



City Research Online

City, University of London Institutional Repository

Citation: Smith, A. T. (1995). The effect of cathodic overprotection on the corrosion fatigue behaviour of API 5L X85 grade welded tubular joints. (Unpublished Doctoral thesis, City, University of London)

This is the accepted version of the paper.

This version of the publication may differ from the final published version.

Permanent repository link: <https://openaccess.city.ac.uk/id/eprint/29606/>

Link to published version:

Copyright: City Research Online aims to make research outputs of City, University of London available to a wider audience. Copyright and Moral Rights remain with the author(s) and/or copyright holders. URLs from City Research Online may be freely distributed and linked to.

Reuse: Copies of full items can be used for personal research or study, educational, or not-for-profit purposes without prior permission or charge. Provided that the authors, title and full bibliographic details are credited, a hyperlink and/or URL is given for the original metadata page and the content is not changed in any way.

City Research Online:

<http://openaccess.city.ac.uk/>

publications@city.ac.uk

**THE EFFECT OF CATHODIC OVERPROTECTION ON THE
CORROSION FATIGUE BEHAVIOUR OF API 5L X85
GRADE WELDED TUBULAR JOINTS.**

by

Alan T Smith, C.Eng, M.Inst.ME, B.Sc. (Eng) Hons.

**A thesis submitted for the degree of Doctor of Philosophy at The
City University, Northampton Sq., London, EC1V 0HB.**

October, 1995

ACKNOWLEDGEMENTS

So many have helped me in the preparation of this thesis, that is difficult to know where to start to thank people. My thanks first and foremost, must go to the staff of the City University and University College London. In particular Professor D. L McDiarmid at the City University for his help and encouragement over the past few years, through the course of several interminable corrosion fatigue experiments, and Professor W. D. Dover at the Non Destructive Evaluation Centre at University College London for his similar patience. This project was funded by the Health and Safety Executive (HSE) and managed through the Marine Technology Support Unit (MaTSU). My thanks also go to these organisations and in particular Mr. Nigel Nichols at MaTSU.

Many people have helped me with the practical work. I am indebted to Mr. Keith Blenkinsopp without whose advice and assistance the experimental work would have proved impossible. Thanks also go to Mr. A. Coombs and Mr. E. Skinner for their advice, encouragement and good humour and to the staff of the engineering departments both at the City University and University College London.

Lastly but by no means least, my thanks go Jenny for her endless patience, support and tolerance, particularly while I was writing.

I grant powers of discretion to the University Librarian to allow this thesis to be copied in whole or in part without further reference to me. This permission covers only single copies made for study purposes, subject to normal conditions of acknowledgment.

The author may be contacted by electronic mail at the following address:

atsmith@twi.co.uk

"The strongest have their moments of fatigue"

F. Nietzsche, *The will to power* (1888)

TABLE OF CONTENTS

ACKNOWLEDGEMENTS	ii
COPYRIGHT	iii
TABLE OF CONTENTS	v
LIST OF TABLES	x
LIST OF FIGURES	xi
ABSTRACT	xv
NOMENCLATURE	xvi
1. REVIEW OF THE LITERATURE	
1.1. Introduction	1
1.2. Scope of Chapter	2
1.3. Stress Analysis	2
1.3.1. Stress Distributions at a Tubular Joint	3
1.3.2. Quantitative Determination of the Hot Spot Stress	5
1.3.2.1. Experimental Model Techniques	5
1.3.2.2. Finite Element Analysis	7
1.3.3. Comparison of Parametric Stress Equations and Experimental Model Results.	8
1.4. Fatigue Design Methods	9
1.4.1. Total Life Prediction Using S-N Curves	9
1.4.1.1. The T' Curve (figure 1.9)	10
1.4.2. Fatigue Life Prediction Using Fracture Mechanics	13
1.4.2.1. Fatigue Initiation	13
1.4.2.2. Fatigue Propagation	14
1.4.2.3. The Application of the Paris Law to Crack Growth in Tubular Joints	15
1.4.2.4. Stress Intensity Factor Solutions for a Crack in Tubular Intersection	19
1.4.3. Summary	21

1.5. Corrosion Fatigue of Structural Steels under Conditions of Cathodic Overprotection	21
1.5.1. The Principle of Cathodic Protection	22
1.5.2. Cathodic Overprotection and Corrosion Fatigue.	23
1.5.3. The Influence of Cathodic Protection on Crack Initiation	25
1.5.4. Crack Propagation	26
1.5.4.1. The Influence of Loading and Environmental Variables on Crack Propagation	27
1.5.4.2. Crack Propagation Under Conditions of Cathodic Overprotection	30
1.5.5. The Influence of Cathodic Protection on the Endurance Life.	34
1.5.6. Summary	35
1.6 Scope of this Thesis	36
2. TEST SPECIMEN DETAILS	
2.1 Scope of chapter	79
2.2 Material Selection	79
2.3. Geometry Selection	80
2.4. Fabrication Details	81
2.4.1 Weld Inspection	82
2.5 Summary	83
3. GLOBAL STRESS ANALYSIS	
3.1. Scope of Chapter	92
3.2 Experimental Stress Analysis of Steel Specimen	92
3.2.1. Test Rig	92
3.2.2. Experimental Method	93
3.2.3. Results	94
3.2.4. Discussion of Results	95
3.3. Experimental Investigation of the Bending to Membrane Stress Ratio and Influence of the Second Brace on the Global Stress System.	97
3.3.1. Experimental Method	97
3.3.2. Results	98
3.3.3. Discussion of Results	98

3.4. Conclusions	99
4. FATIGUE TESTING OF STEEL TUBULAR JOINTS IN AN AIR ENVIRONMENT	
4.1 Scope of Chapter	108
4.2. Determination of the Paris Law Constants for API 5L X85	108
4.2.1 Test Set Up and Procedure	109
4.2.2. Results	109
4.2.3. Discussion of Results	110
4.3. Air Fatigue Testing of Steel Tubular Joints	110
4.3.1. Test Apparatus.	111
4.3.2. Experimental Test Conditions.	113
4.3.3. Experimental Results	114
4.3.4. Discussion of Results	119
4.3.4.1. Fatigue Crack Propagation	119
4.3.4.2. Fracture Mechanics Analysis	121
4.3.5. Stress Endurance Results	126
4.3.5.1. N1 Endurance Data	127
4.3.5.2. N3 Endurance Results	128
4.4. Conclusions	130
5. FATIGUE TESTING OF STEEL TUBULAR JOINTS IN SEAWATER, WITH CATHODIC PROTECTION.	
5.1. Scope of chapter	157
5.2. Corrosion Fatigue, Compact Tension Test Specimen Data	157
5.2.1. Test Set Up and Procedure	158
5.2.2. Results	159
5.2.3. Discussion of Results	159
5.3. Corrosion Fatigue Testing of Steel Tubular Joints	161
5.3.1. Experimental Apparatus and Procedure	161
5.3.2. Results	162
5.3.3. Discussion of the Results	167
5.3.3.1. Corrosion Fatigue Crack Propagation	167
5.3.3.2. Fracture Mechanics Analysis	169

5.3.4. Stress Endurance Results	174
5.3.4.1. N1 Endurance Data	174
5.3.4.2. N3 Endurance Results	175
5.4 Conclusions	176
6. THE IMPLICATIONS OF THE RESEARCH	
6.1 Scope of Chapter	210
6.2 Implications of Research for General Tubular Joint Design	211
6.2.1. The Implications for the Air Fatigue of Tubular Joints	211
6.2.1.1. Stress Field Prediction	211
6.2.1.2. Variation in Crack Path	211
6.2.1.3. Accuracy of SIF Modelling	212
6.2.1.4. Influence of Weld Toe Radius	212
6.2.2. The Implications for the Corrosion Fatigue of Tubular Joints	212
6.2.2.1. Variation of ACPD signal	212
6.2.2.2. Modelling of Tubular Joint Crack Growth Behaviour with Compact Tension Data	213
6.2.2.3. Variation of Crack Growth Rate with Depth	214
6.3 Implications of the Research for Tubular Joints Constructed from Higher Strength Steels	214
6.3.1. Air Fatigue of Higher Strength Steels	214
6.3.1.1. Crack Growth Rate Prediction	214
6.3.1.2. Steel Quality	214
6.3.1.3. Endurance Prediction	215
6.3.2. Corrosion Fatigue of Higher Strength Steels	215
6.3.2.1. Crack Growth Behaviour	215
6.3.2.2. Endurance Behaviour	217
6.4 Application of Constant Amplitude Data to Variable Amplitude Corrosion Fatigue of Tubular Joints	218
6.4.1. Endurance Life Prediction	218
6.4.2. Incremental Crack Growth Prediction and Variable Amplitude Loading	219
6.4.3. Application of Constant Amplitude Data to Variable Amplitude Loading	220
6.5 Summary of Chapter	220

7. SUMMARY, CONCLUSIONS AND FURTHER WORK	
7.1 Scope of Chapter	225
7.2. Summary of Thesis	225
7.3 Summary of Conclusions.	227
7.4 Further Work	228
REFERENCES	230
APPENDICES	
I Weld profiles at crown and saddle positions.	240
II "Irish Penny" test	244
III Calculation of nominal stress in out of plane bending	245
IV Variation of ACPD measured depth with applied load	246

LIST OF TABLES

	Page No.	
1.1	SCF Matrix for selection of parametric equations	38
1.2	Details of design T' Curve [HSE, 1992]	39
1.3	Influence of loading mode on the average fatigue endurance (from HSE 1992)	40
1.4	Comparison of environmental reduction factors for welded plate	40
1.5	Properties of steels referred to in Chapter 1	41
2.1	Metallurgical and physical properties of typical jack up chord steels	84
2.2	Properties of Marathon le Tourneau structural tubing	85
2.3	Specimen geometry	86
2.4	Comparison of weld metal strength with base metal strength	87
3.1	Measured SCFs and values from parametric equations: steel model data	101
3.2	Acrylic model dimensions	102
3.3	Influence of Double T joint on SCF and ratio of bending stress to membrane stress, acrylic model data	102
4.1	Summary of air test details	131
4.2	Initiation and total life endurance data: in air specimens	132
5.1	Chemical composition of substitute seawater	178
5.2	Compact tension test conditions	178
5.3	Tubular joint test conditions	179
5.4	Initiation and total life endurance data: corrosion fatigue specimens	180

LIST OF FIGURES

		Page No.
1.1	A simplified view of a "Jacket" construction, fixed rig	42
1.2	A simplified view of a "Jack Up" construction, mobile rig	43
1.3	Definition of stress distributions	44
1.4	Modes of loading	45
1.5	Definition of hot spot stress	46
1.6	Location of strain gauges for linear extrapolation to weld toe to determine stress concentration factor	47
1.7	The "Hot Spot" stress and bending membrane ratio	48
1.8	Schematic representation of the SN curve	49
1.9	T' curve adapted to 20mm thickness	50
1.10	The effect of plate thickness on crack initiation	51
1.11	Total life for air tested tubular joints compared to T' curve	52
1.12a	Typical stable cyclic stress strain curve	53
1.12b	Coffin Manson curve for strain controlled fatigue	53
1.12c	Derivation of the cyclic strain life from simultaneous solution of the Neuber and cyclic stress strain curves.	54
1.13	Fracture failure modes	55
1.14	Schematic of crack growth as a function of SIF range	56
1.15	Typical fatigue crack growth rates in air for high strength steels	57
1.16	Schematic of typical fatigue crack growth in a tubular joint	58
1.17	Curves of crack depth against percentage of fatigue life for planar and tubular welded specimens	59
1.18	Fatigue crack growth at for X70 steels at four stress ratios	60
1.19	Typical transverse residual stress distributions for a tubular joint	61
1.21	Schematic representation of aqueous corrosion	62
1.22	Polarisation diagram schematically representing the electrochemistry of aqueous corrosion	62
1.23	Schematic diagram showing how corrosion can be reduced or stopped by cathodic protection	63
1.24	Nonogram for the cross referencing of potential readings	64
1.25	Specific conductivity of seawater	65
1.26	Hydrogen permeation current as a function of cathodic potential	66
1.27	Corrosion fatigue by hydrogen embrittlement	67
1.28	The effect of cathodic potential on the initiation life of smooth specimens	67
1.29	Schematic diagram of the effect of cathodic protection on fatigue crack propagation	68

1.30	Effect of frequency on corrosion fatigue crack propagation under freely corroding conditions in seawater	69
1.31	Fatigue crack growth in X65, tested in 3.5% NaCl solution at the Zinc potential, R=0.2 and four frequencies	70
1.32	Influence of applied load ratio on the corrosion fatigue crack growth rate for HY130 tested in 3.5% NaCl at the Zinc potential	71
1.33	Crack growth data for specimens containing through thickness cracks tested in seawater at -1.1V at R=-1 to 0.85	72
1.34	Schematic representation of the effect of cathodic protection of the da/dN Vs SIF plot for short cracks	73
1.35	Effect of potential on the fatigue crack growth rate at 0.1 Hz in seawater at 20C	74
1.36	da/dN versus empirical K for constant amplitude fatigue tests of PWHT BS4360.50D tubular joints in a seawater environment at a potential of -850 mV	75
1.37	Comparison of corrosion fatigue data for high strength steels with cathodic overprotection	76
1.38	Comparison of the corrosion fatigue behaviour of welded high strength steels with BS4360.50D parent plate at a potential of -1100 mV	77
1.39	Corrosion fatigue data for tubular joints c.f. T' curve	78
2.1	Typical leg components for jack up units	88
2.2	Test specimen geometry	89
2.3	Typical "weave" profile of FCAW specimens	90
2.4	Typical "stringer" weld profile of SMAW specimens	90
2.5	Position where weld toes failed the "Irish Penny" test	91
3.1	Experimental rig design	103
3.2	Position of strain gauges relative to weld toe	104
3.4	Experimental stress distribution (brace side)	105
3.5	Position of strain gauges and loading of acrylic model	106
3.6	Inclination of principal stress plane as measured at rosette positions	107
4.1	Compact tension specimen geometry	133
4.2	Schematic of compact tension specimen test rig	134
4.3	Fatigue crack growth rate in air: Marathon Le Tourneau X85 steel	135
4.4	External view of fatigue crack in W2	136
4.5	Section of W2 at 320 mm from crown	137

4.6	W2 air fatigue crack profile: uncorrected depth	138
4.7	Air fatigue crack growth data: specimen W2	139
4.8	External view of fatigue crack in W6	140
4.9a	W6 air fatigue crack profile: uncorrected depth. Depth readings <5mm	141
4.9b	W6 air fatigue crack profile, uncorrected depth. Depth readings >5mm	142
4.10	Air fatigue crack depth data: specimen W6	143
4.11	External view of fatigue crack in S1	144
4.12a	S1 fatigue crack profile: uncorrected depth. Depth <5mm	145
4.12b	S1 fatigue crack profile: uncorrected depth	146
4.13	Air fatigue crack growth data: specimen S1	147
4.14	Example of crack growth shown in a "typical tubular joint fatigue crack	148
4.15a	Shallow crack surface (a<4mm), specimen W6	149
4.15b:	Deep crack surface (a>4mm), specimen W6	149
4.16a	Shallow crack surface (a<4mm), specimen S1	150
4.16b	Deep crack surface (a>4mm), specimen S1	150
4.17	Typical FeMnS inclusions (from W2 parent plate)	151
4.18	In air crack ratio variation	152
4.19	Empirical SIF range for tubular joints	152
4.20	Variation of Y value with a/T	153
4.21	Tubular joint N1 initiation life, X85 c.f. BS4360.50D	154
4.22	Variation of stress intensity factor range with crack depth	155
4.23	Tubular joint N3 air life, X85 c.f. BS4350.50D	156
5.1	Schematic of compact tension corrosion fatigue rig	181
5.2	Corrosion fatigue crack growth rates of X85 structural steel, compact tension specimens with cathodic protection	182
5.3	Comparison of corrosion fatigue data for high strength steels with cathodic overprotection	183
5.4	Schematic of corrosion fatigue rig	184
5.5	Photograph of tubular joint, corrosion fatigue rig	185
5.6	External view of fatigue crack in W5	186
5.7a	W5 corrosion fatigue crack profile uncorrected depth. Depth <5mm	187
5.7b	W5 corrosion fatigue crack profile uncorrected depth	188
5.8	Corrosion fatigue crack growth data: specimen W5	189
5.9	External view of fatigue crack in S2	190
5.10a	S2 corrosion fatigue crack profile uncorrected depth. Depth <5mm	191
5.10b	S2 corrosion fatigue crack profile uncorrected depth. Depth >5mm	192
5.11	Corrosion fatigue crack growth data: specimen S2	193
5.12	External view of fatigue crack in S3	194

5.13	Corrosion fatigue crack profile: uncorrected depth	195
5.14	Corrosion fatigue crack growth data: specimen S3	196
5.15	External view of fatigue crack in S4	197
5.16a	S4 corrosion fatigue crack profile: uncorrected depth. Depth <5mm	198
5.16b	S4 corrosion fatigue crack profile: uncorrected depth. Depth >5mm	199
5.17	Fatigue crack growth data: specimen S4	200
5.18	Seawater crack aspect ratio	201
5.19	Fracture surface for specimen W1/W5 (cracks <4mm)	202
5.19b	Fracture surface for specimen W1/W5 (cracks >4mm)	202
5.20a	Fracture surface for specimen S2 (cracks <4mm)	203
5.20b	Fracture surface for specimen S2 (cracks >4mm)	203
5.21	X85 tubular joint, corrosion fatigue data	204
5.22	Comparison of data for shallow crack growth and deep crack growth	205
5.23a	Corrosion fatigue crack growth data: specimen W5	206
5.23b	Corrosion fatigue crack growth data: specimen S2	206
5.23c	Corrosion fatigue crack growth data: specimen S3	207
5.23d	Fatigue crack growth data: specimen S4	207
5.24	Comparison of corrosion fatigue N1 endurance data with T' curve	208
5.25	Comparison of corrosion of fatigue N3 endurance data with T' curve	209
6.1	X85 tubular joint, corrosion fatigue data	222
6.2	Comparison of corrosion fatigue data for high strength steels with cathodic overprotection	223
6.3	Procedure to calculate equivalent crack growth rate	224

ABSTRACT

A total of eight tubular joints made from a 590 MPa yield strength steel used for Jack Up leg construction have been successfully fatigue tested. Specimens were tested at constant amplitude using out of plane bending in both an air environment and in seawater. Seawater specimens were cathodically overprotected at a potential of -1000 mV (vs Ag/ AgCl). In addition to the endurance life of the specimens, the crack depth was monitored.

Two methods of welding tubular joints have been identified as being used in Jack up construction: flux cored arc welding (FCAW), where the beads are laid perpendicular to the weld toe in a weave action; and shielded metal arc welding (SMAW) beads are laid in a direction parallel to the weld toe as stringer beads. The quality of the weave welds was inferior to that of the string welds. The fatigue properties of both methods have been investigated.

Results show that current fatigue guidelines for the endurance life of offshore grade steels of yield strength less than 400 MPa provide a conservative estimate for the endurance life of both air and cathodically protected test specimens regardless of the weld technique. However there is evidence to suggest that the weave welding technique may give improved fatigue endurance performance compared to the string welding technique.

An empirical fracture mechanics methodology has been derived to estimate the crack growth rate of both the weave and string welded specimens. A difference in the empirical stress intensity factor for the weave welded specimens compared to the string welded specimens has been noted. The string welded specimen Y value showed close agreement with empirical Y value formulae derived at University College London.

Crack growth rates under conditions of cathodic overprotection were comparable to crack growth rates of steels with a yield strength less than 400 MPa under conditions of optimum cathodic protection, however crack growth rates were noticeably higher for the string welded specimens than for the weave welded specimens under comparable loading conditions.

Crack growth paths for the test specimens were quite different from that normally associated with cracks in unstiffened tubular joints. This has implications for the in service inspection, residual strength and stiffness of the joints. The difference in the crack path was particularly noticeable with the string welded specimens. Manganese Sulphide inclusions were observed in the chord material, these may have influenced the crack path.

Nomenclature

a	Crack depth
d	Diameter of brace
l	Length of moment arm
m	Exponent in Paris Law
r	Radius of brace
t	Thickness of brace
C	Constant term in Paris Law
D	Diameter of chord
E	Youngs modulus
I	Second moment of area
K	Stress intensity factor
K_{TH}	Threshold value of stress intensity factor
L	Length of chord
M	Moment
N	Number of cycles
P	Applied Load
R	Applied load ratio
S	Stress
$S_C(\phi)$	Geometric stress concentration factor at displacement ϕ around the weld toe
S_{HS}	Stress concentration factor at the chord "hot spot"
T	Chord thickness
V	Voltage
W	Width of compact tension specimens
IPB	In plane bending
OPB	Out of plane bending
SCF	Stress concentration factor
SIF	Stress intensity factor
α	$2L/D$
β	d/D
γ	$D/2T$
τ	t/T
θ	Angle between chord and brace axis
ϕ	Displacement of point on weld toe measured with respect to brace crown.
ε	Strain
σ	Stress
ν	Poissons' ratio

Other terms are defined within the text.

1. REVIEW OF THE LITERATURE

1.1. Introduction

There are two basic types of oil platforms: fixed and mobile. Fixed platforms are used for continuous production. The most common design of fixed rig in use in the North Sea is the jacket platform (see figure 1.1). The jacket platform is constructed in the form of a framework of vertical or near vertical chords, interconnected by supporting bracing. The primary function of the chords and bracing is to support the topside weight. In addition to this static load, fixed platforms are also subject to dynamic loading from wind, current and wave forces. These dynamic forces can give rise to fatigue crack growth at the welded joint between the chords and braces. The chords and bracing of jacket platforms are usually constructed from a tough, weldable, structural steel BS4360.50D, with a yield strength of 350 MPa.

Research into the fatigue behaviour of tubular joints made from BS4360.50D, has been extensive because of the widespread use of this steel in jacket platforms in the North Sea [Dover & Dharmavasan, 1989; Dover & Dharmavasan, 1992] From this work, a fracture mechanics methodology has been developed, to describe fatigue crack growth in tubular joints under conditions of constant and variable amplitude loading and with varying levels of cathodic protection. Using this fracture mechanics approach, together with a planned inspection policy, it is possible to schedule inspection to detect cracks, or monitor crack growth and make informed decisions about maintenance and safety, as well as to make improvements in the reliability of design life calculations.

Mobile rigs are primarily designed for exploration. Of the various designs available, the Jack-up rig is in common use (see figure 1.2). Jack up rigs are used for exploration and increasingly, for small scale production. Jack-up rigs consist of a central barge or platform and three to four self elevating legs. The barge is towed from site to site with the legs elevated. On site, the legs are lowered on rack and pinion gears to rest on either a "mat", or steel "spud can". The use of high strength steels for jack up construction has the advantage that it is possible to reduce the leg weight. Reduced leg weight gives a lower centre of gravity when the rig is under tow and greater stability as well as greater buoyancy and reduced production costs. This has led to the widespread use of steels with yield strengths in the region of 485 MPa to 690 MPa for Jack-up legs.

Jack-up rigs are also subject to the following dynamic loads, in addition to dynamic loading from current, wind and wave forces:

- (i) high alternating bending moments, induced by the legs swaying when under tow [Kam and Birkinshaw, 1993];
- (ii) loads due to the near resonant response of the platform under service conditions, as a result of the proximity between the natural period of the platform and the natural period of the waves [Hambly, 1985].

The high strength steels used in Jack-up rigs have also been shown to be susceptible to hydrogen assisted cracking [Davey, 1991]. This is further enhanced by the use of excessively negative cathodic protection (overprotection). Susceptibility to hydrogen embrittlement is known to increase with yield strength, therefore, there is likely to be an enhancement of the fatigue crack growth rate of high strength steels in seawater when protected by cathodic protection [Proctor, 1986]. Although some work has been done on fatigue crack growth of steels in the yield stress range of 485 MPa to 700 MPa, there has been little recorded work on fatigue crack growth in representative tubular joints in the 590 MPa to 700 MPa yield stress range, either in-air or under conditions of cathodic protection.

1.2. Scope of Chapter

The corrosion fatigue behaviour of welded tubular steel joints with yield strengths of below 400 MPa, has been the subject of several research programmes. This chapter summarises the existing knowledge of corrosion fatigue of structural steel tubular joints. In particular the following aspects have been investigated and are relevant to the problem of corrosion fatigue in high strength steel tubular joints.

- (i) The stress field at the intersection of the welded tubular joint.
- (ii) The different design procedures for evaluating fatigue damage of welded joints.
- (iii) The influence of cathodic overprotection on the corrosion fatigue process for steel, welded tubular joints

1.3. Stress Analysis

In the following section, only the stress transverse to the weld toe (σ_{xx} in figure 1.3) is considered, as this is the stress component contributing most directly to crack growth. The transverse stress at a welded tubular joint varies in three mutually perpendicular directions: the variation on the chord surface in a direction at 90° to the weld toe; the through thickness variation in a direction perpendicular to the weld toe; and the

circumferential variation in a direction around the tubular intersection (figure 1.3). These stress distributions vary according to the mode of loading: axial loading; in-plane bending (IPB); and out-of-plane bending (OPB) (figure 1.4).

The stress at the weld toe arises from three components: the nominal stresses; the geometric stresses and the notch stresses. The nominal stresses are those which result from the response of the structure, assuming that the joint behaves as a simple beam or column. The geometric stresses are those which result from the need of the tube wall to maintain compatibility, as the chord deforms under load. The notch stresses are due to the stress concentrating effect of the local geometry at the weld toe.

This section will describe:

- (i) the stress distributions in a tubular joint;
- (ii) quantitative determination of the stress in the vicinity of the weld toe.

1.3.1. Stress Distributions at a Tubular Joint

Much of the following discussion is based on work carried out under the United Kingdom Offshore Steels Research Programme Phases I and II [DEn, 1988; DEn, 1987].

The Transverse Stress Distribution Along the Normal to the Weld Toe.

The transverse stress variation on the chord or brace surface, perpendicular to the weld toe is shown in figure 1.5. Notch stresses predominate in a region within $0.2\sqrt{rt}$ of either the brace or chord weld toe (figure 1.6).

The zone marked as lying between B and A (figure 1.6), is characterised by approximately linear stress decay. This region is dominated by geometrical stresses and varies in size according to the circumferential position around the weld toe. The transverse stress ceases to decay linearly beyond the region marked by A in figure 1.6.

In practice, the notch stress at the weld toe is very variable, due to the variation in the weld toe radius. It is therefore necessary to standardise the weld toe stress. This is done by using a fictitious stress, known as the hot spot stress, which is derived from the linear stress decay region described above. The hot spot stress is defined as *"the greatest value around the brace/chord intersection of the linear extrapolation to the weld toe of the geometric stress distributions near the weld toe. This 'hot spot' stress incorporates the effects of overall joint geometry (i.e. the relative size of the brace and chord) but omits the stress concentrating effects of the weld itself which results in a local stress distribution."* [DEn, 1984] (see figure 1.5).

The Transverse Stress Distribution Around the Brace Chord Intersection.

The transverse stress distribution in the circumferential direction is an important parameter for both the Average stress (AVS) and Two Part Method (TPM) solutions of the stress intensity function (see section 1.4.2.4 and 4.3.4).

Hellier *et al* [1990 c] have produced a set of semi empirical functions to describe the stress distribution around the weld toe. The SCF described in the equations is defined as the stress at the weld toe extrapolated from the region of linear stress decay, i.e. the geometric stress at the weld toe, divided by the nominal stress. The equations were obtained by fitting results from nearly 900 finite element analyses to simple circular functions. Typical distributions are :

$$S_C(\phi)=S_{HS}\text{Sin}^2(\phi) \quad (1.1)$$

For OPB in a Y or T joint where $\beta>0.4$

where ϕ represents the angular displacement of the local geometric stress concentration factor with respect to the crown.

UEG guidelines [UEG, 1985] recommend that the geometric weld toe stress has a sinusoidal distribution around the weld toe for OPB in a Y or T joint such that:

$$S_C(\phi)=S_{HS}\text{Sin}(\phi) \quad (1.2)$$

The Transverse Stress Distribution in the Through Thickness Direction

The transverse stress distribution in the through thickness direction is an important parameter for the application of plate solutions such as Newman & Raju [1981] and Niu & Glinka [1989] to the stress intensity function in tubular joints (see section 1.4.2.4).

Analysis of the through thickness distribution of transverse stresses at the weld toe has been carried out by Elliot & Fessler [1987], using photo-elastic techniques. Through thickness analysis was carried out at the crown position of K/T joints with modelled welds, for conditions of out of plane bending. These results show two distinct regions:

- i: An exponential region or through thickness notch stress zone, extending to between 0.06 and 0.08 of the wall thickness,
- ii: A linear region, beyond the through thickness notch zone, where principal stresses decay linearly with distance.

Stresses in the notch stress zone are dependent on the weld toe radius. Monahan [1994] and Niu & Glinka [1987] have suggested suitable distributions to describe the transverse stress distribution in the through thickness direction which include the notch stresses. Monahan [1994] has shown good agreement when these expressions have been used to predict crack growth in tubular joints. The problem with these techniques, is that they require detailed information about the weld toe radius which is seldom available, and the validity of the expressions is limited by weld angle and weld toe radius. It has also been argued that the effect of the weld toe radius on the stress intensity factor is limited to early crack growth [Niu & Glinka, 1987].

For longer cracks ($a > 0.1T$), the transverse stress distribution in the through thickness direction can be simplified to two components: a membrane stress and a bending stress (figure 1.7). These stresses can then be determined using thin shell finite element analysis. Hellier *et al* [1990a] have produced sets of parametric equations to describe the bending stress to membrane stress ratio for T and Y joints under a variety of loading conditions.

1.3.2. Quantitative Determination of the Hot Spot Stress

Following extensive testing of steel and acrylic models of tubular joints and finite element analysis of representative models, there is now an extensive database containing a variety of loading cases and geometries. By modelling these databases in terms of the following tubular parameters:

$$\alpha=2L/D; \beta=d/D; \gamma=D/2T; \tau=t/T; \theta=\text{angle between the brace and chord,}$$

the SCF can be expressed in terms of a set of parametric equations using curve fitting techniques. These parametric equations provide a suitable basis for design calculations. In the following section, the methodology of model tests and finite element analysis will be discussed, together with accepted parametric solutions derived from these solutions. Further details are given in UKOSRP II [DEn, 1987] and UEG Design of Tubular Joints [UEG, 1985].

1.3.2.1. Experimental Model Techniques

Steel Models

The stress distribution in steel models of tubular joints can be determined using electrical resistance strain gauges. The resulting strain analysis is used to determine surface stress distributions and the ratio of bending stress to membrane stress near the weld toe.

Full scale steel models are recommended in preference to other experimental methods where the weld profile needs to be accurately represented. In practice, the work on steel models is limited, not only by the size of the chord and brace sections but also by difficulty in reproducing realistic end restraint.

Acrylic Models

Acrylic models are recommended if the tubular dimensions fall outside the range of existing parametric studies and cost and test time scales are limited. Acrylic models have the advantage that they can be quickly and easily made, can be scaled down in size and have a low material modulus. The low material modulus, combined with the lower loads needed for the scaled models, permits loading without recourse to expensive actuators.

Acrylic models are strain gauged in the same way as steel models, and yield information on the SCF and bending to membrane ratio only, however allowances have to be made for both the creep rate and the different Poisson's ratio in determining stresses.

Photo-elastic Methods

Due to the complexity of this technique, it is only used where detailed information on the transverse stress distribution in the through thickness direction is required.

Parametric Solutions based on Steel and Acrylic Model Results: The Lloyds Registry Equations [Smedley & Fisher, 1991]

This set of parametric equations, has been derived from curve fitting data from a database of 161 steel tubular joints and 149 acrylic tubular joints. The effect of the short chord length is included, by using a correction factor. A stiffening factor is also incorporated, to account for the effect of adjacent braces where K, KT and other multibrace joints are considered. An influence function is also included to model the effect of loading on adjacent braces. In addition, a safety factor is applied to ensure that the mean steel and acrylic model results, plus one standard deviation, fall within the values predicted by the parametric equation. The following validity range applies:

$$4 \leq \alpha \leq \infty; \quad 0.13 \leq \beta \leq 1.0^*; \quad 10 \leq \gamma \leq 35.0; \quad 0.25 \leq \tau \leq 1.0; \quad 30 \leq \theta \leq 90$$

* $\beta=1$ forms a special case in the above equations.

1.3.2.2. Finite Element Analysis

Finite Element Analysis (FEA) forms a comparatively inexpensive and versatile way of approximating the stress levels for an individual welded tubular joint. The results for a variety of different geometries can be fitted to a set of equations. This enables the hot spot SCF to be expressed in terms of the modelling parameters.

Accuracy is determined by two factors:

- a) The complexity of the element and number of nodes.
- b) The size of the mesh used.

When using FEA, the following points should be noted:

- i) The accuracy of methods should be established by convergence studies or comparison with laboratory results;
- ii) The value of stress obtained from FEA, is the result of superimposing the tensile and bending components of stress, induced at the intersection of thin shell elements. This is not the same as the definition of hot spot stress given above and this intersection may be physically remote from the weld toe area. For this reason, thin shell elements are not recommended where $\beta > 0.8$ [UEG, 1985].

There are a variety of solutions based on different finite element analyses. The following two sets of parametric equations are chosen as representative for the following reasons: the Efthymiou equations are accepted by the Health and Safety Executive (HSE), as acceptable for design purposes [HSE, 1992]; the UCL equations also provide for a parametric solution of the bending stress to membrane stress ratio which will be used in subsequent calculations.

Parametric Equations Based on Finite Element Analysis:

The Efthymiou Equations

Using results from FEA of tubular T, Y, and gap/ overlap K joints, a set of widely used parametric equations were developed [Efthymiou & Durkin, 1985]. These equations were developed further to include X and KT joints, and the effect of loading on an adjacent brace was modelled using influence functions [Efthymiou, 1988]. This enables the analysis of multiplanar nodes. The basic parametric equations also include a function to correct for short chord length and a correction factor to account for different end fixity conditions (relevant to axial loading). The following validity conditions apply:

$$4 \leq \alpha \leq 40 \quad 0.2 \leq \beta \leq 1.0 \quad 8 \leq \gamma \leq 32 \quad 0.2 \leq \tau \leq 1.0 \quad 20 \leq \theta \leq 90$$

The University College London (UCL) Equations

Hellier, Connolly and Dover [1990b] derived a set of equations for the hot spot SCF, bending stress to membrane stress ratio and free surface stress distributions around the weld toe for axial loading, OPB and IPB in Y and T tubular joints. The parametric equations were based on results from nearly 900 finite element analyses.

The validity range of the UCL equations, are as follows:

$$6.21 \leq \alpha \leq \infty \quad 0.2 \leq \beta \leq 0.8 \quad 7.6 \leq \gamma \leq 32; \quad 0.2 \leq \tau \leq 1.00; \quad 32 \leq \theta \leq 90$$

1.3.3. Comparison of Parametric Stress Equations and Experimental Model Results.

Current recommended practice for determining the hot spot stress is based on the comparison of the above equations with both acrylic and steel model data [HSE, 1992]. The Efthymiou and the Lloyds Registry equations were chosen as recommended equations, because they are well recognised by industry, have good documentation and their consistency of prediction [HSE, 1992]. However, neither set of equations was recommended for all joint types and loading cases. The applicability of both sets of equations is summarised in table 1.1. In the case of the bending stress to membrane stress ratio, there is little steel model data to compare to the UCL equations. However, Hellier [1990a] claims good agreement between the parametric formulae and acrylic model data.

It should be noted that although the parametric solutions listed above, allow the most accurate assessment of the hot spot stress currently readily available, the equations have several drawbacks. Firstly the results obtained from the laboratory and finite element analyses assume either fixed end or pin jointed restraint. Modelling the degree of end restraint in a realistic case is not easy. Secondly, the parametric equations reflect an upper bound (conservative) estimate of the hot spot SCF. Vinas Pich [1994], has shown that variation of the chord wall thickness within the manufacturers tolerances, combined with the conservative upper bound for the parametric equations, can lead to overestimates of the SCF of up to 45%. Overestimating the hot spot SCF can lead to the remaining life and endurance life of the tubular being considerably underestimated. For the purposes of an experimental investigation, the parametric solutions for the SCF are unlikely to yield a sufficiently accurate solution. It is therefore recommended that in the current study, the SCF should be determined experimentally from electrical resistance strain gauges.

1.4. Fatigue Design Methods

The total life of a welded tubular joint can be determined by using either a stress life (SN) diagram, or from separate calculation of the propagation life, calculated using a fracture mechanics approach, and the initiation life. The SN approach, provides a simple guideline for the design of structures using tubular joints, whereas fatigue propagation calculations provide an indication of the severity of existing flaws and a guide for inspection scheduling. SN calculations are based on a different methodology to that of fatigue propagation calculations and are discussed in section 1.4.1. Fatigue propagation calculations are based on linear elastic fracture mechanics and will be discussed in section 1.4.2. The endurance life and fatigue crack propagation life are complicated by corrosion fatigue and cathodic protection. The influence of these factors is discussed in detail in section 1.5. In the following section, the total life is defined as the number of cycles needed for the fatigue crack to penetrate the chord wall.

1.4.1. Total Life Prediction Using S-N Curves

The total fatigue life is made up of three phases: initiation, propagation and final fracture. Final fracture is a rapid process and compared to initiation and propagation forms an insignificant proportion of the total life. Ideally, the initiation life is considered together with the propagation life, to form the total life and represented by a Stress Life Endurance Curve or S-N curve (figure 1.8). The S-N curve has two notable features:

- (i) The relationship between the stress range and number of cycles to failure is simplified to a straight line on the log stress range versus the log of number of cycles to failure plot ;
- (ii) A stress limit exists for in-air data, below which fatigue crack growth cannot initiate. This is called the fatigue limit.

In practice the number of cycles to failure is subject to statistical variation and individual results may vary considerably from that predicted using the S-N curve. As a result of many experimental fatigue tests, a S-N curve for BS4360.50D welded tubular joints has been developed. Recommended design practice for this curve will be considered, together with current practice for higher strength steels.

1.4.1.1. The T' Curve (figure 1.9)

Constant amplitude, in-air fatigue tests have been conducted on a variety of BS4360.50D tubular joint specimens with different chord wall thicknesses, hot spot stress ranges and loading conditions [DEn, 1988; DEn; 1987]. These have been collated to form the database for the Fatigue Design Guidance Notes S-N curve for tubular joints. From this database, two large subsets have been formed; one of 32-40 mm chord wall thickness joints, the second of 16-19 mm chord wall thickness joints. The fatigue endurance data for each subset has a log normal distribution about the mean endurance line. The data from each subset can therefore be expressed using the following equation adapted to give a 97.6% probability of survival:

$$\text{Log}(N) = \text{Log } k - 2 \text{Log } s - m \cdot \text{Log}(S) \quad (1.3)$$

where

N = The predicted number of cycles to failure under stress range S

k = constant

S = stress range

Log s = the standard deviation of Log N

m = the inverse slope of the S-N curve. To retain consistency with earlier work this slope was fixed at -1/3.

The largest subset of data was based on 54 constant amplitude in air tests of 16-19 mm specimens and is known as the T' curve [HSE, 1992]. The values of the constants are given (table 1.2). There is a change of slope at $N > 10^7$ cycles reflecting the possibility of an endurance limit at longer lives. The T' curve replaced an earlier curve based on a database of 25 constant amplitude, in air tests of 32-40 mm tubular joints known as the T curve.

The Thickness Effect

It has been observed that thick plates and tubulars often have a reduced fatigue life compared to that of thin plates [Gurney, 1989]. This has been accounted for by a higher crack growth rate in the short crack phase of thick plate and a shorter initiation period. The notch stresses are particularly important in considering the crack initiation life. It can be assumed that:

i) The size of the notch stress zone increases with the size of the weld fillet;

ii) The size of the initial crack is constant regardless of the size of the weld fillet.

From figure 1.10, it can be seen that a crack in a thin plate will be subject to a lower stress than a crack in a thick plate. A thick plate will have a reduced initiation life compared with a thin plate and the crack will grow faster in the short crack region. The accelerated growth in the notch region will reduce the overall life. The reduction in fatigue life will depend on:

i) The magnitude of the notch zone stresses, which is dependent on the local weld geometry;

ii) The through thickness variation of transverse stress, dependant on the plate thickness;

iii) The proportion of the total fatigue crack life spent with the crack in the region of high stress.

The Health and Safety Executive [HSE, 1992] has suggested the following empirical correction factors for tubular joints:

$$a > T_0 \quad S = S_0 \cdot (T_0/T)^{-0.3} \quad (1.4)$$

$$a \leq T_0 \quad S = S_0 \quad (1.5)$$

Assuming a value of $m=3$ this translates to:

$$a > T_0 \quad N = N_0 (T_0/T)^{-0.9} \quad (1.6)$$

$$a \leq T_0 \quad T = T_0 \quad (1.7)$$

where S_0 and T_0 are the stress range and thickness of a reference tubular joint (in this case 16 mm).

Other Geometry Effects

The thickness correction factor derived above, was obtained using specimens with either a high bending to tension ratio or significant notch effect. For specimens with a low ratio of τ , and consequently low bending to tension ratio, or with a low SCF, this correction factor may be over conservative. However, evidence from tests on 16 mm chord wall thicknesses show that the effect of τ is small compared to that of thickness. The affects of varying other geometric parameters on the S-N curve appear to be negligible [HSE, 1992].

Influence of Loading Mode.

The influence of loading mode on the endurance life has been considered by the HSE [1992]. The axial mode of loading was shown to give marginally shorter endurance lives than the out of plane bending and in plane bending modes. Out of plane bending was shown to give the longest endurance lives (see table 1.3). However, given the large degree of scatter, the influence of the loading mode is of secondary importance.

Influence of the Applied Load Ratio.

The effect of applied load ratio on the endurance life, has been determined from fatigue tests of transverse, as-welded plate specimens. This was judged to be minimal [DEn, 1988]. The reason why the mean stress appeared to have a minimal effect on the endurance life was attributed to the near yield, residual weld stresses at the weld toe. The presence of high tensile stresses can render the effect of the applied mean stress negligible (see section 1.4.2.3).

The T' curve is limited to tubular joints constructed from steels of yield strength less than 400 MPa and fatigued in air. However, the T' curve provides a useful benchmark against which the endurance life of higher strength steel tubular joint fatigue tests can be compared.

The Endurance Life of Higher Strength Tubular Joints

Endurance life results for welded tubular joints made from higher yield strength steels tested in-air are limited. Vinas Pich [1994] has obtained fatigue data for a 450 MPa yield strength tubular under conditions of constant and variable amplitude loading, and Lopez Martinez *et al* [1994] have obtained data for a steel of yield strength 820 MPa (Weldox700) under variable amplitude loading, tested using in plane bending. The hot spot stresses are standardised to a constant amplitude stress range by using a modified form of Miners summation, the equivalent stress [Hibberd and Dover 1977]. Endurance life data is shown for comparison with the T' curve in figure 1.11.

The endurance life of the Weldox 700 tubular joints falls below that typical of BS4360.50D steels. However, specimens were tested by reacting two braces, welded to a common chord, against each other. Such a mode of loading, results in a higher chord membrane stress compared to where the brace is loaded in true in plane bending. The high membrane stress is believed to contribute significantly to the reduced endurance life. Results from the 450 MPa steel [Vinas Pich, 1994] combined with the Weldox 700 steel are too few to determine precisely the effect of yield

strength on the T' curve. Even though they are lower than those typical of the BS4360.50D steel, they still fall within or close to the overall scatter band. However, these results fail to confirm any increase in the endurance life when the yield strength is increased.

1.4.2. Fatigue Life Prediction Using Fracture Mechanics

The use of fracture mechanics allows an accurate assessment of the propagation life of a fatigue cracked specimen. To obtain the total life requires a separate calculation of the initiation life. For this reason the following section considers methods for evaluating the initiation life in addition to methods for calculating the propagation life of the tubular joint.

1.4.2.1. Fatigue Initiation

It has been argued [Glinka *et al*, 1987; Bhuyan & Vosikovsky, 1989], that the initiation life can be estimated from a modified SN approach using knowledge of the cyclic stress strain curve, the stress concentration factors (through the use of the modified Neuber's rule [Topper *et al*, 1969]), and the strain life curve as defined by the Coffin Manson relationship (see figure 1.12) [Hertzberg, 1989]. A development of this model, relevant to the initiation life analysis of welded joints, is to adapt the Coffin Manson relationship to include the effect of residual weld stress [Morrow, 1979]. Clearly, a great deal of information is required to analyse the initiation life using this method and its validity for use with welded joints is called into doubt by the somewhat arbitrary definition of the initiation life, and by the presence of pre-existing flaws at the weld toe. In addition the question arises as to whether the Coffin Manson relationship should be derived for the parent plate or the weld toe heat affected zone. The total strain approach is clearly more complex than the basic SN approach.

In the case of welded tubular joints, slag intrusions at the weld toe present an obvious site for crack initiation. These intrusions were measured and found to vary in size from 0.15 to 0.4 mm [Sines, 1967; Watkins, 1970]. However, an initial defect size of 0.1-0.25 mm has been shown to be compatible with a subsequent fracture mechanics approach [BS7608:1993]. This provides a simple approach to the calculation of the fatigue life. Given that the initiation life of a typical as-welded tubular joint is typically a small fraction of the total life [Dover & Dharmavasan, 1984], this approach does not seem to be unreasonable.

1.4.2.2. Fatigue Propagation

Fatigue crack propagation can be characterised in terms of the stress field in the immediate vicinity of the crack tip. Cracks can grow in three modes depending on the orientation of the applied load to the crack plane (see figure 1.13). In mode I, a tensile load is applied perpendicular to the crack plane. For a linear elastic material the stress field around the crack tip is defined as:

$$\sigma = \frac{f(\theta)}{\sqrt{2\pi r}} \quad (1.8)$$

Where r is the distance from the tip and K is the stress intensity factor (SIF). The SIF is more commonly expressed as

$$K = Y\sigma\sqrt{\pi a} \quad (1.9)$$

where Y is dependant on the geometry and loading conditions. Standard solutions for K and Y exist and are given in many texts [e.g. Broek, 1991].

Paris [1962] investigated the relationship between fatigue crack growth and the stress intensity factor. He showed that the fatigue crack rate could be characterised as a function of ΔK (figure 1.14). A plot of da/dN versus ΔK shows three regions:

i. Region I: A threshold value of the SIF (ΔK_{th}) below which cracks will not propagate.

ii. Region II: The rate of crack growth is governed by the Paris Law;

$$\frac{da}{dN} = C(\Delta K)^m \quad (1.11)$$

iii. Region III: crack growth tends to infinity.

The use of the Paris Law allows the remaining life of a cracked specimen to be evaluated in terms of the SIF range ΔK , provided that crack growth is confined to region II and that a suitable expression exists for ΔK .

Both ΔK_{th} and region III crack propagation are dependent on the load ratio. This is illustrated in figure 1.18. In the case of ΔK_{th} , the value of the effective K_{min} is thought to have a strong influence on whether the crack propagates. In the case of region III crack growth, propagation is dominated by static modes of failure as K_{min} approaches K_c . The influence of the R ratio is discussed further in the following subsection.

Conservative values for ΔK_{th} , C and m have been determined for carbon and carbon manganese steels and are given in PD6493:1991 as:

$$\Delta K_{th} = 2 \quad R > 0.5$$

$$\Delta K_{th} = 5.4-6.8R \quad 0 \leq R \leq 0.5 \quad (1.10)$$

$$\Delta K_{th} = 5.4 \quad R \leq 0$$

Mean air levels for C and m for carbon and carbon manganese steels with a yield strength of less than 600 MPa, at operating temperatures of less than 100°C are given as:

$$C=9.5 \times 10^{-12}, m=3.00$$

Units: da/dN(m/cycle); $\Delta K(\text{MPa}\sqrt{m})$

Other values of C and m have been determined for the same materials [Dover & Holdbrook, 1979], however the change in values have relatively little influence on the fatigue crack growth calculations [HSE, 1992]. The dependence of C and m on the applied load ratio is discussed in section 1.4.2.3.

At present, PD6493:1991 guidelines are confined to steels of yield strength less than 600 MPa and no recommended values are included for higher strength steels. However a review of in air fatigue data for four structural steels with yield strengths in the range 480 MPa to 890 MPa, has been conducted by King *et al* [1992]. A comparison of in-air fatigue crack growth rates of these materials shows close agreement with $da/dN = 9.5 \times 10^{-12} \Delta K^3$, specified in PD6493:1991 (figure 1.15). Full testing conditions are not known for the Creusot Loire A517Q plate, but lower in air crack growth rates are claimed for this material [Bennett *et al*, 1991].

1.4.2.3. The Application of the Paris Law to Crack Growth in Tubular Joints.

Analysis of in air fatigue tests of tubular joints typically show three principal regions of crack growth (see figure 1.16). These regions are characterised by:

- i. Region 1. A period of initiation and short crack growth.
- ii. Region 2. A period of approximately constant crack growth as the crack propagates through the chord wall.
- iii. Region 3. A period of continuous growth as the crack extends around the chord wall.

In-air fatigue tests of tubular joints, show the majority of the endurance life is confined to Region 2. It should be noted that tests involving flat plate do not reproduce the same crack growth behaviour as tests using tubular joints. The difference in the behaviour is shown schematically in figure 1.17. This shows the life

of plate specimens is dominated by initiation and growth of short cracks whereas the life of tubular specimens is dominated by the propagation of longer cracks at an approximately constant rate. This difference provides the justification for the fatigue testing of full scale tubular joints in place of tests on welded plates.

The Paris Law provides a method of predicting the crack growth propagation rate and remaining life. However, several factors can lead to complications in calculating an accurate value for the SIF and possible inaccuracy in predicting the remaining life in the specific case of a welded tubular joint. These are discussed below:

i) Tubular Joint Geometry

No proven solution exists for the solution of the SIF of a semi elliptical crack, at a tubular intersection, because of the complexity of the geometry. The SIF can be approximated by considering the tubular joint to be equivalent to a flat plate, subjected to the tensile and bending stresses described in section 1.3. Alternatively the SIF can be approximated by using finite element analysis or empirical methods, which make an allowance for the geometry of the specimen. The solution of the SIF is considered in more detail in section 1.4.2.4.

ii) Stress Distribution

The accuracy of any idealised solution for the SIF is dependent on how realistically the assumed stress field approaches that of the tubular joint. In section 1.3.1 the stress field at the weld toe was described in terms of a hot spot stress, transverse stress distribution in the circumferential direction and bending to tension stress ratio. Clearly, cracks less deep than the notch weld toe are also influenced by the magnitude of the notch stresses. Since the notch stress is directly dependent on the notch radius (which has been shown to be extremely variable), this introduces a degree of uncertainty into the calculation of the SIF when describing early crack growth. Different SIF equations show different levels of sophistication when considering the stress distribution.

iii) Applied Load Ratio and Residual Weld Stresses

The effect of the applied load ratio (R ratio) on the Paris curve is shown for a higher strength steel in figure 1.18. Regions I and III are influenced most by the R ratio, however region II is also influenced by the R ratio, though to a lesser degree (see section 1.4.2.2). Many authors have attempted to "correct" the Paris equation for the effect of the R ratio [see Broek 1991], however the suggested corrections lack generality. In the case of a welded joint, contraction during solidification of the weld

metal, results in high residual tensile stresses in the weld toe area [Easterling 1992]. These residual stresses are usually close to the yield stress. Discussion of the effect of the applied mean stress must therefore be considered together with the residual stress.

In considering the effect of residual weld stresses and the applied stress ratio, use is made of the effective stress intensity factor range (ΔK_{eff}), which is defined as the SIF range contributing to actual crack growth and the effective stress ratio (R_{eff}), which is defined as the ratio of the minimum effective stress cyclic stress divided by the maximum effective cyclic stress. The effective R ratio and ΔK_{eff} are given as:

$$(\sigma_{min} + \sigma_{res}) \geq 0; (\sigma_{max} + \sigma_{res}) \leq \sigma_{yield}; \quad R_{eff} = \frac{\sigma_{min} + \sigma_{res}}{\sigma_{max} + \sigma_{res}} \quad 1.13$$

$$\text{and} \quad \Delta K_{eff} = Y \Delta \sigma \sqrt{(\pi a)} \quad 1.14$$

If one assumes a plastic yield condition; where the combined residual stress and maximum stress exceeds the yield stress, the effective stress must fluctuate down from the yield stress so:

$$(\sigma_{min} + \sigma_{res} \geq 0; (\sigma_{max} + \sigma_{res}) \geq \sigma_{yield}; \quad R_{eff} = \frac{\sigma_y - \Delta \sigma}{\sigma_y} \quad 1.15$$

$$\text{and} \quad \Delta K_{eff} = Y \Delta \sigma \sqrt{(\pi a)} \quad 1.16$$

However, where part of the combined residual and applied stress cycle is compressive it is generally recognised that the compressive part of the cycle does not contribute to fatigue crack growth.

$$(\sigma_{min} + \sigma_{res}) \leq 0; 0 \leq (\sigma_{max} + \sigma_{res}) \leq \sigma_{yield} \quad R_{eff} = 0 \quad 1.17$$

$$\text{and} \quad \Delta K_{eff} = Y (\sigma_{max} + \sigma_{res}) \sqrt{(\pi a)} \quad 1.18$$

It can be seen that there are three principal regions affected by the applied mean and residual stresses: a region where high residual stresses mean that applied mean stress has little influence on the effective SIF and the Paris Law constants can be determined from fatigue tests conducted at a high mean stress (high applied load ratio); an intermediate region where the effect of residual stress is less dominant and applied mean stress ratio is more significant; and a region of zero effective stress ratio where the effective SIF range is equal to the magnitude of the maximum effective SIF [Stacey, 1993]. Under conditions of high residual stresses, the applied mean stress makes little difference to the effective stress ratio. It is therefore reasonable to model values of C, m and ΔK_{th} to be used on tubular joints, on crack growth data obtained at

a high load ratio. The residual stress and applied load ratio would be expected to have a greater influence on fatigue crack growth where the threshold SIF is affected.

Porter Goff *et al* [1987] have studied the residual stress distributions of welded tubular joints using hole drilling and block sectioning techniques. This work has confirmed that near yield tensile residual stresses occur within a few millimetres of the inner and outer surfaces. However, mid section compressive residual stresses were also recorded (see figure 1.19). In regions of compressive residual stress, one would expect significant crack closure and a subsequent reduction in K_{eff} . Experiments on tubular joints by Monahan [1994] using clip gauges, have not recorded any crack closure at crack depths of up to $0.6T$. This suggests that the residual stresses redistribute as the crack grows. Monahan has argued that the residual stress in a tubular joint is subject to partial stress relief and partial residual stress redistribution as the crack grows (see figure 1.20). In effect, the crack tip is subject to a tensile residual stress regardless of the crack length. Although this remains a hypothesis and the exact nature of any residual stress redistribution is unknown, the explanation for the lack of crack closure proposed by Monahan, appears plausible.

iv) Load Redistribution.

A tubular joint is a redundant structure. As the crack grows the load redistributes around the brace chord intersection. The actual nature of load redistribution in tubular joints is unknown. Various models have been proposed as an aid to incorporating load redistribution into calculations for the SIF. One of the simplest of these is linear moment release [Aaghaakouchak *et al* 1989]. Using this model, the tensile stress transmitted across the remaining ligament remains constant, however, the bending moment supported by the remaining ligament is assumed to decrease linearly to zero as the crack grows, in the following manner:

$$M=M_0(1-a/T) \quad (1.19)$$

v) Crack Position

Normally cracks initiate at the hot spot and grow with the deepest point at the hot spot. This is at the saddle position for out of plane bending and axial loading, and at the crown for in plane bending. If cracks initiate at other positions the stress can be determined from the appropriate stress distribution and the deepest point of the crack would normally migrate towards the hot spot.

vi) Multiple Crack Initiation and Crack Aspect Ratio.

It is very rare for cracks in a welded tubular joint to start and propagate as a single crack. The welding process provides many initiation sites. Generally speaking, these cracks will start as flaws of a given aspect ratio and later interact with each other as they coalesce to form a long, but shallow, crack [Dover *et al*, 1984]. The crack will then grow to a preferred aspect ratio depending on the joint stress distribution [Morgan, 1987]. The shape of the crack is normally assumed to be that of a semi-ellipse for tubular joints [Dover *et al*, 1984], where the crack geometry is described by the aspect ratio (crack depth divided by half the surface length). Current recommended design practice [BS PD6493:1991] accounts for multiple cracks by assessing the structure using a single crack encompassing the smaller defects, however this can lead to over estimating of the aspect ratio especially for early crack growth. Morgan [1987] and Twaddle & Hancock [1988] have argued that these guidelines are over conservative and that each crack can be considered as acting independently, prior to coalescence. The aspect ratio has a significant effect on the SIF, and is therefore important in calculating the crack growth rate.

Empirical formulae have been derived for the aspect ratio of cracks in tubular joints both by Dover *et al* [Dover *et al*, 1988] and Monahan [Monahan, 1994]. These formulae provide a simple method of establishing the aspect ratio, however, the accuracy of such formulae in the early stages of crack growth is debatable. These formulae will be reviewed in more detail in chapter 4.

1.4.2.4. Stress Intensity Factor Solutions for a Crack in a Tubular Intersection

The solution for the SIF is not straightforward and ideally should take many factors into account. Several methods can be used to approximate the SIF for a crack in a tubular joint. These are discussed below.

Calculation of the SIF using Numerical Techniques

Direct calculation of the SIF can be made using either three dimensional FEA or two dimensional techniques. The SIF can be found from the local crack tip stress strain field using either the "crack tip response" or the "energy release rate" methods. However, finite element methods only provide a solution for a particular geometry and results are difficult to generalise. In practice, accurate modelling of the SIF in the vicinity of the crack is complex and expensive.

Empirical Solutions for the SIF

The SIF range can be determined from full scale constant amplitude fatigue tests provided that crack growth is within region II of the Paris Law curve and crack growth data can be accurately monitored. The SIF can be determined by transposing the Paris Law so:

$$\Delta K_{\text{eff}} = \left(\frac{1}{C} \frac{da}{dN} \right)^{\frac{1}{m}} \quad 1.20$$

It is assumed that:
$$\Delta K_{\text{eff}} = S_{\text{HS}} Y_{\text{exp}} \sqrt{\pi a} \quad 1.21$$

It follows that:

$$Y_{\text{exp}} = \frac{1}{S_{\text{HS}} \sqrt{\pi a}} \left(\frac{1}{C} \frac{da}{dN} \right)^{\frac{1}{m}} \quad 1.22$$

This allows the SIF to be obtained for a similar joint. Y_{exp} is an all embracing function which accounts for bending stress to membrane stress ratio, load redistribution, crack aspect ratio, stress distribution around the weld toe, residual stress and notch stresses. The Y_{exp} value can be found for a variety of geometries, tested under various loading conditions and expressed as a parametric function of the geometry. The use of such parametric functions provide a means of determining the SIF using a minimum of geometrical inputs. However, as residual stress, weld notch stress concentration, aspect ratio and redundancy can have an effect on the SIF, any change in these conditions from those obtained for the reference test may lead to errors. Two sets of equations have been derived from crack growth data: the "Average Stress" (AVS) Method [Dover and Dharmavasan, 1982]; and the Two Phase Method (TPM) [Kam, 1988], both developed at University College London using results from large scale tubular joints. These are only valid within strict limits and will be considered in greater detail in chapter 4.

Estimation of the SIF using Plate Solution Formulae.

Any comprehensive solution for the SIF in a tubular joint would have to make allowance for the following: crack position, crack profile, stress distribution, residual stress, load redistribution and multiple crack interaction. The approximations described here are solutions for the SIF in more simple applications, which have then been applied to tubular joints.

Various solutions for the SIF of a semi elliptical, surface breaking crack in a flat plate exist. Of these, the Newman & Raju [1981] equations form one of the most widely

accepted sets of solutions . The solutions are based on fitting finite element solutions for the SIF to a parametric model and allow the SIF to be determined from the bending to membrane stress, hot spot stress, crack aspect ratio and a minimum of geometrical information. However, many assumptions are made in applying these equations to the SIF in tubular joints and the accuracy of this method is low. The accuracy can be improved by incorporating load redistribution [Aaghaakouchak, 1989] and by making other modifications to accommodate the local weld geometry [Niu & Glinka, 1987; Thurlbeck & Burdekin, 1992] and a correction for aspect ratio effects [Monahan 1994]. The application of the plate solution techniques will be discussed further in chapter 4.

1.4.3. Summary

Both the SN approach and the fracture mechanics approach present a valid means of evaluating the fatigue design life. The fracture mechanics approach can be used to evaluate the remaining life of the specimen and has advantages because of its versatility. In view of the fact that no definitive solution exists for the SIF in a welded tubular joint, it seems reasonable for the purposes of the current study, to fatigue test a tubular joint in air under conditions of constant amplitude with the purpose of deriving an empirical solution for the Y value in terms of crack depth and hot spot stress range. It can then be assumed that the SIF of subsequent corrosion fatigue tests can be obtained using the same Y value solution, provided the geometry of the specimens, the fabrication history and the crack profiles are similar. The empirical Y values can then be compared to adapted plate solutions and semi empirical solutions such as TPM and AVS to assess the accuracy of these methods. In addition, an air fatigue test will enable actual endurance data to be obtained, for a comparison with the predicted endurance life.

1.5. Corrosion Fatigue of Structural Steels under Conditions of Cathodic Overprotection

The fatigue initiation and crack propagation processes considered above, result from mechanical processes. It is assumed that the effect of environment for structures fatigued in air is negligible. Where structures are fatigued in a corrosive environment, one would expect the corrosion fatigue process to be much more complex than the air fatigue process, and corrosion fatigue data to reflect the complex interaction between mechanical and environmental variables. The relationship between corrosion and fatigue is further complicated by the application of cathodic protection. The literature on corrosion fatigue is extensive. This section will concentrate on the effect of

corrosion fatigue on offshore structural steels with a yield strength of over 350 MPa and subject to cathodic overprotection. In particular the following aspects will be examined:

(i) the principle of cathodic protection and the effects of cathodic overprotection on corrosion fatigue, including crack propagation and retardation mechanisms arising from cathodic protection.

(ii) the influence of environmental and loading variables on the corrosion fatigue process, with a view to establishing test conditions which accurately simulate in service conditions.

(iii) existing test data for the corrosion fatigue of offshore structural steels will be examined, so that a comparison with test data from the current test programme can be made.

1.5.1. The Principle of Cathodic Protection

Corrosion of steel in sea water is an electrochemical process involving oxidation of iron and reduction of oxygen. Oxidation is accompanied by the parent metal going into solution and is known as anodic dissolution (see figure 1.21).

The anodic reaction involved is:
$$\text{Fe} \Rightarrow \text{Fe}^{2+} + 2\text{e}^- \text{ (oxidation) } \quad (1.23)$$

The principal cathodic reaction involved is:

Oxygen reduction (neutral or basic solutions)
$$\text{O}_2 + 2\text{H}_2\text{O} + 4\text{e}^- \Rightarrow 4\text{OH}^- \quad (1.24)$$

During corrosion, the driving force for the anodic and cathodic reactions is provided by the potential difference between the cathodic and anodic sites. This can be represented electrochemically by the Tafel plot (figure 1.22) or potential diagram. If the anodic sites and cathodic sites are connected together, so that a current flows between them, the potential of the steel moves spontaneously to a value between E_c and E_a , shown by E_{CORR} giving a current of I_{CORR} . Under conditions of free corrosion, the rate of anodic dissolution can be measured using I_{CORR} .

By adding electrons to the metal surface, the anodic reaction can be suppressed while the cathodic reaction rate is maintained. This is shown schematically on the potential diagram (figure 1.23). When a current CA is applied, I_{CORR} is reduced to I_p and the potential of the steel falls to E_p . Increasing the applied current to equal to the limiting current will eventually stop the anodic dissolution and depress the potential to E_a .

The effectiveness of a cathodic protection system is measured by the potential of the steel relative to a reference electrode. The potential can be measured indirectly by connecting to a half cell reference electrode, such as a standard calomel electrode (SCE), Cu/CuSO₄ or Ag/AgCl electrode. A nomogram and resistivity chart to aid conversion from one potential to another are included in figure 1.24 and 1.25. Unless otherwise stated, the potentials stated in the following test can be assumed to be measured relative to a Ag/AgCl electrode.

Cathodic protection can be applied through the following two methods:

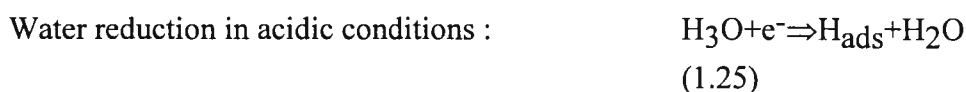
i) Impressed Current Method. A potential difference is applied between the work to be protected (the cathode) and the anode (the counter electrode), allowing a current to flow across the sea-water and electrons to flow to the work, suppressing anodic dissolution. The potential of the cathode can be controlled using a reference electrode and potentiostat.

ii) Sacrificial Anode. The work to be protected is galvanically coupled to a more active metal, such as zinc. Galvanic coupling causes a current to flow to the more noble metal, suppressing corrosion in the protected specimen but causing the anode to be consumed. Typical potentials achieved using Zinc anodes lie in the region -950 mV to -1030 mV [Marine Technology Directorate, 1990].

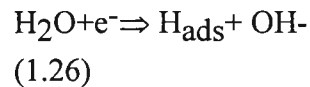
Under conditions of free corrosion, the potential of steel is about -670 mV. The generally accepted potential for protection of steel structures in sea-water is -850 mV [Marine Technology Directorate, 1990]. Cathodic overprotection can occur locally as a result of changes in the electrical conductivity of the seawater due to variations in oxygen concentration, temperature and location with respect to the anode. Measurements taken for the HSE on platforms in service, measured cathodic protection levels of between -950 mV and -1020 mV next to high strength steels painted with coal tar. Sacrificial anode systems using zinc, achieve potentials of -1000 mV to -1050 mV [Davey, 1991]. Cathodic overprotection of -1000 mV, therefore represents a realistic operating condition likely to be encountered in some joints.

1.5.2. Cathodic Overprotection and Corrosion Fatigue.

Cathodic protection and cathodic overprotection can result in the following reactions taking place, depending on the pH of the seawater:



Water reduction in neutral or basic conditions (such as seawater):



and Oxygen reduction in neutral or basic solutions: $\text{O}_2 + 2\text{H}_2\text{O} + 4\text{e}^- \Rightarrow 4\text{OH}^-$ (1.27)

Under normal circumstances, seawater is alkaline and the reduction of water and oxygen would be expected to take place. The electron exchange takes place at the steel surface. The adsorbed hydrogen atoms can either recombine to form molecular hydrogen gas, or be absorbed into the steel. The principal means of measuring the amount of hydrogen available for crack growth, is to measure the hydrogen permeation current. Neilsen & Maahn [1987] have determined the hydrogen permeation current in BS4360.50D steel as a result of cathodic protection and shown a near logarithmic increase in hydrogen permeation with increasing levels of cathodic overprotection (see figure 1.26).

Atomic hydrogen has a detrimental effect on crack growth through two mechanisms. Firstly, the surface energy is related to the fracture stress through the following equation [Congleton & Craig, 1982]:

$$\sigma_{FR} = \sqrt{\frac{E\gamma}{b}} \quad (1.28)$$

where

σ_{FB} is the fracture strength

γ is the surface energy

b is the interatomic spacing

E is Young's modulus

Hydrogen at the crack tip can reduce the surface energy, thereby reducing the fracture stress and embrittling the steel.

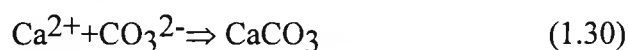
Secondly, atomic hydrogen can contribute to the corrosion fatigue process through the mechanism of hydrogen embrittlement. The exact nature of hydrogen embrittlement is uncertain, but it has been proposed that the hydrogen adsorbed to the steel surface can become absorbed into the steel and migrate to the front of the plastic yield zone ahead of the highly strained crack tip. The hydrogen is interstitially absorbed ahead of the crack tip, where it can interfere with dislocation movement, thereby embrittling the steel (figure 1.27) [Suresh, 1991]. Hydrogen embrittlement can lead to a dramatic

increase in the fatigue crack growth rate and is particularly prevalent in higher strength steels with cathodic protection. Fractography has shown that, in an X70 steel, at increasingly negative potentials, the proportion of brittle failure modes such as intergranular and transgranular cleavage increases compared to ductile failure modes such as tearing and microvoid coalescence [Saenz de Santa Maria & Proctor, 1986]. This helps to confirm hydrogen embrittlement as the main crack growth mechanism under cathodic protection.

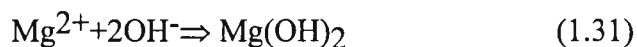
Cathodic overprotection can also have an influence on the fatigue crack growth rate, through the formation of calcareous deposits in the crack enclave. Under the influence of cathodic overprotection, water is reduced to hydrogen and hydroxyl ions (equation 1.25), the increased number of hydroxyl ions displace the carbonate ions from the hydrogen bicarbonate ions in solution.



The carbonate ions are then free to combine with calcium ions in solution, to form calcium carbonate, which precipitates as an insoluble salt.



The hydroxyl ions are also free to combine with magnesium ions to form magnesium hydroxide which precipitates as an insoluble salt.



Magnesium salts can delay initiation of short cracks, but enhance crack propagation, whereas calcium salts appear to retard crack propagation [Marine Technology Directorate, 1990]. This is by two mechanisms: firstly, calcium salts particularly, act as a barrier to prevent further water reduction and absorption of hydrogen; secondly, the precipitation of salts acts as a plug helping to wedge the crack open, thereby reducing the effective value of ΔK . This second mechanism may be responsible for crack retardation at the early stages of crack growth [Neilsen and Maahn, 1987]. The formation of calcareous deposits also helps to act as a protective film and reduces the current supplied by the CP system [Marine Technology Directorate, 1990].

1.5.3. The Influence of Cathodic Protection on Crack Initiation

The initiation of fatigue cracks in seawater is dependent on the level of cathodic protection and the total strain for smooth or notched specimens. Bignonnet [Bignonnet *et al*, 1987] has shown that the fatigue initiation life of 350 MPa yield strength steels can be restored to that of air specimens at potentials of -800 mV. With

overprotection, low strain cycling ($\Delta\varepsilon_T < 0.5\%$) shows initiation lives approaching or improving on those of the air specimens. However at higher strain ranges the initiation lives are inferior to those of the air specimens by a factor of 2 or more (see figure 1.28). It has been suggested that the principal reason for the restoration of fatigue lives to those of the air specimens is due to the prevention of anodic dissolution and consequent initiation from crack pits [Congleton & Craig, 1982]. At lower potentials and high cyclic plastic strain, hydrogen can diffuse into the lattice, causing embrittlement and increasing cyclic work hardening, thereby reducing the fatigue initiation life. In a series of tests investigating the fatigue limits of different higher strength steels under conditions of cathodic overprotection (-1100 mV(SCE)), Rajpathak & Hartt [1988] found that a fatigue limit was restored by cathodic protection for key hole notch specimens. The fatigue limit with cathodic protection increased with tensile strength to a limit of 550 MPa at a tensile strength limit of 700 MPa, this compares with air data showing an increase in fatigue limit with tensile strength to a ceiling of $\sigma_{UTS} = 1050$ MPa. However, in the presence of high tensile residual stresses, such as occur in welded joints, one would not expect the higher strength materials to show an increased fatigue limit.

In the case of welded tubular joints it is normal to consider the weld toe to contain pre-existing cracks in the form of slag inclusions (see section 1.4.2.1). If it is assumed that such flaws are in existence, the problem of crack initiation is replaced by the problem of propagation of short cracks. Whether the crack propagates from the pre-existing flaw will depend on crack propagation rates, crack retardation due to corrosion product crack closure and the threshold SIF [Dickson *et al* 1986, Neilsen & Maahn 1987] (see section 1.5.4).

1.5.4. The Influence of Cathodic Protection on Crack Propagation

To simplify discussion of the general effect of the environmental and loading variables, a fracture mechanics approach is adopted. A typical plot of SIF range against crack growth rate is shown schematically in figure 1.29. At low SIF ranges, cathodic protection can restore the value of ΔK_{TH} to that of air value and the environmental contribution to the fatigue process is low. The environmental contribution increases dramatically at higher SIF ranges leading to a typical "plateau" region of crack growth where the crack growth rate is independent of the SIF range. At higher ranges of the SIF the mechanical contribution again takes dominance and the crack growth rate tends to that of air specimens.

The corrosion fatigue crack growth rate is strongly influenced by the rate with which hydrogen can diffuse to the triaxial stress region ahead of the crack tip. The crack

growth rate is therefore likely to be strongly influenced by such variables as the temperature, stress waveform and frequency. However, in addition, the availability of hydrogen will be a function of dissolved oxygen content, salinity, pH, and electrical potential. One can also expect the residual weld stress and the applied mean stress to have a significant influence on the crack growth rate. This is further complicated because properties such as potential and pH are likely to be significantly different at the crack tip compared to the bulk solution and are interrelated both to each other and such factors as the SIF, R ratio, temperature etc.

1.5.4.1. The Influence of Loading and Environmental Variables on Crack Propagation

i) Dissolved Oxygen Content:

It has been suggested that the supply of oxygen can affect the crack propagation rate by limiting the supply of hydrogen to the crack tip. This is because dissolved oxygen in the water affects the degree to which hydrogen can permeate into the steel. This has been shown experimentally by Lucas & Robinson [1986], using hydrogen permeation tests in aerated and deaerated 3% Na Cl solution. It has been suggested that increased proportions of adsorbed oxygen can lead to hydrogen being discharged on the adsorbed oxygen layer, rather than being discharged on the metal surface and absorbed into the lattice. Increasing the proportion of dissolved oxygen will also increase the internal pH of the crack enclave, though this will be nullified by the pumping action of the crack.

In the North Sea, dissolved oxygen content varies from that of fully oxygenated at the splash zone, to anaerobic conditions below the mudline. It is therefore difficult to pitch a level for the dissolved oxygen content to represent "typical" offshore conditions. Thorpe *et al* [1983] have shown that reducing the oxygen content from 7 to 1 mg/l has only a second order effect on the crack growth rates at the free potential, though the effect of oxygen content at more negative potentials is likely to be more influential for the reasons discussed above. In experimental work, a fully aerated water supply is maintained to provide compatibility with other results.

ii) Temperature.

Increased temperature can have a direct effect on corrosion fatigue rates by increasing the adsorption of hydrogen to the steel surface and the diffusivity of hydrogen through the steel. The effect of temperature has been the subject of several studies. Thorpe *et al* [1983] have shown that increasing the temperature of sea-water from 5 to 10°C, doubles the crack growth rate under free corrosion . Vosikovsky [1975]

has measured the rate of crack growth for cathodically protected specimens and measured the crack growth rate to increase by a factor of four times with an increase of temperature from 0°C to 25°C. For the purposes of laboratory tests, a temperature of 8 to 10°C is chosen to allow comparison between tests and approximate North Sea conditions [DEn, 1988].

iii) Salinity:

Work by Monahan & Hopkins [1990] has shown that the chemical composition of the seawater influences the propagation rates through the formation of crack tip deposits. It can therefore be expected that changing the salinity and constituents of the seawater will have a direct effect on corrosion product crack closure, by influencing the ratio of calcium to magnesium salts and the total quantity precipitated. However, corrosion fatigue tests conducted at the free potential show that changing the salinity from 1.75% to 3.5% by weight has only a second order effect on crack growth rates at the free corrosion potential [Thorpe *et al*, 1983]. In practice, the composition of seawater varies widely. For the purpose of comparison with other tests ASTM D1141 [1992] synthetic sea-water is used for standard laboratory tests.

iv) pH.

The pH has a direct influence on crack growth by determining the rate of water reduction and controlling the deposition of magnesium and calcium salt deposits. The influence of cathodic protection is generally to increase the pH of the electrolyte through the reduction of oxygen and water. It has been shown by Turnbull and Gardner [1982] that for static cracks at pH values less than 10, and potentials higher than -1100 mV the rate of water reduction is not significantly affected by pH. However, for pH greater than 10, water reduction decreases significantly with increased pH. This would have a significant effect on limiting the availability of hydrogen. In addition, calcium carbonate can precipitate at pH levels of above 8.2 [Maahn, 1986] and together with magnesium hydroxide can influence the crack growth rate through the crack closure mechanisms listed in section 1.5.2.

Experimental readings within typical crack enclaves show the pH to be between 10 and 13 [Hodgkiess & Cannon, 1986; Turnbull & Ferriss, 1986]. This is confirmed by the presence of magnesium hydroxide, which is unable to precipitate below pH 10. However, the relationship between the crack depth, crack tip potential, stress intensity function and crack tip pH is complicated. Moreover, the pH value within the crack enclave, will be moderated by solution pumping. The standard pH for the bulk solution used in representative tests is taken as pH 8.2 [ASTM D1141, 1992].

vi) Frequency and Stress Waveform.

Both the frequency and the waveform, can be expected to influence the crack growth rate by affecting the time with which hydrogen can diffuse through the steel and accumulate ahead of the crack tip. Vosikovsky [1980] has measured the effect of frequency on corrosion fatigue crack propagation rates in X65 steel protected at the zinc potential. He has shown the plateau crack growth rate increases by a decade with each decade decrease in frequency from 0.01 Hz to 10 Hz (see figure 1.31). However, at higher frequencies than 10 Hz, hydrogen diffusion has difficulty keeping up with mechanical fatigue crack propagation and cathodic protection has a negligible effect on corrosion fatigue crack growth rates.

The form of the stress wave appears to be important. Studies conducted by Atkinson & Lindley [1977] have shown that positive sawtooth and triangular waves give much higher fatigue crack growth rates than square and negative sawtooth waves. Sinusoidal waves behave in a similar way to positive sawtooth and triangular waves. This supports a view that for the environment to contribute to the fatigue process, the rise time is crucial. During the rise time, new metal is constantly being exposed to the environment, while the metal is in a state of high strain and any passivating oxide/hydroxide layer is being broken. This allows for anodic dissolution or absorption of reactant products. Hold time is less significant than rise time and has less influence at longer hold times. For the purposes of simulating North Sea conditions, a sinusoidal wave was chosen. The frequency adopted to simulate North Sea conditions was 0.167Hz.

v) Residual and Applied Mean Stress.

The applied mean stress can be expected to influence the corrosion fatigue crack growth rate in much the same way as it influenced the air crack growth rate (section 1.4.2.3). In addition, it can be expected to:

- i) affect the threshold SIF by decreasing crack closure effects at higher levels of applied stress;
- ii) affect region II crack growth by influencing the plateau growth rate;
- iii) influence region III crack growth by increasing the mechanical stress contribution as K_{MAX} approaches the embrittled value of K_C .

Work done by Vosikovsky [1978] on the corrosion fatigue of HY130 and X70 showed that for tests in 3.5% NaCl solutions the strongest effect of the stress ratio can be seen at the lowest values of ΔK (figure 1.32), with relatively little difference being made to intermediate rates of crack growth. In compact tension specimen tests on BS4360.50D reported in UKORSP 1 [Thorpe, 1983], the general effect of increasing

applied load ratios has been noted as enhancing the crack growth rate including plateau rates (see figure 1.33).

The interaction of residual weld stress fields and applied load ratios was discussed in section 1.4.2.3. In conditions of corrosion fatigue, the effective load ratio could have a significant affect on crack growth rate via an effect on plateau corrosion fatigue crack growth rates.

vi) Crack Length

It should be noted that short crack lengths can lead to substantially higher crack growth rates than long crack growth at equivalent values of the SIF range, depending on the environment and material. Kim & Hartt [1993] have summarised the effects of short crack length at a potential of -950 mV (SCE), for a series of higher strength steels, is to restore ΔK_{TH} to air values, but to enhance crack growth rates up to a depth of 0.3 - 0.6 mm. The effect of short crack growth at other potentials is shown in figure 1.34. For a crack in a tubular joint, this has implications for whether cracks start to propagate from pre-existing flaws (section 1.5.3), but has little significance for cracks deeper than 1 mm.

It is worth pointing out that the potential at the crack tip can vary considerably from those in the bulk solution due to the electrical resistance of the crack solution [Congleton & Craig, 1982]. Maahn [1986] has modelled the crack tip potential mathematically, using a model which compares favourably with experimental results. He has shown that, for a crack of 10mm deep at 0.13 Hz and an external potential of -1000mV, the crack tip potential varies between approximately -900 mV and -850 mV. However, experimental measurements taken by Hodgkiess and Cannon [1985] for 5mm deep cracks, suggest that the crack tip potential is closer to that of the bulk solution at -900 mV(Ag/AgCl). It has also been noted by Turnbull & Ferriss [1986], that under cathodic protection more negative than -1000 mV(SCE), the generation of hydrogen atoms on the external surface is more significant to crack growth, than that at the crack tip.

1.5.4.2. Crack Propagation Under Conditions of Cathodic Overprotection.

From consideration of the environmental and loading variables, a set of conditions representative of North Sea conditions can be derived. By holding these conditions constant between tests, the effect of cathodic protection on the crack growth rate can be modelled on a da/dN versus ΔK plot.

The influence of cathodic protection on the threshold SIF has been studied by Dolphin & Tice [cited in HSE, 1992]. In tests involving low levels of calcareous deposits, they confirmed that ΔK_{th} is restored to in-air values by cathodic protection. Work on BS4360.50D tubular joints tested at a potential of -1000 mV, supports the use of a threshold SIF of $\Delta K_{th} = 7 \text{ MPa}\sqrt{\text{m}}$ [Austin, 1994] for welded tubular joints.

The general effect of lowering the cathodic potential on stage II growth is to increase the plateau crack growth rate. This is illustrated by compact tension tests on BS4360.50D (see figure 1.35). By comparing crack growth rates at similar levels of SIF range, usually in the plateau region of crack growth, a "snap shot" can be made of the effect of cathodic protection levels on crack propagation rates. Cowling & Appleton [1986] have derived such a graph for BS4360.50D. This shows a decline in crack growth rates from those measured in free corrosion (as anodic dissolution is reduced as a possible crack growth mechanism), to crack growth rates just above those measured in air. The minimum crack growth rate is actually achieved at a bulk potential just below that considered to be optimum. The rise in crack growth rates corresponds to the increase in the hydrogen permeation current noted by Neilsen & Maahn [1987] and is clear evidence for an increased contribution of hydrogen embrittlement to the crack growth process.

PD6493:1991 guidance for the values of C and m is currently limited to steels of yield strength less than 400MPa. These are selected to provide a generous upper bound to the available crack growth data from compact tension data tested at a potential of -1100 mV and R=0.85:

$$C=7.3 \times 10^{-11}, m=3.00$$

Units: da/dN(m/cycle); $\Delta K(\text{MPa}\sqrt{m})$

It should be noted that some of the plateau data exceeds this line, however to increase the value of C would make the line over conservative [HSE, 1992].

Actual data for tubular joints is largely confined to BS4360.50D steels. Wilson & Dover [1986] have conducted constant amplitude, corrosion fatigue tests on post weld heat treated (PWHT) tubular joints at a cathodic protection level of -850 mV (vs Ag/AgCl) and a low mean stress ratio (R=0.1). Using this crack growth data and the AVS model to predict crack growth (section 1.4.2.4.), a multi segment model has been derived to predict crack growth, as shown in figure 1.36.

Austin [1992] fatigue tested as-welded BS4360.50D tubular joints in conditions of variable amplitude loading, with cathodic protection of -1000 mV. Austin compared

corrosion fatigue crack growth rates for the variable amplitude corrosion fatigue tests of BS4360.50D tubular steel joints with those for constant amplitude crack growth in a PWHT joint [Wilson & Dover, 1986]. Austin found the constant amplitude results underpredicted the plateau rate of crack growth by a factor of 5, for cracks of between 2 and 7 mm deep, while the constant amplitude crack growth data correlated more closely with the variable amplitude data for deeper cracks. Austin suggested that increasing the crack growth rate by a factor of 5 to account for this, was not unreasonable given the scatter in experimental data. It is the author's view that at least part of the measured difference between the PWHT crack growth data of the constant amplitude, low mean stress tubular joints and the crack growth data from the as welded tubular specimens, can be ascribed to differences in the residual stress fields.

Austin also modelled the variable amplitude crack growth process by using the equivalent crack growth rate concept of Kam and Dover [1988], the AVS Model to determine the SIF [Dover and Dharmavasan, 1982], a rainflow counting method and crack growth data from a variety of constant amplitude, compact tension specimen tests [Austin, 1994]. Austin came to several conclusions which have consequences for constant amplitude, corrosion fatigue tests. As well as finding that crack growth modelling was greatly improved by incorporating a SIF threshold at $7 \text{ MPa}\sqrt{\text{m}}$, Austin also found the crack growth rate differed from that predicted using the corrosion fatigue compact tension specimen data of Thorpe and Scott [1983]. Austin has suggested that under conditions of rapid crack growth, corrosion fatigue growth rates can be limited by the diffusion rate of the available hydrogen through the material lattice or by the supply of hydrogen. Where specimens had previously been subject to high loads, such as storm states, the process zone could become enlarged and lead to subsequent higher than normal crack growth rates when the load was reduced. He suggested that the size of the process zone (where hydrogen embrittlement takes place) is fundamental to the rate of crack growth and that this is dependent on the size of the crack tip plastic zone and consequently the stress state and load history. In the case of high rates of crack growth, the crack grows faster than the hydrogen can diffuse to the crack tip, and tubular crack growth rates are consequently lower than those experienced by small scale compact tension specimens.

Unfortunately, little data is available for steel tubular joints of higher yield strength under conditions of cathodic overprotection. Vinas Pich [1994] has conducted two variable amplitude tests of a 450 MPa yield strength steel using a Wave Action Standardised History (WASH) derived from offshore experience. Vinas Pich modelled data using the equivalent crack growth rate concept developed by Kam and Dover [1988], a rainflow counting method, crack growth rate data from Brook and Zhang [1992] and a variety of SIF solutions. Vinas Pich claimed that corrosion fatigue

crack growth could be modelled reasonably accurately by assuming an AVS solution for the SIF [Dover and Dharmavasan, 1982] and by treating sea states on an individual basis. However, Vinas Pichs' work was primarily concerned with the prediction of corrosion fatigue crack growth rates under conditions of variable amplitude loading and provided little information on corrosion fatigue crack growth in higher strength steels not contained in other literature.

The influence of CP on crack propagation of steels with a yield strength higher than 450 MPa has been reviewed by King *et al* [1992], using results from plate tests on 50D, X70, HT80, and HY130 (for properties see table 1.5). Crack growth data for these steels are shown collectively for comparison with each other and current recommended design practice in figure 1.37. Comparison of the corrosion fatigue crack growth rates for HT80 and HY130 materials shows close agreement. The X70 steel shows a higher crack growth rate than that exhibited by the other steels in the region $13 \text{ MPa}\sqrt{m} < \Delta K < 20 \text{ MPa}\sqrt{m}$ but converges to the same crack growth rates outside of these limits. Many of these higher strength steels have crack growth rates at, or above, that predicted using HSE guidelines for steels with a yield strength of less than 400 MPa. However, there seems to be no consistent correlation between increasing strength and higher crack growth rates. As steels of this grade are likely to be used in jack up construction, there is clear evidence that existing guidelines may need to be revised to account for higher crack growth rates in steels with yield strengths of more than 400 MPa.

Brook and Zhang [1994] have fatigue tested RQTuf 501 steel (470 MPa yield strength) under conditions of variable, sequential and constant amplitude loading in seawater with cathodic protection of -850 mV and -1000 mV using standard edge notched bend specimens. They found that RQTuf 501 exhibited similar plateau crack growth rates to those observed in BS4360.50D steel. Brook and Zhang [1994], also conducted corrosion fatigue tests for BS 7191.450 steel at a potential of -1000 mV. Corrosion fatigue crack growth rates were shown to be approximately equivalent to those of BS4360.50D.

Billingham and Laws [1994] have determined corrosion fatigue crack growth rates in the coarse grained HAZ region of several higher strength steels (table 1.5), with yield strengths in the region of 460 MPa to 640 MPa, at cathodic potentials of -800 mV to -1100 mV. Corrosion fatigue crack growth rates were noted to increase at potentials more negative than -950 mV. This finding was in agreement with Kim and Hartt [1993]. Billingham and Laws also noted that even at cathodic protection levels of -1100 mV, corrosion fatigue crack growth rates were equivalent to, or better than those BS4360.50D (see figure 1.38).

1.5.5. The Influence of Cathodic Protection on the Endurance Life.

The effect of the environment on the total life of a tubular joint can be evaluated in terms of the Environment Reduction Factor or ERF. The ERF is the ratio of mean fatigue endurance in air to the fatigue endurance in a particular environment at the same stress range. To enable comparison, the ERF is calculated by normalising endurance data to the T' curve using a thickness exponent of 0.3.

Existing fatigue guidance for tubular joints is confined to steels with a yield strength of less than 400 MPa. As only a limited number of corrosion fatigue tests of tubular joints at optimum cathodic protection and cathodic overprotection have been carried out [Dijkstra & de Bach, 1981; Wilson & Dover, 1986] it is necessary to consider results from welded plate tests. From these results two trends emerge:

- i. At low stress ranges and endurance lives beyond 10^7 cycles, the initiation and total life are restored to the in-air values, reflecting extended initiation lives obtained at low stress ranges;
- ii. At high stress ranges, the fatigue life is reduced by a maximum factor of 2.7, reflecting the relatively short initiation life and faster crack propagation rate obtained under conditions of cathodic overprotection.

This would support a change of slope when adapting the T' curve to conditions of cathodic protection. Data from cathodically protected tubular joint tests is shown for comparison with the T' curve in figure 1.39. The corrosion fatigue data includes data obtained at a higher than normal cyclic frequency. However, taking this into account, test data for tubular joints under cathodic protection and cathodic overprotection supports the use of a less conservative ERF of 2.1. In practice, an ERF of 2 has been adopted at higher stress ranges and no change of slope is made. The fatigue limit, noted at lower stress ranges is catered for by extending slope of -1/5 back to intercept the lowered line. No distinction is made between the optimum level of cathodic protection and overprotection at -1V to -1.1V (figure 1.39, table 1.2) [HSE, 1992].

At present, there are no guide-lines on the use of S-N curves for welded tubular joints made from steels of higher yield strengths than 400 MPa, other than to note that excessive cathodic protection may reduce the fatigue life to below that predicted by the T' curve [HSE, 1992]. S-N curve data for higher strength structural steel tested under conditions of cathodic overprotection is available for as welded plate specimens of a 430 MPa yield strength steel (MACS steel produced by Kawasaki), 470 MPa yield strength steel (SAR 60) [Tubby and Booth, 1991] and a 490 MPa yield strength steel (RQT501) [Bateson *et al*, 1988]. Little difference was noted between the

endurance life of either the SAR60 or the MACS steel and that of BS4360.50D under similar conditions of optimum and cathodic overprotection of -1100 mV. The RQT 501 steel shows similar endurance lives to BS4360.50D at -850 mV, however the endurance life deteriorates below that predicted of BS4360.50D at potentials of -1100 mV. The environmental reduction factors for the RQT 501 steel protected at a potential of -1100 mV are greater than those allowed under current HSE guidelines for steels with a yield strength of less than 400 MPa [HSE, 1992]. This data is summarised in table 1.4. This would point to the need for the T' curve to be modified, before it is applied to steels of yield strength greater than 400 MPa, protected using cathodic overprotection.

Vinas Pich [1994] has shown that the endurance lives of two welded tubular specimens made from a 450 MPa steel (corrosion fatigue tested at variable amplitude and a potential of -1000 mV (vs Ag/AgCl)) are compatible with HSE guidelines for steels with a yield strength less than 400 MPa (figure 1.39). However, other than this, there is no corrosion fatigue data available for higher strength tubular joints under conditions of corrosion fatigue and cathodic overprotection.

1.5.6 Summary

The effect of cathodic protection on the corrosion fatigue of high strength steel, can be summarised by the effect on the fatigue initiation and propagation lives. Cathodic protection has been shown to restore the initiation life of smooth specimens at low strain ranges. However, welded specimens are known to harbour small defects as a result of the welding process. Initiation is therefore more a matter of propagation from small initial flaws.

Any analysis of corrosion fatigue propagation is complex. However, a meaningful evaluation of corrosion fatigue crack growth can be made by holding the environmental and physical variables constant and at levels equivalent to offshore conditions. For lower grade steels, the effect of cathodic protection is to increase the crack growth rate at potentials more negative than the optimum. Higher strength steels also show this tendency at potentials more negative than -950 mV. At these more negative potentials, corrosion fatigue crack growth rates for higher strength steels vary from being lower than those experienced by BS4360.50D steels, to being marginally higher. The higher crack growth rates experienced at these low potentials is a cause for concern, as these conditions are likely to be met in practice.

The endurance life of higher strength steel welded joints, varies from being equivalent to BS4360.50D, to being just below that predicted using existing guidelines.

Knowledge of the endurance life and the corrosion fatigue propagation process for the higher strength steels is restricted by a shortage of test data for realistic offshore structures.

1.6 Scope of this Thesis

It has been established that corrosion fatigue under conditions of cathodic overprotection presents a serious and real problem for the use of jack up platforms for extended periods of use in the North Sea. Although the corrosion fatigue behaviour of steels currently used in fixed jacket platforms is well documented, there is little data on the corrosion fatigue behaviour of the higher strength steels commonly used for jack up legs. A fully representative study of the corrosion fatigue of jack up legs, would require a realistic stress history [Kam & Birkinshaw, 1993]. However, as there is a general shortage of information on higher grade steel tubular joints, it was decided to fatigue test specimens using constant amplitude and obtain crack growth and endurance data. The constant amplitude data can then be compared to representative variable amplitude data, when a relevant stress history can be established.

The observations made in this chapter provide a basis with which the study of corrosion fatigue in a higher strength steel tubular joint was undertaken. Two double T joints were fatigue tested at constant amplitude and conditions of cathodic overprotection of -1000 mV (vs Ag/AgCl) and air fatigue. The methodology adopted below, would work equally well with either axial loading, in plane bending or out of plane bending, provided that the loading mode is adhered to throughout the test programme. It was decided to test the specimens in out of plane bending, as this represents a mode commonly found in service. The test programme was divided into four stages: stress analysis of test specimens; determination of Paris Law constants for the test material; air fatigue of tubular specimens and determination of the Y value, and corrosion fatigue of the tubular specimens under conditions of cathodic protection.

The hot spot stress was determined using experimental strain analysis (section 1.3.2.1), in order to characterise both the air and corrosion fatigue endurance lives and the crack growth rate. The hot spot stress was related to the applied load through the SCF, which was determined experimentally. The test load was then selected to give the chosen value of hot spot stress in each test. The transverse stress distribution in the circumferential direction was also determined using experimental strain analysis and is used to calculate the Y value from the AVS and TPM equations (section 1.4.2.4). It was also decided to compare the SCF for the double T joint with that of a single T joint.

Paris Law constants have been determined for some higher strength steels and show general agreement with data from lower strength steels (section 1.4.2.2), However, for the steel chosen in this study, this information was not available. For this reason, it was necessary to fatigue test a compact tension specimen in an air environment.

Specimens were fatigue tested in air at a known hot spot stress range. From the crack depth and number of elapsed cycles, an empirical curve for the calibration of the SIF was obtained. The empirical "Y value" was used to characterise the SIF range for the specimen geometry and mode of loading and was obtained by transformation of the Paris Law (equation 1.22), as discussed in section 1.4.2.1. Data on the air fatigue, endurance life was also obtained from these tests.

From corrosion fatigue tests conducted under representative North Sea conditions, the fatigue endurance life, crack depth and crack growth rate were also determined. The SIF range was calculated from the hot spot stress, the crack depth, and the Y value. From the above information a graph of the SIF versus the crack growth rate was obtained. This was then used to obtain appropriate constants for the calculation of the corrosion fatigue crack growth rate in a tubular joint under conditions of cathodic overprotection. The endurance life was obtained for comparison with existing fatigue guidelines. A compact tension specimen was also tested under similar environmental conditions, to enable a comparison with tubular joint crack growth data and to see if compact tension data could be used to successfully predict crack growth in tubular joints.

The above data was used to prove the validity of a fracture mechanics methodology for the fatigue design of high strength steel tubular joints under conditions of cathodic overprotection.

TABLE 1.1 SCF MATRIX FOR SELECTION OF PARAMETRIC EQUATIONS

Joint Type	Loading	Position	Efthy[1988] ¹	LR[1991] ²
X JOINTS	Balanced Axial	Chord Saddle	Y	N
		Chord Crown	N*	N*
		Brace Saddle	Y	Y
		Brace Crown	Y	Y
	Balanced OPB	Chordside	Y	Y
		Brace Side	Y	Y
Balanced IPB	Chordside	Y	Y	
	Brace Side	Y	Y	
K JOINTS	Balanced Axial	Chordside	N	Y
		Brace Side	N	Y
	Unbalanced OPB	Chordside	Y	Y
		Brace Side	Y	Y
Balanced IPB	Chordside	N	Y	
	Brace Side	YC	Y	
T/Y JOINTS	Axial	Chord Saddle	Y	Y
		Chord Crown	Y	Y
		Brace Saddle	Y	Y
		Brace Crown	YC	N
	OPB	Chordside	Y	Y
		Brace Side	Y	Y
	IPB	Chordside	Y	Y
Brace Side		Y	N	

Key To Table 1.1

- Y Recommend the equation.
- YC Recommend the equation, but note the equation is generally conservative.
- N Not recommend the equation, fails to meet HSE acceptance criteria.
- N* Not recommended because of size of relevant database.

- 1 Efthymiou, 1987
- 2 Smedley & Fisher, 1991

TABLE 1.2. DETAILS OF DESIGN T' CURVE [HSE, 1992]

$$\text{Log}_{10}(N) = \text{Log}_{10}(K_1) - m \cdot \text{Log}_{10}(S_B)$$

Environment	Log₁₀K₁	m	S₀ (N/mm²)
Air	12.476	3	67
	16.127	5	
Seawater (Free Corrosion)	12.00	3	-
Seawater (with CP)	12.175	3	95
	16.127	5	

S₀ represents the stress at which the T' curve changes slope.

Table 1.3 Influence of Loading Mode on the Average Fatigue Endurance (from HSE 1992)

Loading Mode	Number of Joints	Average Value of <u>Fatigue Endurance</u> Predicted Fatigue Life
AXIAL	21	0.80
I.P.B	9	1.47
O.P.B	29	1.31

Table 1.4 Comparison of Environmental Reduction Factors for Welded Plate (from King *et al* 1992)

STEEL TYPE	YIELD STRENGTH MPa	ENVIRONMENT	ENVIRONMENTAL REDUCTION FACTOR	
			N<10 ⁶	N>10 ⁶
BS4360:50D	375	CP 850 mV	2.46	1.20
		CP 1100 mV	2.70	1.40
		FC	3.20	2.70
SAR60	470	CP 850 mV	2.00	1.00
		CP 1100 mV	2.00	3.50
		FC	3.00	4.00
RTQ501	490	CP 850 mV	2.25	1.20
		CP 1100 mV	4.00	5.50
		FC	3.00	4.50
A514	760.00	FC	3.00	7.00

**TABLE 1.5: PROPERTIES OF STEELS REFERRED TO IN CHAPTER 1
(VALUES ARE MINIMUM SPECIFIED WHERE AVAILABLE).**

Steel	σ_{YS} (MPa)	σ_{UTS} (MPa)	Elong %	Charpy (J)
BS4360.50D BS4360.355D	345	490	18	41J@ -40°C
MACS	431	556	25	263J@ -60°C
BS7191.450F	450	550	19	41J@ -40°C
X65	458	570	32	
SAR 60	470	594	77	189J@ -20°C
RQT 501	490			
X70	527	672	35	
Weldox 700	700	780	14.5 RA	40J@ -40°C
A517Q	700	805	16% RA	40J@ -40°C
A514	760			
HT80	784	843	12	
HY130	993	1034	22	

Figure 1.1 A Simplified View of a "Jacket" Construction, Fixed Rig.

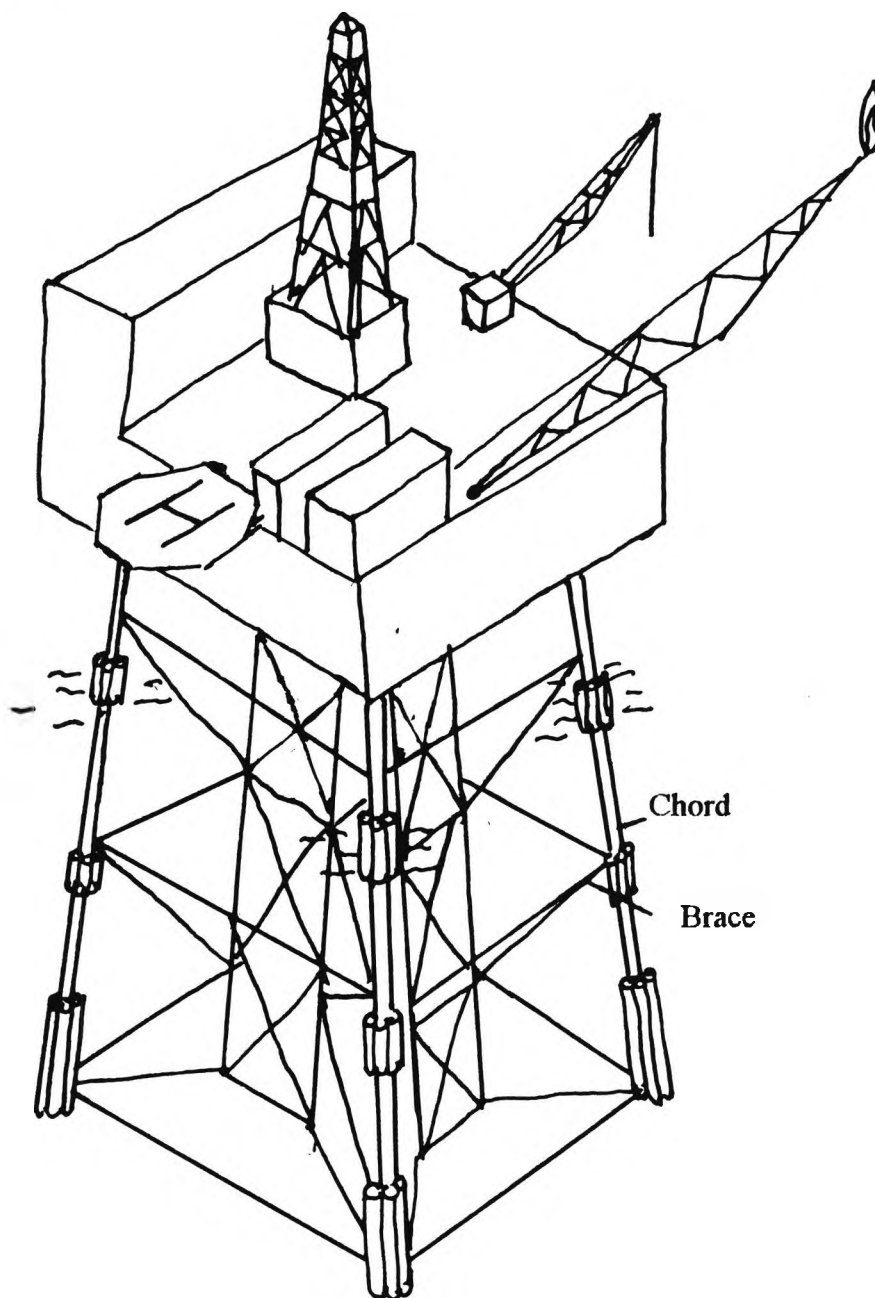


Figure 1.2 A Simplified View of a "Jack Up" Construction, Mobile Rig.

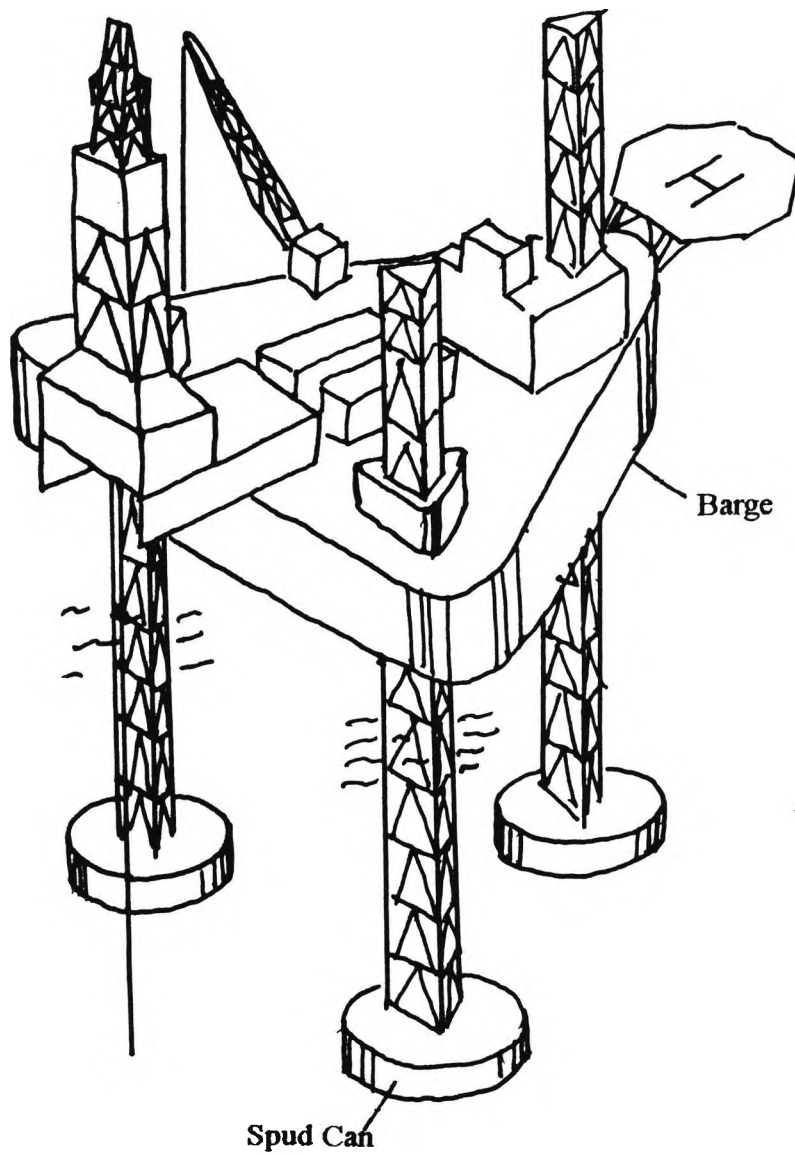


Figure 1.3 Definition of stress distributions

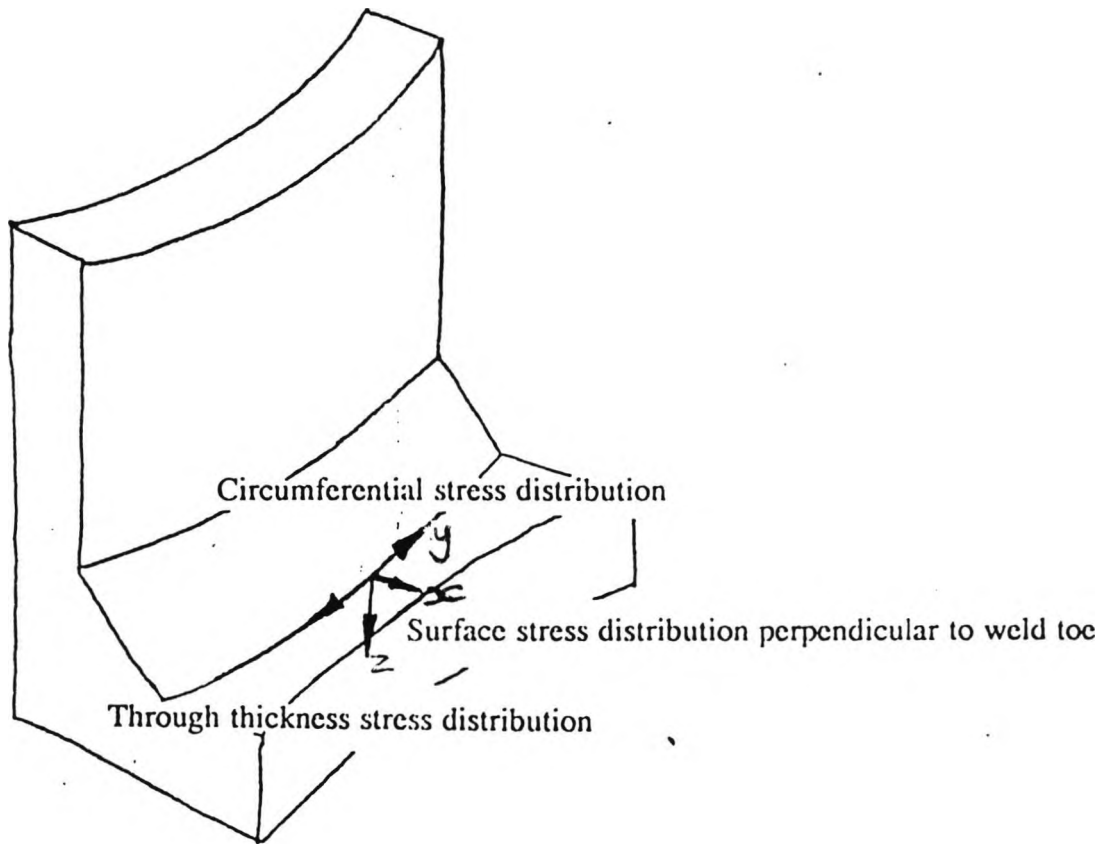


Figure 1.4 Modes of loading

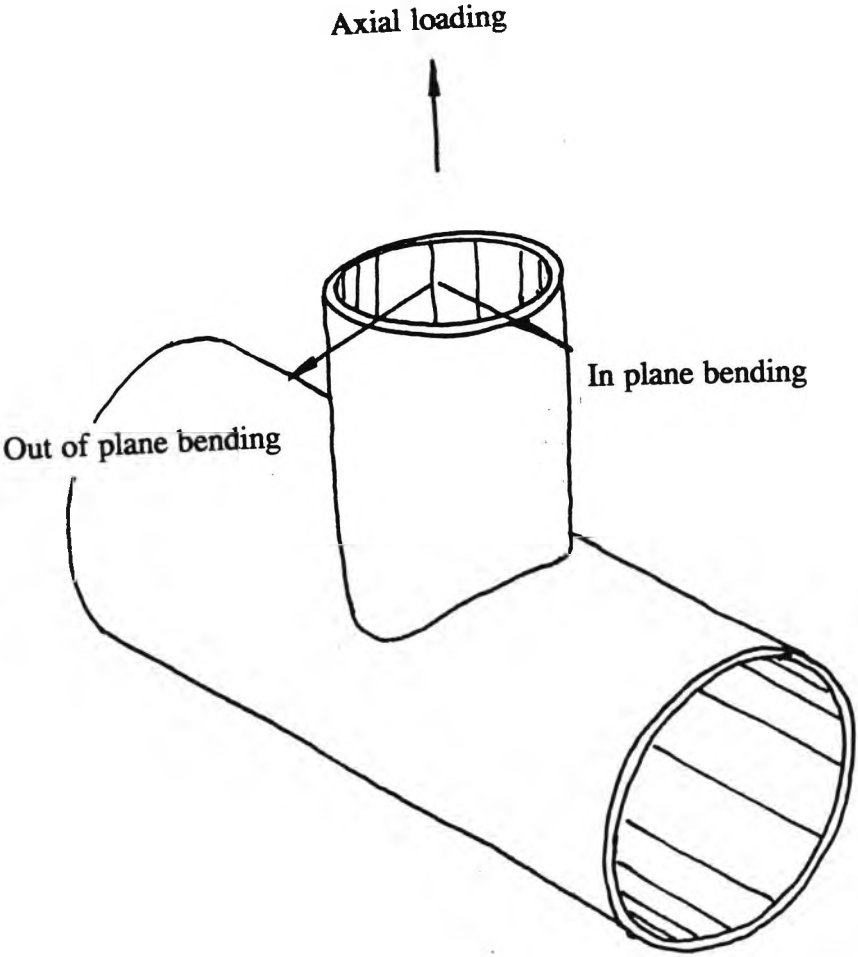
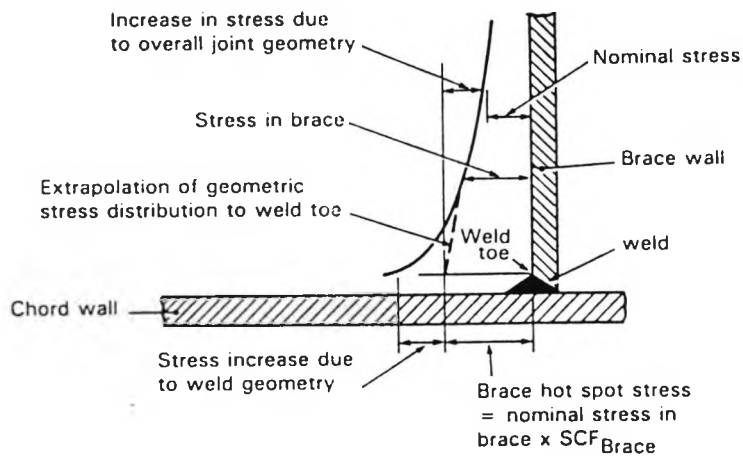
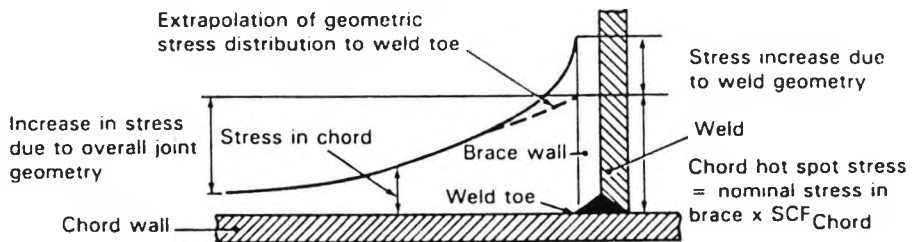


Figure 1.5: Definition of Hot Spot Stress [from UKORSP 1, 1988]



Stress distribution in brace



Stress distribution in chord

Figure 1.6: Location of Strain Gauges for Linear Extrapolation to Weld Toe to Determine Stress Concentration Factor [from UKORSP 1, 1988].

$x = 0.2 \sqrt{rt}$ but not less than 4 mm

Range of linear stress distribution extends between A and B

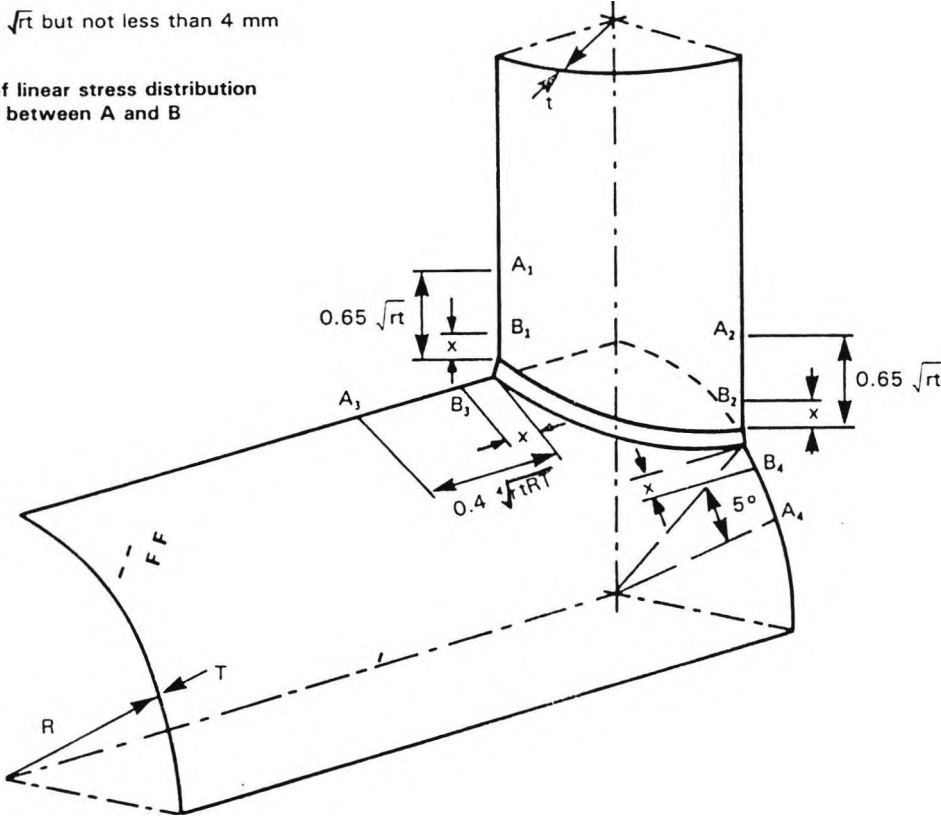
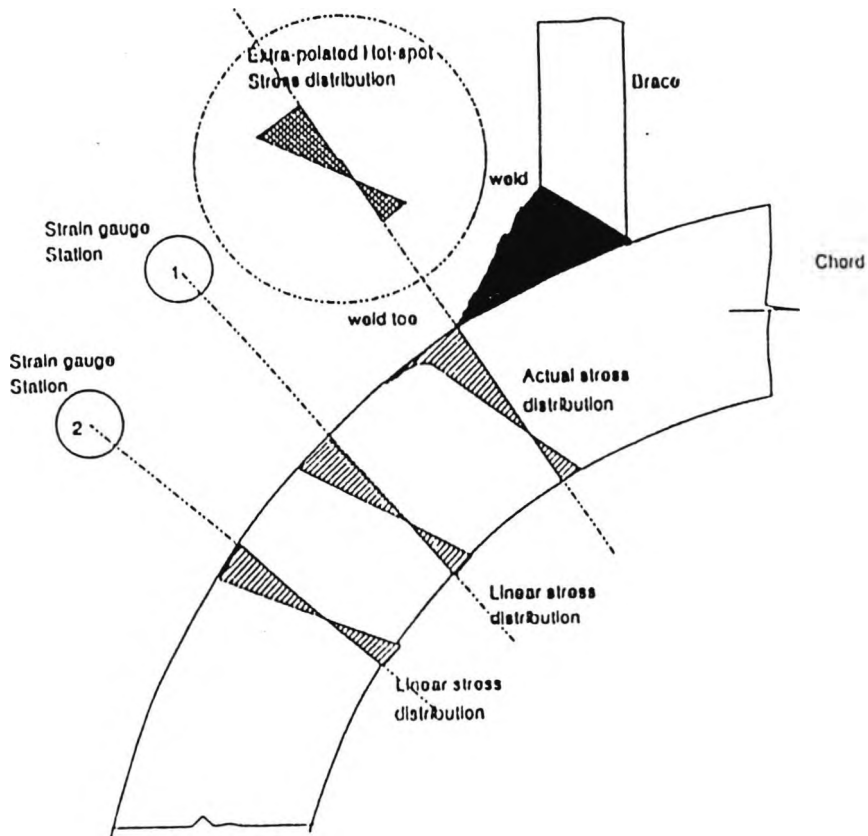


Figure 1.7 The "Hot Spot" stress and bending to membrane ratio



Through Stress Distribution = Tensile Stress + Bending Stress

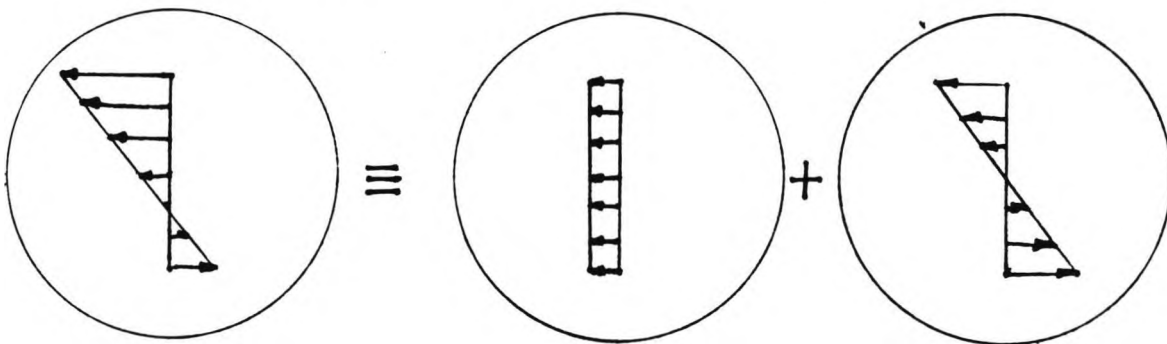


Figure 1.8 Schematic representation of the SN curve

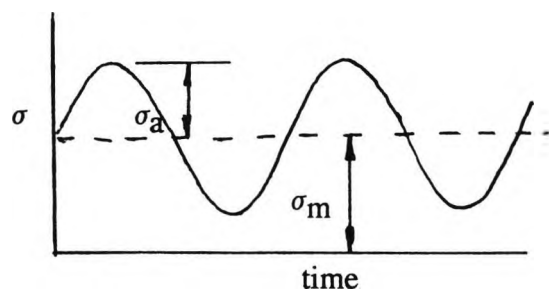
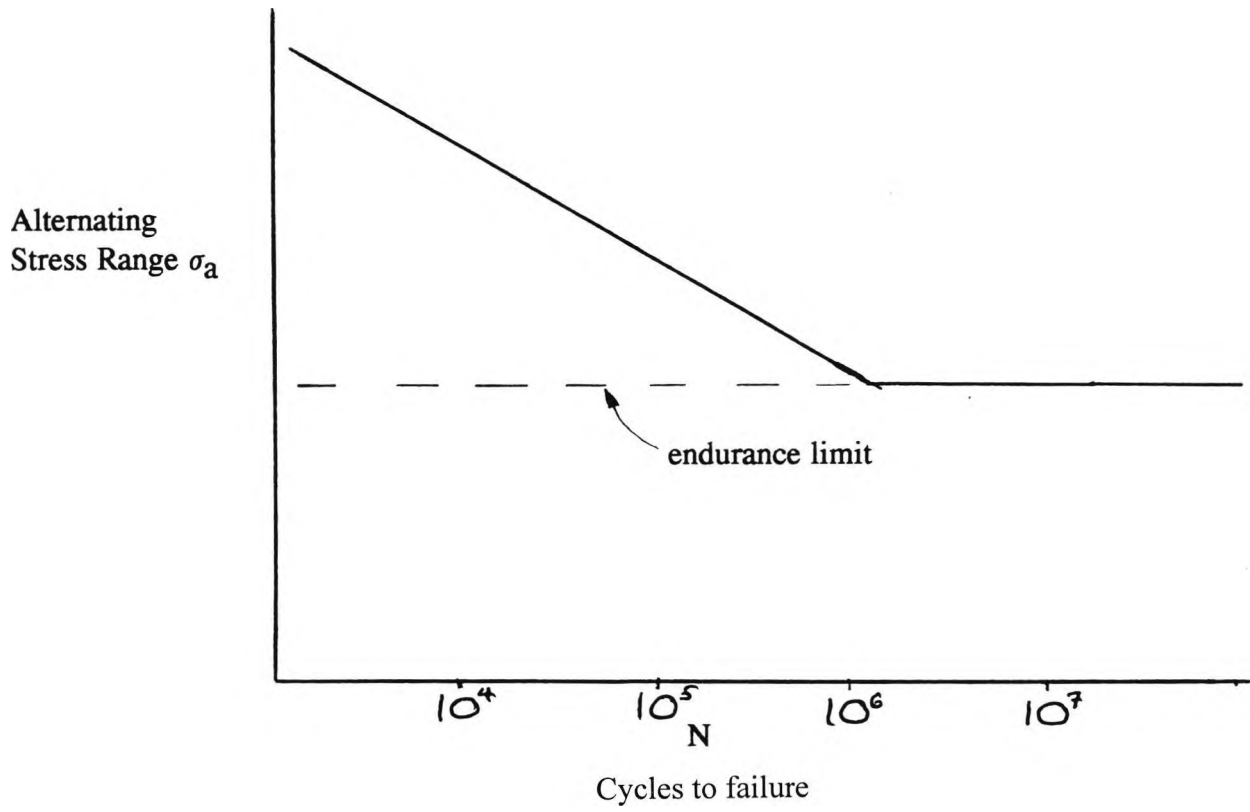


Figure 1.9: T' Curve Adapted to 20mm Thickness

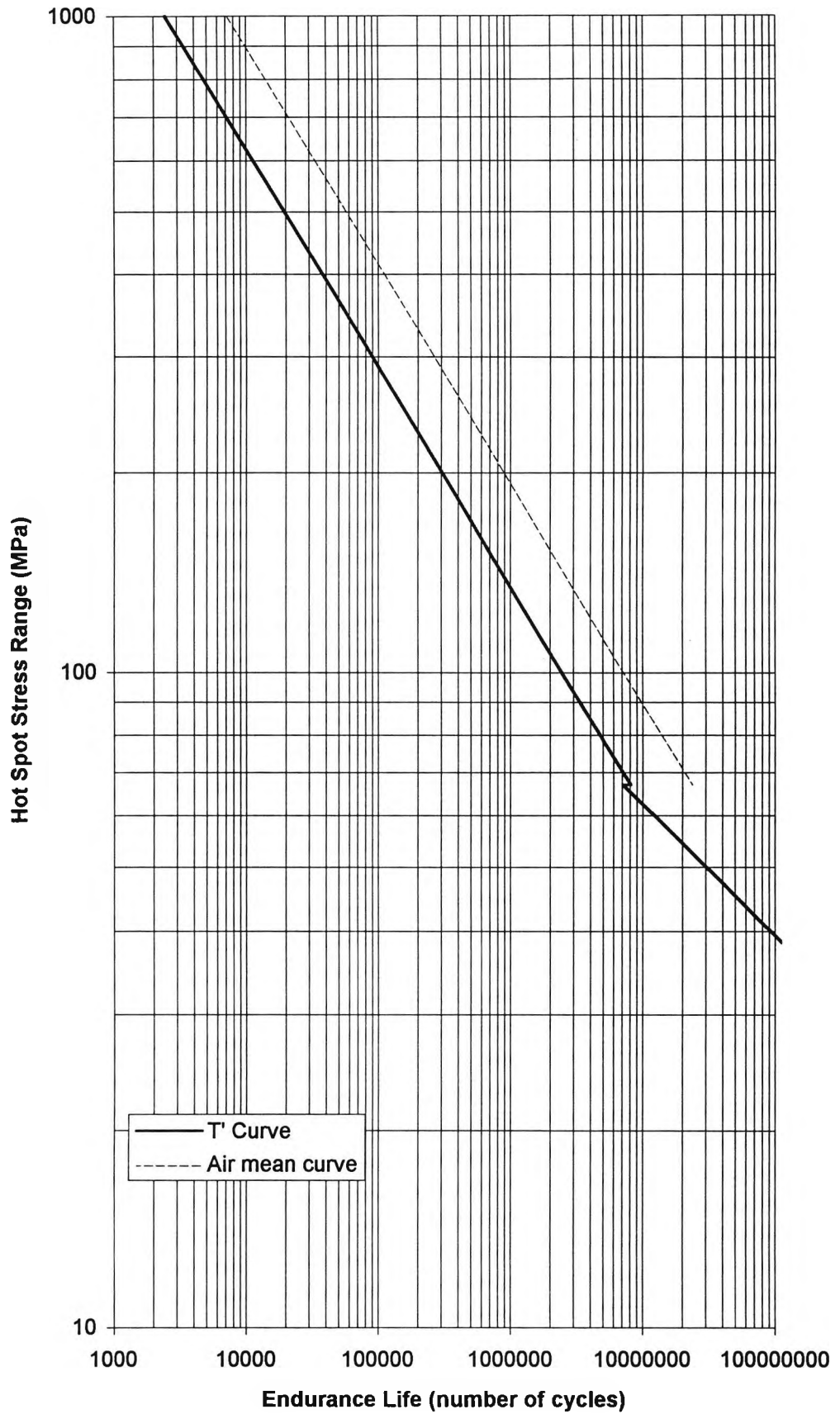
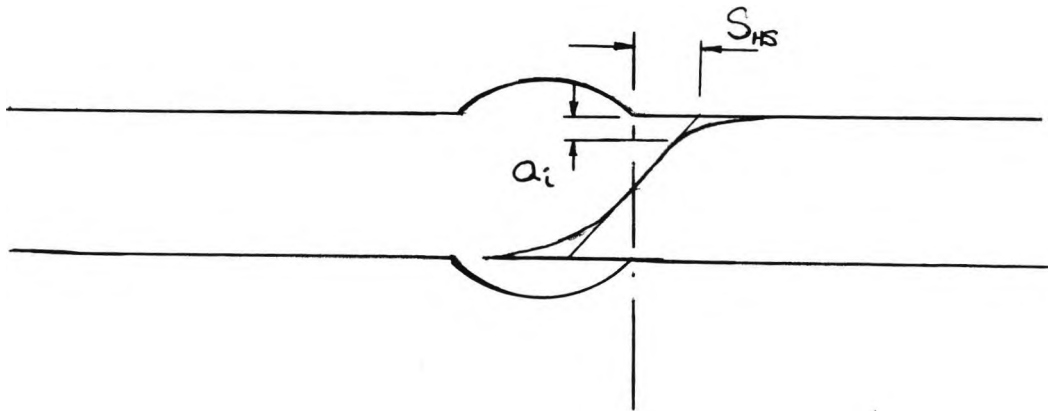
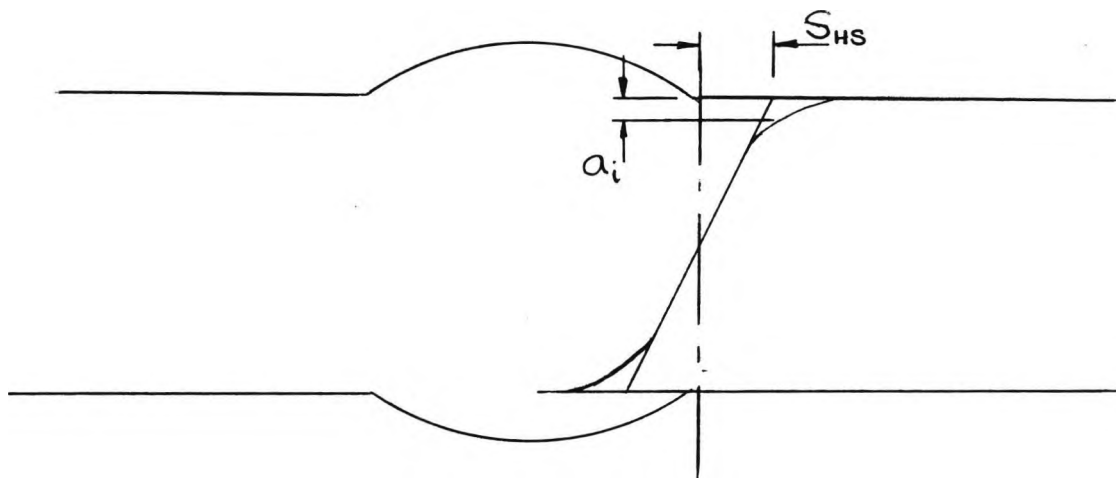


Figure 1.10 The effect of plate thickness on crack initiation

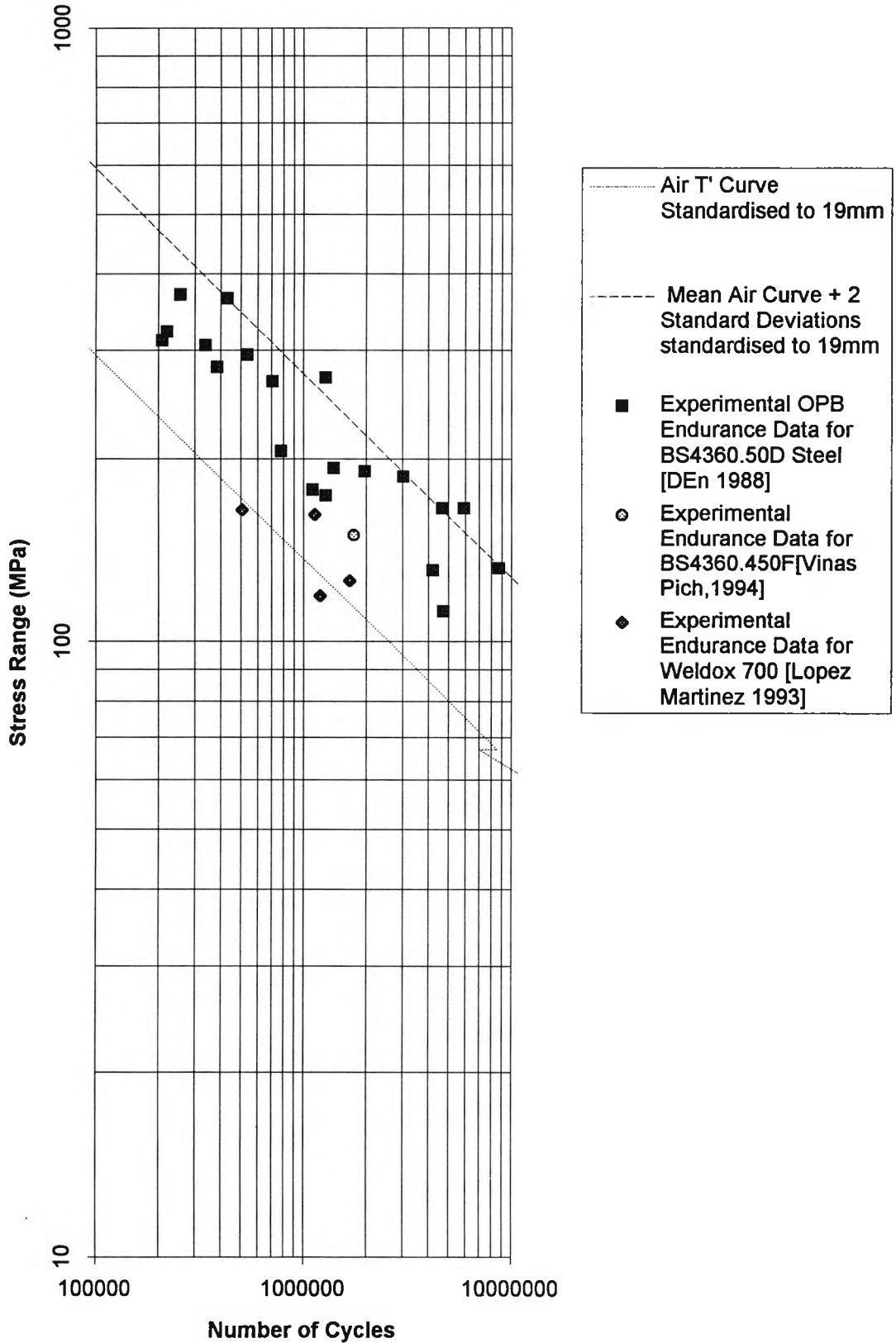


a) Through thickness stress distribution in a thin plate



b) Through thickness stress distribution in a thick plate

Figure 1.11: Total life for air tested tubular joints compared to T' Curve



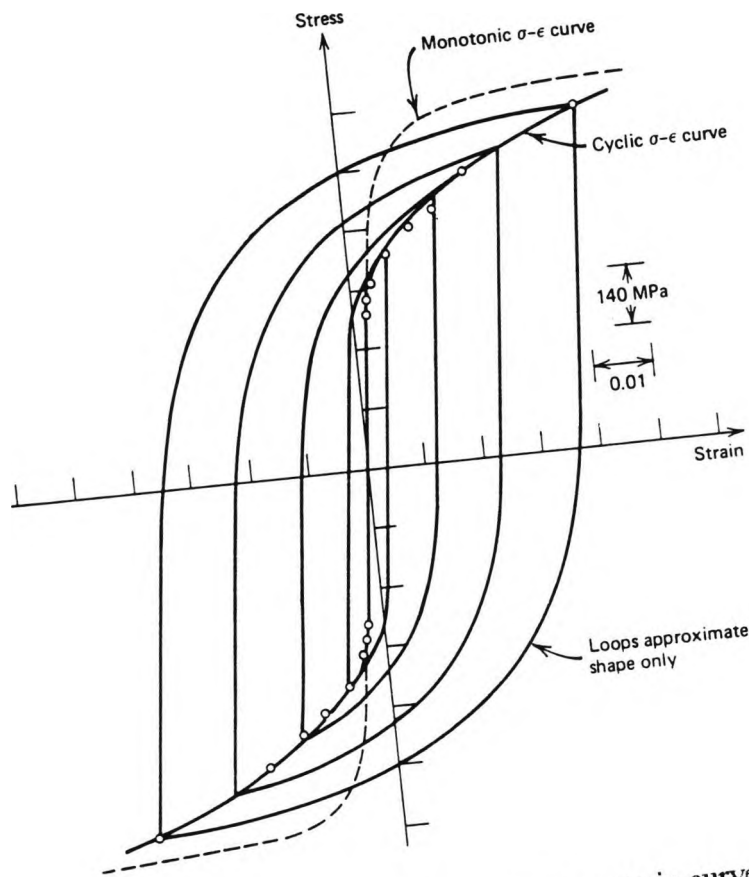


Figure 1.12a. Typical stable cyclic stress strain curve.

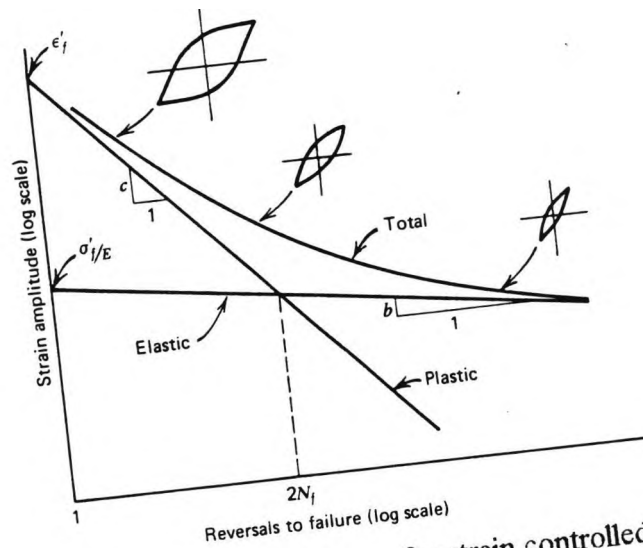


Figure 1.12b. Coffin Manson curve for strain controlled fatigue:

$$\frac{\Delta \epsilon_T}{2} = \frac{\sigma_f}{E} (2N_f)^b + \epsilon_f' (2N_f)^c$$

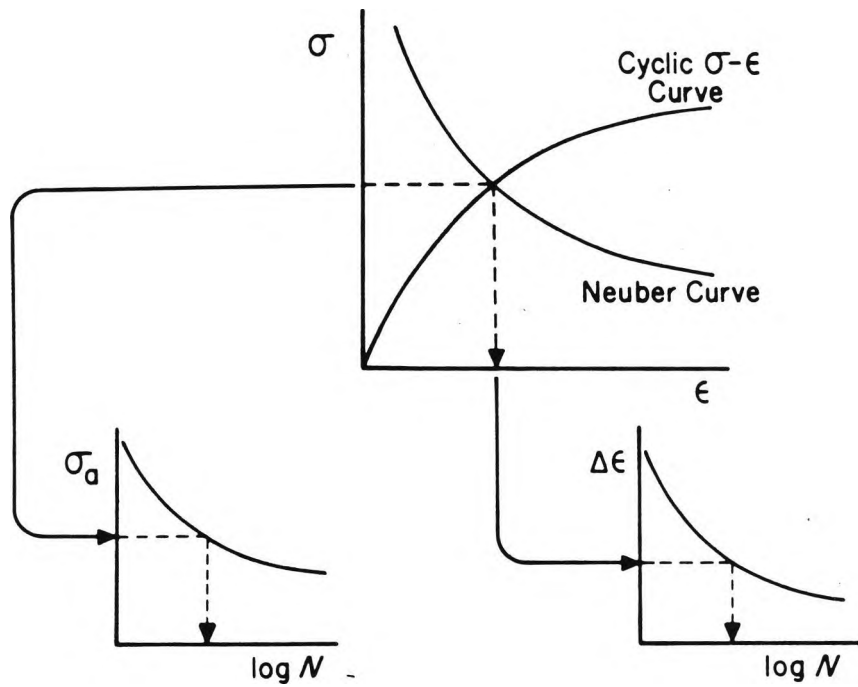


Figure 1.12c. Derivation of the cyclic strain life from simultaneous solution of the Neuber and cyclic stress strain curves. The cyclic life is determined from the Coffin Manson curve.

Figure 1.13 Fracture failure modes

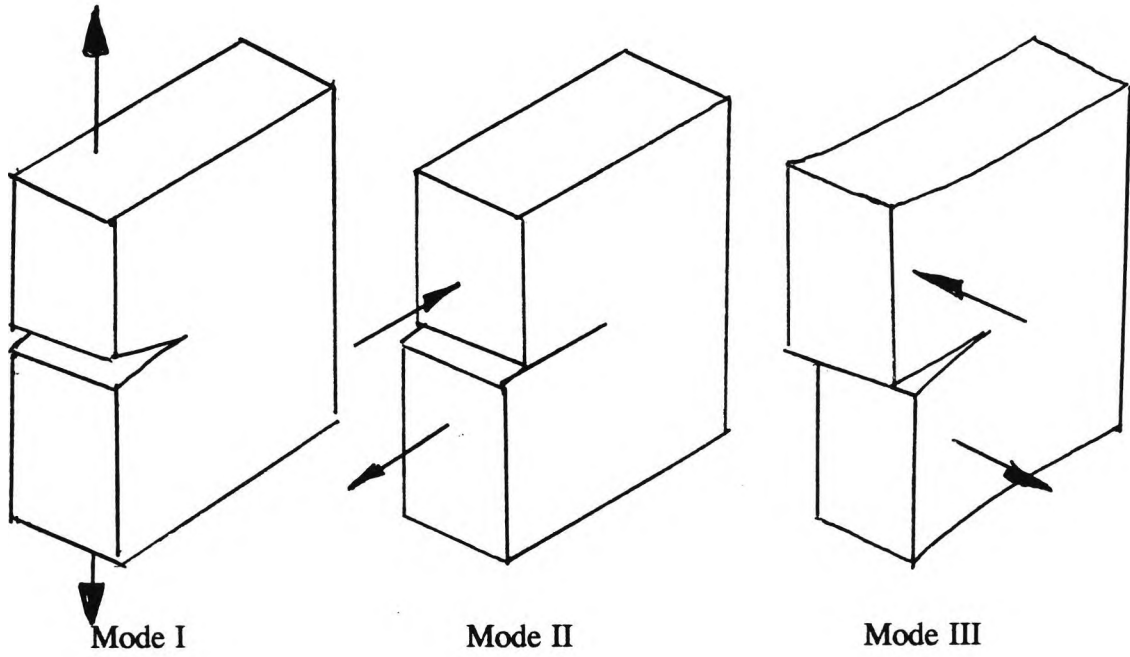


Figure 1.14 Schematic of crack growth as a function of SIF range

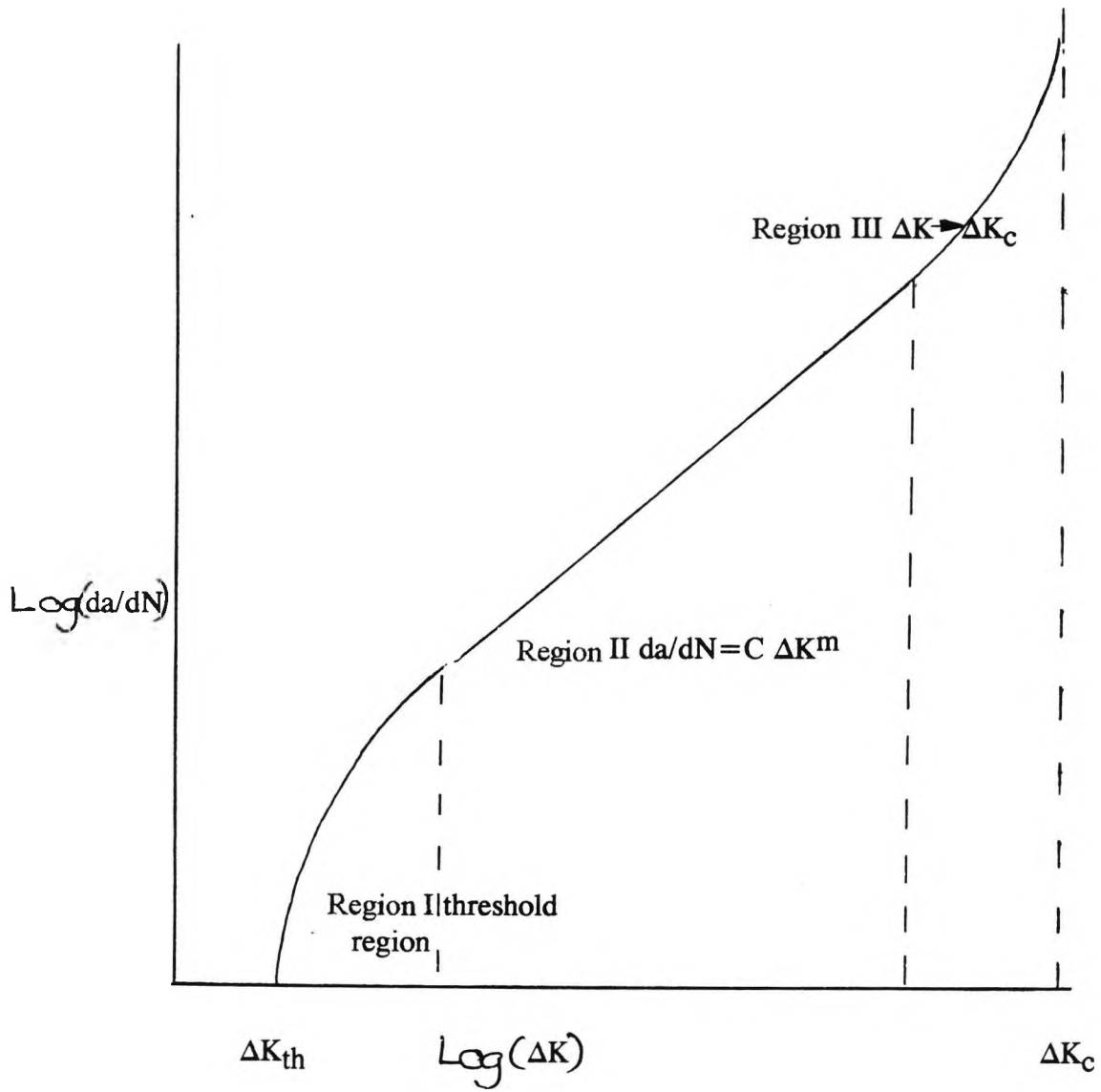


Figure 1.15 Typical fatigue crack growth rates in air for high strength steels

[from King et al, 1993]

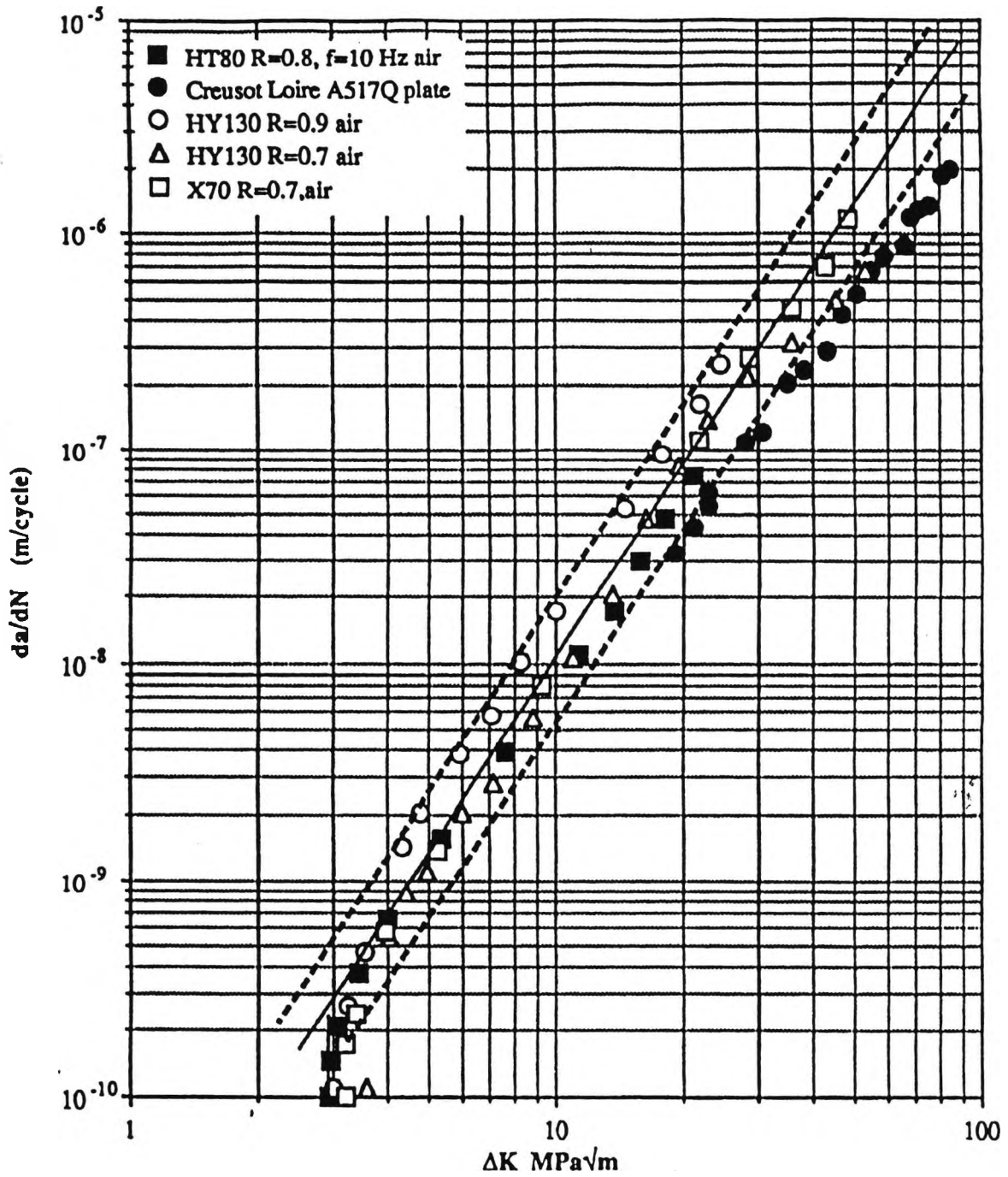
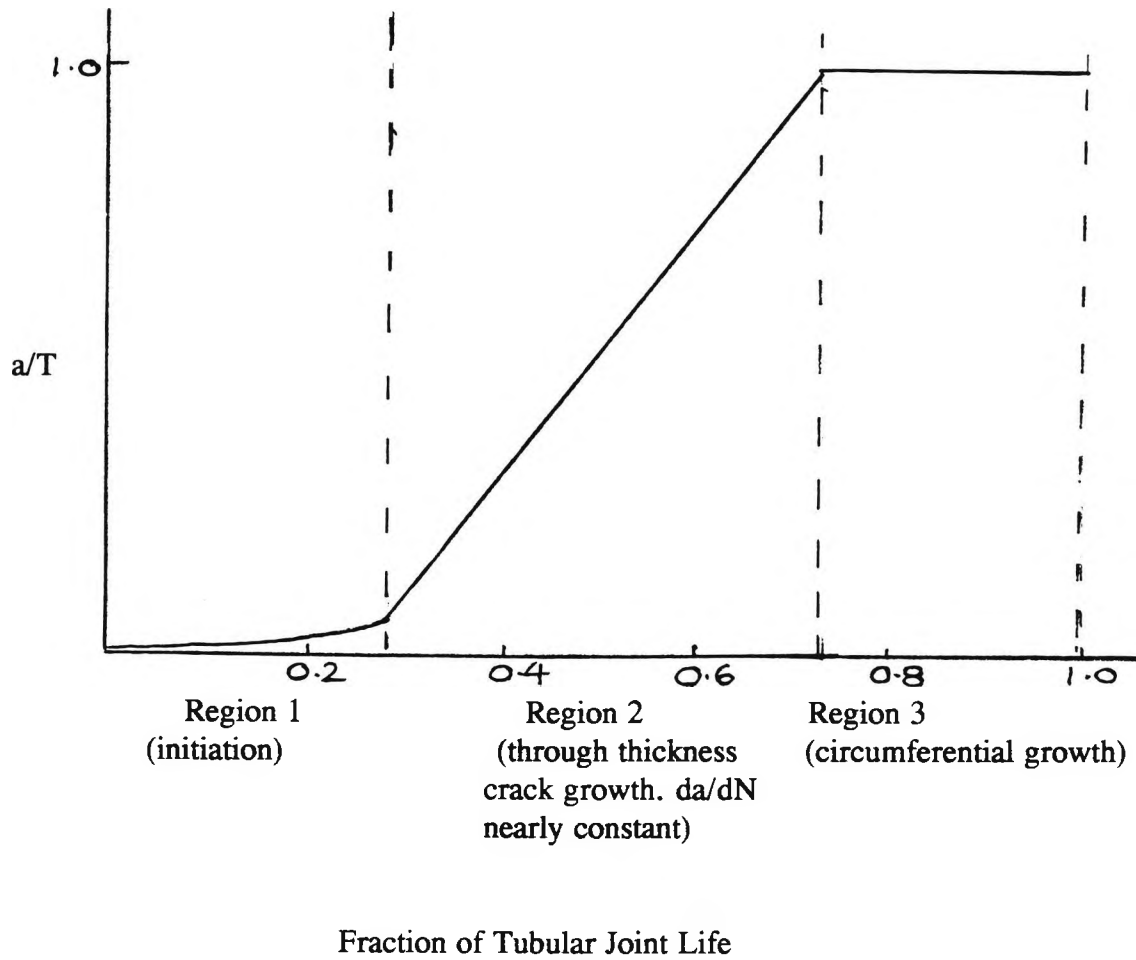


Figure 1.16 Schematic of typical fatigue crack growth in a tubular joint



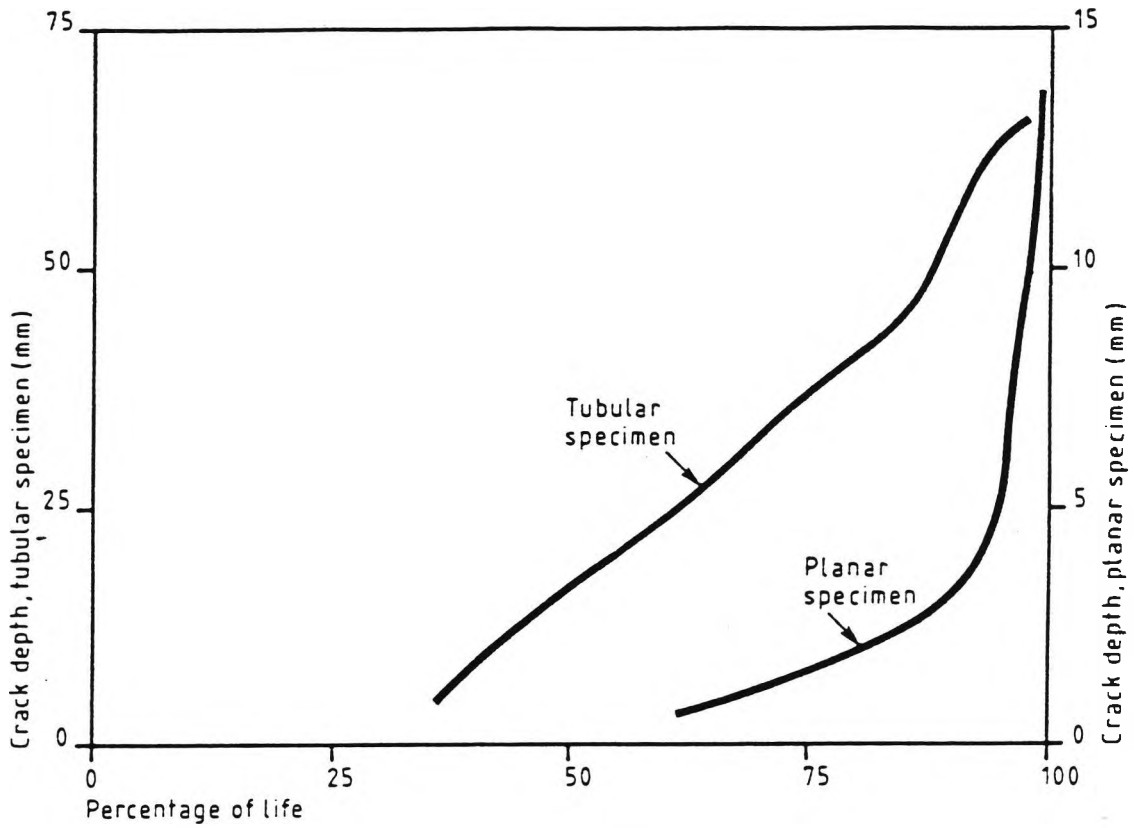


Figure 1.17 Curves of crack depth against percentage of fatigue life for planar and tubular welded specimens [from MTD, 1990]

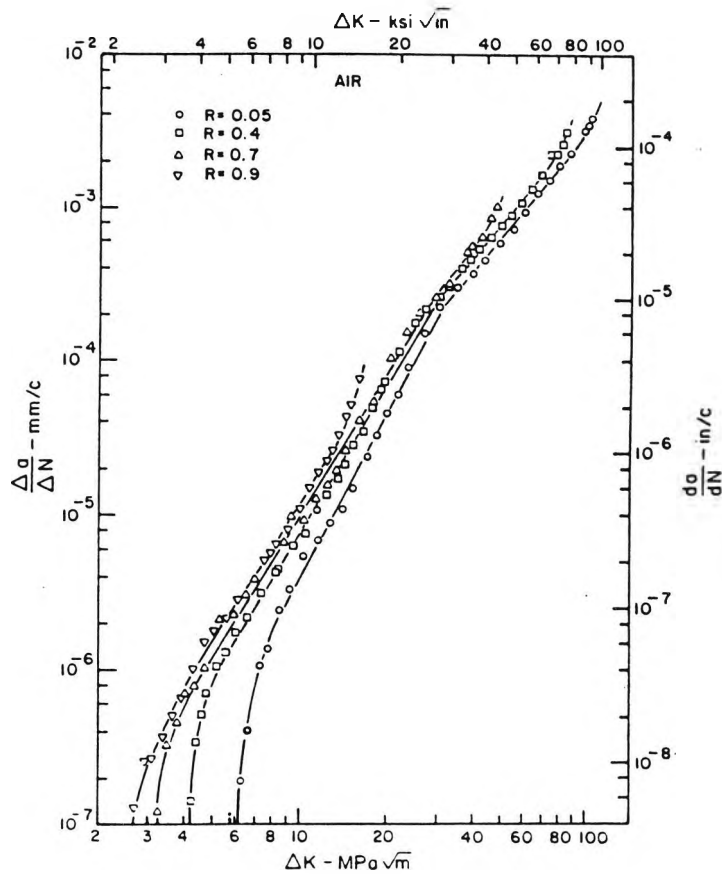


Figure 1.18 Fatigue crack growth at for X70 steels at four stress ratios
 [Vosikovsky, 1979]

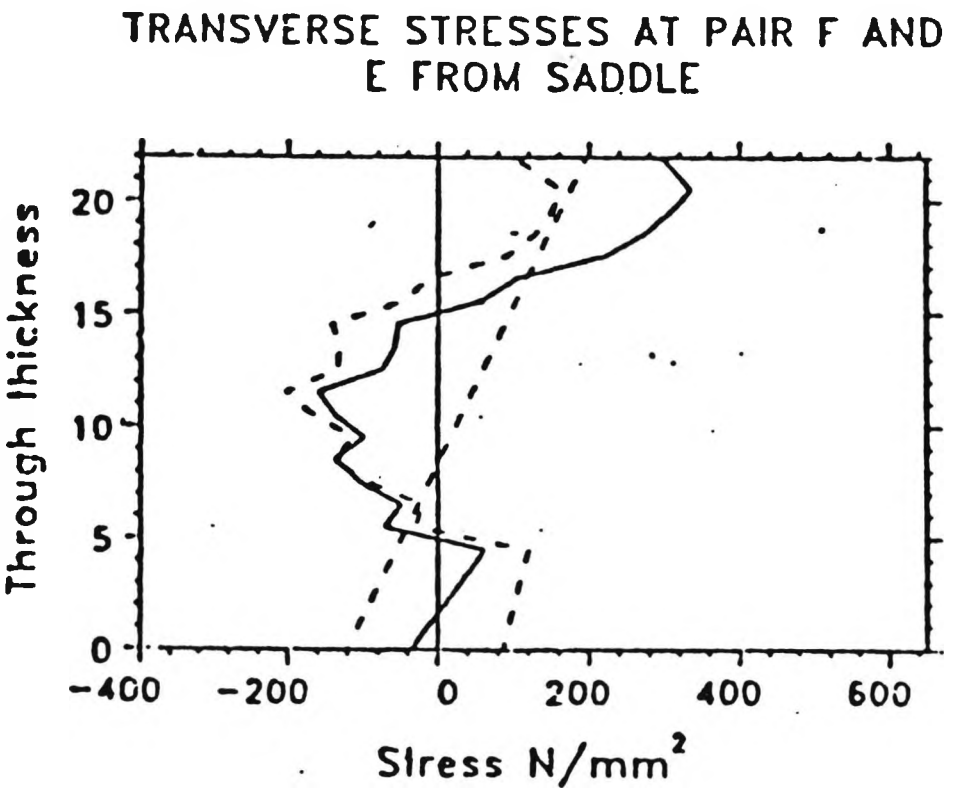


Figure 1.19 Typical transverse residual stress distributions for a tubular joint
 [Porter Goff, 1987]

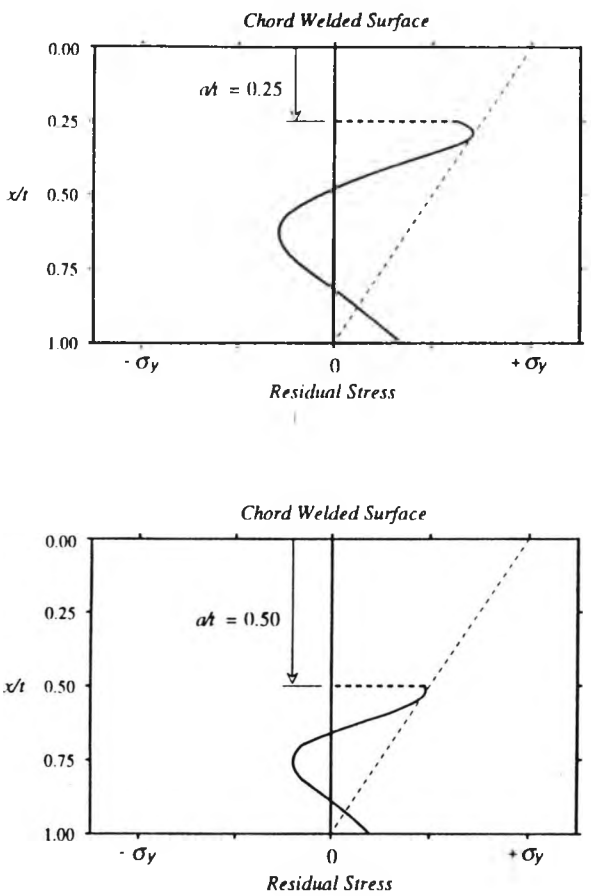


Figure 1.20 Residual stress redistribution model proposed by Monahan [1994]

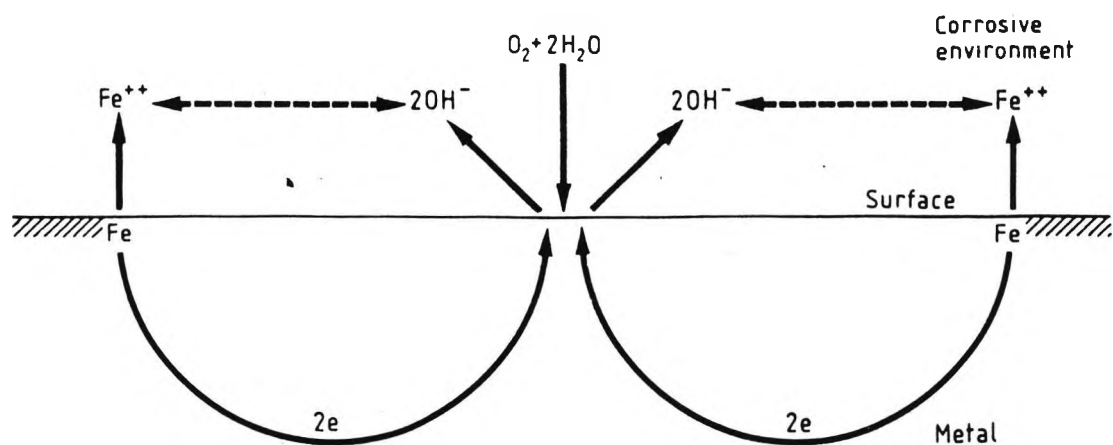


Figure 1.21 Schematic representation of aqueous corrosion [MTD, 1990]

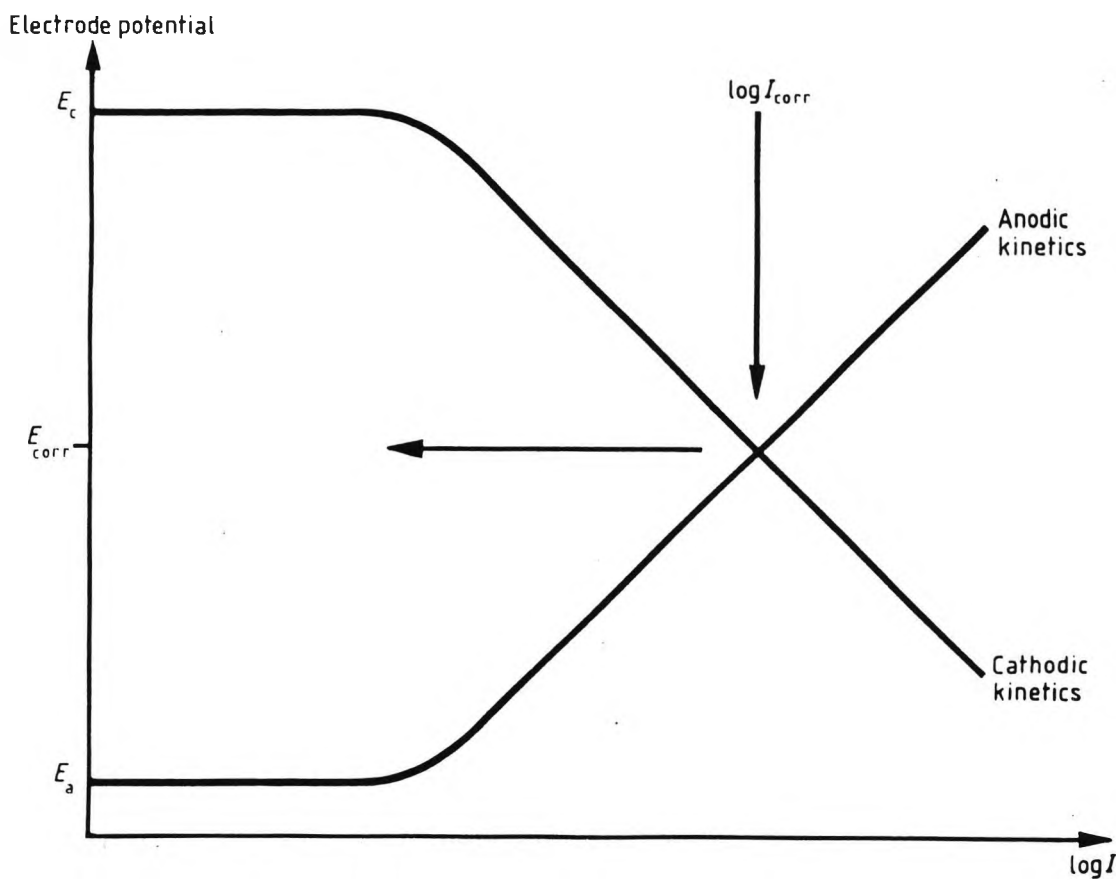


Figure 1.22 Polarisation diagram schematically representing the electrochemistry of aqueous corrosion [MTD, 1990]

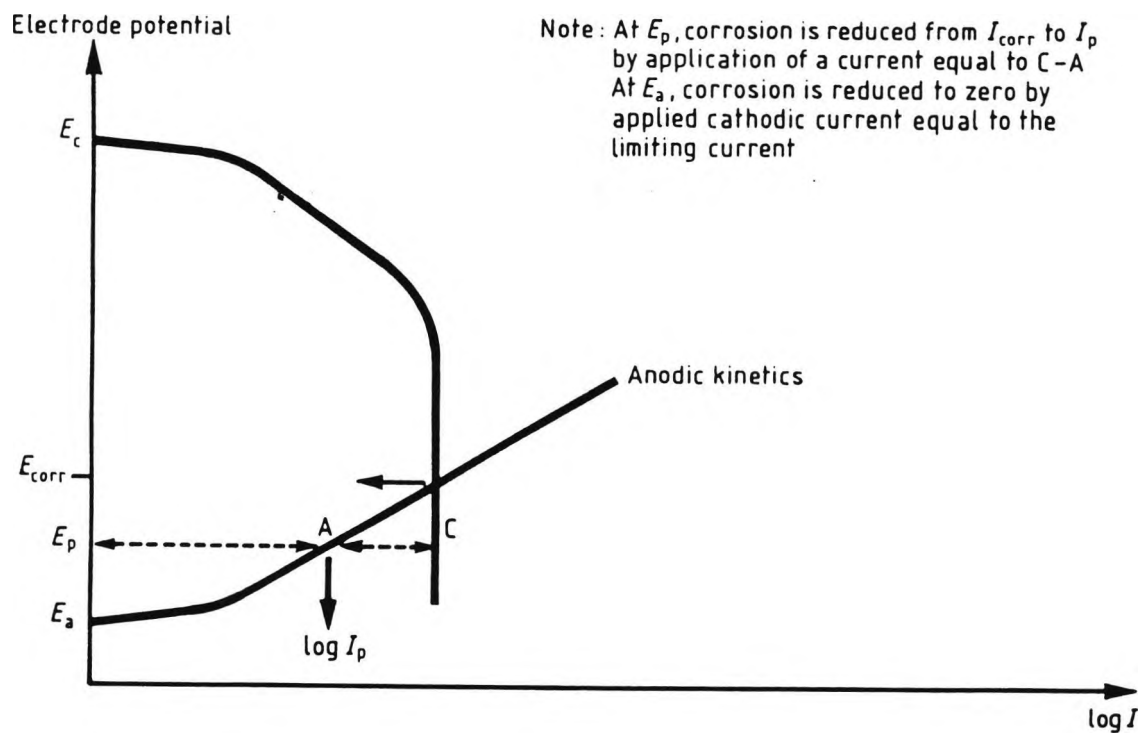


Figure 1.23 Schematic diagram showing how corrosion can be reduced or stopped by cathodic protection [MTD, 1990]

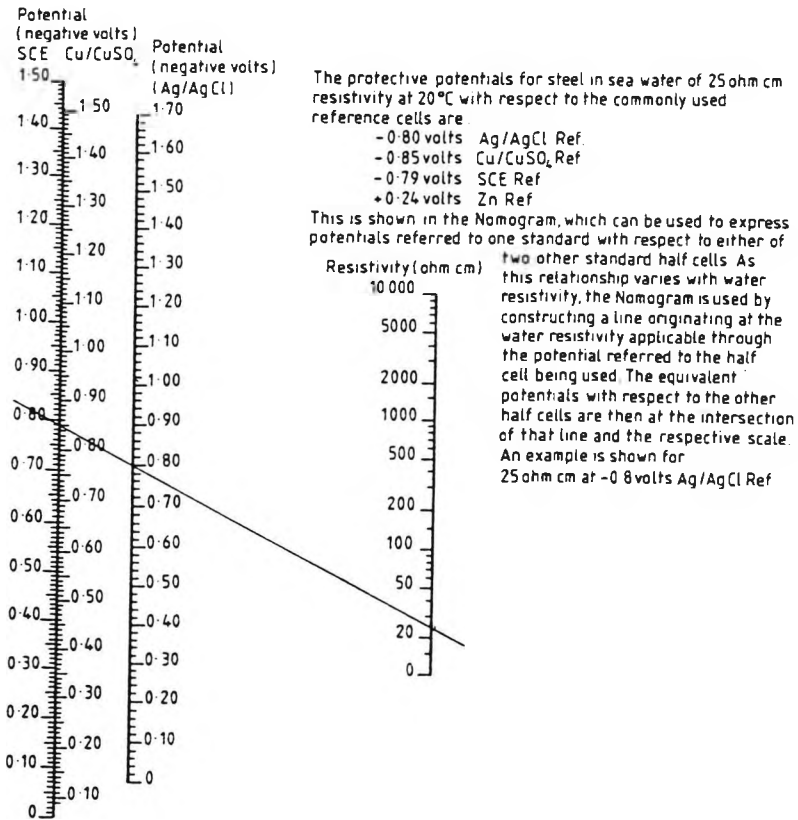


Figure 1.24 Nomogram for the cross referencing of potential readings [MTD, 1990]

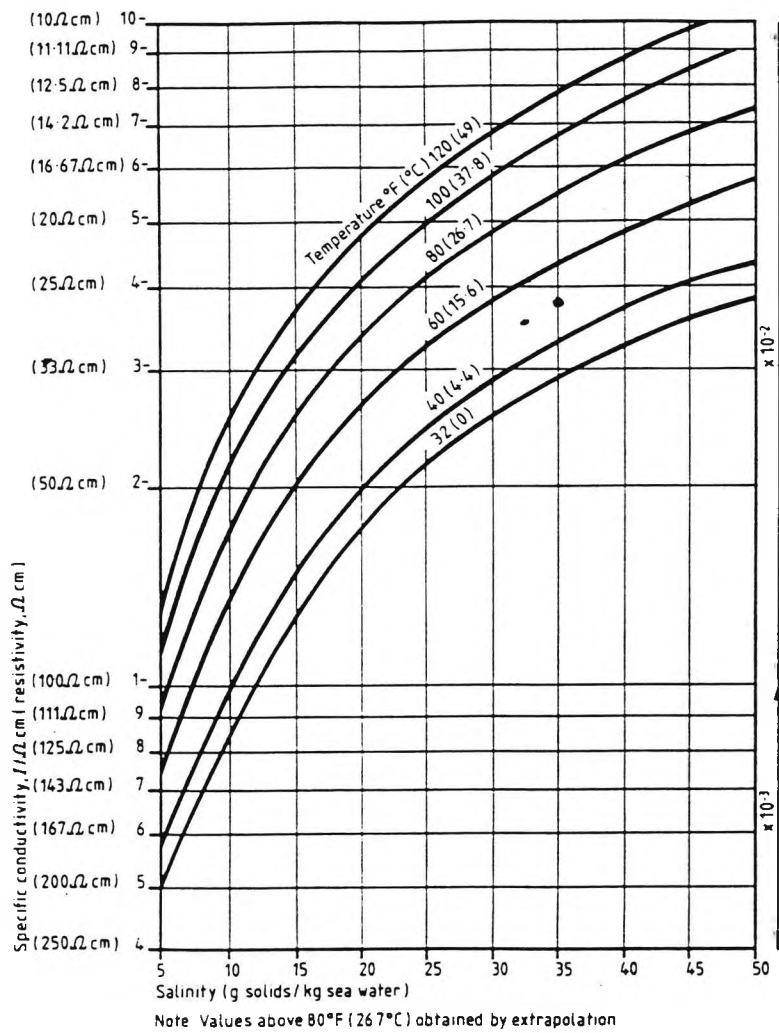


Figure 1.25 Specific conductivity of seawater [MTD, 1990]

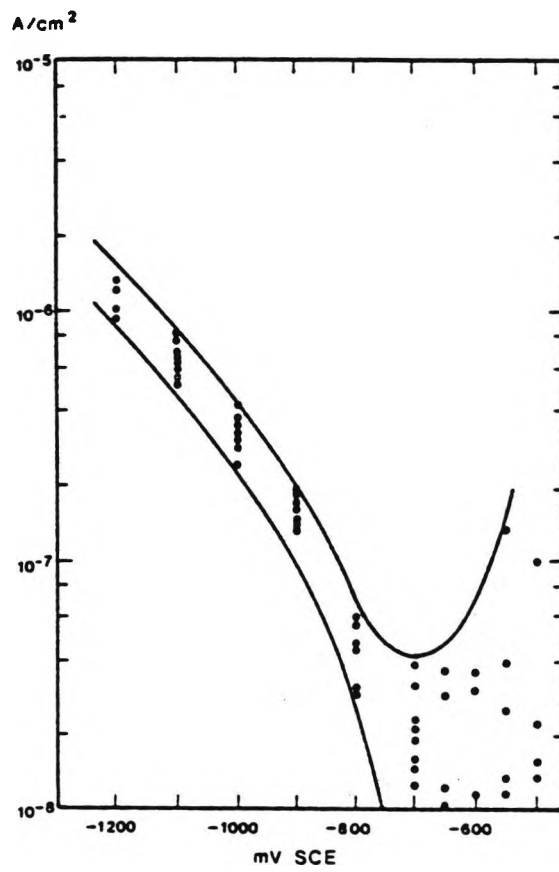


Figure 1.26 Hydrogen permeation current as a function of cathodic potential [Nielsen & Maahn, 1987]

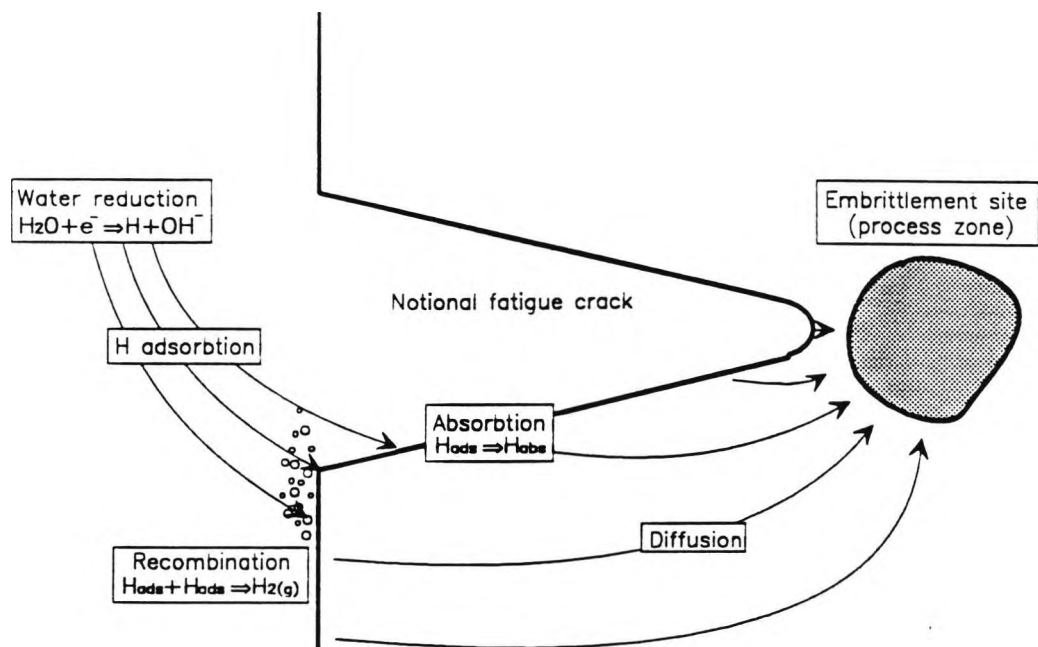


Figure 1.27 Corrosion fatigue by hydrogen embrittlement

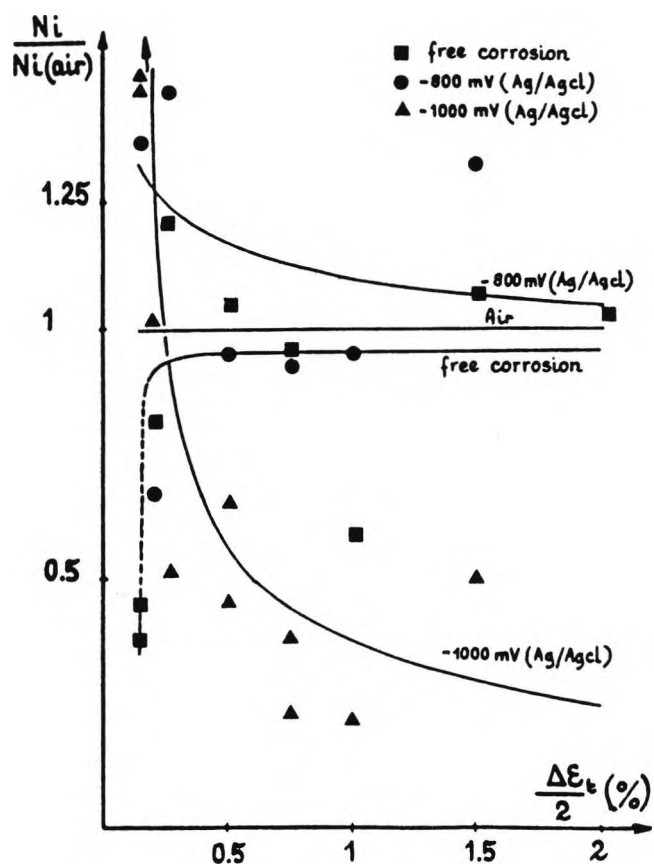


Figure 1.28 The effect of cathodic potential on the initiation life of smooth specimens [Bignonnet, 1987]

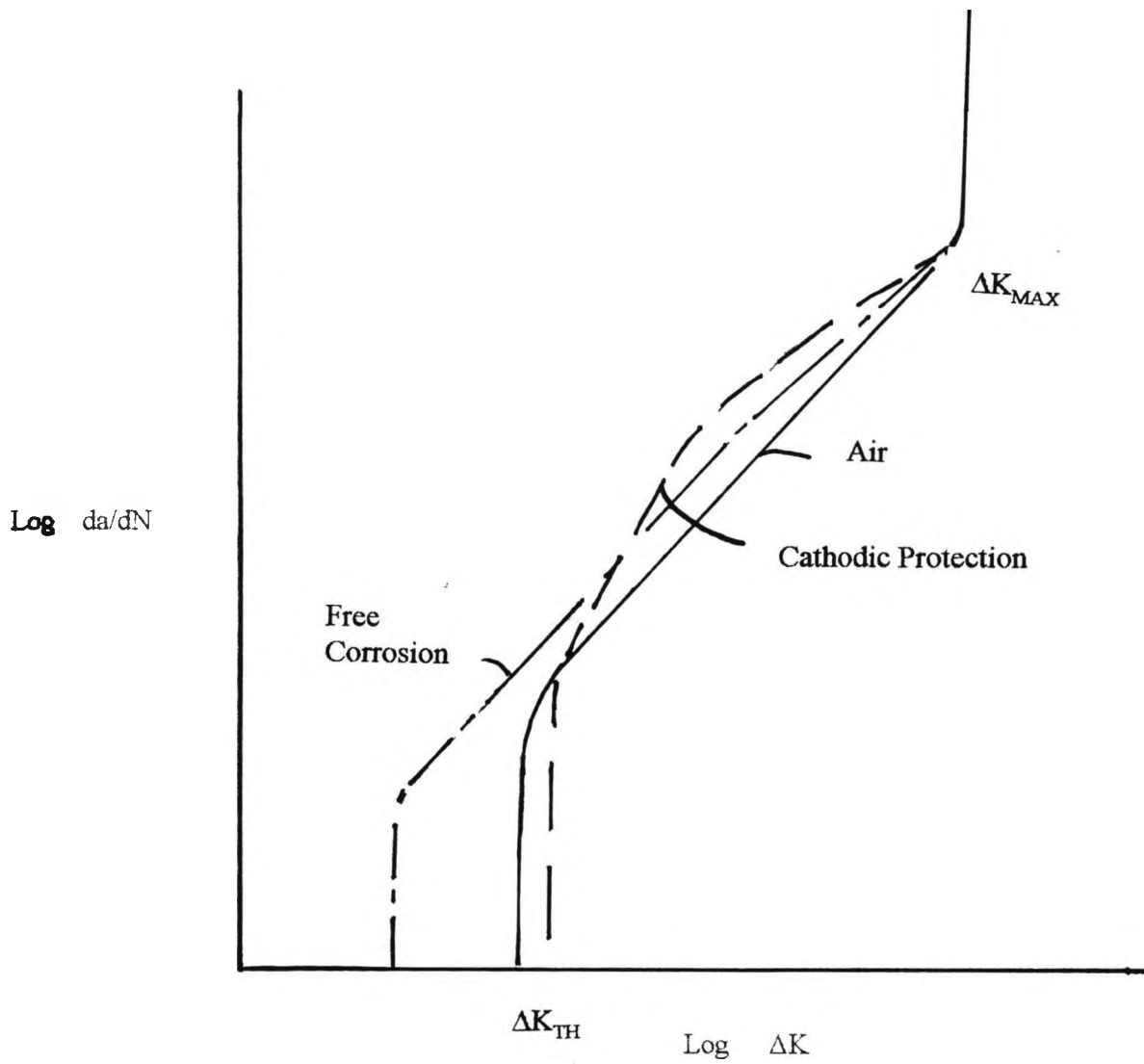
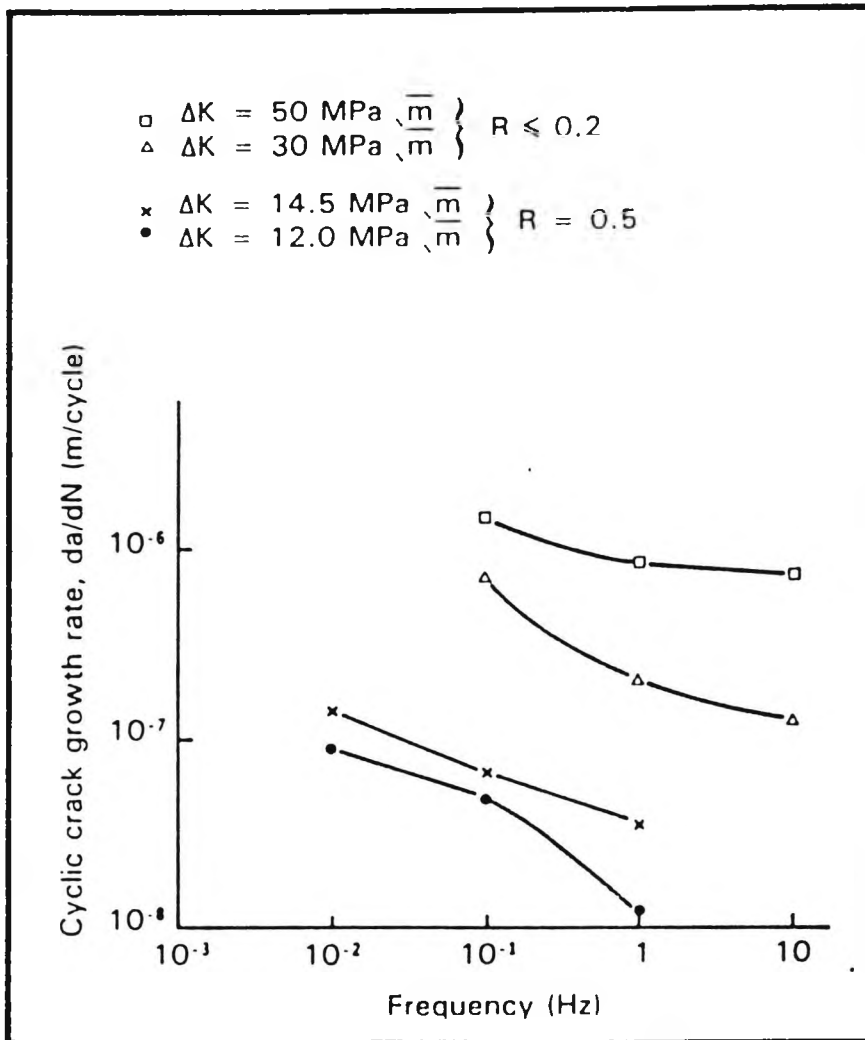


Figure 1.29 Schematic diagram of the effect of cathodic protection on fatigue crack propagation.

Figure 1.30 Effect of frequency on corrosion fatigue crack propagation under freely corroding conditions in seawater [Thorpe *et al*, 1983]



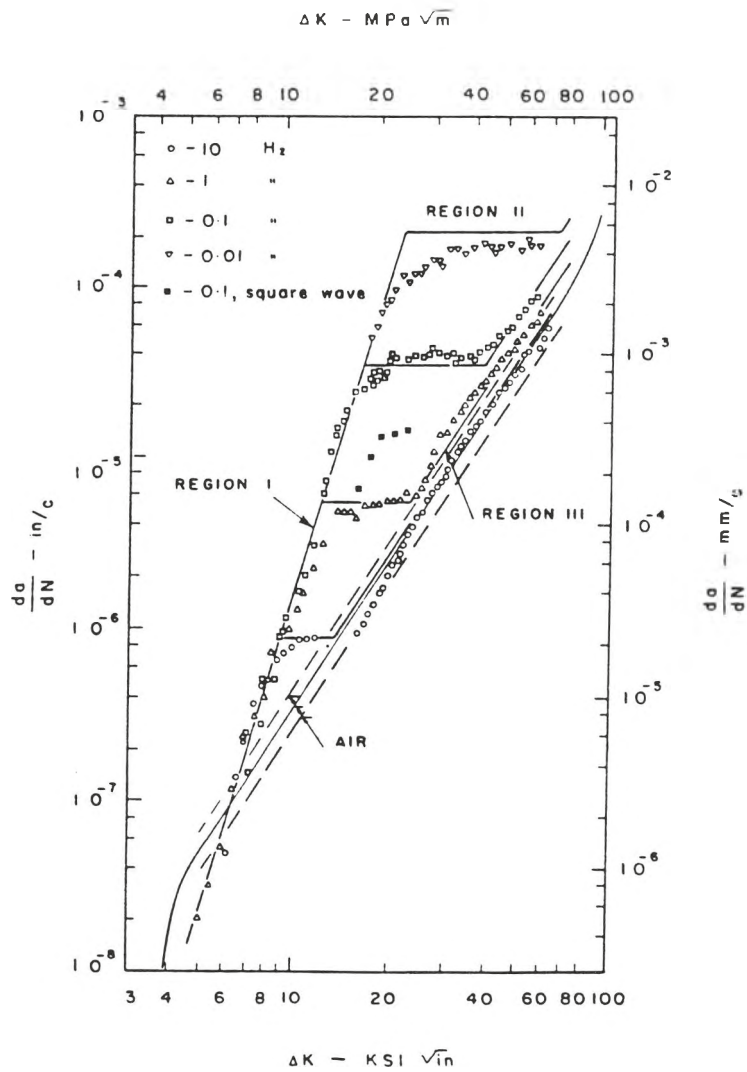


Figure 1.31 Fatigue crack growth in X65, tested in 3.5% NaCl solution at the Zinc potential, $R=0.2$ and four frequencies [Vosikovskiy, 1980]

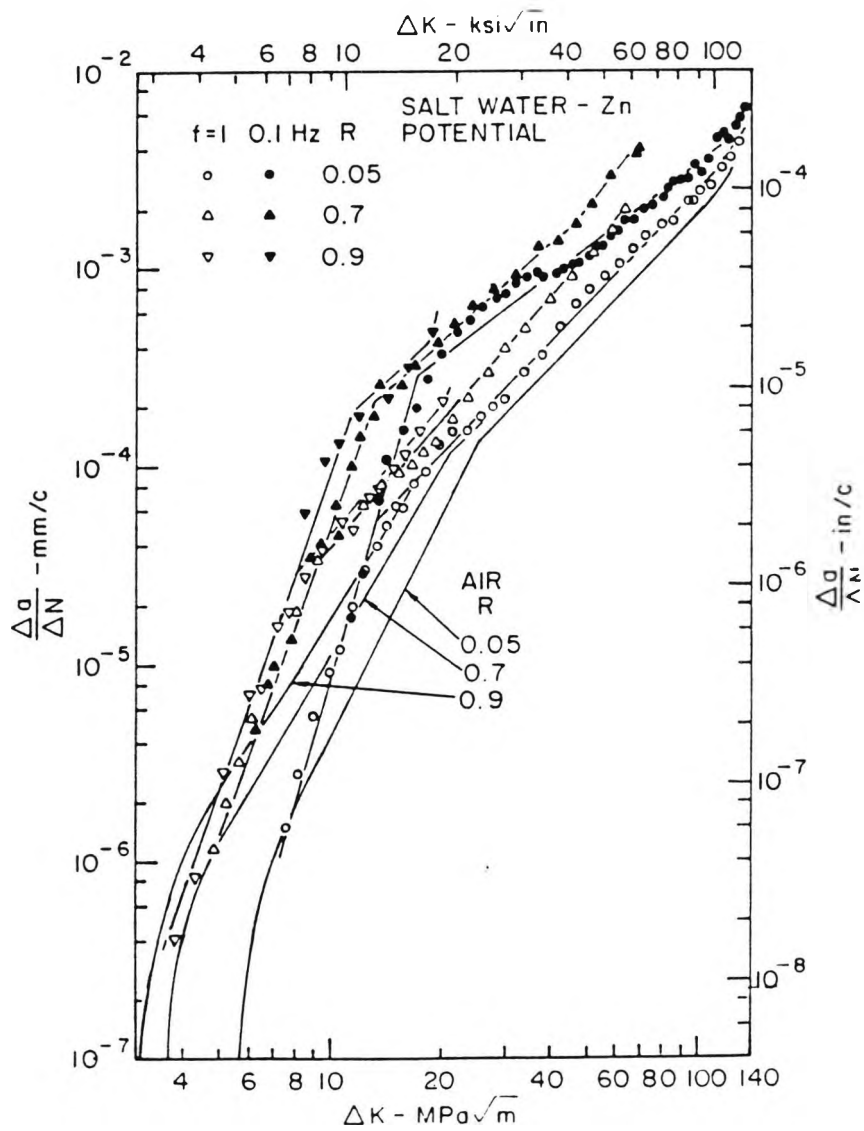
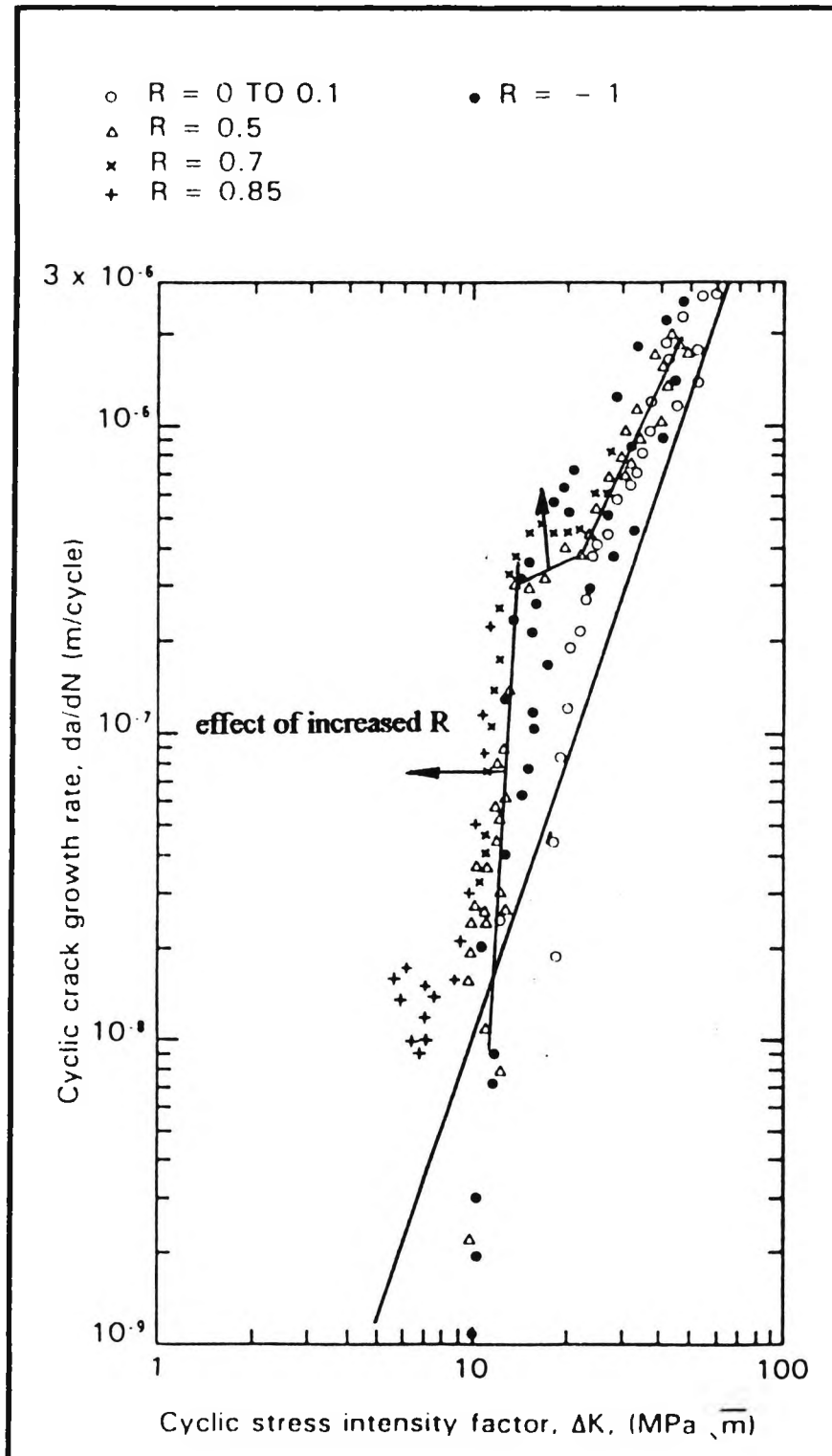


Figure 1.32 Influence of applied load ratio on the corrosion fatigue crack growth rate for HY130 tested in 3.5% NaCl at the Zinc potential [Vosikovsky, 1980]

Figure 1.33 Crack growth data for specimens containing through thickness cracks tested in seawater at -1.1V at R=-1 to 0.85 [DEn, 1988]



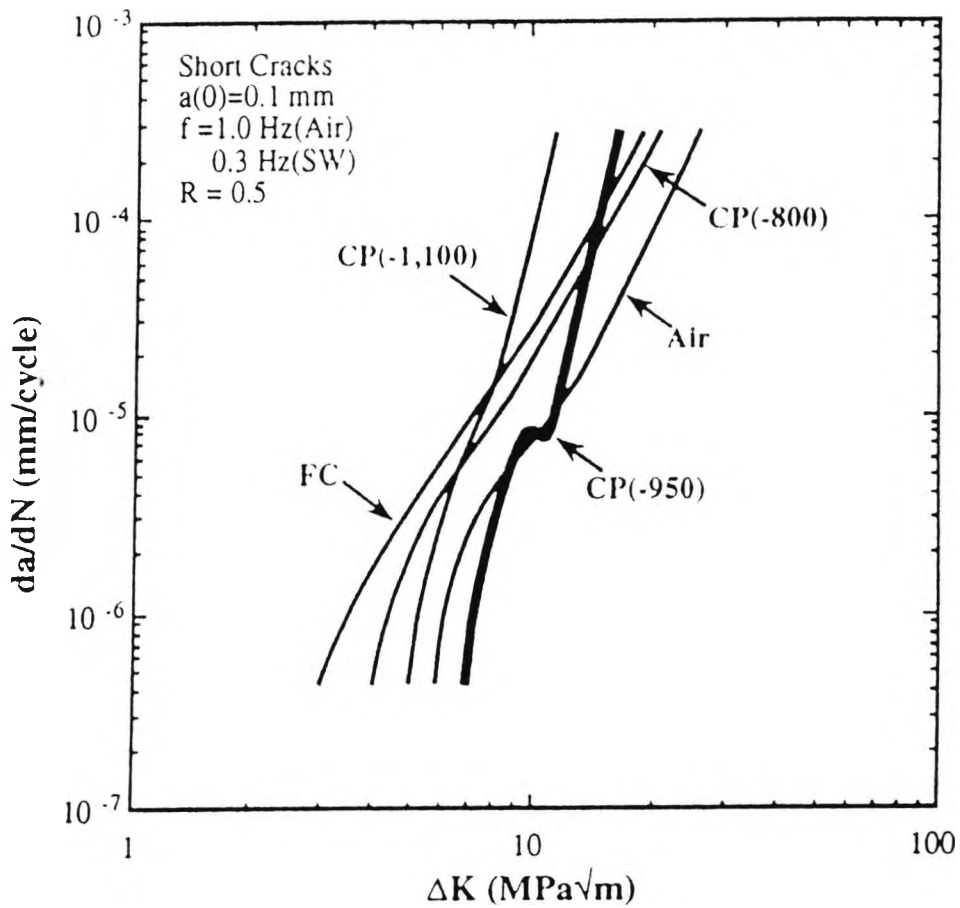


Figure 1.34 Schematic representation of the effect of cathodic protection on the da/dN Vs SIF plot for short cracks [Kim & Hartt, 1993]

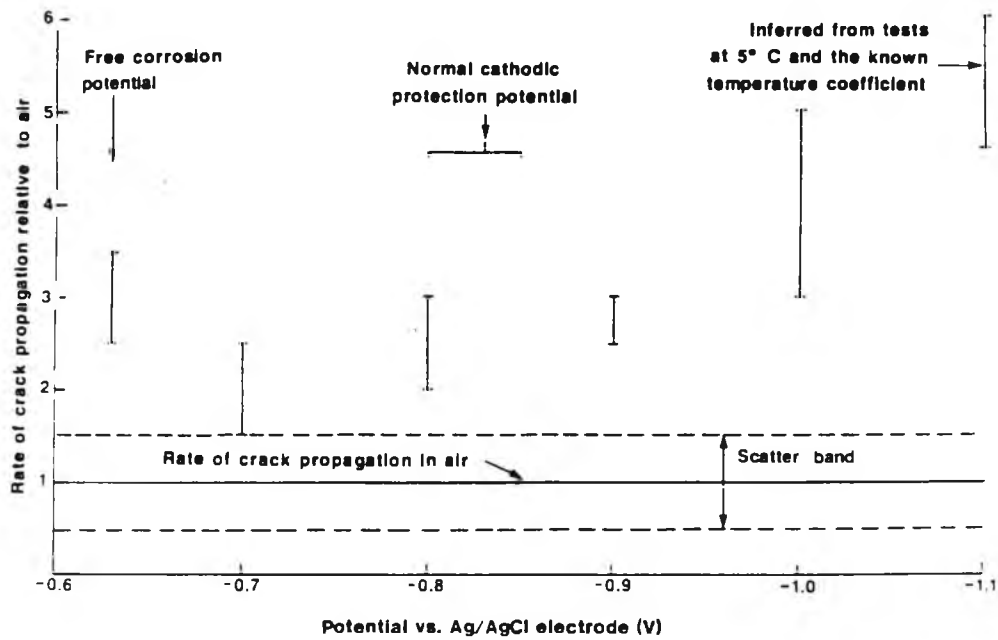


Figure 1.35 Effect of potential on the fatigue crack growth rate at 0.1 Hz in seawater at 20C, $\Delta K = 20-24 \text{ MPa}\sqrt{m}$, $R \leq 0.1$ [from Silvester & Scott, 1975; cited in Vosikovsky & Tyson, 1986]

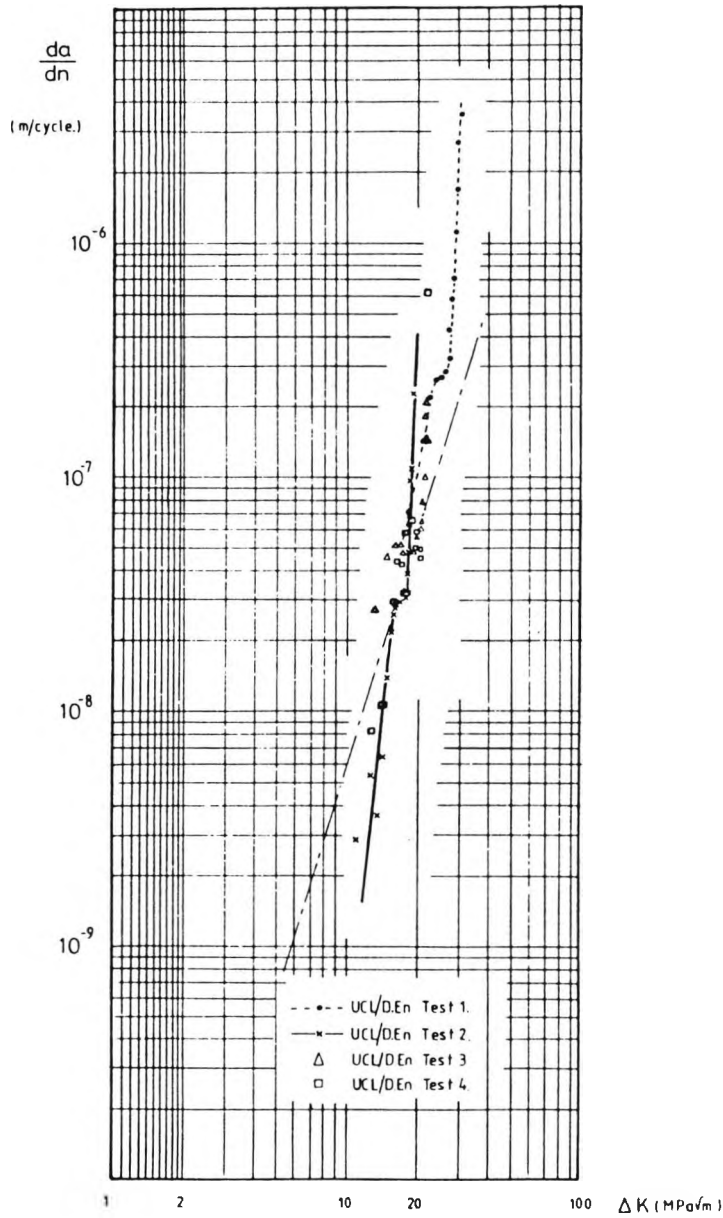
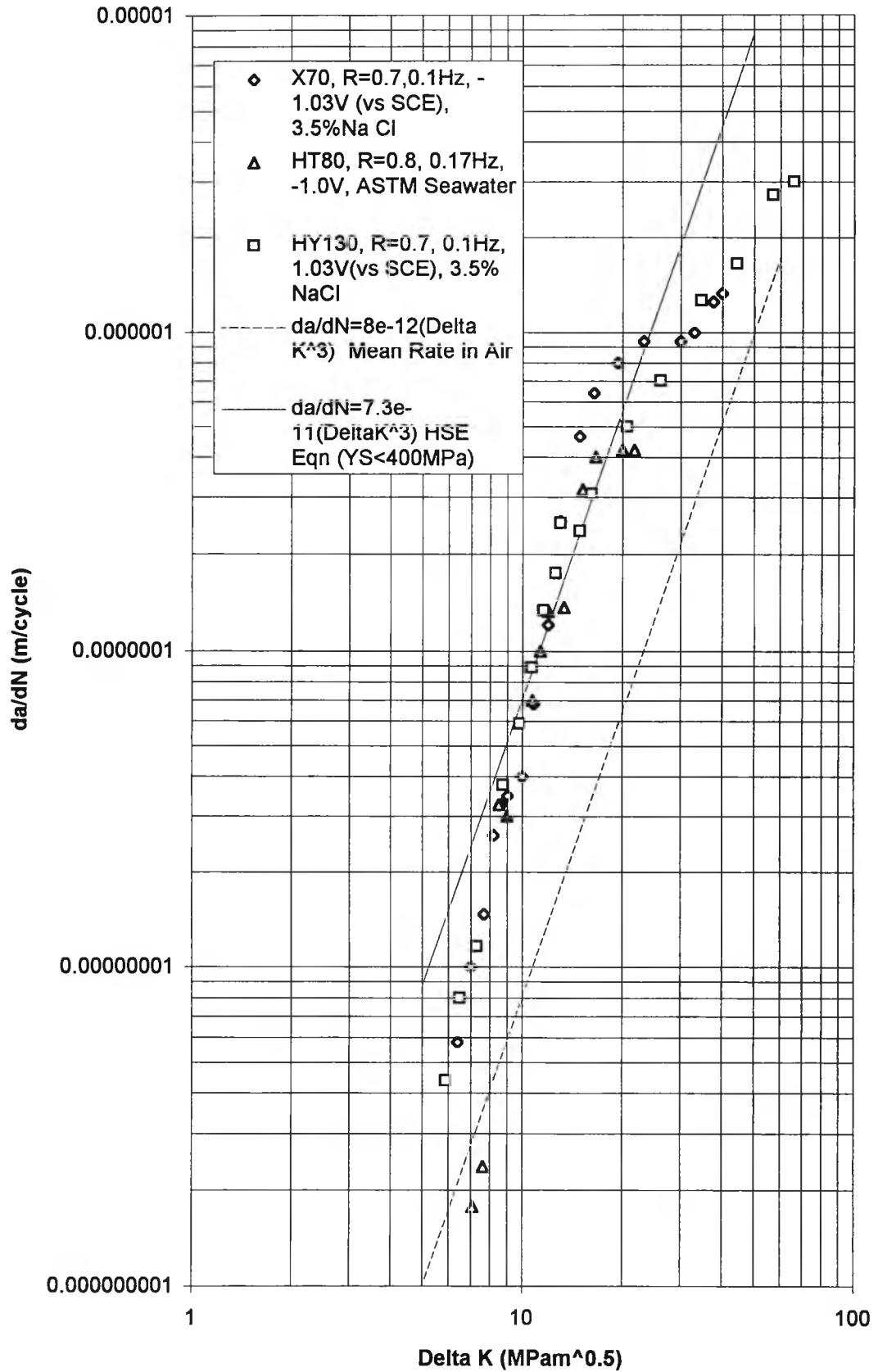


Figure 1.36 da/dN versus empirical K for constant amplitude fatigue tests of PWHT BS4360.50D tubular joints in a seawater environment at a potential of -850 mV [Wilson & Dover, 1986]

Figure 1.37: Comparison of corrosion fatigue data for high strength steels with cathodic overprotection



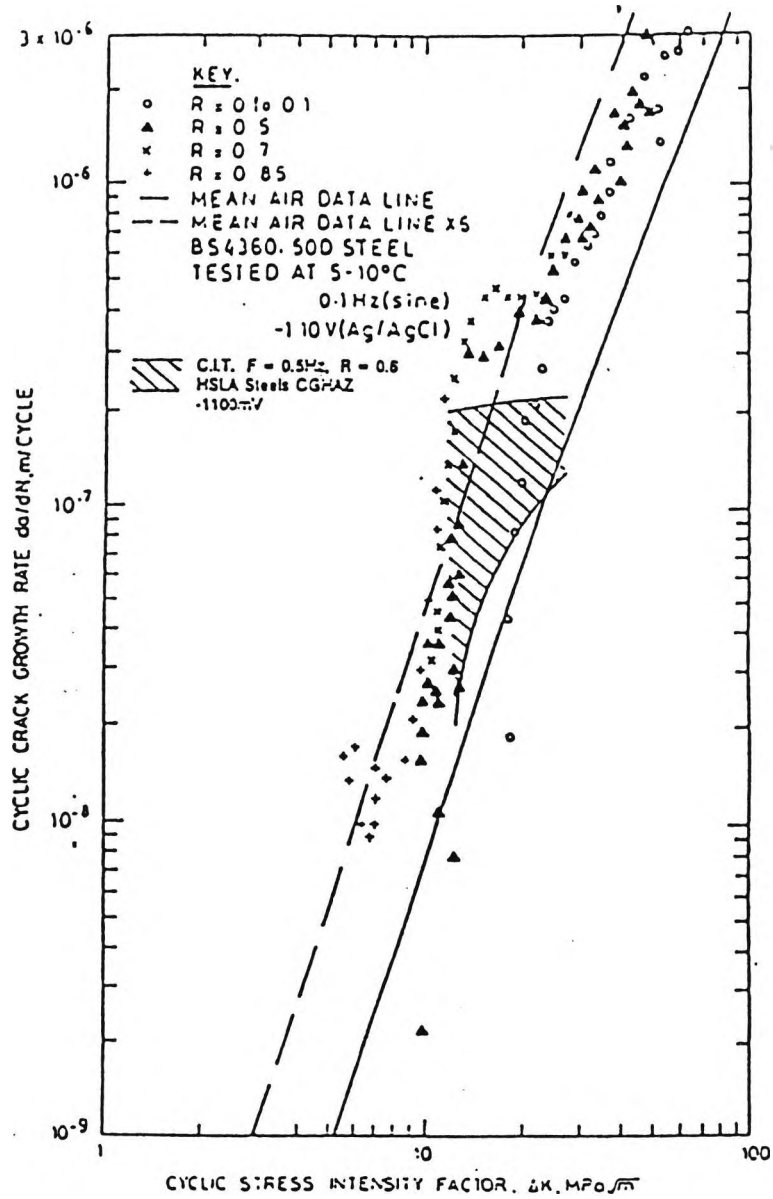
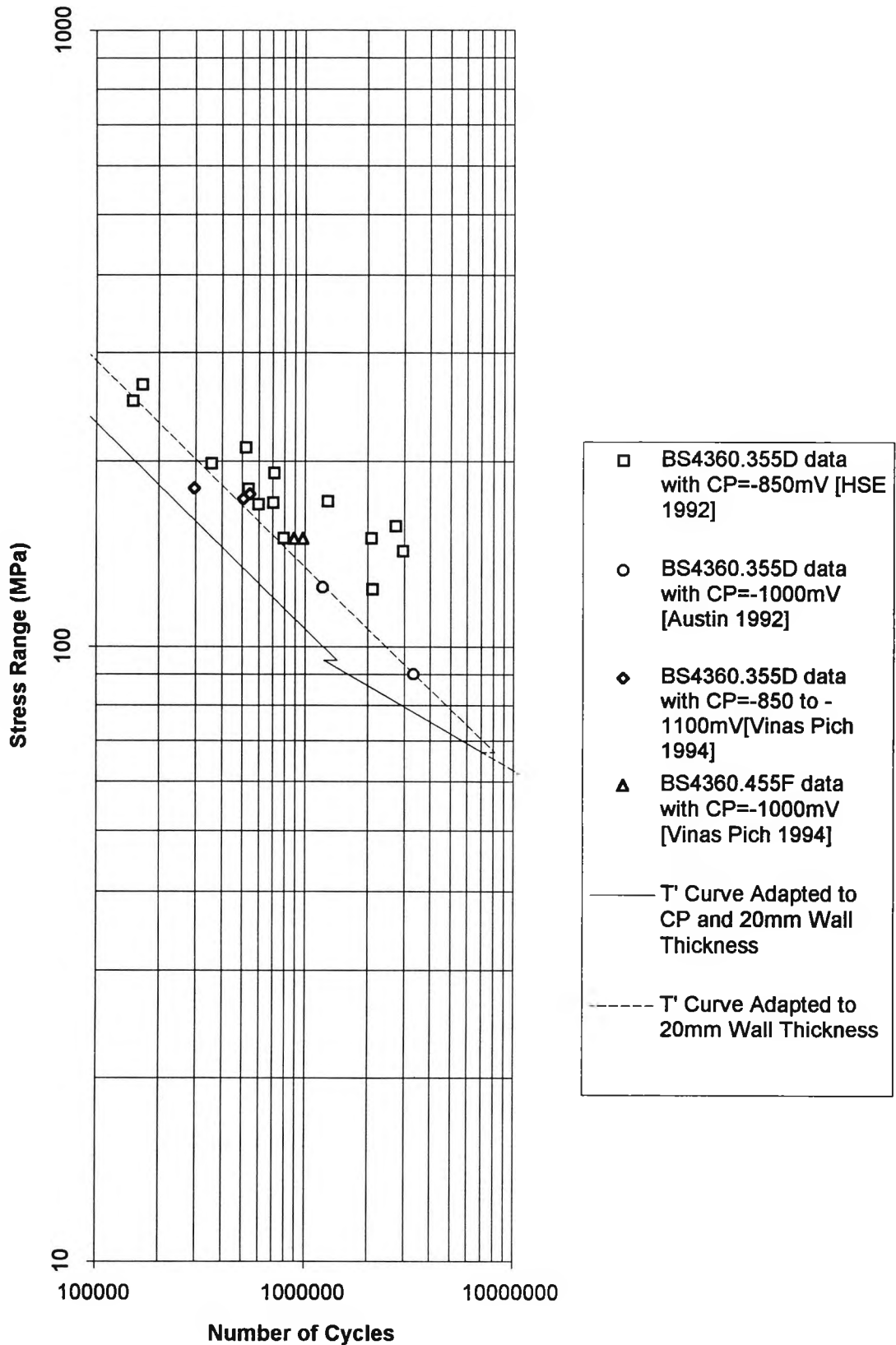


Figure 1.38 Comparison of the corrosion fatigue behaviour of welded high strength steels with BS4360.50D parent plate at a potential of -1100 mV [Billingham and Laws, 1994].

**Figure 1.39: Corrosion Fatigue Data for Tubular Joints
c.f. T' Curve (Adjusted to 19mm chord thickness)**



2. TEST SPECIMEN DETAILS

2.1 Scope of chapter

This chapter will review the materials commonly used for the construction of jack up legs, the types of jack up chord to brace joints and the fabrication processes used. The reasons for selecting the test material, the joint geometry and the fabrication process used in test programme will also be described, together with a comparison of the specified mechanical properties and the measured properties.

2.2 Material Selection

Jack up rigs have progressed from using steels with a yield strength of 300 MPa for the chords, to steels with a yield strength of 510 MPa to 650 MPa for rigs constructed in the 1980s. In the future, it is envisaged that chords will be constructed from steels of up to 900 MPa [Bennett *et al*, 1991]. The problem with such steels is to increase the yield strength, while maintaining the weldability and toughness. Higher strengths can be achieved through quenching and tempering carbon steels. However, quench and tempered carbon steels are prone to quench cracking and have poor weldability. This can be avoided by substituting elements such as manganese, nickel, chromium and molybdenum in place of some of the carbon, so that the quench and tempered steel retains a refined grain structure at depth. In addition, the use of such alloying elements improves the weldability by decreasing the tendency for martensite to form in the heat affected zone. Steels based on the alloying system described above, have been identified as currently used on jack up rigs [Bennett *et al*, 1991; Nichols *pers. comm.*].

As steel making has progressed it has become possible to improve the quality of the steel and reduce the cost. Vacuum degassing has resulted in greatly reduced levels of impurities. In addition, alloying levels can be reduced through the use of boron. Additional grain refinement is promoted through the addition of aluminium and vanadium. As a result of these improvements, several other high strength steels have been identified as suitable for offshore use [Healy *et al*, 1993].

In view of the wide choice of steels, it was decided that criteria should be set for the selection of a suitable steel for the chord material to be used in the experiment. The criteria were as follows:

- i. The steel for the chord member should be of a similar grade and composition to that used currently in the construction of jack up legs.
- ii. Weld procedures should be documented and similar to those used in the construction of jack up rigs.

The use of the above criteria led to the identification of three steels: Nippon Steel Welten 80 [Nippon Steel, 1984]; Creusot Loire A517Q [Creusot Loire, 1990]; and Marathon Le Tourneau MM Structural Tubing [Marathon Le Tourneau, 1983.]. The metallurgical and physical properties of the three materials are described in table 2.1. Of the three steels considered, the Marathon Le Tourneau MM structural tubing represents the lowest strength steel and is more representative of the steel used in serving jack up rigs such as the 116C and Gorilla designs [Bowes, *pers. comm.*]. The Nippon Welten 80 and the Creusot Loire A517Q are currently used for Jack Up chord construction and represent the trend to higher strength steels [Bennett *et al*, 1991].

Marathon Le Tourneau, API 5L X85, MM structural steel was selected for the tubular test specimens because it met the criteria listed above and was readily available as welded tube. Chord and brace material of a nominal yield strength of 590MPa was supplied by Marathon Le Tourneau, Vicksburg, Mississippi, USA. On receipt of the specimens, coupons were taken from the chord material, remote to the weld, and the metallurgical characteristics were measured using optical emission analysis [Stanger, *pers. comm.*]. The specified physical and metallurgical characteristics are compared with the measured values in table 2.2.. The measured metallurgical properties are in general agreement with those specified, although the presence of Nickel, Chromium and Copper were detected, even though these were not mentioned in the original specification. The International Institute of Welding measure of carbon equivalent [IIW, 1971] for the test specimens is 0.51%, this is lower than the level recommended for the use of preheat.

2.3. Geometry Selection

Representative designs of typical jack up leg chord-brace joints are shown in figure 2.1 [King, 1992]. A wide variety of joints are used, depending on the design of the particular jack up rig. To test all the different varieties of jack up leg chord brace joints, would require a costly research programme and take considerable time. The tubular joint shares many common features with the jack up, brace chord connections and it is anticipated that many of the principles of tubular joint analysis can be used with jack up joints.

Double T joints were selected to give two tests per specimen. Specimen dimensions were chosen to ensure that the chord SCF exceeded the brace SCF, so that the probable site for crack initiation was at the chord weld toe (see section 1.3.2). The chord length was determined to minimise unrepresentative boundary effects due to the end restraint.

The specified and measured dimensions and geometry of the test specimens, are given in table 2.3 and figure 2.2. The chord and brace wall thickness were measured close to the saddle positions, the maximum thickness was 20.6 mm (c.f. nominal thickness 19 mm). The inclination of the brace to the chord was measured; this was less than 1° in all cases.

2.4. Fabrication Details

Two welding procedures were used in the fabrication of welded tubular joints: flux-cored arc welding (FCAW) and shielded metal arc welding (SMAW). The FCAW process is a semi-automatic process using carbon dioxide shielding. The FCAW specimens were welded using a "weaved" weld technique, as shown in figure 2.3. The FCAW weldments were smoothly blended into the chord at the saddle position and exhibited a series of connected cusps at the weld toe, resulting in a large weld toe radius at the saddle position. This type of welding is favoured by Marathon Le Tourneau, probably because it allows high weld metal deposition rates and it is claimed to be more tolerant of poor joint fitup. The latter is important in a complex structure such as a jack up leg [Pisarski *et al* 1987]. The SMAW process is a manual process, resulting in a conventional "string" appearance and smaller radius at the weld toe as shown in figure 2.4. This type of welding is more commonly used in the construction of rigs for the North Sea.

The use of FCAW has been called into question because of doubts about the fracture toughness compared to that of the SMAW process [Pisarski *et al*, 1987]. This is particularly important where thick section joints are intended to operate in conditions of high static stresses and cold temperatures. From an investigation of the influence of welding procedure on the fracture toughness of a 340 MPa yield strength steel, Pisarski *et al* [1987] have concluded that the FCAW technique, using a wide weave procedure, produces a satisfactory toughness, provided that the weave layer thickness can be kept below 3.5 mm thick (resulting in a more refined grain structure). Pisarski has noted that maintaining the layer thickness to less than 3.5 mm, is difficult using the weave technique. The stringer technique normally uses a faster travel speed, weld layers are therefore thinner and are more inclined to have a refined structure. The more refined grain structure of the stringer bead welds gives higher values of fracture

toughness. It should also be noted that the weaved technique is associated with much higher heat inputs than than the stringer weld technique. This has the effect of: firstly, increasing the size of the grain coarsened heat affected zone, which generally has inferior toughness properties compared to parent plate; secondly, the residual stresses are increased, which has consequences for the fracture behaviour of the joint [PD6493: 1991]. It is for these reasons, and the difficulty of confirming the weld layer thickness by subsequent inspection, that certifying authorities are prejudiced against the use of the wide weave technique.

As jack up rigs are mobile and see service globally, it was decided that it was valid to investigate both FCAW weave welded and SMAW stringer welded joints. Four tubular welded, double T joint specimens were tested in this test series, a total of eight welded joints. Four of the joints were constructed using a flux cored wire arc welding process (FCAW), at Marathon Le Tourneau. The weave welded joints were initially referred to as joints W1 to W4. The other four joints were constructed at Highland Fabricators of Scotland, using a conventional manual shielded metal arc welding process (SMAW), to a weld procedure supplied by Marathon Le Tourneau and were referred to as joints S1 to S4. All joints were specified as full penetration welds. The SMAW joints were preheated to a minimum of 100°C and the electrodes oven dried to minimise hydrogen embrittlement. No post weld heat treatment was used.

2.4.1 Weld Inspection

The FCAW and SMAW specimens were inspected by magnetic particle inspection (see section 4.3.1) on arrival at the laboratory, no cracks were found. In addition the SMAW specimens were inspected using ultrasonic inspection at the fabrication yard, again no defects were reported.

The weld profile for all specimens was measured at regular intervals around the chord brace intersections. The weld profile at the crown and saddle positions are included in Appendix I.

The degree of weld toe blending was measured using the Irish Penny Test (Appendix II). The FCAW joints failed in the regions shown (figure 2.5). The weld as a whole does not fail unless more than 10% of the weld fails. Using this criterion, joints W1, W3 and W4 failed. However the failed regions lie close to the crown positions and failure in these regions was thought unlikely to affect the fatigue performance for out of plane bending (OPB). The poor weld profile revealed by the Irish Penny Test is thought to be more significant where the joint is subjected to in plane bending (IPB),

or multiplane bending, as is likely to occur offshore. The SMAW specimens passed the Irish Penny Test at all positions.

In addition, the weld toe radius was measured by replicating the weld toe with a high resolution two part polymer. The polymer was later removed and sectioned at 20 positions. The sections were viewed with the aid of a shadow graph. The SMAW specimen was found to have an average weld toe radius of 2.1 mm with a standard deviation of 1.6 mm. This compares with a FCAW specimen average weld toe radius of 6.1 mm and standard deviation of 2.1 mm. The smaller weld toe radius measured for the SMAW specimens may result in a shorter fatigue initiation life for reasons discussed in chapter 4.

On sectioning, the FCAW welds were found to have poor penetration. An example is shown later in figure 4.5. It should be noted that the poor penetration was analogous to a crack on the inside of the brace (see chapter 4). This poor penetration was not found in the SMAW specimens.

On completion of the test programme, tensile test specimens were taken from the weld metal (the axis of the specimens aligned to the circumferential direction). The yield strength tensile strength and ductility of the weld metal was measured. These were compared to the properties of the weld metal specified by the manufacturers, and the properties of the parent plate material in table 2.4. The yield strength and tensile strength of the chord material were all greater than those specified. The specified and measured yield and tensile strength of the weld metal were below those of the parent plate material. The toughness of the parent plate was measured by the Charpy V test with specimens taken from the L-S and L-T directions and tested at a temperature of -40C.

The minimum of 3 results for each direction are given in table 2.4. It should be noted that the minimum measured toughness was just below that specified.

2.5 Summary

Marathon Le Tourneau MM structural tubing was chosen as a suitable representative material for the tubular joint tests. The corrosion fatigue behaviour of two types of welded tubular joint, differentiated by their weld procedures, were investigated. The specimens obtained from the suppliers were defective in a number of locations due to poor weld profiling and poor weld penetration. However, the areas which failed to meet the specification were not thought to influence fatigue crack initiation or propagation in OPB tests.

TABLE 2.1 METALLURGICAL AND PHYSICAL PROPERTIES OF TYPICAL JACK UP CHORD STEELS

Element %	Nippon Welten 80A [3.2]	Creusot Loire A517Q [3.3]	Marathon Le Tourneau MM Structural Tubing [3.4]
Carbon	0.16Max	0.15 Max	0.13-0.23
Silicon	0.15-0.35 Max	-	0.18-0.53
Manganese	0.6-1.2	0.8-0.12	1.05-1.45
Sulphur	0.03 Max	0.004 Max	.04 Max
Phosphorus	0.03 Max	0.012 Max	.04 Max
Copper	0.15-0.5	-	-
Nickel	0.4-1.5	0.85-2.0	-
Chromium	0.4-0.8	0.4-0.7	-
Molybdenum	0.3-0.6	0.4-0.6	.12-.23
Aluminium	-	-	added for grain control
Vanadium	0.10 Max	.05 Max	-
Boron	0.006 Max	-	-
Carbon Equivalent	0.6 ² Max	0.58 ¹ Max	0.51 ¹ Max
Yield Strength	685MPa	689MPa	585MPa
UTS	780-930MPa	805-945MPa	689MPa
El/RA	RA 16% in 50mm	RA 16% in 2"	El 18% in 2"
Charpy Values	39J @ -20C	40 J @ -40C	20.3J @ -45C

¹ International Institute of Welding definition of carbon equivalent.

$$C_{eqiv} = C + Mn/6 + (Cr + Mo + V)/5 + (Cu + Ni)/15$$

² Japanese Standard definition of carbon equivalent.

$$C_{eqiv} = C + Mn/6 + Cr/5 + Mo/4 + Si/24 + V/14 + Ni/40$$

TABLE 2.2 PROPERTIES OF MARATHON LE TOURNEAU STRUCTURAL TUBING

Element	Specified %	Measured %
Carbon	0.13-0.23	0.18
Silicon	0.18-0.53	0.27
Manganese	1.05-1.45	1.44
Sulphur	0.04 max	0.020
Phosphorus	0.04 max	0.015
Nickel	-	0.19
Chromium	-	0.11
Copper	-	0.19
Molybdenum	0.12-0.23	0.24
Aluminium	added for grain control	0.02

Heat treatment: 1600-1700F. Water quench draw 1150-1275F

Hardness range: 14-25 Rockwell "C" Scale

PHYSICAL PROPERTIES (MINIMUM VALUES)

	Yield Strength	Tensile Strength	Elongation	Toughness
Specified	586 MPa	689 MPa	18% in 2"	34J @ -40C (27J min)
Measured	670 MPa	795 MPa	25% in 25 mm	75J average (LT direction) 34J average (TS direction) 32J @ -40C

1 Tested by optical emission, Stanger Consultants Ltd

2 Worst of 12 tensile tests, 3 in rolling direction, 3 transverse to rolling direction, 6 from FCAW specimens, 6 from SMAW specimens.

TABLE 2.3 SPECIMEN GEOMETRY.

Specimen	Chord			Brace			θ
	L	D	T	l	d	t	
nominal	2000	406	19	1000	325	19	90°
W1	2000	403	20.4	1025	324	19.4	90 ⁺¹ ₋₁
W2	2000	403	19.8	1015	324	19.6	90 ⁺¹ ₋₁
W3	2003	404	19.8	1025	323	19.9	90 ⁺¹ ₋₁
W4	2003	404	20.0	1005	325	20.0	90 ⁺¹ ₋₁
S1	2000	405	20.4	1010	326	19.8	90 ⁺¹ ₋₁
S2	2000	405	20.2	1020	324	20.2	90 ⁺¹ ₋₁
S3	2000	406	20.6	1010	325	20.1	90 ⁺¹ ₋₁
S4	2000	406	20.0	1020	323	19.7	90 ⁺¹ ₋₁

All dimensions in mm

d varied by +/- 2 mm

D varied by +/- 2 mm

W1 -W4: Weave welded specimens.

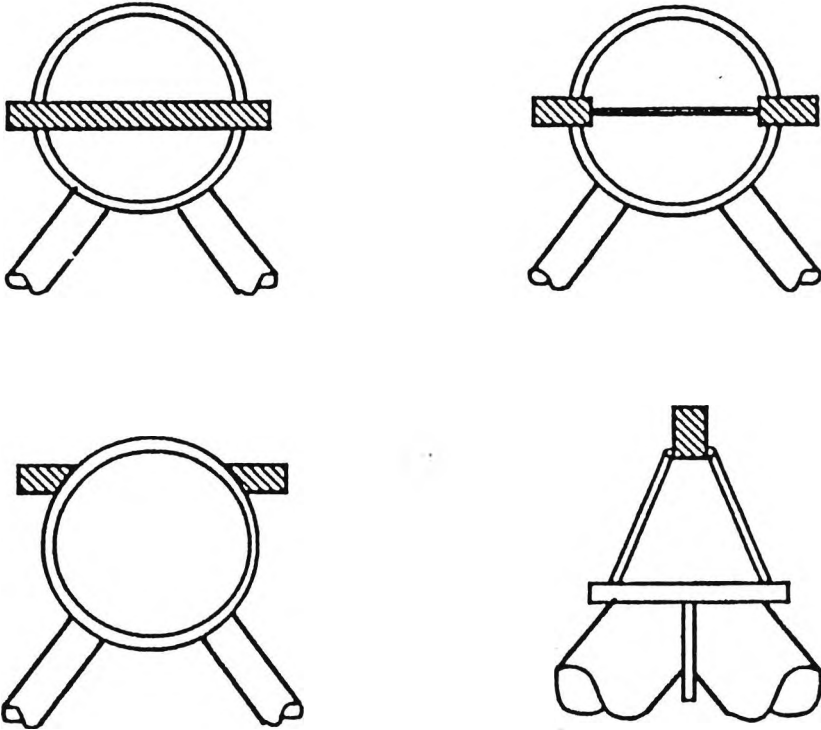
S1 - S4: Stringer welded specimens.

TABLE 2.4: COMPARISON OF WELD METAL STRENGTH WITH BASE METAL STRENGTH

		Yield Strength (MPa)	Ultimate Tensile Strength (MPa)
FCAW	Specified	520	644
	Measured	517	602
SMAW	Specified	580	658
	Measured	550	640
M LeT MM	Specified	586	689
Structural Tubing	Measured	670	795

Measured yield strength and ultimate tensile strength are lowest values from 3 tensile tests.

Figure 2.1 Typical leg components for jack up units (from King *et al*, 1993)



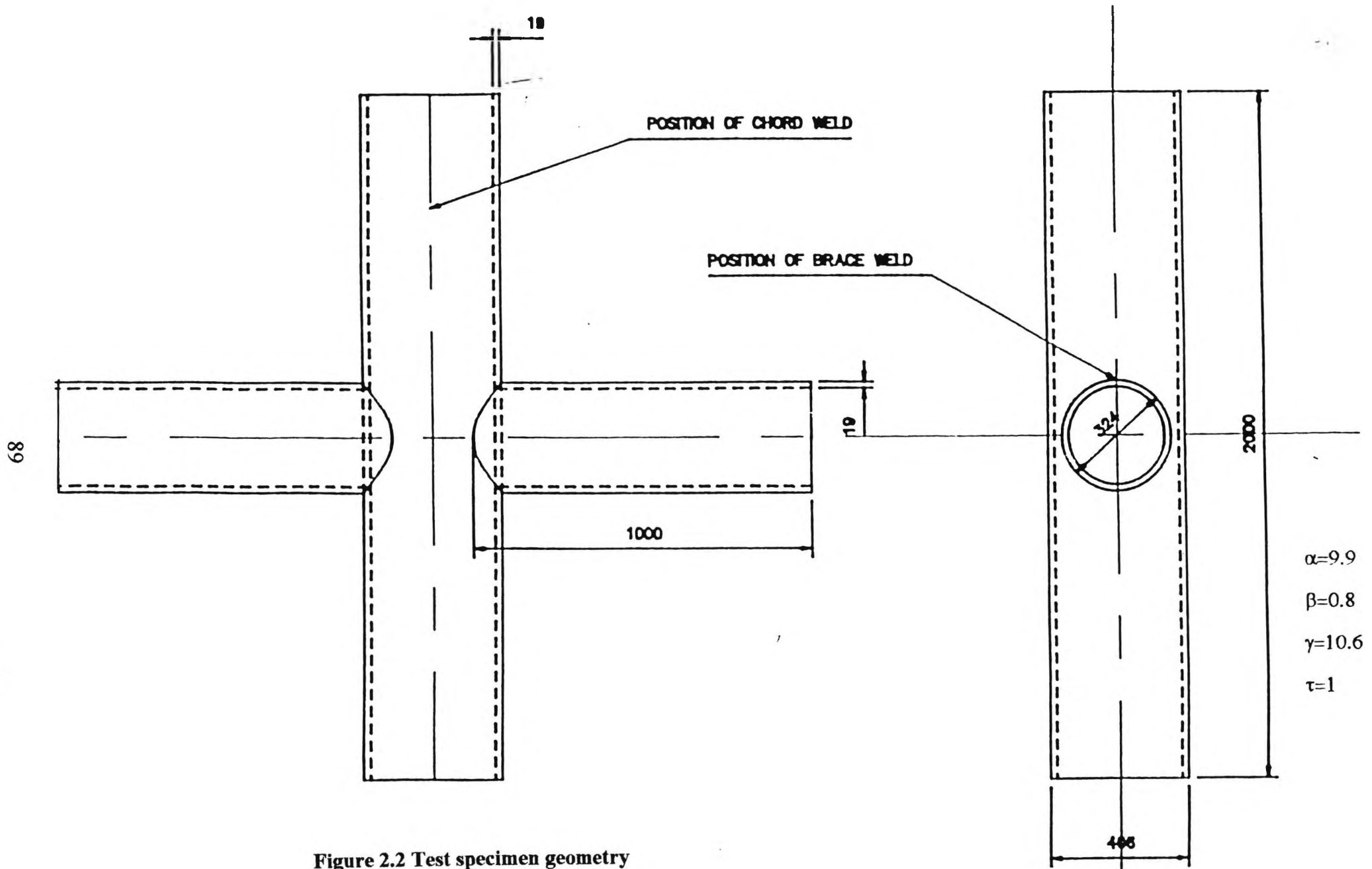


Figure 2.2 Test specimen geometry



Figure 2.3: Typical "weave" profile of FCAW specimens

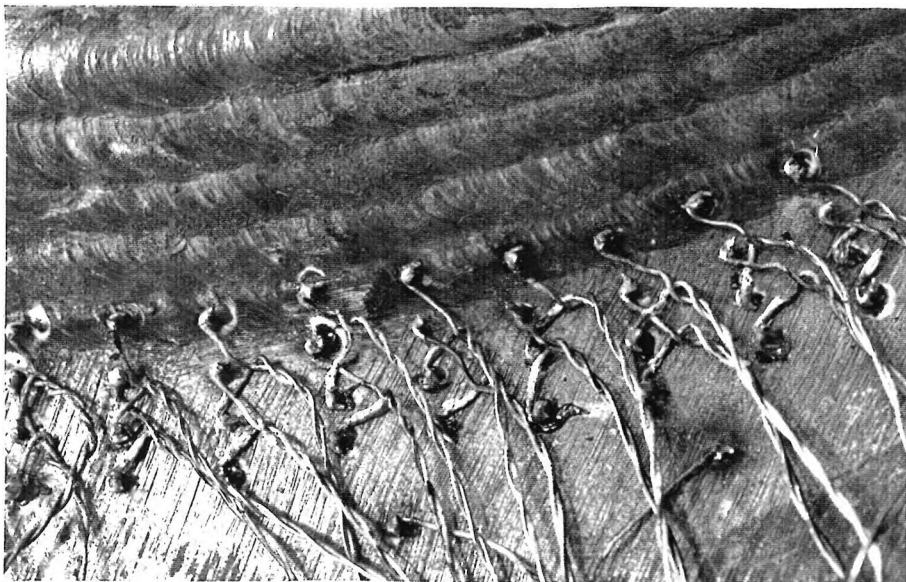
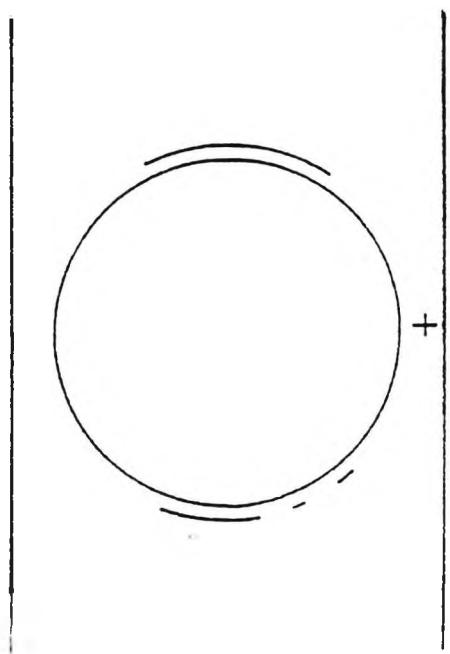


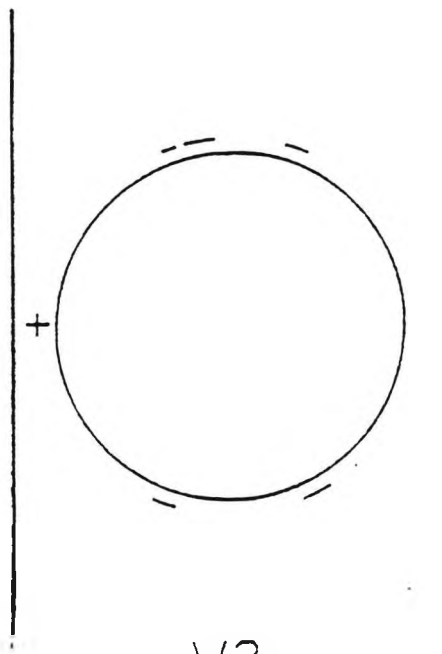
Figure 2.4: Typical "stringer" weld profile of SMAW specimens

Figure 2.5 Position where weld toes failed the "Irish Penny" test



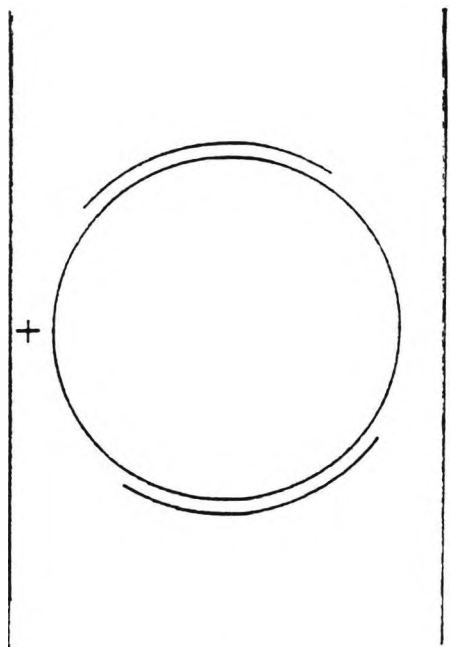
W1

Failed on 24% of weld



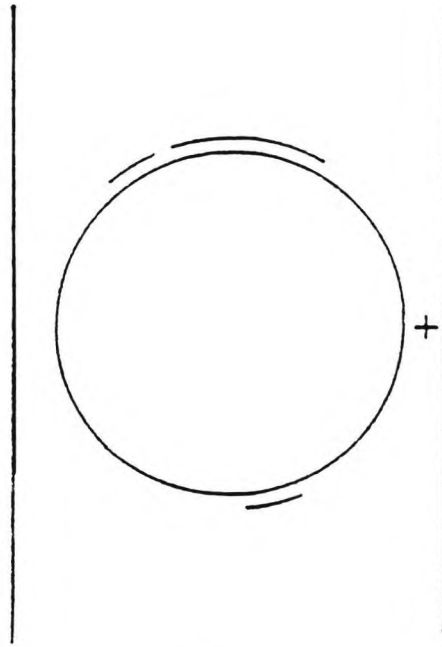
W2

Failed on 8% of weld



W3

Failed on 42% of weld



W4

Failed on 19% of weld

+ indicates cracked saddle

3. GLOBAL STRESS ANALYSIS

3.1. Scope of Chapter

Various stress analysis techniques were reviewed in section 1.3. It was concluded, that the most accurate method of characterising the stress in the region most susceptible to fatigue damage, was to measure the hot spot stress and distribution of stress around the chord brace intersection distribution, through the use of electrical resistance strain gauges, directly attached to the steel specimen. The purpose of this chapter is to report on the stress analysis techniques used in the experimental investigation of the specimens described in chapter 2, and compare the results with those obtained from parametric solutions, based on finite element analysis and acrylic model tests. In addition to the hot spot stress and the transverse stress distribution around the brace chord intersection, the bending stress to membrane stress ratio was also required for evaluation of the stress intensity function, using adapted plate solutions (section 1.4.2). The bending stress to membrane stress ratio was determined from acrylic model tests, the experimental results are reported in this chapter.

As a result of experimental tests, it became apparent that the parametric formulae overestimated the hot spot stress. It was hypothesised that this was due to load interaction effects from the second brace. This chapter reports on a simple test designed to evaluate the influence of the second brace on the chord hot spot stress.

3.2 Experimental Stress Analysis of Steel Specimen

All tubular joints were strain gauged in accordance with UKORSP guidelines [DEn, 1988], prior to fatigue testing. The following section describes the test procedure and results and compares test data to that obtained from the commonly used parametric stress concentration factor (SCF) and transverse stress distribution equations as described in section 1.3.2.

3.2.1. Test Rig

Two double T welded tubular joints were tested in out of plane bending, by reacting one specimen against another using a purpose built servo-hydraulic test facility as shown in figure 3.1. Rigid chord end supports were provided by a strong floor at one end of the chord and an overhead beam at the other. The beam was designed to provide high stiffness. The chord ends were restrained from movement by the use of

clamping blocks gripping to a ring, which was welded to the chord rim. The clamping blocks were designed to give maximum practical purchase. Prior to loading, the rig was adjusted, to minimise the difference in the corner to corner lengths A-A' and B-B' (figure 3.1).

Loading was provided through a 250 kN dynamic load capacity, servo hydraulic actuator controlled through an Instron control console. The load cell was calibrated and was found to have an accuracy of 99%. Load was applied through a swivel bearing plate held rigidly to the brace end by clamping blocks. The actuator was "floated", by suspending it from an A frame in two positions using adjustable slings. This had the effect of confining loading to out of plane bending (OPB).

3.2.2. Experimental Method

The chord weld toe was strain gauged in accordance with UKORSP guidelines using stacked triple gauge rosettes located at the positions shown (see figure 3.2). All chord hot spots were strain gauged. Specimens W2 and S1 were strain gauged at positions of 30°, 60°, 90°, 120° and 150° relative to the crown, to determine the chord circumferential stress distribution. The strain gauge closest to the weld toe was placed 12 mm from the chord weld toe and the outer gauge at 17.5 mm from the chord weld toe. In addition the brace weld toe hot spot of specimens W2, W4, and S1 were strain gauged. The brace of specimen W2 was strain gauged at positions of 30°, 60°, 90°, 120° and 150° relative to the crown to determine the brace circumferential stress distribution. Brace strain gauges were attached in accordance with UKORSP guidelines at 12 mm and 22 mm from the weld toe. Where the weld toe was poorly defined, such as the FCAW chord weld toe, measurements were taken from the point of inflexion. This places all the strain gauges within the linear stress decay region as defined in figure 1.6.

The two braces were loaded in OPB in steps of 5 kN from a load of 5 kN to 25 kN. This was followed by unloading in steps of 5 kN, reloading to 15 kN and 25 kN, unloading to 15 kN and 5 kN, loading to 25 kN and finally unloading to 5kN. Strain readings were taken at each change of load. The maximum load corresponds to a maximum hot spot stress of 152 MPa, or 26% of the yield stress. The hot spot stress induced during strain analysis was less than that of the maximum test hot spot stress and there was no overload effect to influence subsequent fatigue tests.

3.2.3. Results

The slope of the strain versus load graph was determined using engineering judgement. From the slope, the principal strain was determined for both the outer and inner gauges using the following relationship [Benham & Warnock, 1976]:

$$\varepsilon_{1,2} = \frac{1}{2}(\varepsilon_l + \varepsilon_n) \pm \frac{\sqrt{2}}{2} \sqrt{[(\varepsilon_l - \varepsilon_m)^2 + (\varepsilon_m - \varepsilon_n)^2]} \quad 4.1$$

where: $\varepsilon_1, \varepsilon_2$ is the maximum and minimum principal strain

$\varepsilon_l, \varepsilon_m, \varepsilon_n$ are the mean strain/ unit load for individual gauges at 45 degrees to each other.

The maximum principal strain was extrapolated to the weld toe and converted to the maximum principal stress [Benham & Warnock, 1976] using the greater of:

$$\sigma_1 = \frac{E(\varepsilon_1 + \nu\varepsilon_2)}{1 - \nu^2} \quad 4.2$$

$$\sigma_2 = \frac{E(\varepsilon_2 + \nu\varepsilon_1)}{1 - \nu^2} \quad 4.3$$

where: E is the Young's Modulus (210 GPa)

ν is the Poisson's Ratio (0.3)

The SCF was determined by dividing the greatest maximum principal stress by the nominal stress in the brace. For OPB the nominal stress was calculated from simple beam theory, and the moment arm was taken from the swivel pivot to the chord saddle position as shown in Appendix III.

The SCF at the saddle position for all chord saddle positions is given in table 3.1. The experimentally derived SCFs were compared to results from parametric equations. The chord saddle SCFs were found to vary between values of 6.0 and 6.7 with an average value of 6.4. There was no significant variation between the chord saddle SCF of the FCAW and SMAW specimens.

The chord, transverse stress distribution around the brace chord intersection is compared with both the UCL transverse stress distribution [Hellier *et al* (c), 1990] and the UEG transverse stress distribution [UEG, 1985] in figure 3.3. The orientation of the plane of principal stress to the weld toe for the chord gauges is shown in figure 3.6. The brace hot spot SCF varied between 4.7 and 4.8. Both the brace hot spot stress

and brace transverse stress distribution in the circumferential direction, are compared with parametric solutions in table 3.1 and figure 3.4 respectively.

3.2.4. Discussion of Results

Chord Hot Spot SCF

Comparison with the hot spot SCF, predicted using the parametric solutions, shows that the parametric equations overestimate the SCF. The closest approximation was that of the UCL equations [Hellier *et al* (b), 1990], which overestimated by a factor of 28%. Of the HSE recommended equations [HSE, 1992], the Efthymiou equations [Efthymiou, 1988] overestimated the hot spot SCF by 42% and the Lloyds Registry equations [Smedley & Fisher, 1991] overestimated by 59%. The Lloyds Registry equations are based on the regression analysis of acrylic and steel model results, and include a safety factor to account for variations from the mean. To obtain an accurate comparison between the steel specimen experimental results and typical results for acrylic and steel models, the Lloyds Registry equations were adjusted to eliminate the safety factor. The adjusted Lloyds Registry equations show closer agreement and give an overestimate of 31%. Allowing for their conservative nature, all of the parametric stress equations overestimate the chord hot spot SCF. However, the UCL equations predicted the hot spot SCF most accurately.

It was hypothesised that the reason for the parametric equations overestimating the hot spot SCF, was because the parametric equations were all based on solutions for single brace nodes. The second brace may restrain the chord being from being deformed, explaining the overestimate of the SCF in the double brace node. The influence of the second brace is examined further in section 3.2.

It should also be noted that the plane of principal stress (as measured at the rosette positions) was not parallel to the weld toe (figure 3.6). This will be referred to in later chapters.

Brace Hot Spot SCF

The average brace hot spot SCF for the three specimens tested was 4.8. The use of either FCAW or SMAW as a welding process has no influence on the brace hot spot SCF. Again, the parametric solutions were all conservative. However, if the Lloyds Registry equations are adjusted to eliminate the safety factor, they underestimate the hot spot stress by 14%. The Lloyds Registry equations provided the most accurate solution with an overestimate of 12.5%, while the UCL and Efthymiou equations

provided overestimates of 54% and 69% respectively. It is possible that the second brace led to a reduction in the brace SCF compared to the single brace node.

Chord Side Transverse Stress Distribution in the Circumferential Direction

Comparison of the experimental circumferential stress distribution with the predicted transverse stress distribution in the circumferential direction, showed close agreement between experimental results and the UCL stress distribution [Hellier *et al* (c), 1990] and poor agreement with the UEG recommended stress distribution [UEG, 1985]. It was therefore decided to use the UCL stress distribution:

$$S(\varphi) = K_{HS} \sin^2 \varphi \quad 3.4$$

where: $S(\varphi)$ is the characteristic distribution formula for SCF
 K_{HS} is the SCF at the hot spot
 φ is the angle measured around the hot spot

with both the Average Stress [Dover & Dharmavasan, 1982] and Two Phase Method [Kam, 1988], equations for the stress intensity factor (see section 1.4.2). Both the SMAW and FCAW stress distributions were similar and the weld profile makes no difference to the transverse stress distribution around the weld toe. The transverse stress distributions showed a high degree of symmetry about the saddle position (figure 3.3). This confirmed that the top and bottom chord fixity of the test rig was evenly balanced.

It should be noted that the the principle stress was not normal to the weld toe at positions other than the saddle. This will be referred to later chapters.

Brace Side Transverse Stress Distribution in the Circumferential Direction

There was limited agreement between the experimental transverse stress distribution in the circumferential direction and the UCL distributions. The UEG recommended stress distribution did not apply to the brace side, transverse stress distribution.

3.3. Experimental Investigation of the Bending to Membrane Stress Ratio and Influence of the Second Brace on the Global Stress System.

The bending stress to membrane stress ratio was needed to evaluate the transverse stress distribution in the through thickness direction. The bending stress to membrane stress ratio is an important parameter for adapted plate solutions for the stress intensity function. The bending stress to membrane stress ratio can be determined from:

$$\frac{\sigma_b}{\sigma_m} = \frac{\sigma_{hss} - \sigma_i}{\sigma_{hss} + \sigma_i} \quad 3.5$$

where: σ_b is the bending stress;

σ_m is the membrane stress;

σ_{hss} is the hot spot stress per unit load;

σ_i is the maximum stress on the internal chord wall per unit load.

Unfortunately, the narrow internal diameter of the chord did not allow for the inside of the tubular joint to be strain gauged. It was therefore decided to replicate the joint using a bonded cast acrylic joint and to determine the bending to membrane ratio from the acrylic joint. The bending stress to tension stress ratio of the acrylic model can be assumed to accurately predict that of the steel specimen, provided there is close agreement between the hot spot stress concentration factor of the steel specimen and the double T joint acrylic model.

A secondary objective of the acrylic model test was to compare the hot spot stress concentration factor and bending stress to tension stress ratio of the single T joint to that of the double T joint. This was done by testing a single T joint acrylic model in out of plane bending and then bonding a second brace to the acrylic model and retesting.

3.3.1. Experimental Method

An acrylic model of the steel tubular joint was constructed at a scale of 1:3.33 (table 3.2). The weld fillet was not replicated. The test was conducted in two parts: one brace attached to the chord and the load applied in OPB; two braces attached to the chord with the load applied in OPB. For both tests, the inside and outside of the chords were strain gauged as shown in figure 3.5. Two, triple stacked, rosette gauges were placed as shown in figure 3.5, to confirm that the maximum principal stress

acted on a plane parallel to the weld toe, and that the minimum principal stress acted on plane perpendicular to the weld toe and the minimum principal stress was effectively zero. Manufactured gauges, accurately spaced at 2 mm intervals over 10 mm, were applied to the outer and inner chord. These gauges were used to confirm the linear surface stress distribution.

The load was applied using dead-weights, as shown in figure 3.5. After an initial loading sequence, the strain was determined and recorded on a computer datalogger one minute after applying the load. The joint was tested so that the outer strain gauges remained in compression during the test.

On completion of the double brace test a test coupon of the chord material was cut from the specimen and loaded using weights. To make the results compatible with those of the tubular joint, strain readings were taken one minute after the load was applied. From the resultant load strain curve, Young's Modulus ($E=3.62\text{GPa}$) and Poisson's ratio ($\nu=0.3$) were determined .

3.3.2. Results

Results from the two reference gauges indicated that the minimum principal stress acting on the plane perpendicular to the weld toe, was zero at the chord and brace saddle positions. The five linear external and internal gauges were therefore assumed to record the maximum principal strain and that the minimum principal strain was zero. The maximum principal stress was extrapolated from the linear stress region, using equations 3.1, 3.2 and 3.3. The maximum principal stresses are presented as non-dimensional values, by dividing them by the nominal stress determined from simple beam theory.

The chord saddle hot spot SCF was multiplied by an empirical correction factor of 0.95 to correct for the weld leg length [HSE, 1992]. The bending stress to membrane stress ratio was calculated using the hot spot stress corrected for weld leg length and the minimum value of internal chord wall stress (equation 3.4). The hot spot SCF and bending stress to tension stress ratios for both the single brace and double brace acrylic models are given in table 3.3.

3.3.3. Discussion of Results

The hot spot SCF for the acrylic model, double T joint was within 12% of the average hot spot SCF of the steel specimens. The acrylic model reproduced the global stress state of the steel specimen, relatively accurately. The error in the acrylic model can be

ascribed to differences between the scaled dimensions and the model dimensions and errors associated with weld toe modelling.

The hot spot SCF of the single T joint acrylic model, was 3% higher than the hot spot SCF of the double T joint, acrylic model. This was due to the stiffening effect of the second brace restraining the chord wall from deforming under load. However, the discrepancy between the experimental value of the steel specimen, hot spot SCF, and the parametric solutions to the hot spot SCF, was much greater (approximately 28%). The addition of the second brace does not account for the difference and this must be explained by error in the finite element analysis. Efthymiou [1988], has reported that the influence of the second brace on the hot spot stress is negligible for a double T joint and that the hot spot stress can be predicted using appropriate formulae for a single T joint, for the loading case described above. The above test agrees with Efthymiou.

The bending stress to membrane stress ratio increased from 7.17 for the single brace, acrylic model, to 7.95 for the double brace, acrylic model, a factor of over 10.8%. However, the change in the degree of bending (bending stress to total stress ratio) varied from 0.879 for the single brace specimen to 0.888 for the double brace specimen, a change of 1.0%. The degree of bending is reasonably typical of a T joint [Eide et al, 1993]. Moreover, the effect of the additional brace on the degree of bending, agrees with other researchers findings [Haswell, 1992]. As the UCL equations were formulated for a single brace T joint specimen, it is reasonable that the bending stress to tension stress ratio of 7.95 should be used in calculations relating to the double T joint. The development of influence functions, to quantify the load interaction effects of adjacent bracing on the bending stress to tension stress ratio, would prove useful if adapted plate solutions for the stress intensity function, are to be used with multibrace joints. The effect on the endurance of the change in the degree of bending is discussed further in the addenda.

3.4. Conclusions

- 1) The use of either FCAW or SMAW as a welding process had no significant effect on either the chord or brace hot spot SCF, or on the transverse stress distribution in the circumferential direction.
- 2). The most accurate method of determining the hot spot stress concentration factor was by stress analysis with strain gauges on steel tubular joint. There was little difference between the hot spot stress distributions of the SMAW and FCAW specimens. This led

to an average hot spot SCF value of 6.4. The hot spot stress ranges of individual tests could be determined using the chord hot spot SCF for that joint.

3) The transverse stress distribution around the brace chord intersection was accurately modelled using the UCL stress distribution.

4) Stress analysis of a scaled acrylic model gave a bending stress to membrane stress ratio of 7.95.

5) The hot spot stress and degree of bending of the single T joint specimen are similar to the hot spot stress and bending to membrane ratio of the double T joint .

TABLE 3.1 MEASURED SCFS AND VALUES FROM PARAMETRIC EQUATIONS: STEEL MODEL DATA

Test Ref.	Measured Values									Parametric Equations			
	W1/ W5	W2	W3/ W6	W4	S1	S2	S3	S4	Average SCF	LR ¹	$\frac{LR^1}{SF}$	UCL ²	E ³
Chord SCF	6.5	6.7	6.7	6.4	6.4	6.0	6.6	6.2	6.4	10.2	8.4	8.2	9.1
Brace SCF	-	4.8	-	4.7	4.8	-	-	-	4.8	5.4	4.2	7.4	8.1
Bending to Membrane Ratio	Not Recorded									-	-	5.3	-

1. Smedley and Fisher [1991]:
2. Hellier, Connolly and Dover [1990].
3. Efthymiou [1988].

TABLE 3.2 ACRYLIC MODEL DIMENSIONS: NOMINAL SCALE 1:3.36

Specimen	Chord			Brace			θ (degrees)
	L	D	T	l	d	t	
nominal	591	120	6	298	97	6	90
acrylic actual based on average	596	119.8	5.9	297	100.1	6.4	90

TABLE 3.3 INFLUENCE OF DOUBLE T JOINT ON SCF AND RATIO OF BENDING STRESS TO MEMBRANE STRESS, ACRYLIC MODEL DATA.

	SCF	<u>Bending Stress</u> Membrane Stress	<u>Bending Stress</u> Total Stress
Single Brace Model	7.68	7.17	0.879
Double Brace Model	7.47	7.95	0.888

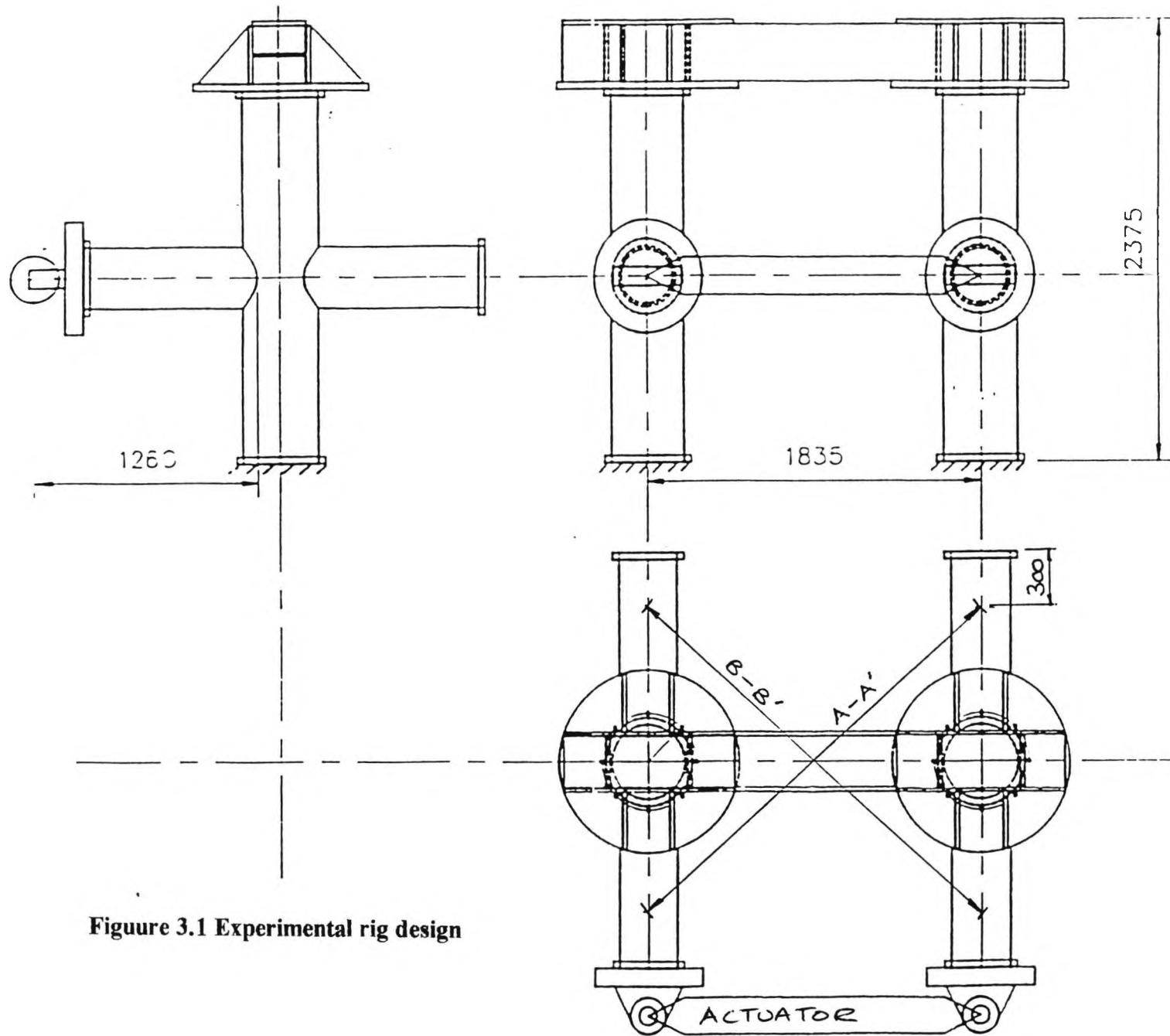


Figure 3.1 Experimental rig design

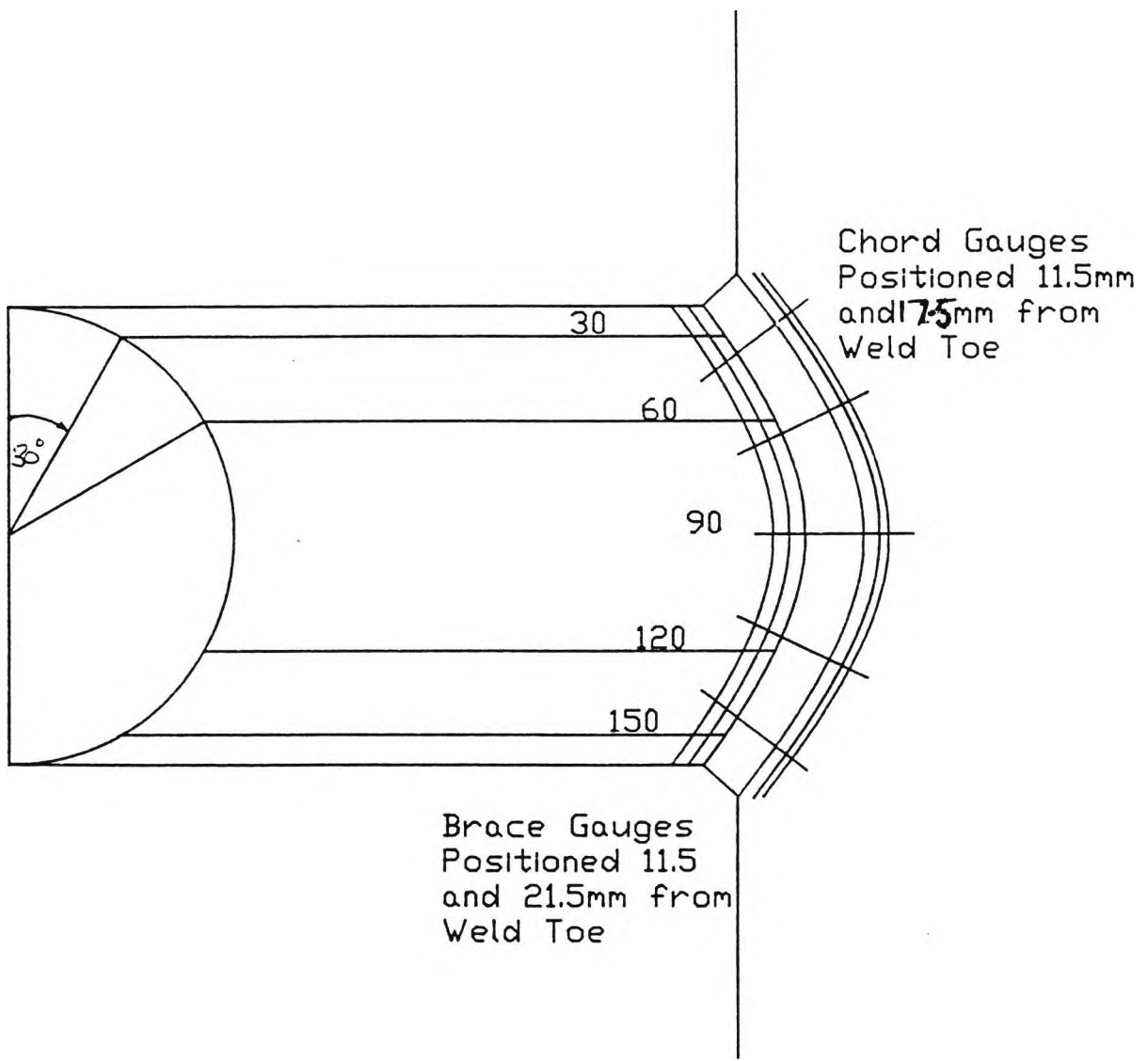


Figure 3.2 Position of strain gauges relative to weld toe

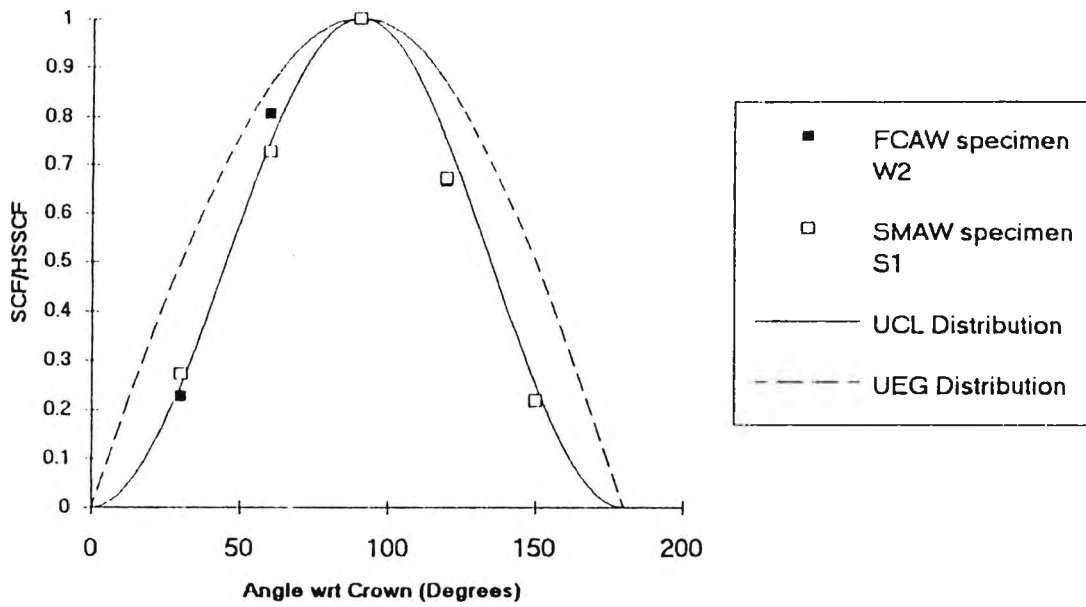


Figure 3.3 Experimental stress distribution (chord side)

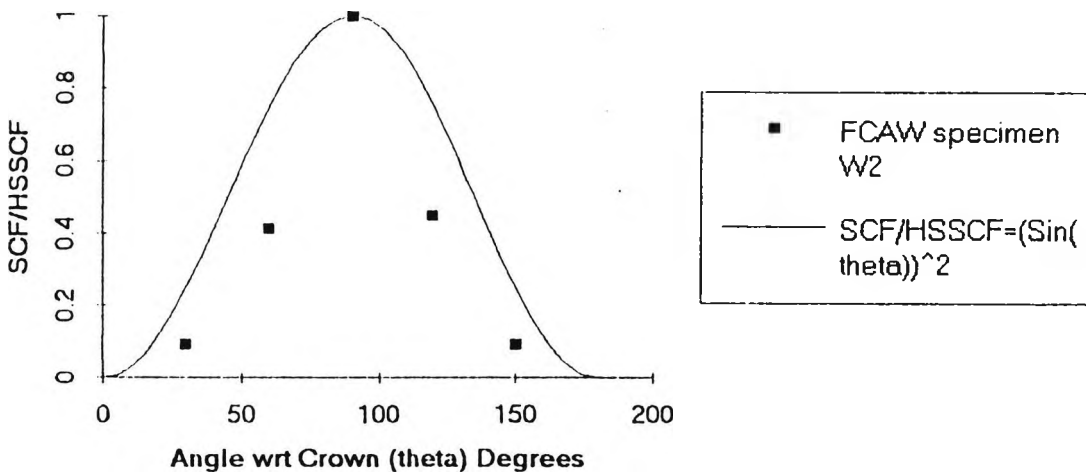


Figure 3.4 Experimental stress distribution (brace side)

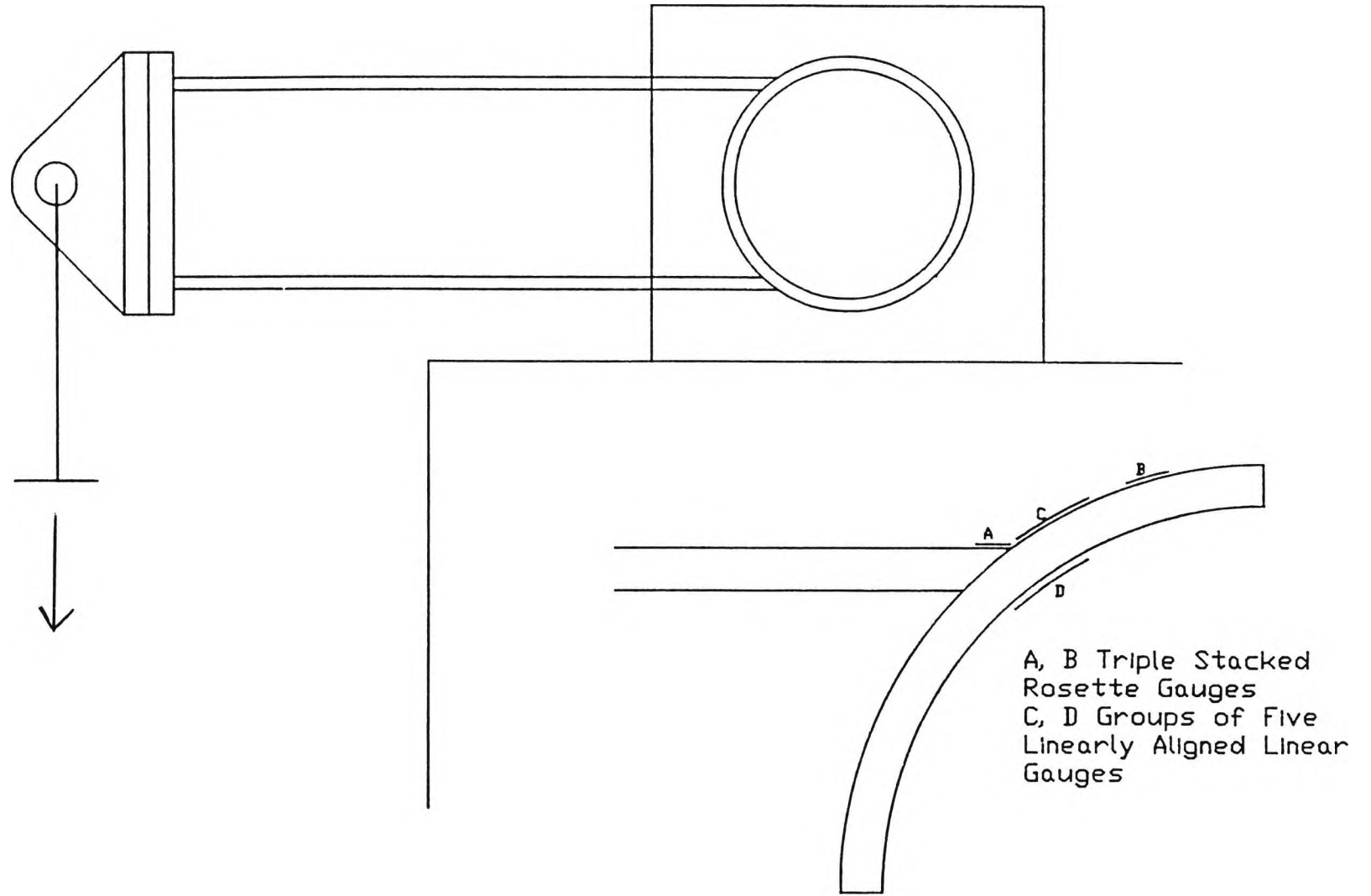


Figure 3.5 Position of strain gauges and loading of acrylic model

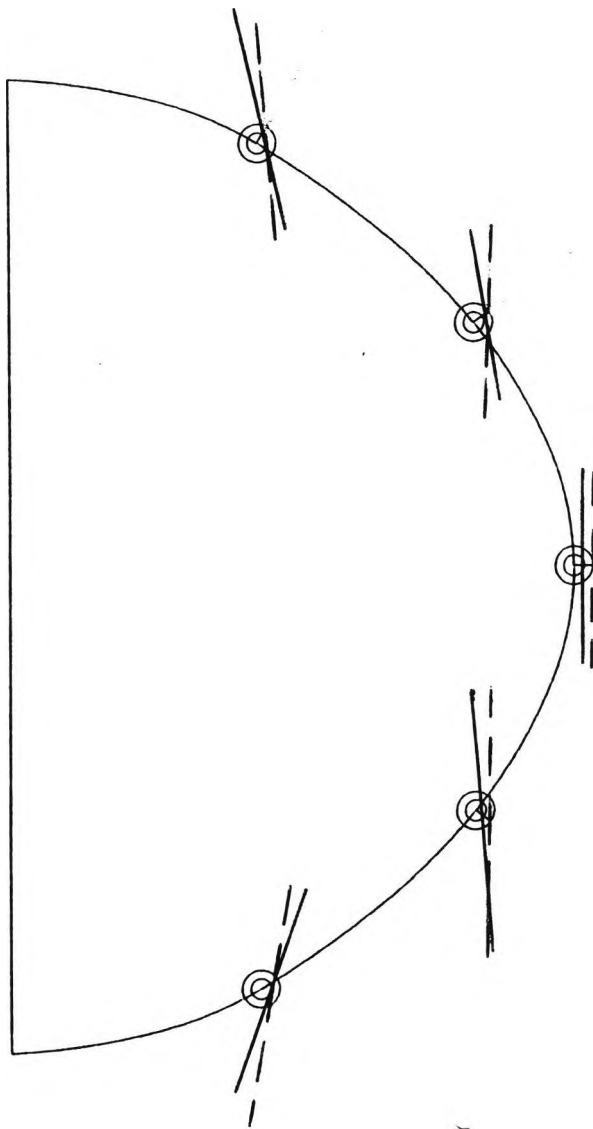


Figure 3.6 Inclination of principal stress plane as measured at rosette positions (Specimen W2)

- 11.5 mm from weld toe
- - - - - 17.5 mm from weld toe

4. FATIGUE TESTING OF STEEL TUBULAR JOINTS IN AN AIR ENVIRONMENT

4.1 Scope of Chapter

The purpose of this chapter is to describe the experimental procedure used to determine the stress intensity factor (SIF) for surface cracks in the tubular joints described in chapter 2. As the determination of the SIF is dependent on the Paris Law constants (section 1.4), the experimental determination of these constants is also described. The Y value is used to characterise the SIF and is determined experimentally for both the FCAW and SMAW specimens. The difference between the Y value equations for the FCAW and SMAW specimens is discussed. The empirical Y values are then compared to generalised empirical solutions for the SIF in a tubular joint and adapted plate solutions for the SIF.

The air fatigue experiments obtained initiation and endurance data for the X85 material. These data are compared against similar data obtained from BS4360.50D tubular specimens tested in an air environment.

4.2. Determination of the Paris Law Constants for API 5L X85

The Paris Law constants, m and C (equation 1.11), need to be determined prior to evaluating the Y value. Conservative design values of the Paris Law constants of offshore structural steels were reviewed in section 1.4.2.2 (see also figure 1.16). No data were established for Marathon Le Tourneau MM, X85 structural steel. For the purpose of this study, mean values of C and m need to be verified for Marathon Le Tourneau MM structural steel. As the Paris Law constants will be used to calibrate the Y values, the values of C and m should reflect mean crack growth rates, rather than the conservative design values. A secondary purpose of the following test is to establish if threshold SIF effects are significant for the SIF ranges experienced during the tubular joint tests.

The Paris Law constants were determined from fatigue tests of compact tension specimens, prepared from the same chord material as the tubular joints.

4.2.1. Test Set Up and Procedure

The test procedure for the determination of C and m is described in detail in British Standard 6835 [1988]. Compact tension specimens were used throughout. The dimensions of the compact test specimens are given in figure 4.1. Test coupons were cut from the chord material at least 100 mm from any weld or flame cut edge and the notch aligned in the L-T direction.

The specimens were fatigue tested using a 50 kN servo hydraulic test frame, controlled from a Dartec control console. Prior to testing, the load cell was calibrated using a proof ring. The crack depth was measured using the alternating current potential drop (ACPD) technique (see section 4.3.1). To minimise depth sizing errors, the initial crack depth indicated by the ACPD reading was subtracted from all subsequent depth readings to give the change in depth. The modified ACPD depth was then compared to the optically measured depth, ACPD readings were then adjusted to account for any discrepancy. All depth readings were based on the average of two readings at two sites. The ACPD readings were recorded regularly using a TSC U10 crack microgauge connected to a personal computer, via an automatic recording programme "Flair". The number of elapsed cycles were counted by use of an electronic counter attached to the test frame. The frequency, time and count were recorded at regular intervals. The compact tension specimens were precracked to a depth of 3 mm, using the procedure recommended in BS6835 [1988].

The compact tension test specimens were then tested at a relatively high R ratio of 0.7, in an attempt to reproduce the effect of high residual stress on crack growth in tubular joints. Two specimens were fatigue tested. One specimen was tested using a load range from 8 kN to 11.4 kN. The second test specimen was fatigue tested using a load range of 11.7 kN to 16.7 kN. The test frequency was set to 2.5 Hz and the wave form was monitored with an oscilloscope. Tests were conducted at a standard room temperature of 16-20 C.

4.2.2. Results

Crack growth readings were taken at approximately 0.5 mm intervals and corrected as described above. The corrected depth was then recorded against the number of elapsed cycles. The crack growth rate was determined using the seven point incremental polynomial method as recommended in ASTM E 647 [1993]. This fits a parabolic curve to seven experimental points and determines the slope from differentiation of the fitted parabolic curve. The SIF was determined, using the closed form approximation for the SIF for compact tension specimens [Srawley, 1976]:

$$\Delta K = \frac{1000\Delta P}{B\sqrt{W}} \times \frac{(2 + \alpha)(0.886 + 4.64\alpha - 13.32\alpha^2 + 14.72\alpha^3 - 5.6\alpha^4)}{(1 - \alpha)^{1.5}} \quad (4.1)$$

where: $\alpha = a/W$ and $\alpha > 0.2$

Values of the SIF range were plotted against the fatigue crack growth rate and are shown in figure 4.3.

4.2.3. Discussion of Results

The fatigue crack growth data for the two specimens agreed closely [1992] (figure 4.3). Inspection, showed that a Paris Law exponent of 3 was compatible with the experimental data. An exponent of 3 also agreed closely with crack growth data obtained for other materials (see section 2.3.2.). The Paris Law was modelled by setting m to 3 and using linear regression to determine the value of C. This resulted in:

$$10^{-8} \text{ m/cycle} < da/dN < 10^{-7} \text{ m/cycle} \quad da/dN = 8 \times 10^{-12} \Delta K^3 \quad (4.2)$$

units: MPa \sqrt{m} , m

The experimental data obtained fitted the above equation with a coefficient of determination of 99%, the high correlation justified setting the exponent m to 3. The experimental data for the X85 specimens, agreed closely with that shown for similar steels in figure 1.16. The mean values of C and m (quoted in equation 4.2 above), can therefore be used to determine the empirical Y value (equation 1.22) with a high degree of confidence. However, calculation of the remaining life of welded tubular joints requires conservative values of C and m. It is therefore recommended that the Paris Law constants for fatigue crack growth in X85 steel, in an air environment, are kept at C=9.5x10⁻¹² and m =3, as recommended by PD6493:1991.

The other principal finding of the compact tension air fatigue tests was that no evidence of threshold effects was seen in the interval 10 MPa \sqrt{m} < ΔK < 25 MPa \sqrt{m} .

4.3. Air Fatigue Testing of Steel Tubular Joints

The tubular joint air fatigue tests provided crack growth, fatigue endurance and fatigue initiation data. The crack growth data were used to determine the SIF from the empirical procedure outlined in section 1.4.2.4 (equation 1.22). This enabled the SIF to be characterised in terms of the hot spot stress, crack depth and Y value. This section describes the experimental procedure used to determine the SIF and to derive the Y value. Differences in the weld profile and possible variations in the residual stress distributions between the FCAW specimens and the SMAW specimens may

lead to differences in the Y value. It was therefore decided to test both the FCAW and SMAW specimens independently, to confirm the Y value calibration curve for each type of specimen. FCAW specimens were designated W1 to W6. SMAW specimens were coded S1 to S4.

4.3.1. Test Apparatus.

The test rig was described in section 3.2.1. The accurate determination of the crack depth is essential for the characterisation of the Y value. Crack depth was monitored using the ACPD techniques. Crack initiation was detected by using magnetic particle inspection MPI and by monitoring changes in the apparent depth as determined by the ACPD technique. The ACPD and MPI techniques are described below:

Magnetic Particle Inspection MPI

This is a quick and easily used method of detecting surface breaking defects down to very shallow depths. It operates by setting up a magnetic circuit around the suspected flaw site. If a crack is present within the circuit, there will be a certain amount of flux leakage around the flaw. If the flaw is then surrounded by finely divided ferromagnetic particles in suspension (magnetic ink), the ferromagnetic particles will be drawn to the flux leakage site and indicate the presence of the defect.

This technique is dependent on the strength of the magnetic field set up within the specimen. An electromagnet was used for this task. The strength of the magnetic field is measured using a "Burmah Castrol" strip. When placed in the magnetic field and sprayed with magnetic ink, the lines on the strip become visible, indicating the field is of sufficient strength.

For the purpose of these tests, a fluorescent magnetic ink, which glows in the presence of ultraviolet light was used. After testing with MPI, the specimen was demagnetised by slowly drawing the energised electromagnetic yolk away from the specimen.

The Alternating Current Potential Drop Technique

Crack depth monitoring was achieved using the Alternating Current Potential Drop method. This sets up an alternating electric field around the crack so that the current flows around the crack tip. The high frequency forces the current to flow in a thin layer close to the surface of the material using the "skin effect". The thickness of the current carrying layer, is given by the following formula:

$$d = (\pi\sigma\mu_r\mu_0f)^{-0.5} \quad (4.3)$$

where

μ_0	is the permeability of free space
μ_r	is the permeability the material
f	is the frequency of the alternating current
σ	is the conductivity of the metal

For a ferro-magnetic material such as the test specimen, the skin depth is in the order 0.1 mm at the chosen frequency of 5 kHz. A potential difference across the crack is generated, this is monitored using a two point contacting probe. The crack depth can then be determined using a simple one dimensional model:

$$d_1 = \Delta / 2 (V_c / V_r - 1) \quad (4.4)$$

where:

d_1	= one dimensional crack depth
Δ	= probe spacing
V_c	= voltage across crack mouth
V_r	= reference voltage drop adjacent to crack mouth

This formula is only true for long cracks with a thin skin effect. In the case of a crack with a significant crack aspect ratio, say $a/c > 0.1$, then a two dimensional modification factor called a multiplier is used [Collins & Michael, 1982]:

$$d_2 = d_1 M \quad (4.5)$$

where d_2 is the two dimensional multiplier ACPD crack depth and M is the multiplier.

One important condition of the ACPD technique, is that, in the event of the crack being inclined to the vertical, then the crack depth obtained is that of the inclined length, rather than the depth resolved to a plane perpendicular to the plate surface.

The accuracy of the ACPD technique has been the subject of several studies [Topp & Dover, 1987; Monahan *et al*, 1992; Dover & Monahan, 1994]. Dover & Monahan [1994] compared the true crack depth with the ACPD crack depth (equation 4.2), corrected where necessary for two dimensional effects, using machined T butt plates. They obtained the following correlation for a probe spacing of 10 mm:

$$(a/c < 0.1) \quad d_{\text{actual}} = (1.09d_1 + 0.09) \text{ mm} \quad (4.6)$$

$$(a/c > 0.1) \quad d_{\text{actual}} = (1.32d_2 - 0.03) \text{ mm} \quad (4.7)$$

Dover & Monahan have suggested that the accuracy of the ACPD technique at high aspect ratios is dependent on the ratio of probe spacing to crack depth. These findings cast doubt on the accuracy of the ACPD technique with high aspect ratio cracks, especially where the probe spacing is large with respect to the surface crack length (2c). However, comparison of measured crack depth with the ACPD crack depth for tubular joints tests, gave the following calibration for a 10 mm probe spacing [Dover & Monahan, 1994]:

$$d_{\text{actual}} = (1.05d_1 + 0.92) \text{ mm} \quad (4.8)$$

This gives a much lower proportional error, at the expense of a larger constant error. This is possibly due to more scatter in the tubular joint data than in the machined T plates. Dover & Monahan [1994] have also pointed out that the two dimensional modifier has been used successfully in the past for crack sizing in tubular joints.

Prior to fatigue testing of the tubular joints in the current test programme, the crack voltage, reference voltage and a calculated initial depth reading were determined. Subsequent depth readings were then adjusted to account for the initial depth reading and the two dimensional modifier. The initial crack depth was in the order of 1 mm and in agreement with equation 4.8. By adjusting the crack depth to account for the initial reading, the error was close to 5%. Given the previous successful use of ACPD multipliers, it was decided that the error was acceptable and no further correction factor was applied.

4.3.2. Experimental Test Conditions.

The hot spot stress was determined using the hot spot SCF, derived for individual specimens in chapter 3. The hot spot stress range for specimens W2, W3 and W4 was selected so that the endurance life of the test specimens would be less than 3 million cycles *i.e.* approximately 200 MPa. The target life was derived by assuming the endurance lives of the specimens would be similar to those of tubular specimens constructed from BS4360.50D and that the endurance life could be predicted from the T' curve adapted to give a 97.6% probability of failure (section 1.4.1.1). The hot spot stress range was raised for subsequent tests, when fatigue cracks failed to initiate in specimens W4 and W3. Details of individual test hot spot stress ranges are given in table 4.1.

Specimens were tested at the highest frequency the test equipment would permit, without distorting the sinusoidal load waveform. Where air tests were coupled to

seawater tests the test frequency was limited to 0.167 Hz. The load was varied sinusoidally and controlled through a function generator. The R ratio was set at 0.05 to prevent bearing damage in the rig and provide sinusoidal loading. The actuator was set to dump pressure in the event of the load exceeding 110% of the prescribed maximum load. The maximum load was also monitored independently with a peak reading digital volt meter.

The points of ACPD field injection were located so the reference voltage readings were as near uniform as possible. The crack depth was monitored at 10 and 5 mm intervals around the chord weld toe using spot welded terminals. The ACPD system was set up, so that the reference voltage at any site was greater than 80% of the maximum reference voltage to ensure a relatively uniform field. The probe signals were then multiplexed to an ACPD instrument, the Crack Microgauge [TSC, U10] and recorded automatically into a computer database [TSC, FLAIR].

The endurance lives of the specimens are defined by the following terms [HSE, 1992]:

N1: The first discernible surface cracking as noted by any available method. In the case of in air joints this was determined by noting the number of cycles at which ACPD readings showed an incontrovertible increase in crack depth and confirmed by MPI;

N2: Intermediate surface cracking as detected by optical examination without the use of crack enhancement or optical aids. It was decided that N2 would not be used in this analysis;

N3: First through wall cracking. In the case of air tests this can be determined by inspection of the inner surface of the chord wall and by a rapid increase in the indicated crack depth;

N4: End of Test as determined by extensive cracking or exhaustion of actuator stroke. It was decided that N4 would not be used in this analysis.

4.3.3. Experimental Results

W2 was reacted against W4; W1 was reacted against W3; W5 was reacted against W6; S1 was reacted against S3; and S2 was reacted against S4. Respective tests therefore have similar test histories. Only the air tests W2, W4, W3, W6 and S1 are considered in this chapter. Specimens W2, W6 and S1 were fatigue tested until the crack achieved partial or full chord penetration. The specimens were then sectioned. Section planes and positions along the cracked chord surface, were identified by their distance (in millimetres), from the crown position.

W2 (figures 4.4, 4.5, 4.6, 4.7)

W2 was fatigue tested at a hot spot stress range of 200 MPa. This test was designed to provide initial data for air endurance lives and the Y value calibration curve. During set up, the actuator became unstable and moved to the extended position. W2 and W4 both rotated by slipping on their restraining blocks. The magnitude of the possible overload was not measured. However, no visible physical damage occurred and the fault was rectified. The test was terminated at a recorded depth of 17.9 mm in W2 at 1,369,151 cycles, so that a comparison could be made between the recorded and actual crack size. Fatigue crack initiation, as defined by N1, was detected at 412,000 cycles. The ratio of N1/N3 was less than 0.3.

Figure 4.4 shows an external view of the fatigue crack. The fatigue crack initiated at 330 mm from the crown or 12° below the saddle position. The initiation site was at a weld overlap in an area of grinding parallel to the weld toe. The comparatively deep grinding marks may have contributed to the crack initiating at this site. The crack was confined to the weld toe in one direction, but grew away from the weld toe and into the chord material in the other direction. A second crack initiated at a position 260 mm from the crown and was not confined to the weld toe. Both of these cracks were parallel to the plane of maximum principal stress as measured in chapter 3 (figure 3.6).

Figure 4.5 shows a view of a section taken at 320 mm from the crown. The crack plane at the saddle position is approximately perpendicular to the brace axis, this is in contrast to that typical of fatigue cracks in tubular specimens and will be discussed later. The measured crack depth from the section at 320 mm from the crown showed the ACPD measurement at this section to underestimate the crack depth by only 6%. There was no evidence of crack branching in this specimen so depth readings can be assumed to be accurate for most of the test.

Figure 4.6 shows the crack depth as a function of distance from the crown position. Comparison with figure 4.4 shows two separate cracks. Unfortunately, the depth of the secondary crack could only be effectively measured at position 260 and 250 because of the position of the ACPD probes in relation to the crack. A line contact was identified at position 290. A line contact is where an electrical short bridges the crack and leads to an underestimate of the crack depth. For this reason the crack depth reading at position 290 was disregarded. The primary crack had an approximate semi elliptical shape, typical of surface flaws in tubular joints. The aspect ratio was estimated from figure 4.6. The variation in the aspect ratio with the crack depth is shown together with the aspect ratio variations from other tests in figure 4.18.

The crack depth has been corrected for the two dimensional AC field. Crack depth readings for the primary crack at the deepest position are shown in figure 4.7. The crack grew to a depth of 8 mm, at a steadily increasing rate in a direction normal to the weld toe, this was followed by an acceleration in crack growth (to 10 mm) and then by approximately constant crack growth.

W4

No sign of crack initiation was recorded at a hot spot stress range of 191 MPa at 1,369,151 cycles, when the test was terminated.

W3

W3 was tested in air at a hot spot stress range of 207 MPa for 3,085,000 cycles. This test was designed to provide endurance life data and to corroborate the Y value calibration curve derived in test W2. No crack was detected on termination of the test.

W6 (figures 4.8, 4.9, 4.10)

W3 was retested as W6 at a hot spot stress range of 310 MPa. The test was terminated when the crack in the corresponding corrosion fatigue specimen W5, penetrated the chord wall. The aim of test W6 was to provide endurance life data and to corroborate the Y value calibration curve derived in test W2, but at a higher hot spot stress level than test W3. All cycle counts for W6 were taken from the point at which the hot spot stress was increased to 310 MPa. A fatigue crack started growing in specimen W6 as soon as the hot spot stress range was increased to 310 MPa. The crack penetrated the chord wall at approximately 317,000 cycles. Chord wall penetration was determined from a sudden change in the ACPD crack voltage.

Figure 4.8 shows an external view of the fatigue crack. The crack initiated at the saddle position and grew along the weld toe, except for the region greater than 320 mm from the crown where it deviated away from the weld toe and into the chord and at position 140 where the crack deviated into the chord material.

Sections were cut at the positions shown in figure 4.8. In common with W2, the crack plane at the saddle position was approximately perpendicular to the brace axis. Sections cut at 205, 220 and 240 show evidence of crack branching. Sections cut at 260 to 340 showed no evidence of crack branching. The measured depth of 22 mm at section 280 agreed closely with the ACPD recorded depth of 22 mm.

Figure 4.9 shows the crack depth as a function of distance from the crown position. Unfortunately, the crack depth could only be effectively measured at position 130 to

310 because of the position of the ACPD probes in relation to the crack. As the test was stopped at 423,000 cycles, the crack depth at sections 280 to 320 continued to increase after the 317,000 cycles profile, shown in figure 4.9. The profile was principally of value in estimating the aspect ratio. The variation in the aspect ratio with the crack depth is shown together with the aspect ratio variations from other tests in figure 4.18.

The crack depth was corrected for the two dimensional field. Crack depth readings for the crack at the deepest position are shown in figure 4.10. The fatigue crack growth plot shows a gradual transition from increasing crack growth rates to constant crack growth rates.

S1 (figures 4.11, 4.12, 4.13)

S1 was tested at a hot spot stress range of 300 MPa until the crack in the corresponding corrosion fatigue specimen S3, showed indications of gross failure. This test was designed to provide endurance life data and the Y value calibration curve for the SMAW specimens. A fatigue crack initiated in specimen S1 at approximately 43,000 cycles. The fatigue crack was terminated at a crack depth of 33 mm after 327,000 cycles. The ratio of N1/N3 was less than 0.13. The low ratio of N1/N3 was representative of typical tubular joints (section 1.4.2.3).

Figure 4.11 shows an external view of the fatigue crack and sectional views of the crack. The crack initiated at the saddle position and was confined to the weld toe. This was in contrast to the deviation away from the crack path away from the weld toe shown in specimens W2 and W6. The crack path shown in the sectional views, contrasted with that of specimens W2 and W6. The path of the crack in specimen S1 was initially along a plane normal to the weld toe, but then deviated to grow along a plane approximately parallel to the chord wall. Some signs of crack branching were evident, especially at sections further away from the saddle e.g. sections 230 and 380. However, at the saddle itself, no branching was evident and the measured section length was in close agreement with the recorded ACPD depth of 33 mm.

Figure 4.12 shows the uncorrected crack depth as a function of the distance from the crown position. The crack aspect ratio was estimated using this diagram. The variation in the aspect ratio with the crack depth is shown together with the aspect ratio variations from other tests in figure 4.18.

The crack depth was corrected for the two dimensional field. Crack depth readings for the crack at the deepest position are shown in figure 4.13. The fatigue crack growth

plot shows a gradual transition from increasing crack growth rates to constant crack growth rates, typical of that seen in other tubular joints.

Crack Fractography

It was noted that the crack plane observed in the FCAW specimens was approximately perpendicular to the brace axis, and the crack plane observed in the SMAW specimens was approximately parallel to the chord wall. This was in contrast to that typical of fatigue cracks in tubular joints (figure 4.14). The fracture surfaces were examined using a scanning electron microscope to see if there were any other distinctive features.

The crack surface of specimen W3/ W6, as shown in figures 4.15a and 4.15b, was typical of the crack surfaces of the FCAW specimens. Figure 4.15a shows the crack surface for early crack growth ($a < 4$ mm). This was distinguished by growth on a plane normal to the weld toe. The fracture surface was relatively smooth. Figure 4.15b shows crack growth for later crack growth ($a > 4$ mm). Later crack growth was distinguished by a fibrous appearance. Due to the irregular surface, features typical of fatigue crack growth, such as striation banding and beach marking could not be seen.

The crack surface of the SMAW specimen S1 is shown in figures 4.16a and 4.16b. Figure 4.16a shows the crack surface for early crack growth. The crack surface is comparatively smooth and on a plane normal to the weld toe, similar to the early crack growth surface of specimen W6 (figure 4.15a). Figure 4.16b shows later crack growth. Later crack growth was characterised by flat platelets approximately parallel to the chord surface.

In addition, the chord plate was sectioned along a plane parallel to the rolling direction and perpendicular to the chord surface. This section was then polished and examined under an optical microscope. Figure 4.17 shows the polished surface, several "stringers" were observed. These stringers were due to iron manganese sulphide compounds, segregating out at the grain boundaries during solidification of the steel and being rolled flat during the rolling process. The inclusions, formed natural planes of weakness within the steel and gave a preferential path for crack growth. These inclusions were believed to be responsible for the flat platelets observed in figure 4.16b.

4.3.4 Discussion of Results

4.3.4.1 Fatigue Crack Propagation.

The deviation of the dominant crack away from the weld toe noted in specimens W2 and W6 was in contrast to the adherence of the surface crack to the weld toe noted in specimen S1. This was probably due to the difference between the weld toe radii and the difference in the notch stresses. The high notch stress of the SMAW technique, forced the crack to conform to the weld toe and grow laterally along the weld toe. In the case of the FCAW technique, the notch stresses were much lower and the crack was free to grow laterally along the plane of maximum principal stress (see figure 3.6). The FCAW crack was therefore straighter than the SMAW crack when viewed from the outside of the chord.

The sectional views of W2 and W6 showed crack growth on a plane perpendicular to the brace stub, this contrasted with crack growth in similar joints of BS4360.50D structural steel, which was on a plane perpendicular to the chord surface (figure 4.14). This supports the view that the plane of principal stress was perpendicular to the brace stub and that there were substantial through thickness stresses in the X85 test specimens. The crack path of both the FCAW and SMAW specimens differed significantly from those typical of previous tubular joint experiments. Spurrier and Healy [1995], have proposed a mechanism which suggests that mismatch between the yield strength of the parent plate and weld metal can lead to an imbalance in the size of the plastic zones either side of the crack tip. This in turn can lead to the crack deviating towards the lower yield strength material. Comparison of the weld metal yield strengths of the FCAW and SMAW specimens with the parent plate yield strength (see table 2.4) show that the weld metal is undermatched. This would cause the crack to grow in the direction shown in figures 4.5 and 4.11. However, it should also be pointed out that the deviation was greatest in the SMAW specimen, where the degree of mismatch was lower. It therefore seems probable that although mismatch could have led to an initial deviation of the crack towards the weld metal, the dominant stress field and manganese sulphide inclusions were responsible for the marked difference between the SMAW and FCAW crack paths.

The later stages in fatigue crack growth in specimen S1 were characterised by growth on a plane nearly parallel to the chord surface. From inspection of the fracture surface it could be seen that crack growth in this plane was associated with manganese sulphate "stringers". The presence of these inclusions provided a preferential path for the cracks to run along (see figures 4.16b and 4.17). This raises the question, why do the SMAW and FCAW specimens show different crack growth paths? It is suggested

that the crack in the SMAW specimen was forced to conform to the weld toe, whereas the lateral growth of the FCAW crack was not restrained by the weld toe. As the crack in the SMAW specimen extended around the weld toe, the crack front would become a continuous straight front. Evidence for this is provided by comparing the sectional views of crack S1, to the outside view. This would have had the effect of turning the crack, so that the plane of crack growth was closely aligned to that of the manganese sulphate inclusions. The SMAW crack would then grow on a plane parallel to the chord surface, whereas the FCAW cracks would grow on the plane of principal maximum stress.

Fatigue tests on ring stiffened joints carried out at the National Engineering Laboratory [Slater, 1991], have shown similar crack growth paths to those of the FCAW and SMAW specimens. However, ring stiffened joints are known to be subject to through thickness stresses. The similarity between the crack growth paths of the ring stiffened joints and the test specimens, supports the view that there are substantial through thickness stresses in the test specimens. The presence of through thickness stresses in unstiffened tubulars has important implications for the fracture mechanics analysis of crack growth. Many fracture mechanics models assume that the crack is perpendicular to the chord wall and that the stress system can be represented by tension and bending stresses in the chord wall. If, as suggested, the through thickness stress component is not negligible, then the crack cannot be represented by a simple plate model. The effect of geometry on the stress system should be investigated, with the aim of determining the value of the non dimensional geometric parameters, at which the through thickness stress component becomes significant. This may be especially important for jack up tubular joints, where the chord wall is often thick in comparison to the chord diameter and the chord wall may be stiffened by the rack.

The variation of the crack aspect ratio with crack depth is shown in figure 4.18. Monahan [1994] has developed an expression for the crack aspect ratio in terms of the crack depth for tubular joints, the CSC function, based on data obtained from tubular joint tests:

$$\frac{a}{2c} = 291 \times 10^{-0.023/(S-1)} \cdot (S-1)^{0.66} \cdot (a/t)^2 \cdot e^{-25.7a/t} + 0.11(a/t)^{0.60} \quad (4.9)$$

$$\text{for } .31 \leq S \leq 2.52$$

where: S is the average stress parameter defined as:

$$S = S_{HS} / S_{AV} \quad (4.10)$$

$$S_{AV} = (1/\pi) \int_0^{\pi} S_c(\phi) d\phi \quad \text{for axial and OPB} \quad (4.11)$$

$$S_{AV} = (1/\pi) \int_{-\frac{\pi}{2}}^{\frac{\pi}{2}} S_c(\phi) d\phi \quad \text{for IPB} \quad (4.12)$$

($\pi/2$ is the saddle position).

From figure 4.18 it can be seen that, for crack growth greater than 20% of the chord thickness, the crack aspect ratio is similar to that of other tubular joints. There is less agreement at shorter crack depths, but this may be due to inaccuracy in determining the aspect ratio for short cracks ($a < 0.2t$). The crack aspect ratio of the air and corrosion fatigue tests should be similar if the Y value of the air fatigue test is to represent the Y value of the corrosion fatigue tests.

Some crack branching was observed in specimen W6. It is thought that branching in section 240 may have occurred after the crack penetrated the chord wall at 280. This is because the chord wall would bend, once the crack penetrated the chord wall at position 280. The branching seen at position 220 was due to multiple crack interaction. Other branching was observed in specimen S1, at sections 380 and 230. This was believed to be due to the presence of manganese sulphate inclusions. The presence of crack branching, was not thought to have influenced the crack depth measurements used in the fracture mechanics analysis.

4.3.4.2. Fracture Mechanics Analysis

The crack growth rates for the test specimens, were all characterised by a gradual transition to constant crack growth rates. This is typical of fatigue crack growth in tubular joints [Dover *et al*, 1986]. The exception to this is a rapid increase in crack depth observed in specimen W2 in the region $a \approx 10$ mm. The reason for the rapid increase in the crack growth rate is unclear. However, it may have been linked to either crack coalescence between the primary and secondary crack, or to the presence of a large inclusion. There is no evidence from the section data to indicate the presence of a large inclusion.

The crack growth data for specimens W2 and S1 was shown to be accurate. It was therefore assumed that crack growth data from tests W2, W6 and S1 could be used to obtain an empirical Y value calibration chart. The crack depth and rate of crack growth were determined for the deepest point in each crack. With the exception of W2, the deepest point of the crack was located close to the saddle. A computer program was written to determine the crack depth and crack growth rate, using the

seven point incremental polynomial method [ASTM E647, 1993]. This method fitted seven data points to a parabolic equation of a vs N , and obtained the fitted crack depth and crack growth rate for the third data point. This procedure was repeated for successive data points. In the event of a major discontinuity in the crack growth rate, such as observed in specimen W2 at a depth of 10 mm, three data points either side of the discontinuity were disregarded.

The SIF was obtained by transformation from equation 4.2. Figure 4.19 shows the SIF as a function of crack depth for specimens W2, W6 and S1. It can be seen that the SIF fell within the range $8\text{MPa}\sqrt{\text{m}} \leq \Delta K \leq 28\text{MPa}\sqrt{\text{m}}$. This was in close agreement with the data range used to establish equation 4.1. It was therefore reasonable to characterise the SIF using equation 1.22. The calibration chart of Y value against crack depth for all the air specimens is shown in figure 4.20.

FCAW specimens

The Y value data for the FCAW specimens W2 and W6 (figure 4.20), showed close agreement in the region $0.07 < a/T < 0.15$ and $0.5 < a/T < 0.8$. Crack growth data for specimen W2 in for the region $0.15 < a/T < 0.5$ was disregarded because of the anomalous effect of the discontinuity in the crack growth rate. The data for specimens W2 and W6 were fitted to a log Y versus log (a/T) line using a least squares regression curve. The Y value for the FCAW specimens was modelled by:

$$Y_{\text{exp}} = 0.3279\left(\frac{a}{T}\right)^{-0.3077} \quad (4.13)$$

with a coefficient of determination of 0.969.

SMAW specimen

Only one curve was available for SMAW specimens and this was for test S1. The data for S1 is included in figure 4.20. The data for specimen S1 were fitted to a log Y versus log (a/T) line using a least squares regression curve. The Y value for the SMAW specimens was modelled by:

$$Y_{\text{exp}} = 0.354\left(\frac{a}{T}\right)^{-0.3768} \quad (4.14)$$

with a coefficient of determination of 0.998

Discussion of the Experimental Y Calibration Chart

Figure 4.20 shows the following features:

Firstly, there appears to be close agreement between the Y values of specimen W2 and W6 in the region $0.07 < a/T < 0.15$ and $0.5 < a/T < 0.8$. This confirms that the Y value is independent of the hot spot stress range. Since some of the W2 data was excluded from the best fit analysis, equation 4.13 should be used with caution;

Secondly, data points for S1 were remarkably consistent with the log normal, best fit line. Crack growth in the region of the weld toe and crack growth parallel to the chord surface had quite different crack surfaces. The latter was influenced by growth along flat plates associated with manganese sulphate inclusions (figures 4.16b and 4.17). One would expect that the crack growth rate would be influenced by the presence of the manganese sulphate inclusions and that higher crack growth rates would be reflected in the Y value calibration chart. In fact, the consistency of the Y value calibration chart, suggests that the presence of the inclusions had less influence on the crack growth rate than might be expected. The SMAW, Y calibration curve can therefore be used with a high degree of confidence;

Thirdly, there was considerable difference between the Y value curves for the W and S type cracking in the region $a/T < 0.4$. This was due to a considerably slower rate of crack growth for the FCAW specimen cracks, compared to the SMAW specimen cracks at a depth of $a < 0.4T$. It is suggested that the principal reason for the difference in the Y value was due to the difference in the local weld toe geometry and associated weld toe notch stresses. Thurlbeck & Burdekin [1992] have modelled the effect of weld toe radius and weld angle on the SIF for weld radii of up to $0.5T$, and found that the weld radius has a strong influence on the SIF in the region $0 < a/T < 0.2$. However, this does not fully account for the difference between the Y values of the weave welded FCAW specimens compared to the stringer welded SMAW specimens, shown in region $0.2 < a/T < 0.4$.

The influence of the residual stress distribution on the crack growth rate was discussed in section 1.4. The residual stress distribution in the FCAW specimens is unknown, but it was thought that the peak residual stress in the FCAW specimen may be lower than the peak residual stress level of the SMAW specimen. If the FCAW process resulted in residual stresses being relieved to such a degree that the maximum stress was below the yield stress, the value of C in the Paris law might effectively be lowered, resulting in a lower crack growth rate. However crack growth data for BS4360.50D, showed that the mean stress ratio had relatively little influence on region II of the Paris fatigue crack growth (see section 1.4.2.3) provided that the minimum stress was tensile. Changes in the residual weld stress were therefore thought to have little influence on the crack growth rate for fatigue specimens tested in an air environment.

Finally, Y values for the S and W type cracks converged at crack depths of a/T greater than 0.4. At these depths manganese sulphate inclusions were aligned with the plane of fatigue crack growth in the SMAW specimen, whereas the inclusions were not aligned to the plane of fatigue crack growth in the FCAW specimen. The convergence of the Y values would suggest that the crack growth rate was not influenced by the change in the orientation of the crack growth plane. This was a surprising result, as the inclination of the crack plane to the plane of principal stress and the plane of any inclusions would be expected to have a direct influence on the crack growth rate. The evidence from crack growth data for depths of a/T less than 0.4 and the consistency of Y value data for specimen S1, supports the contention that the presence of manganese sulphate inclusions has an influence on the crack growth path, but has little influence on the crack growth rate.

The Y value calibration chart for the FCAW process was shown to be different to that of the SMAW process. In addition, the fatigue crack paths in the FCAW and SMAW specimens were shown to differ. The type of cracking shown in S1, section 310 (figure 4.11) was defined as S type cracking and that shown in W6, section 280 (figure 4.8) was defined as W type cracking. It is uncertain whether the crack path or the weld process determined the SIF and the Y value. It was therefore decided that type S cracking should be associated with the Y value calibration curve for the stringer welded SMAW specimens, and type W cracking should be associated with the Y value calibration curve for the weave welded FCAW specimens.

Comparison of Experimental Data with Generalised Fracture Mechanics Solutions

Various techniques for determining the SIF for a surface crack in a tubular joint were reviewed in section 1.4. Of the techniques discussed, the empirical AVS and TPM equations were derived using a similar technique to the empirical method described above. The advantage of these equations is that SIF can be determined for a variety of tubular joint geometries and loading cases. However the AVS and TPM equations cannot be used outside the specified validity limits.

The advantage in using adapted plate solutions for surface breaking cracks in tubular joints is the potential applicability of these equations to a wide variety of tubular joints and non tubular joints. The adapted plate solutions assume that a crack in a tubular joint is analogous to that of a surface breaking crack in a flat plate, where the through thickness component of stress is negligible. However, flat plate solutions are invalid where the through thickness component of stress is considerable. The use of

adapted plate solutions was therefore considered inappropriate for the specimens described in this test.

It may be possible to extend the use of the AVS and TPM equations to the crack growth data obtained in the current programme. Both the AVS and TPM models are derived by curve fitting crack growth data for BS4360.50D steel tubular joint air fatigue tests conducted in a similar manner to those described above. The AVS model fits crack growth data to a single curve, whereas the TPM model fits crack growth data to two curves split at $a = 0.25T$.

The AVS model is given as:

$$Y = D(T)P(T/a)^j \quad (4.15)$$

D , p and j were observed to vary linearly with the average value of the stress concentration factor S (equation 4.9):

$$D = 1.18 - 0.32S$$

$$p = 0.13 - 0.02S$$

$$j = 0.24 + 0.06S$$

The empirical nature of the formula means that the following validity limits apply:

- $2.66 < S_c < 9.1$
- $1.5 < S_{AV} < 6.35$
- S_{AV} defined in equations 4.10 to 4.12
- Formula is only empirically derived for $t = 16$ mm.

The TPM model is given as:

$$Y = M_I B (T/a)^k \quad (4.16)$$

for $a/T < 0.25$: $M_I = (0.25T/a)^{-P}$

and $a/T > 0.25$ $M_I = 1$

where : $B = (0.669 - 0.1625S)(T/0.016)^{0.11}$

$$k = (0.353 + 0.057S)(T/0.016)^{-0.099}$$

$$p = 0.231(T/0.016)^{-1.71}(\beta)^{0.31}S_c^{0.18}$$

and the following validity limits apply:

- $0.21 < \beta < 0.76$
- $2.66 < S_c < 9.4$
- $1.51 < S_{AV} < 6.35$
- $16 \text{ mm} < t < 45 \text{ mm}$

The transverse stress distribution in the circumferential direction (equation 3.4) is used to derive the AVS and TPM equations. The data from specimen S1 agreed closely with those obtained from the AVS model, however the TPM model was slightly more conservative. This was not surprising as the AVS and TPM models were derived for string welded specimens. However, the difference between the crack path typical of a X85 steel tubular and a BS4360.50D specimen was expected to lead to a significant variation in the Y value. In reality, the crack path appears to have only a small influence on the Y value. Both the AVS and TPM methods could be used to derive the air fatigue crack growth rate in string welded, SMAW tubular specimens.

The data from tests W2 and W6 agreed less closely with the AVS and TPM calculated Y values. The reasons for this are similar to the reasons for the difference between the FCAW and SMAW, Y values and are thought to be principally due to the effect of the large weld toe radius. However, both the AVS and TPM methods of calculating the Y value could be used to derive a conservative value of the air fatigue crack growth rate in weave welded, FCAW tubular specimens.

4.3.5 Stress Endurance Results

The following section makes a comparison between the N1 and N3 endurance lives obtained for specimens W2, W3, W4, W6 and S1, with the endurance life predicted using the T' curve (equation 1.3). N1 and N3 results from the current programme are also compared with data from out of plane bending, fatigue tests conducted on 457 mm diameter chord specimens of 16 mm chord thickness BS4360.50D tubular specimens [HSE, 1992]. All results were standardised to a 20 mm wall thickness using equations 1.4 and 1.6. The results for the endurance life of the API 5L X85 tubular joints were too few to allow statistically significant conclusions to be made. Individual results are reported in table 4.2.

4.3.5.1 N1 Endurance Data

Crack initiation in welded tubular joints was discussed in section 1.4.2. It was noted that initiation was assumed to take place from pre-existing flaws, due to slag inclusions or weld defects. The initiation life for a welded tubular joint has been approximated by N1, where N1 is the first discernible sign of cracking by any available means. The determination of N1 is clearly dependent on the resolution of the detection method. The use of MPI allows the detection of cracks of approximately 4 mm long and 0.6 mm deep [Kare, 1989], whereas the resolution of the ACPD method was dependent on the position of the probes relative to the crack. For specimens W2, W6 and S1 it proved possible, once the crack had been detected using MPI, to examine the ACPD crack growth readings and determine at which point the crack started increasing in depth. This allowed for a lower estimate of N1 than would be possible using MPI alone and allowed detection of crack initiation to a depth of approximately 0.3 mm..

The results obtained from the current test programme were too few to allow a statistically significant assessment of the effect of yield strength on the N1 life, or to quantify the effect of the welding process on the N1 life. However, comparison of the N1 life of the X85 steel tubular joints and the N1 life for BS4360.50D steel joints (figure 4.22) allows a qualitative assessment of the effect of yield strength and welding process. The N1 lives of the specimens are also presented in table 4.2.

The weld toe radius and weld process were thought likely to have an influence on the initiation life. The effect of yield strength is therefore best assessed, by comparing the N1 life of specimen S1 with the BS4360.50D tubular data, since the BS4360.50D specimens were welded under similar conditions and have a similar weld profile. Figure 4.22 shows that the N1 life of S1, is within the range of N1 data for the BS4360.50D tubular joints. There was no evidence for an improvement in the N1 life as a result of using higher yield strength steels.

The effect of the welding process on the N1 life was assessed by comparing the data for test W3 with that of S1 and the BS4360.50D tubular data. The N1 life of W3 was greater than the 97% probability of N3 failure for the BS4360.50D specimens. This indicates an improvement in the fatigue life as a result of the welding process. The N1 life of specimen W2 was comparable to that of the BS4360.50D specimens, however this data was compromised by a possible overload. In addition, the poor weld profile shown in figure 2.5, indicated that an extended initiation life in the OPB loading mode may have been at the expense of a reduced initiation life in other modes of loading.

A possible reason for the extended initiation life of the FCAW specimens compared to the SMAW specimens, is that stress intensity factor threshold effects (section 1.4.2.4) are responsible. Small cracks varying in size from 0.1 to 0.4 mm deep are usually present at the weld toe (section 1.4.2.1). Fatigue cracks would propagate from these flaws, provided that the stress intensity range was greater than ΔK_{TH} . The stress intensity factor range can be modelled using equations 4.12 and 4.13. This assumes that crack growth can be described using linear elastic fracture mechanics for cracks as small as 0.1-0.4 mm. Recent work by Monahan [1994] suggested that linear elastic fracture mechanics can be successfully applied to cracks in tubular joints of 0.3 mm deep. However, linear elastic fracture mechanics may apply at even shorter cracks, provided there is no notch plasticity. From figure 4.23 it can be seen that at a hot spot stress range of 200 MPa, a 0.1 mm deep crack in a FCAW corresponded to $\Delta K \approx 6$ MPa, whereas identical conditions in a SMAW specimen corresponded to $\Delta K \approx 9$ MPa. Austin *et al* [1992] have suggested that a stress intensity factor threshold of $7\text{MPa}\sqrt{\text{m}} \leq \Delta K \leq 9\text{MPa}\sqrt{\text{m}}$ was applicable to fatigue crack growth in tubular joints constructed from BS4360.50D. No SIF threshold data was available for the X85 steel, but the existence of a SIF threshold in the region suggested by Austin, would explain the lack of crack initiation in the FCAW specimens at a hot spot stress range of 200 MPa. It should be noted that raising the hot spot stress range to 300 MPa would raise the SIF range to above the threshold level suggested by Austin (figure 4.22), and result in immediate propagation in the FCAW specimen. This was observed in specimen W6. It follows that lowering the hot spot stress range to 150 MPa, would lead to greatly improved N1 lives for the FCAW specimens compared to the SMAW specimens, even with lower strength steels. Evaluation of the initiation life using a strain life approach would require additional material data (section 1.4.2.1).

It is interesting to note that no crack initiated at the intersection of the inner brace wall to the chord of W2 (figure 4.5), despite the lack of weld penetration. The initiation of cracks at the inner brace/ chord intersection has been a cause for concern in tubular joint design, partly because such a crack would be extremely difficult to detect. Although it is not possible to generalise on the basis of one result, the lack of fatigue initiation despite an ideal "starter notch", should provides reassurance to those involved with certification and inspection.

4.3.5.2 N3 Endurance Results

Direct comparison between the T' curve and the FCAW specimens was provided by test W3. Test W3 provided evidence that the fatigue life of the FCAW specimens exceeded that predicted by the T' curve (see figure 4.23). The extended fatigue life was due to an extended N1 life and was discussed above. However, the comparatively

low experimental Y value of fatigue cracks in the FCAW specimens (figure 4.20) indicate that the fatigue crack propagation lives of the weave welded specimens were longer than those typical of the string welded joints. The extended N1 and slower crack growth rate should lead to an extension in the N3 endurance life.

The fatigue life of test W6 was approximately equal to that of the BS4360.50D specimens even though the specimen had been previously tested as W3 (figure 4.23). The endurance results for W2 and W4 were compromised by a possible overload. However, the total fatigue life for specimen W2 was greater than or equal to that of the BS4360.50D specimens. The evidence is that the existing fatigue endurance guidelines predict a conservative value for the endurance life of the weave welded FCAW, X85 tubular joints. There is some evidence that the joints constructed using the FCAW welding process, have a longer endurance life than those predicted by the T' curve, particularly at lower hot spot stress ranges. However, the quality of the FCAW process would need to be improved and more joints would need to be tested before any improvement on the existing T' curve, could be recommended.

The S type crack growth plane, reported for the SMAW specimens, was almost parallel to the chord surface, this was in contrast to "typical" tubular joint crack growth. If the N3 definition of chord life is applied to S type fatigue crack growth, unusually high endurance lives are noted as a result of the increased path length. It therefore seems reasonable to relate the damage to the crack length. For convenience a new definition of endurance has adopted, N3*. N3* is defined as the number of cycles for a crack to grow to a length equal to the chord wall thickness, measured using the ACPD technique. The loss of stiffness and the residual yield strength of N3* for an S type crack, should be approximately equivalent to that of N3 for a conventional through thickness crack, given the same aspect ratio. While the difference between N3* and N3 was considerable for S type cracking, the difference for W type cracking was less.

Fatigue testing of specimen S1 was terminated at a depth of 33 mm, before the crack penetrated the chord wall. The N3* endurance life was determined from figure 4.13. Comparing N3* with figure 4.23, one can see that the N3* life was similar to N3 data obtained from BS4360.50D tests. It should be noted that the N1 life, Paris Law data and Y value calibration data, for the SMAW specimen were similar to those of the BS4360.50D tubular specimens. One would therefore expect a similar total life to that of the BS4360.50D tubular joints. The evidence suggests that the existing fatigue endurance guidelines can be used for SMAW specimens constructed from API 5L X85 steel, to predict a conservative value for the endurance life. However, more joints

would need to be tested before the T' curve could be verified, or adapted for use with X85 grade tubular joints.

It was suggested, that the improvement in fatigue life was primarily due to the low notch stresses associated with the weave welded, FCAW process. The advantages of the low notch stresses could be combined with the higher toughness values of the stringer welded, SMAW process by weld toe grinding or TIG dressing the stringer welded joints. The use of weld improvement techniques with high strength steel joints is worthy of further research.

4.4. Conclusions

1) It has been established that crack growth in an X85 steel, for the range $10 \text{ MPa}\sqrt{\text{m}} < \Delta K < 20 \text{ MPa}\sqrt{\text{m}}$, can be described using the Paris Law with values of $C=8 \times 10^{-12}$, $m = 3$ (units $\text{MPa}\sqrt{\text{m}}$).

2) The fatigue crack growth path for the tubular specimens tested in the current test programme, have been shown to differ from typical crack growth paths in tubular joints tested in previous test programmes. It is believed that the different crack path is due to a combination of weld mismatch effects, local geometry effects, stresses acting in the through thickness direction and the presence of inclusions in the steel.

3) A fracture mechanics model has been developed to describe crack growth in both the FCAW and SMAW specimens. The empirical SIFs obtained for the test specimens, are in close agreement with those predicted using the AVS and TPM equations.

4) Evidence from the current test programme suggests that the T' curve can be used to conservatively predict the air fatigue life of specimens constructed from an X85 grade steel. However further tests are needed to verify this.

TABLE 4.1. SUMMARY OF AIR TEST DETAILS

Test No.	Weld Process	Hot Spot Stress Range (MPa)	R Ratio	Test Frequency (Hz)
W2	FCAW	200	0.05	0.7-1.2 ¹
W3	FCAW	207	0.05	0.167
W4	FCAW	191	0.05	0.7-1.2 ¹
W6 ²	FCAW	310	0.05	0.167
S1	SMAW	300	0.05	0.167

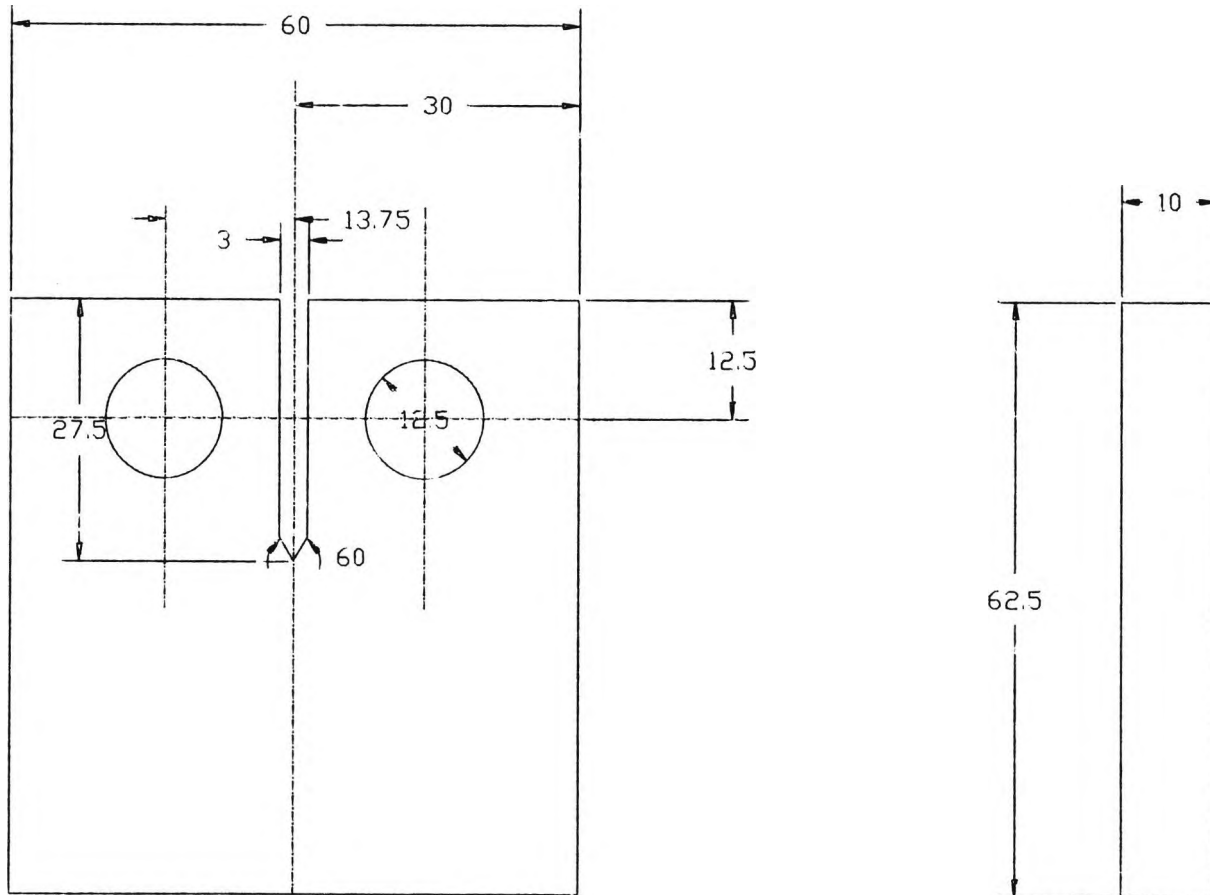
¹ Frequency was increased to 1.2Hz after 1,082,909 cycles

² Previously tested as W3.

TABLE 4.2. INITIATION AND TOTAL LIFE ENDURANCE DATA: IN AIR SPECIMENS

Specimen	Hot Spot Stress Range MPa	Initiation Life N1	Through Wall Thickness Life N3	Comments
W2	200	412,179 cycles	1,369,151 cycles Test stopped at recorded depth of 18mm	Possible overload
W3	207			No sign of initiation after 3,085,000 cycles
W4	191			Possible overload No sign of Initiation after 1,369,151 cycles
W6	310	0 cycles	317,173 cycles	Specimen previously fatigued as W3
S1	300	43,000 cycles	327,173 cycles Test terminated at apparent depth of 32 mm. N3* = 220,000 cycles	

Figure 4.1 Compact tension specimen geometry



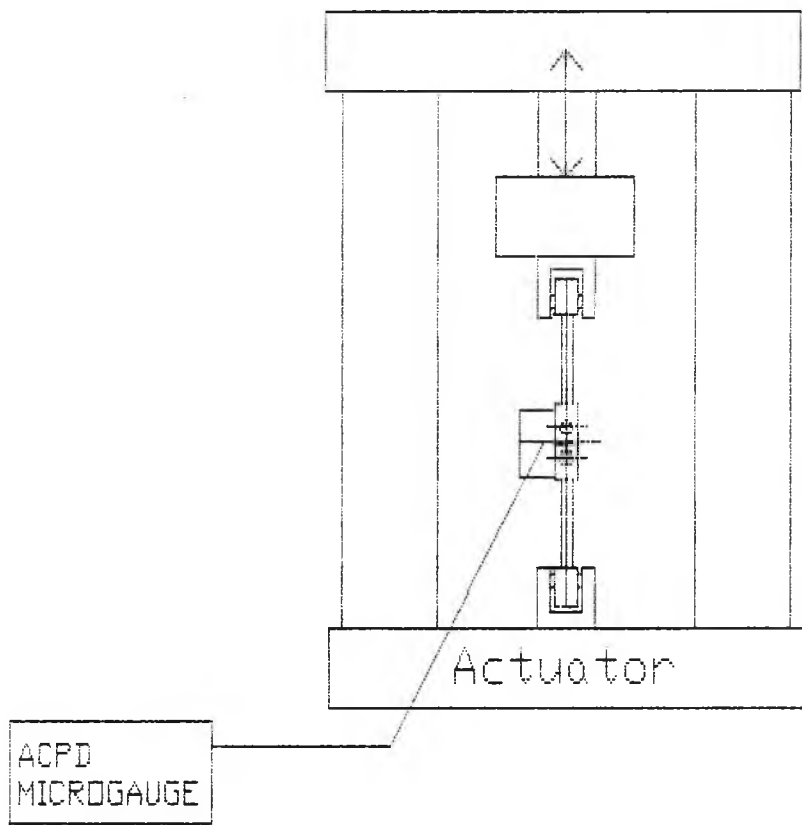
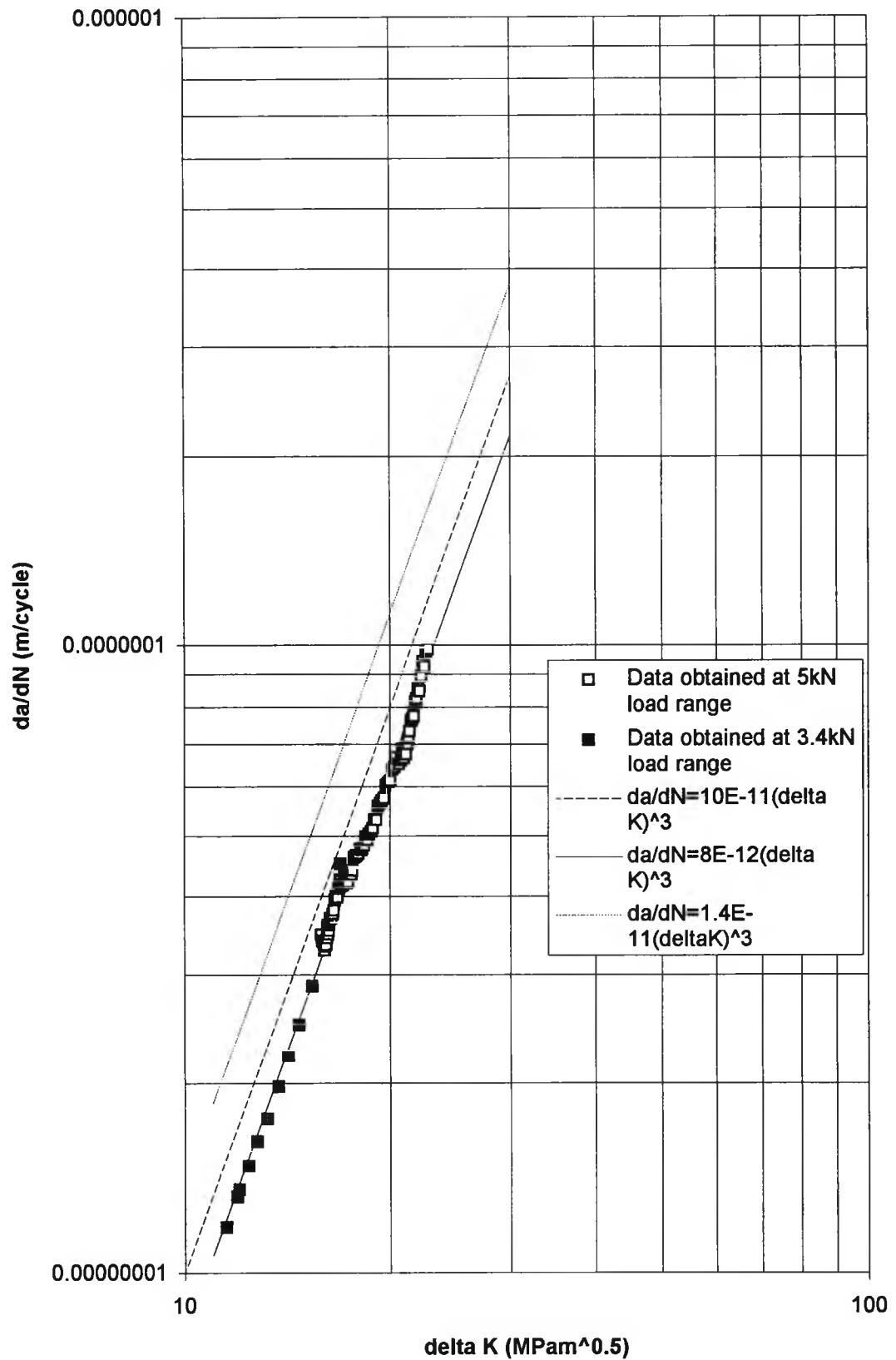


Figure 4.2 Schematic of compact tension specimen test rig

Figure 4.3 Fatigue Crack Growth Rate In Air: Marathon Le
 Tourneau X85 Steel
 CT Specimen, R Ratio=0.7



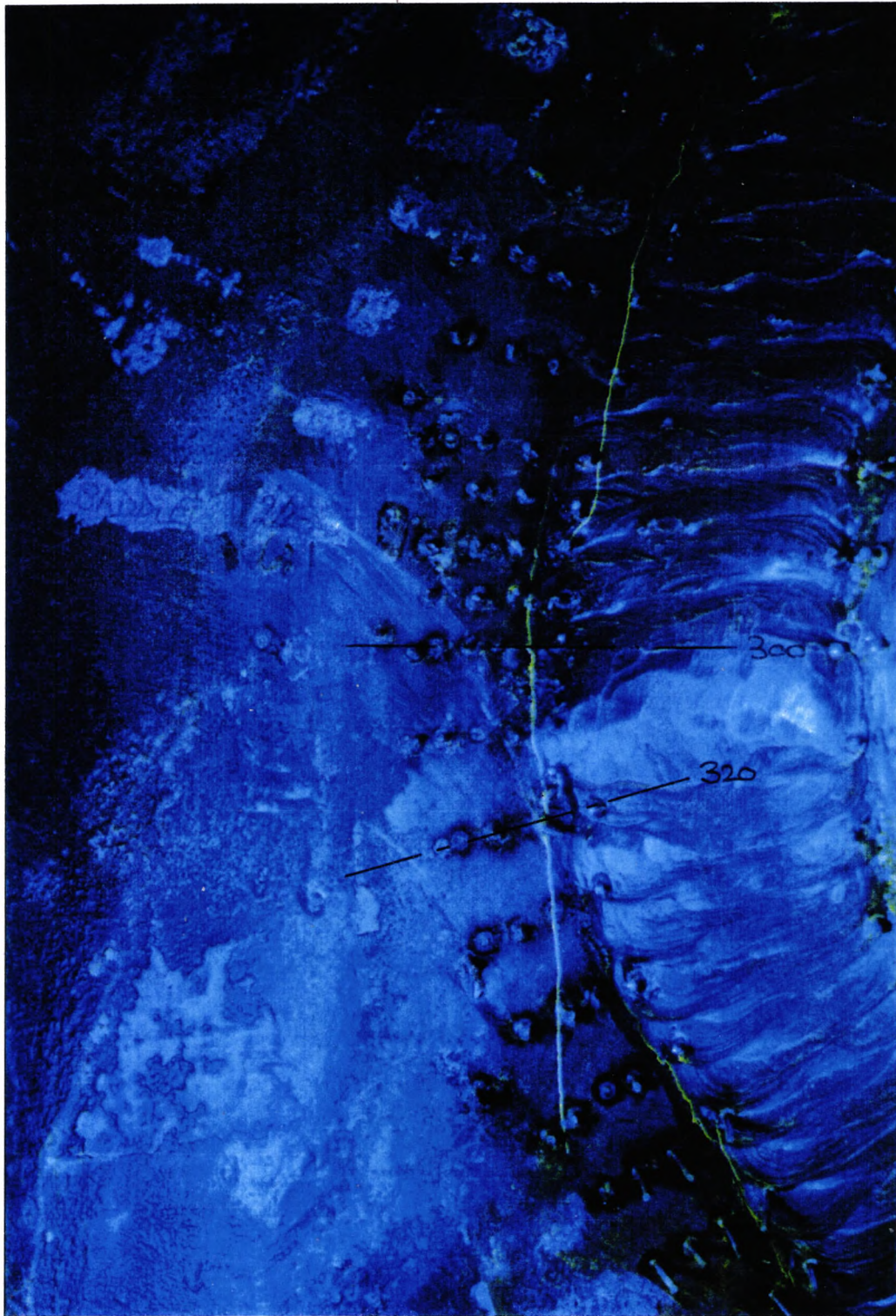
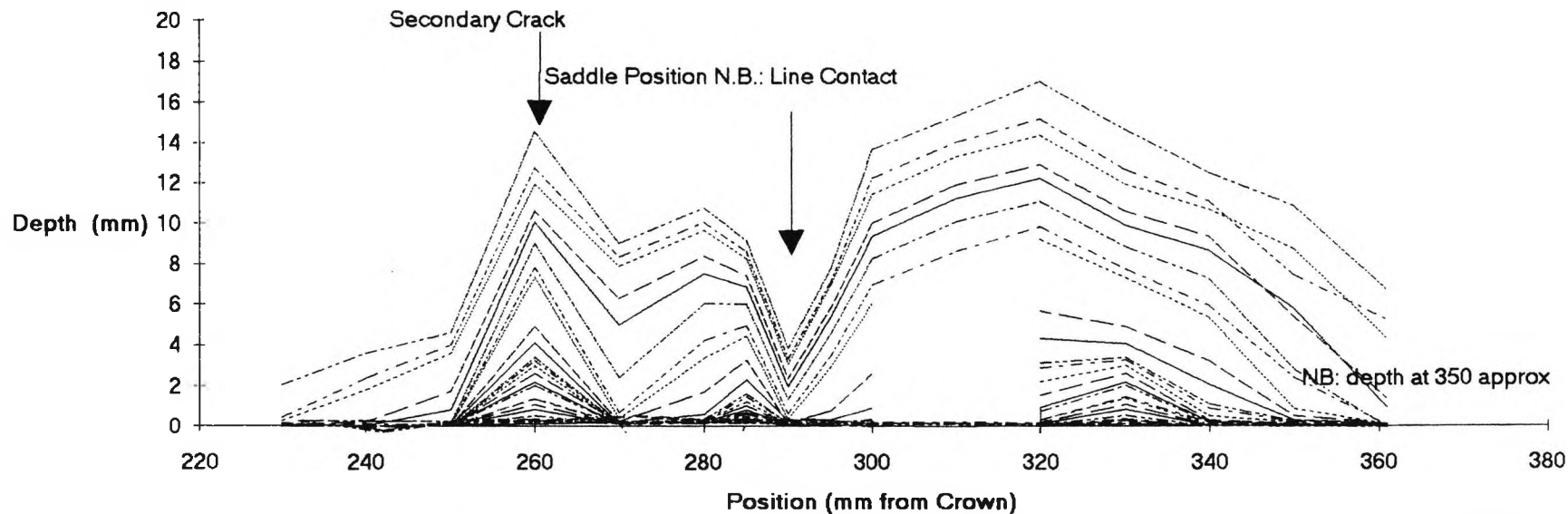


Figure 4.4 External view of fatigue crack in W2



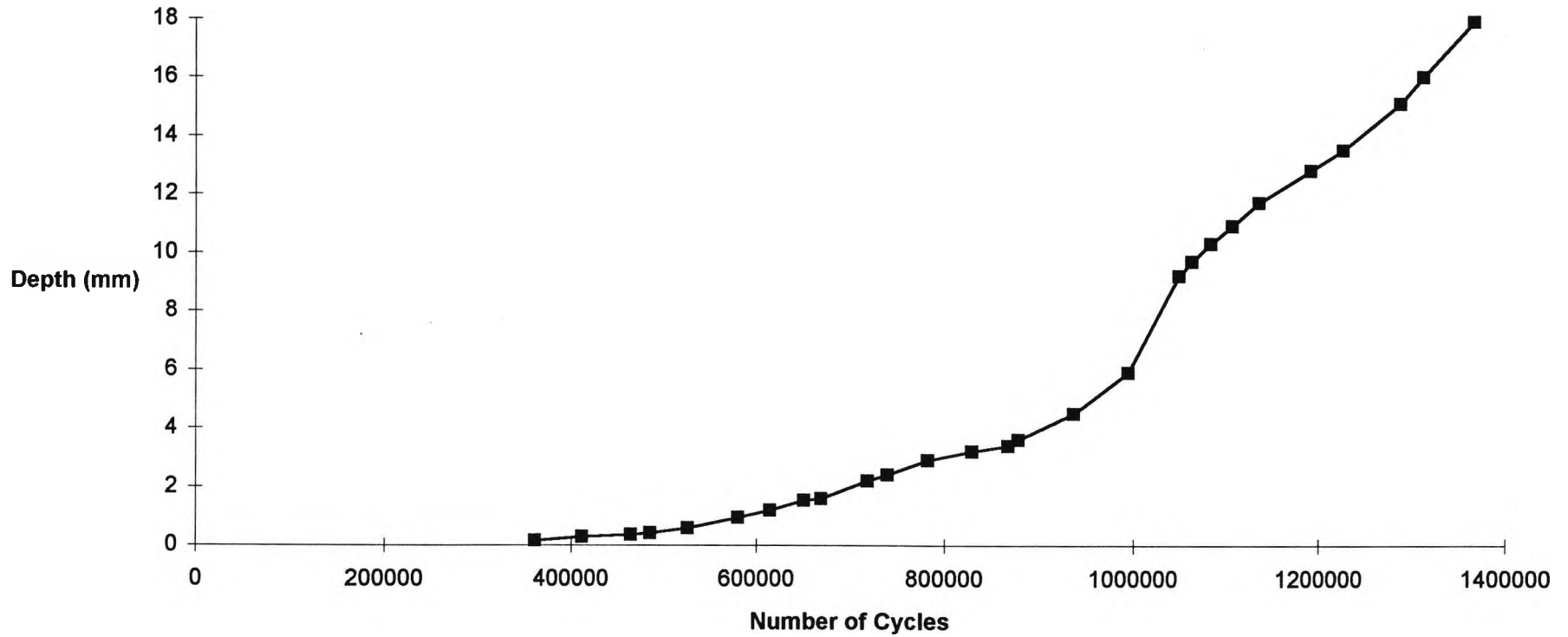
Figure 4.5 Section of W2 at 320 mm from crown

Figure 4.6 W2 Air Fatigue Crack Profile: Uncorrected Depth



—————	361,138 cycles	-----	412,179 cycles	464,578 cycles	-----	485,660 cycles	526,400 cycles
—————	580,670 cycles	-----	615,397 cycles	651,700 cycles	-----	670,192 cycles	719,467 cycles
—————	740,267 cycles	-----	782,220 cycles	828,763 cycles	-----	866,913 cycles	877,526 cycles
—————	936,500 cycles	-----	994,670 cycles	1,062,929 cycles	-----	1,082,909 cycles	1,135,810 cycles
—————	1,192,250 cycles	-----	1,227,062 cycles	1,289,842 cycles	-----	1,315,124 cycles	1,369,151 cycles

**Figure 4.7 Air Fatigue Crack Growth Data: Specimen W2
Hot Spot Stress Range: 200MPa**



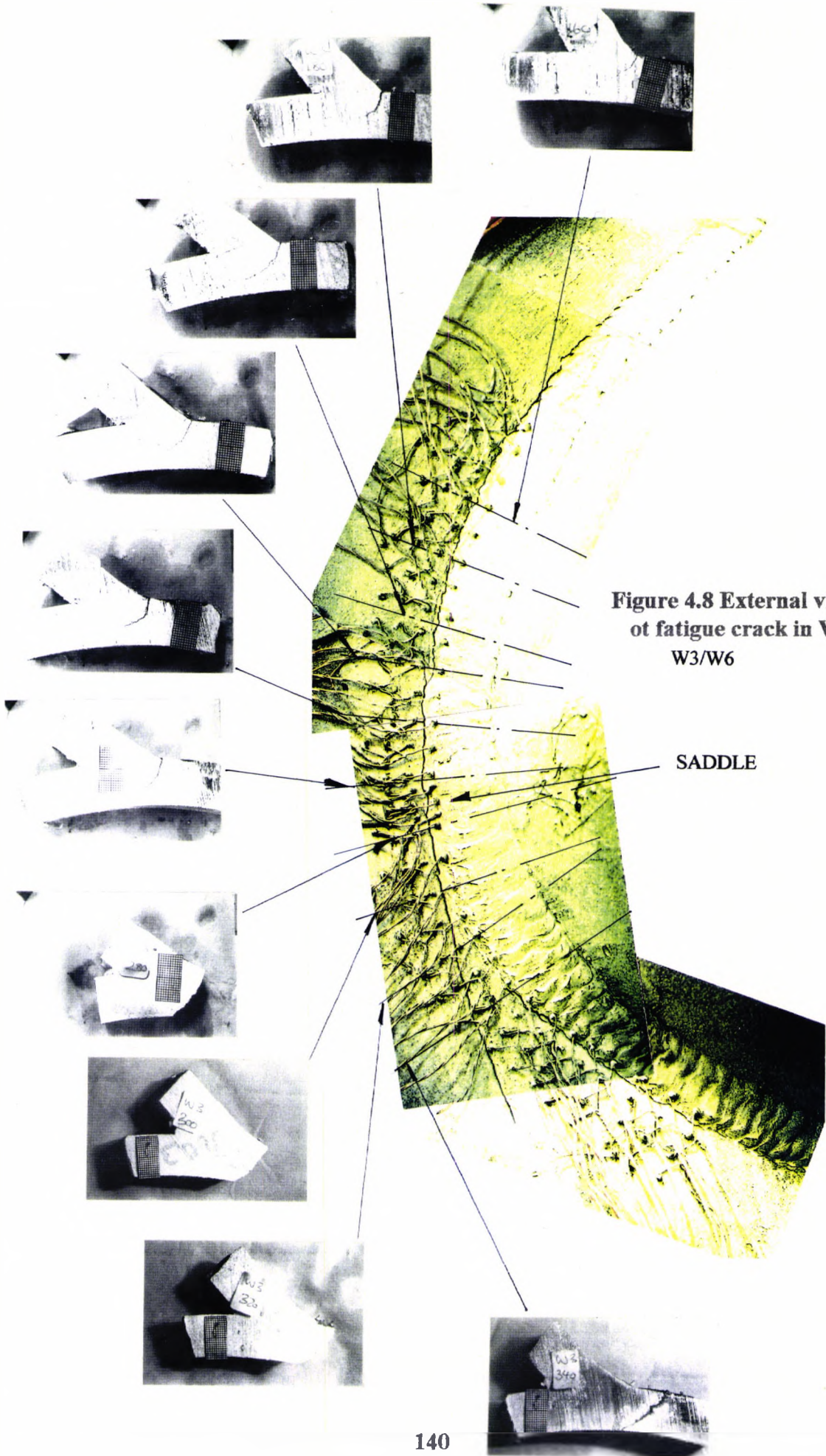
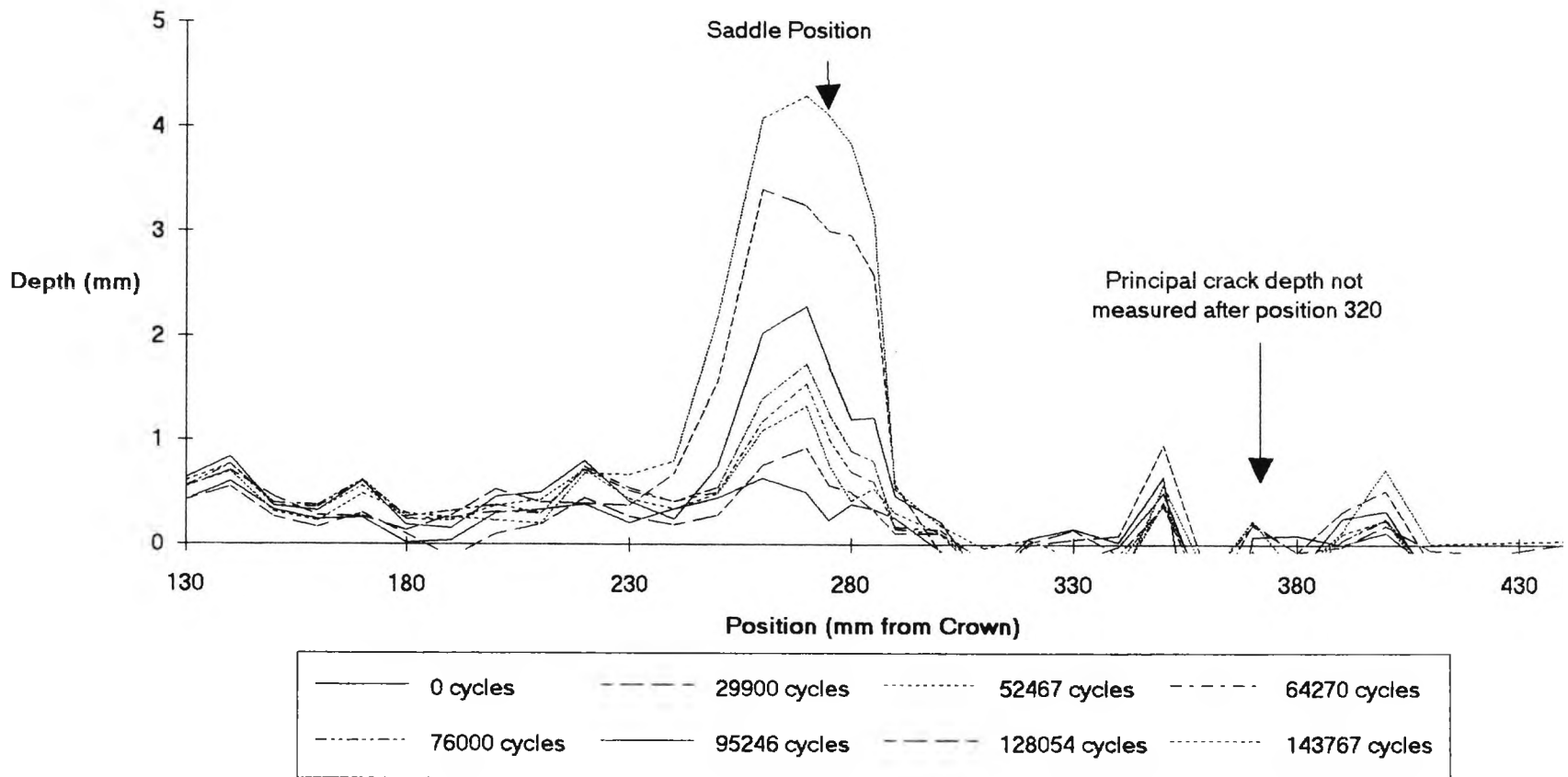


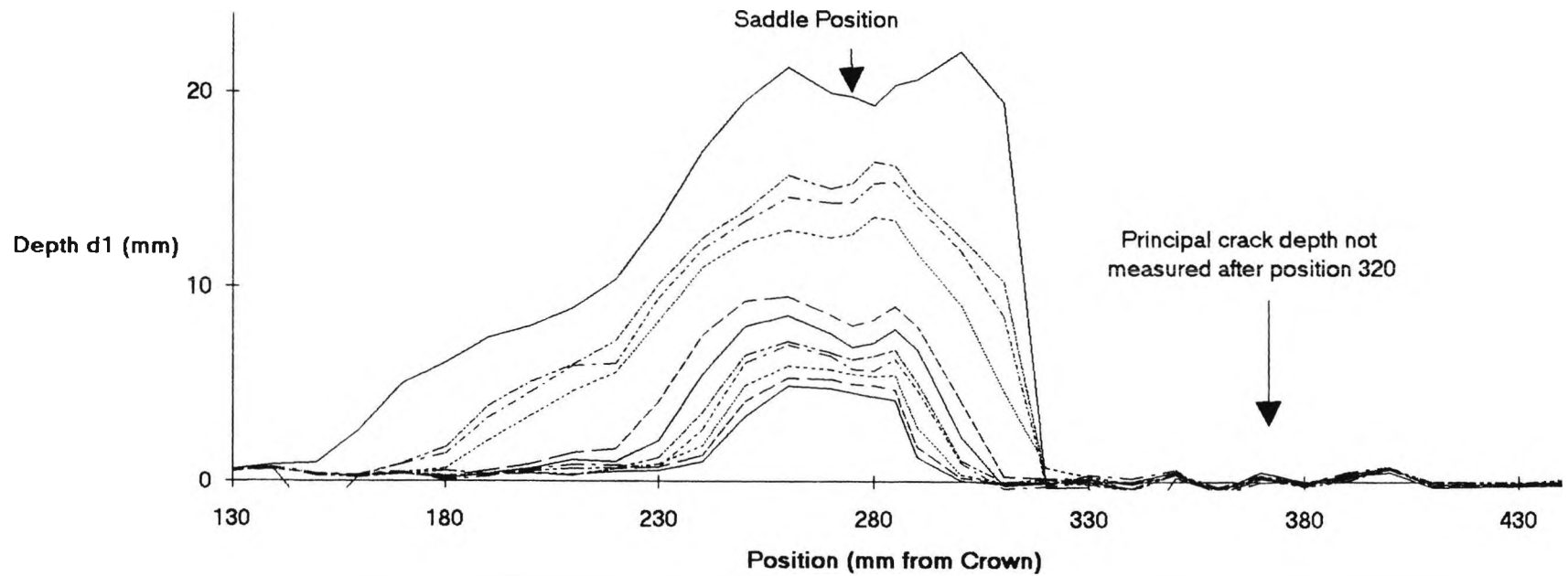
Figure 4.8 External view of fatigue crack in W6. W3/W6

SADDLE

**Figure 4.9a: W6 Air Fatigue Crack Profile: Uncorrected Depth
Depth Readings < 5mm**

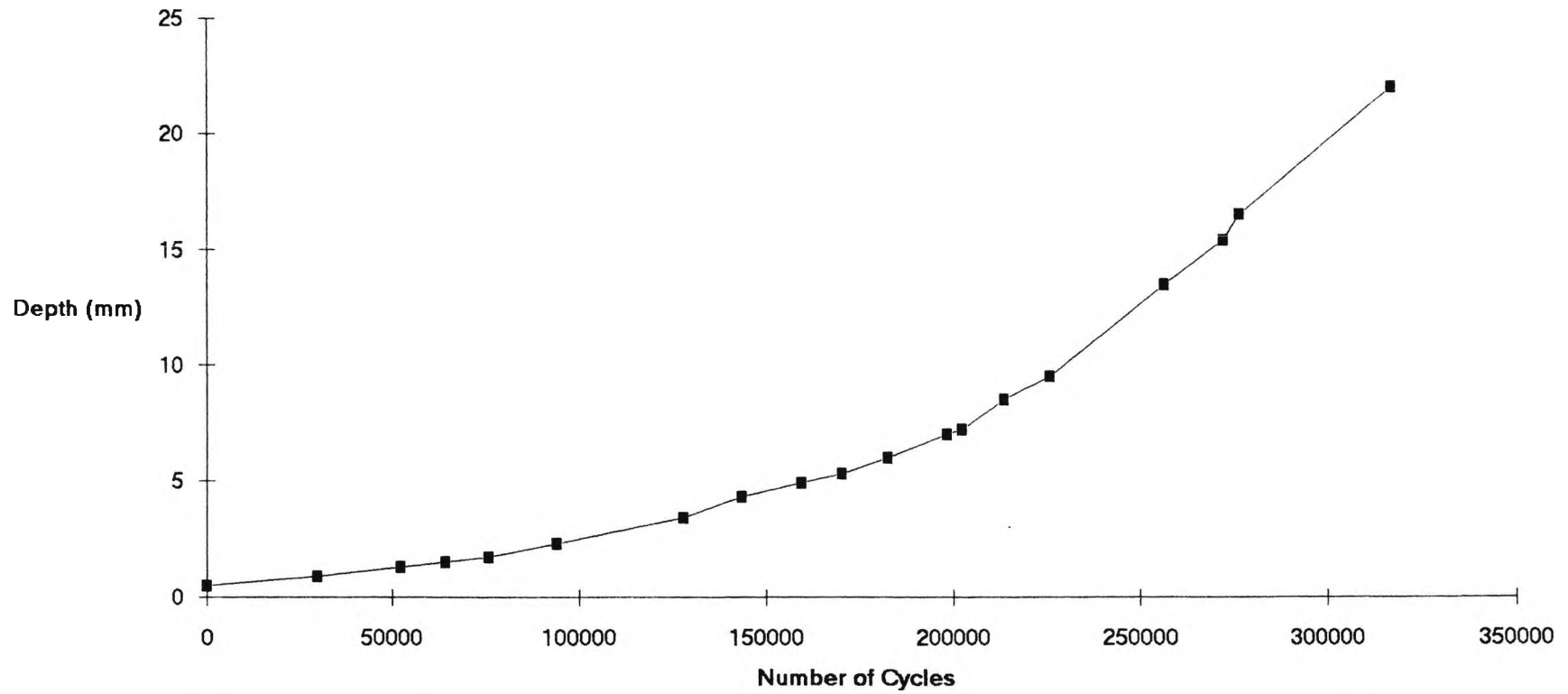


**Figure 4.9b: W6 Air Fatigue Crack Profile, Uncorrected Depth
Depth Readings > 5 mm**



—————	159598 cycles	- - - - -	170232 cycles	182462 cycles	- . - . -	198303 cycles
- . - . -	202348 cycles	—————	213847 cycles	- - - - -	226305 cycles	256467 cycles
- . - . -	272410 cycles	276703 cycles	—————	317173 cycles		

**Figure 4.10: Air Fatigue Crack Depth Data: Specimen W6
Hot Spot Stress Range: 300MPa**



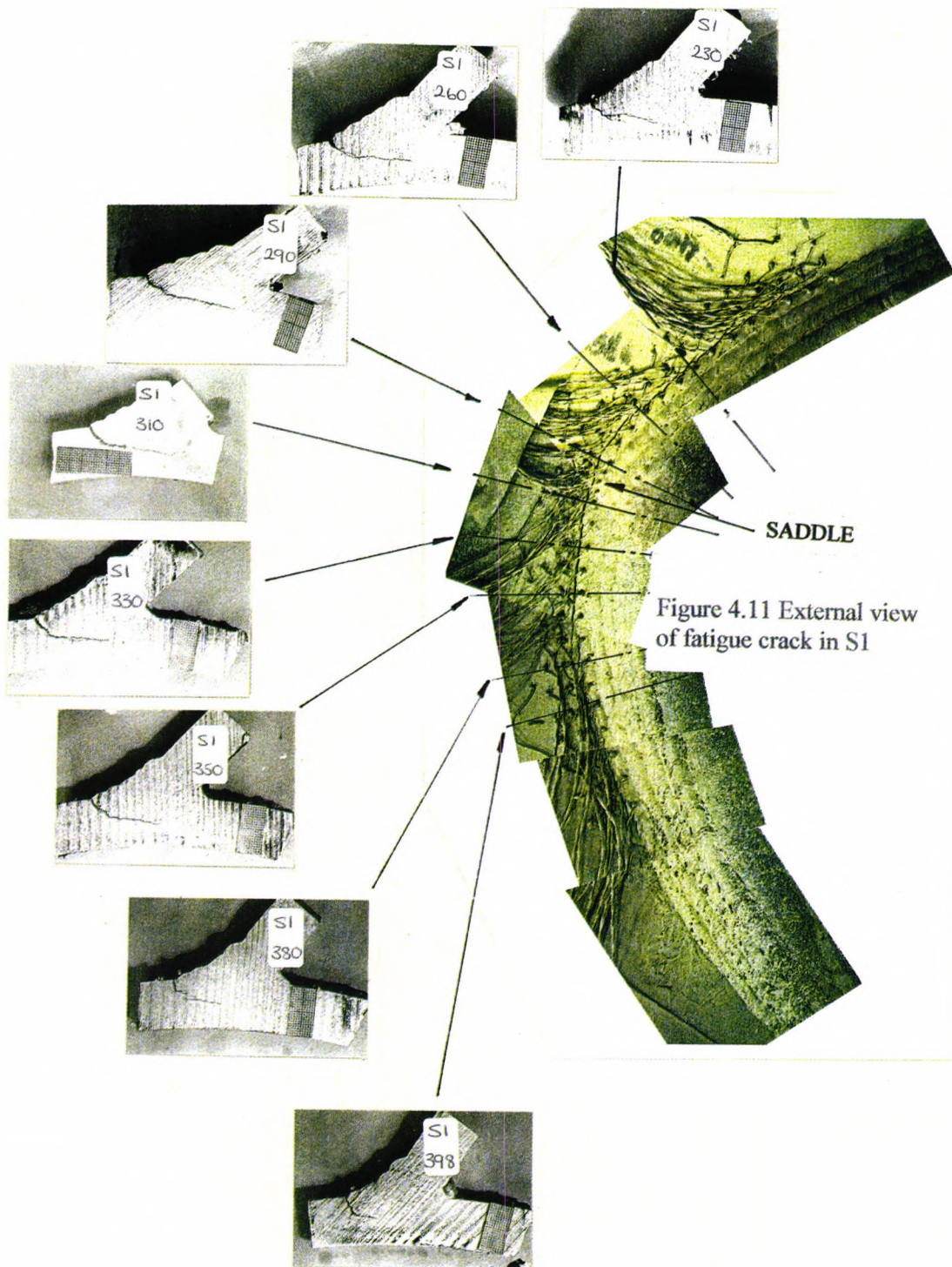


**Figure 4.12a: S1 Fatigue Crack Profile: Uncorrected Depth
Depth <5mm.**

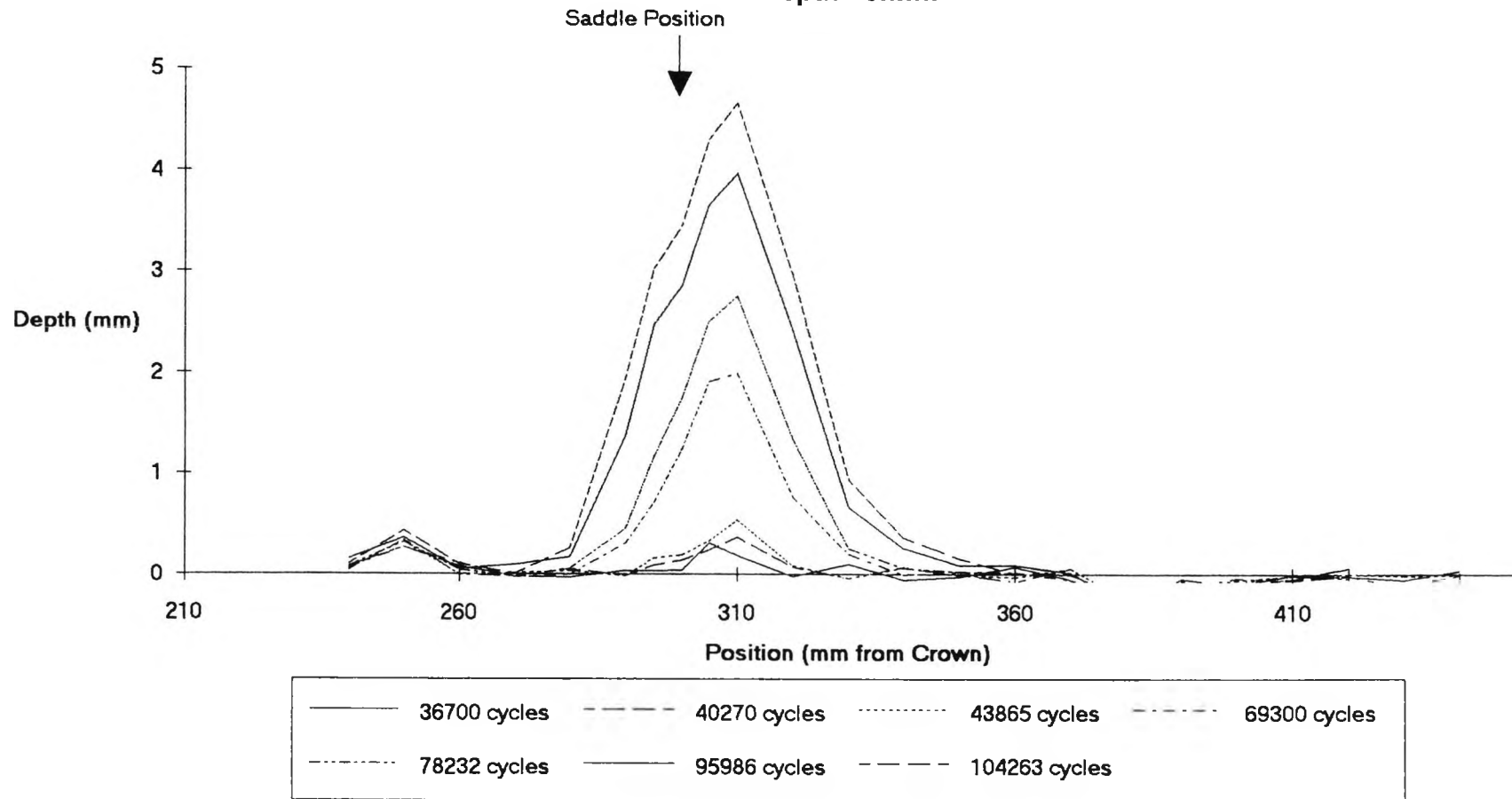
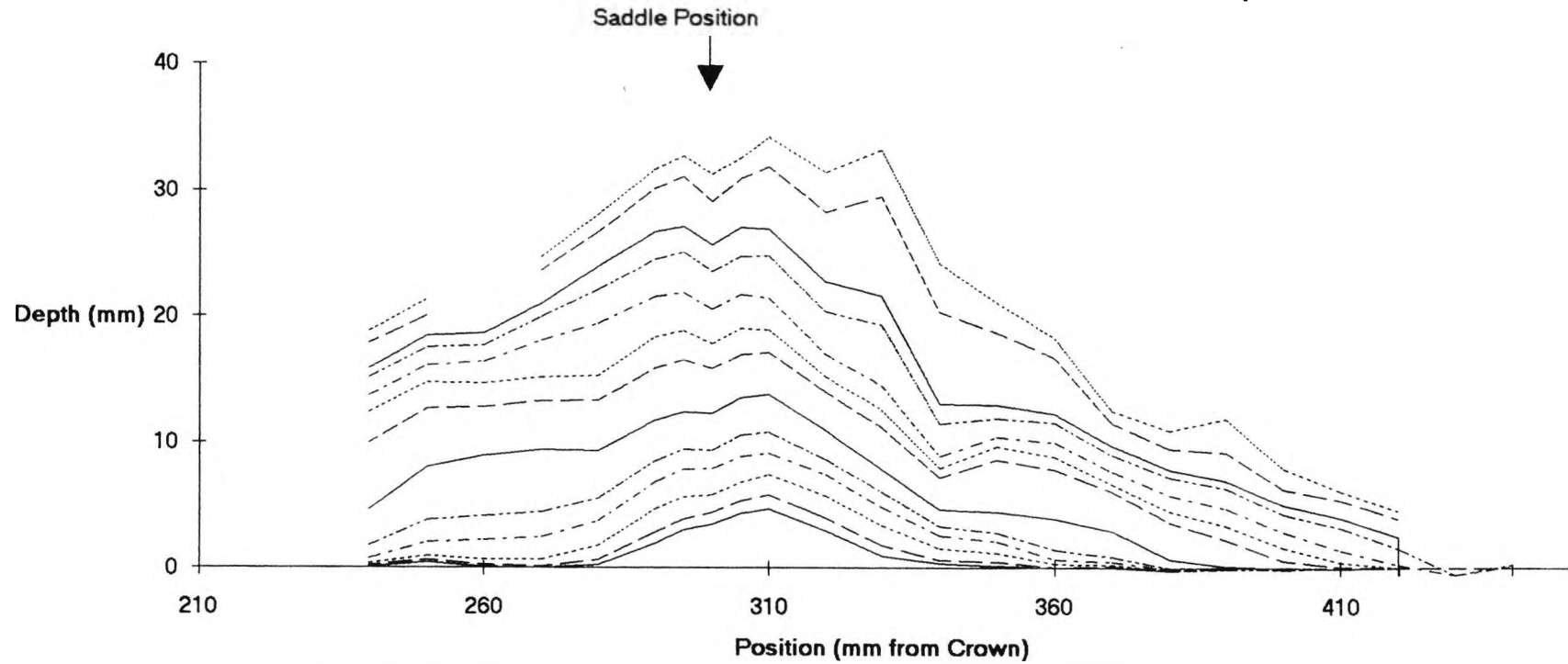
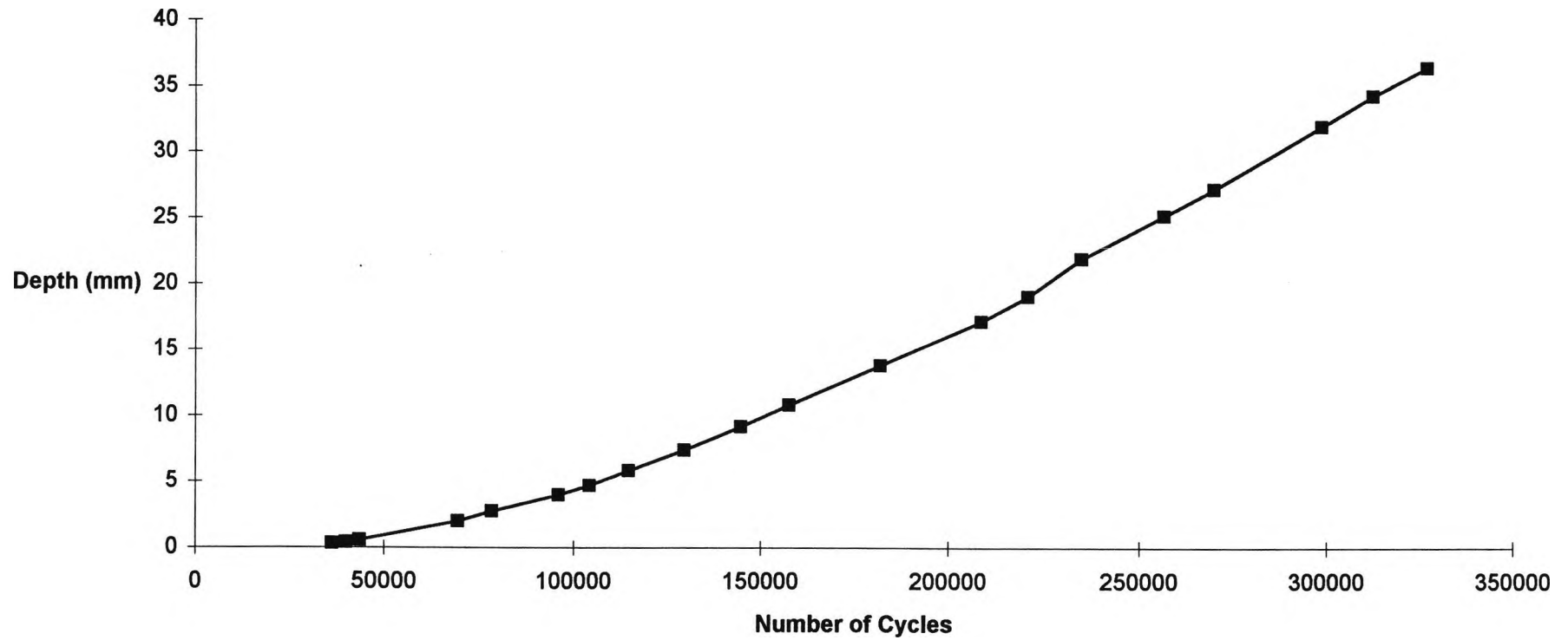


Figure 4.12b: S1 Fatigue Crack Profile: Uncorrected Depth



— 104263 cycles	- - - 114701 cycles 129639 cycles	- - - - 144789 cycles 157682 cycles
— 182105 cycles	- - - 208,780 cycles 221017 cycles	- - - - 235108 cycles 256515 cycles
— 269700 cycles	- - - 298761 cycles 312529 cycles		

**Figure 4.13: Air Fatigue Crack Growth Data: Specimen S1
Hot Spot Stress Range: 300MPa**



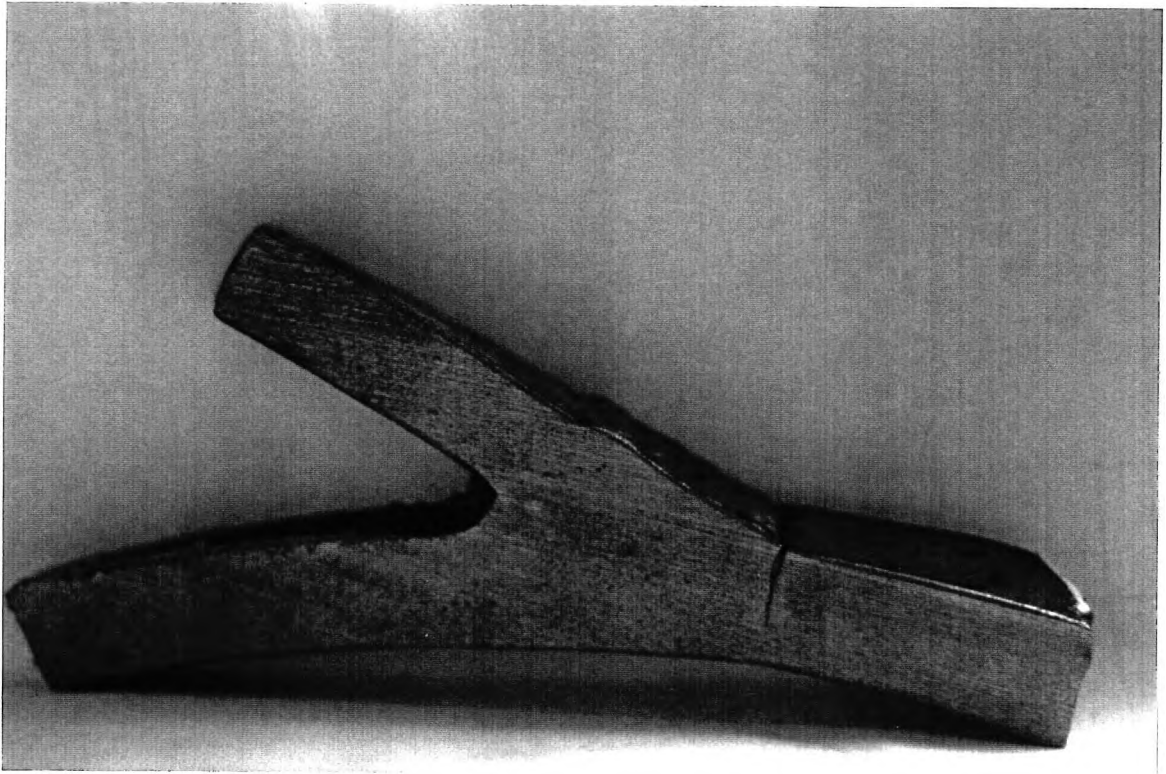


Figure 4.14 Example of crack growth shown in a "typical" tubular joint fatigue crack



Figure 4.15a: Shallow crack surface ($a < 4$ mm), Specimen W6



Figure 4.15b: Deep crack surface ($a > 4$ mm), Specimen W6

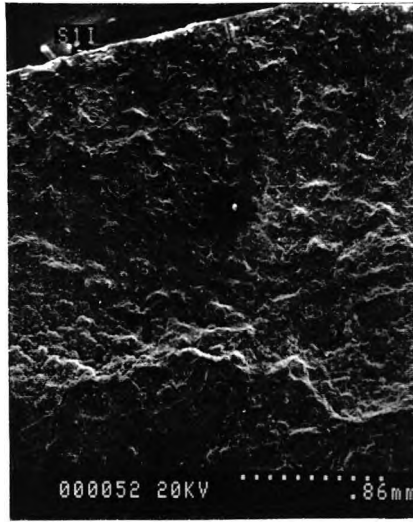
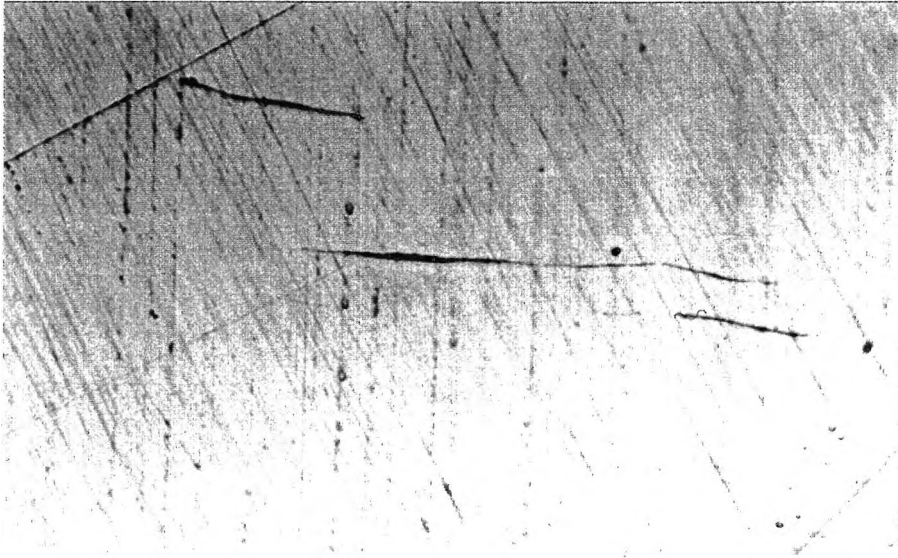


Figure 4.16a: Shallow crack surface ($a < 4$ mm), Specimen S1



Figure 4.16b: Deep crack surface ($a > 4$ mm), Specimen S1



**Figure 4.17 Typical FeMnS inclusions (from W2 parent plate)
Scale 134:1**

Figure 4.18: In Air Crack Aspect Ratio Variation

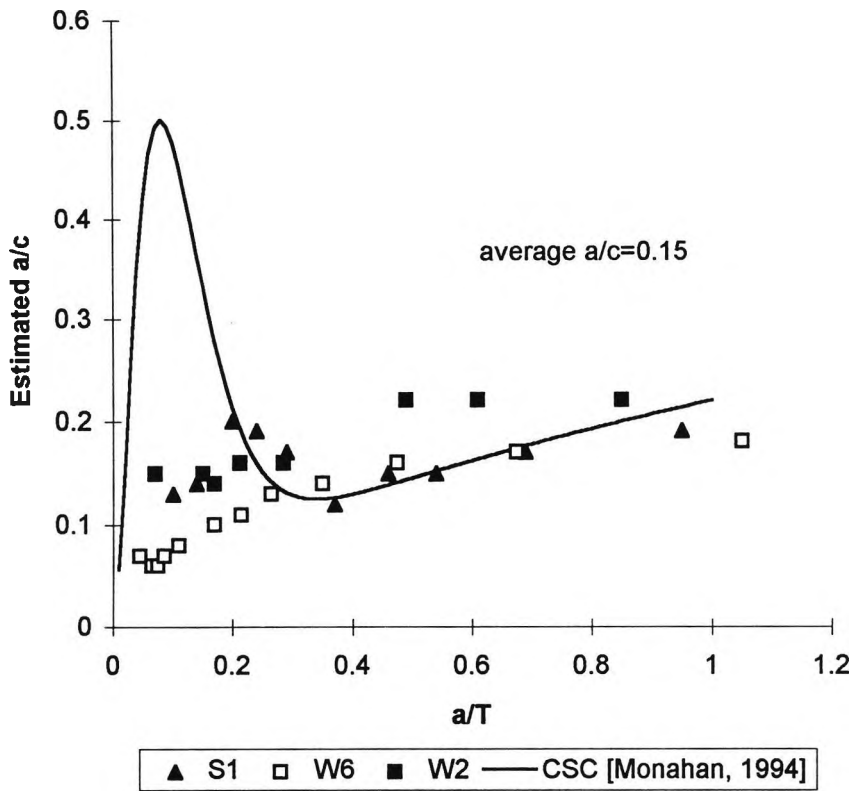


Figure 4.19 Empirical SIF Range for Tubular Joints

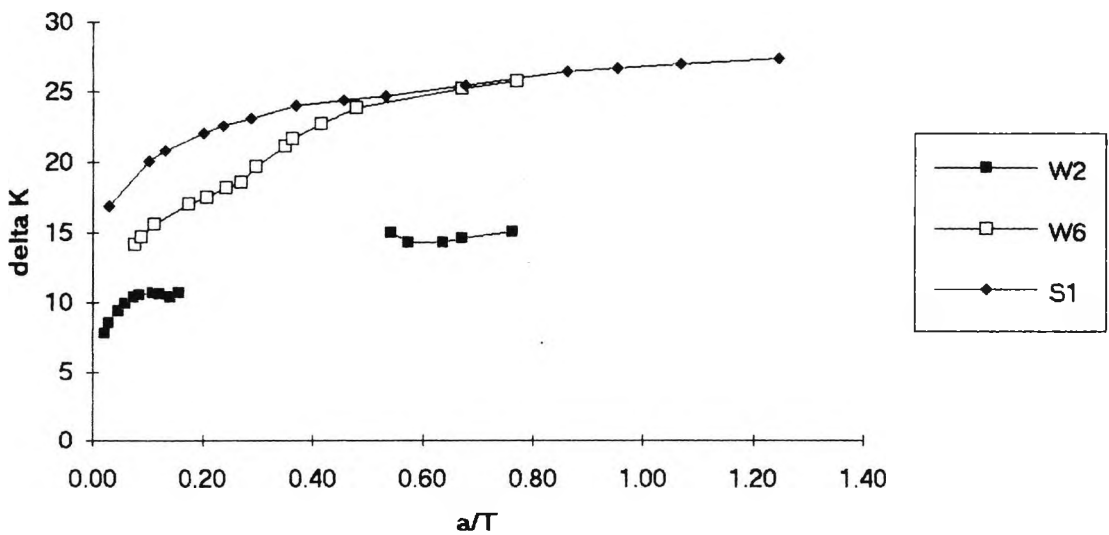
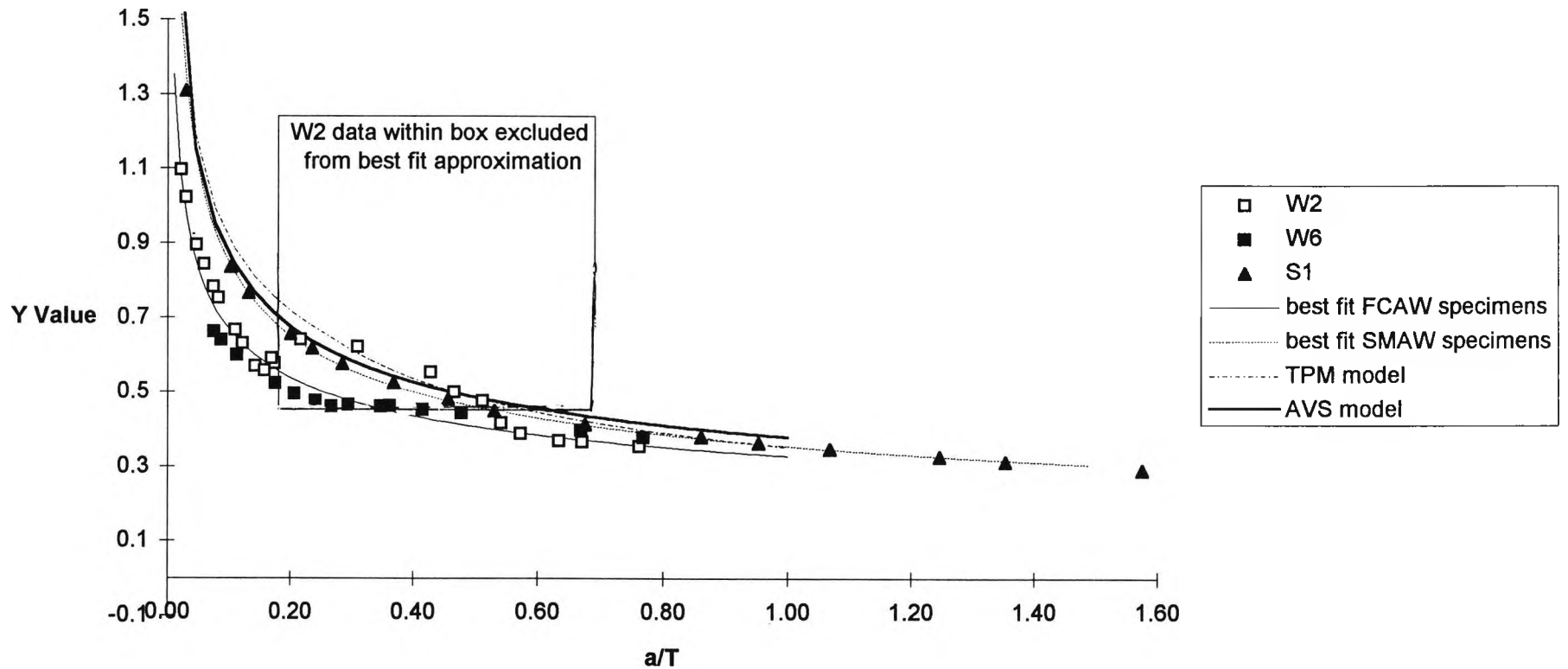


Figure 4.20: Variation of Y Value with a/T



**Figure 4.21 Tubular Joint N1 Initiation Life, X85 c.f.
BS4360.50D
(Adjusted to 20mm chord thickness) n/i no initiation**

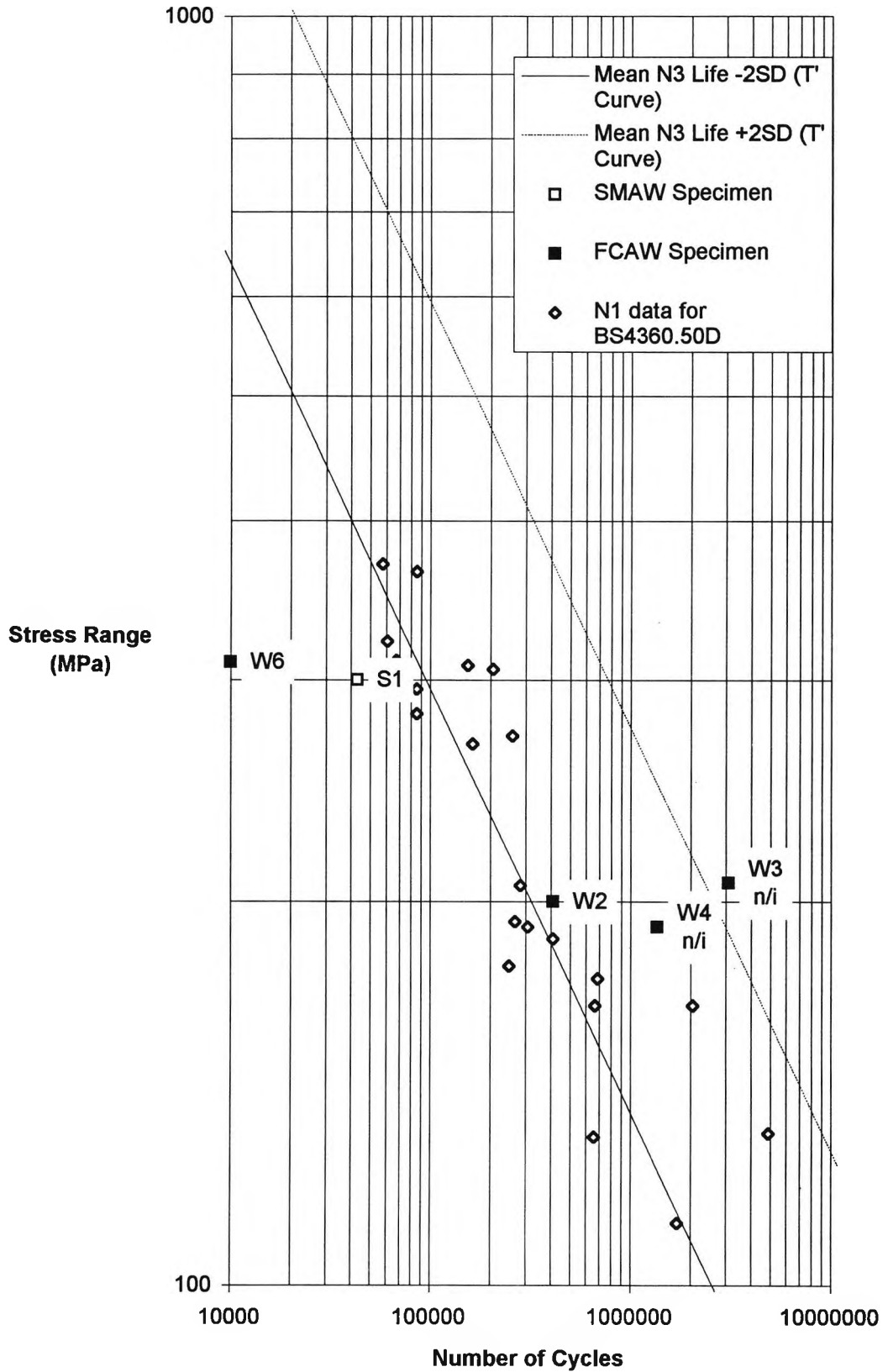


Figure 4.22 Variation of Stress Intensity Factor Range with Crack Depth

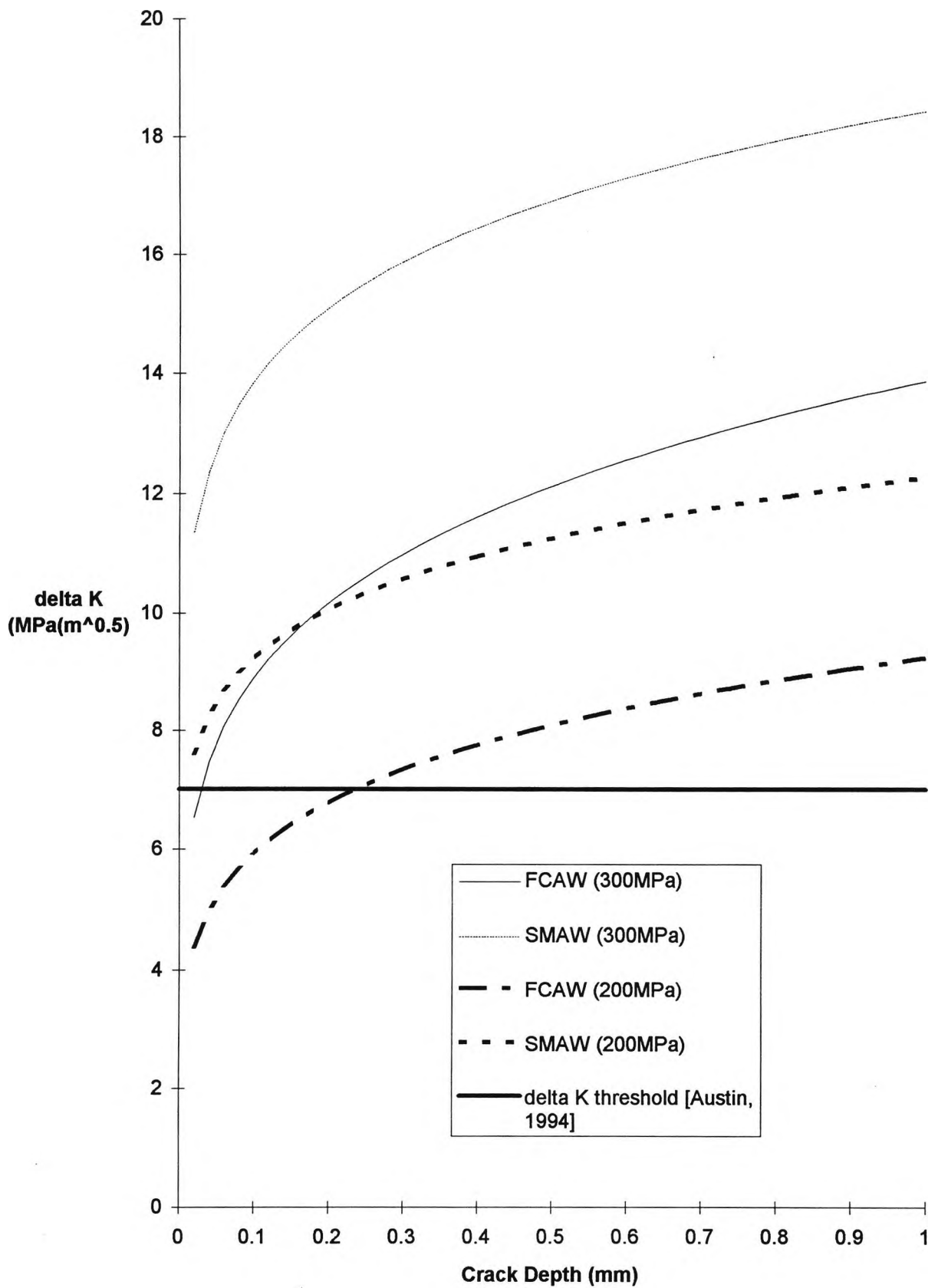
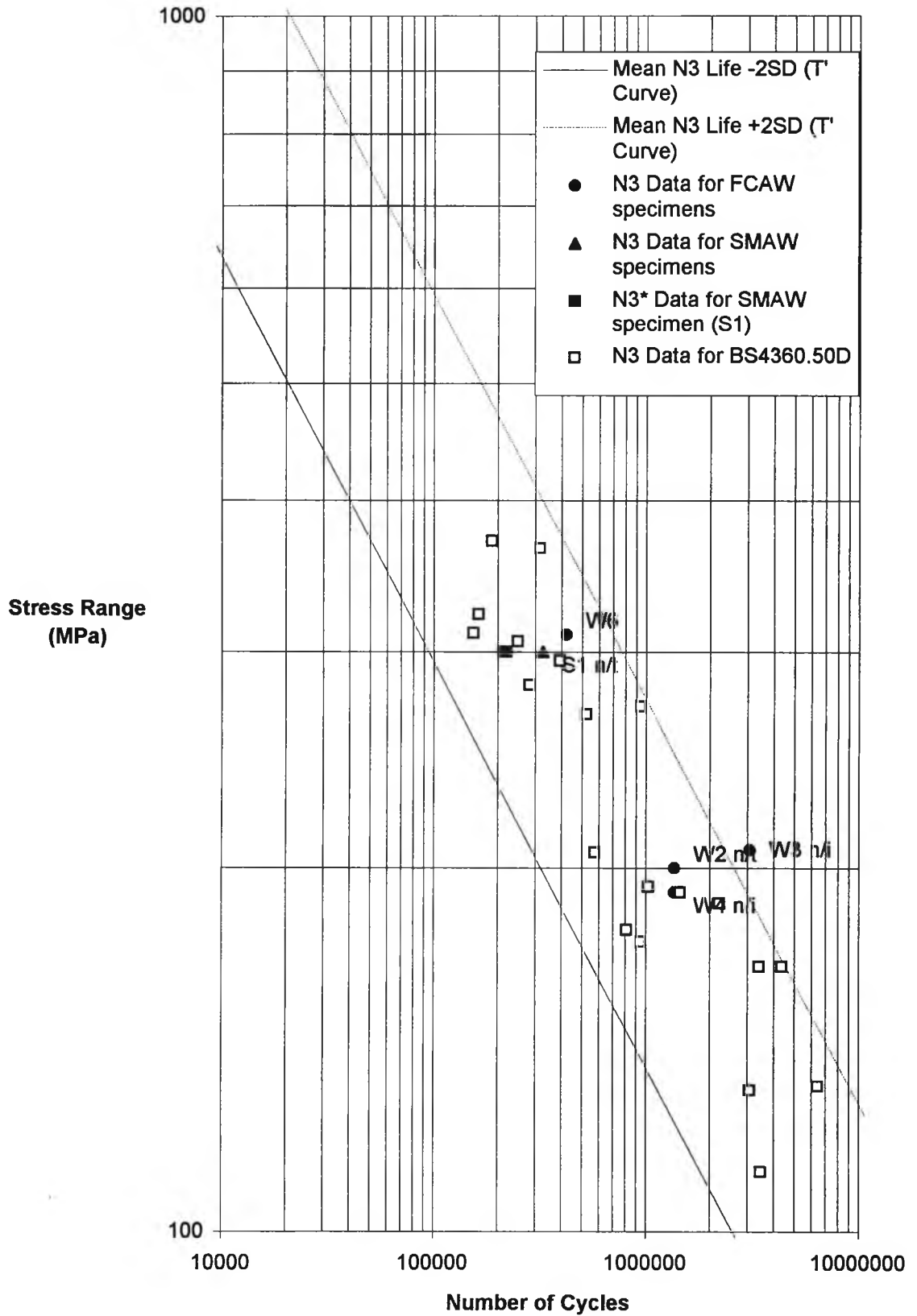


Figure 4.23. Tubular Joint N3 Air Life, X85 c.f. BS4360.50D
 (Adjusted to 20mm chord thickness) n/i no initiation; n/t not through.



5. FATIGUE TESTING OF STEEL TUBULAR JOINTS IN SEAWATER, WITH CATHODIC PROTECTION.

5.1. Scope of chapter

The influence of various environmental and physical variables on the corrosion fatigue rate was discussed in chapter 1.5. The interaction of these factors is complex. However, fatigue crack growth can be realistically modelled by holding variables such as dissolved oxygen content, temperature, salinity, pH, stress waveform and stress frequency constant, and as close to service conditions as possible. This allows the corrosion fatigue process to be studied by determining the crack growth rate as a function of the stress intensity factor range at different levels of cathodic protection. It was also concluded that cathodic overprotection was a situation likely to be experienced under service conditions, and that there was a lack of information on the corrosion fatigue crack growth of higher strength steels, under conditions of cathodic overprotection.

The purpose of this chapter is to present the crack growth data obtained from the fatigue of tubular joints constructed from API 5L X85 steel, cathodically protected at a potential of -1000mV (vs Ag/ AgCl). Using the empirical model for the stress intensity factor derived in chapter 4, the fatigue crack growth rate for the cathodically protected specimens is described in terms of the stress intensity factor range. This chapter will also present the corrosion fatigue crack growth rate data for FCAW specimens in addition to that of stringer welded, SMAW specimens. Data from a compact tension specimen test, fatigued under similar environmental conditions, was obtained so that it could be compared to the tubular joint crack growth data.

The corrosion fatigue experiments obtained initiation and endurance data for the X85 tubular joints. The endurance data will be compared to equivalent data obtained from the corrosion fatigue of BS4360.50D type steels and existing HSE guidelines for the prediction of the endurance of steels with a yield strength of less than 400 MPa.

5.2. Corrosion Fatigue, Compact Tension Test Specimen Data

The compact tension specimen test provided an inexpensive and relatively simple way of studying the corrosion fatigue behaviour of the API 5L X85 steel. The objective of the test was to provide data on the corrosion fatigue crack growth rate as a function of

the stress intensity factor range for the SIF range $0\text{MPa}\sqrt{\text{m}} \leq \Delta K \leq 22\text{MPa}\sqrt{\text{m}}$. These data will be compared to similar data obtained from tubular joint tests.

5.2.1. Test Set Up and Procedure

Test coupons were cut from the X85 chord material with the notch aligned in the LT direction as described in section 4.2. Dimensions are given in figure 4.1. In total two coupons were tested, one at a load range of 3.4 kN and the second at a load range of 5 kN. A load ratio of 0.7 was used to simulate the residual weld stress effect in the region of the weld toe. The test frequency was set to 0.167 Hz to simulate the wave frequency.

The effect of environment on the crack propagation rate was discussed in detail in section 2.4.2. The environmental conditions in the following tests were aimed at reproducing typical North Sea conditions and represent similar environmental conditions to those of both the X85 tubular joint tests and corrosion fatigue tests of BS4360.50D tubular joints. Corrosion fatigue tests were conducted by surrounding the joint with an environmental chamber, as shown in figure 5.1. Synthetic (biologically inert) sea water, prepared to ASTM D1141 (see table 5.1), was continuously circulated around the joint and chiller reservoir. The temperature of the sea water was maintained at 8-10°C and fully aerated. The pH of the sea water was monitored and observed to stay between 8.0 and 8.3.

During corrosion fatigue tests, the cathodic protection current was applied to the tubular joint through a platinum wire gauze, positioned to provide a uniform field. Control of the current was through a purpose built potentiostat with a back up external power supply. The potential controlled through a Ag/AgCl reference electrode and maintained at -1000mV. In addition the potential of the steel was monitored independently using a second Ag/AgCl reference electrode. The crack depth was monitored using the Alternating Current Potential Drop ACPD method at a frequency of 5 KHz. The temperature and pH of the seawater, cathodic protection voltage and current, crack depth, cycle count, and time were also monitored regularly.

Prior to corrosion fatigue testing the specimens were precracked to a depth of 3 mm in air using the procedure recommended in BS6835:1988. This was followed by a "presoak" period of 15 days. During this period chilled seawater was continuously cycled around the unloaded specimen. The test was terminated when the specimen fractured. Test conditions are summarised in table 5.2.

5.2.2. Results

The crack growth rate was determined using the seven point incremental polynomial method as recommended in ASTM E 647 [1993]. The SIF was determined using the closed form approximation for the SIF range, given in BS6835:1988 (equation 4.1). Values of the SIF range are plotted against the fatigue crack growth rate and shown in figure 5.2.

5.2.3. Discussion of Results

Figure 5.2 shows the rate of fatigue crack growth as a function of the SIF range. The crack growth rate decreased as the crack grew to a depth of 7 mm. This was followed by an increase in the corrosion fatigue crack growth rate, to a region where the fatigue crack growth rate could be approximated by a linear log da/dN versus log ΔK curve relationship.

The decreasing fatigue crack rate shown in early crack growth ($a < 7$ mm), was contrary to expectations. Comparison with the air data, shows that the corrosion fatigue crack growth rate was lower than that measured in air fatigue specimens for $\Delta K=12$ MPa \sqrt{m} . The decreasing crack growth rate was probably due to calcareous deposit crack closure and was confined to cracks of low crack mouth opening displacement. It is interesting to note that crack deceleration occurred, despite the presence of a high mean stress ratio. This would suggest that there was a competitive effect between calcareous deposition accumulation per cycle and the crack tip opening displacement per cycle, and that calcareous deposit crack closure can occur even in the presence of high residual tensile stresses.

An explanation for the rapid change from decelerating crack growth to accelerating crack growth is that the specimen requires a period of time for the atomic hydrogen to diffuse to the crack tip and start the hydrogen embrittlement process, and that the immersion period has to be combined with mechanical strain. Scully & Moran [1990] have studied the influence of immersion and strain on the subsequent fracture ductility of tensile specimens protected at -900 mV. They concluded that for cathodic protection to have an influence on the fracture process the period of immersion had to be combined with tensile strain. The above explanation would account for the delayed rapid crack growth propagation and suggest that for future tests the immersion period should be combined with loading at the mean applied load. Relating the above to the crack growth chart of the X85 test specimen and other high strength steels (figure 5.3), suggested that the corrosion fatigue crack growth data in the region $10\text{MPa}\sqrt{m} \leq \Delta K \leq 13\text{MPa}\sqrt{m}$ were unrealistically low.

Data in the region $13\text{MPa}\sqrt{\text{m}} \leq \Delta K \leq 22\text{MPa}\sqrt{\text{m}}$ agreed closely with data for other high strength steels (figure 5.3). The crack growth data in the interval $13\text{MPa}\sqrt{\text{m}} \leq \Delta K \leq 22\text{MPa}\sqrt{\text{m}}$ was approximated by a log log linear relationship. Unlike equation 4.1 there was no reason for the exponent to be fixed to 3. The mean crack growth rate was represented by the following relationship:

$$13\text{MPa}\sqrt{\text{m}} \leq \Delta K \leq 22\text{MPa}\sqrt{\text{m}} \quad da/dN = 9.98 \times 10^{-11} (\Delta K)^{2.79} \text{m/cycle} \quad (5.1)$$

(coefficient of determination of 97.6%). This represented an increase in the corrosion fatigue crack growth rate of between 6.5 and 7.3 times the mean air fatigue crack growth rate. The increase in the corrosion fatigue crack growth rate was attributed to hydrogen embrittlement (section 1.5.2). Caution should be used in applying these crack growth rates to corrosion fatigue in tubular joints. Austin [1994] noted that the rate of corrosion fatigue crack growth was dependent on the size of the crack tip process zone and was limited by hydrogen diffusion from the external surface to the crack tip. Both hydrogen diffusion and process zone are dependent on the thickness and stress state of the specimen. Cracks in tubular joints are predominantly in a state of plane strain. This contrasts with thinner compact tension specimens where the crack tip is often at an intermediate state between plane stress and plane strain. It is also likely that hydrogen is more readily available to the process zone in a thin specimen, than in a thicker specimen, due to bulk charging from the specimen surface [Turnbull, 1986] (section 1.5.4.2). Given the above considerations, the rate of crack growth from a relatively thin compact tension specimen tested at a high load ratio, should provide a conservative guide to crack growth in a tubular joint.

The intention of the above test was to provide background data for comparison with subsequent tubular joint corrosion fatigue tests. It has been shown, that although compact tension specimen tests can provide useful crack growth data, the crack growth rate is influenced by crack retardation effects, the duration and loading conditions of the immersion period and the stress state of the specimen. There is therefore a limit to which corrosion fatigue crack growth can be modelled by compact tension specimen tests. The most reliable measure of the corrosion fatigue crack growth rate as a function of SIF range, is obtained from full scale tests of tubular joints. Comparison of the X85 steel data with other materials is reserved to chapter 6.

5.3. Corrosion Fatigue Testing of Steel Tubular Joints

The results of full scale corrosion fatigue tests on tubular joints are discussed in the following section. The test procedure, in as far as it differed from the air fatigue tubular joint tests, is described. The results from the test included crack growth data and fracture surface are examined in detail. The N1 and N3 endurance lives are also discussed.

5.3.1. Experimental Apparatus and Procedure

The experimental apparatus and rig used was essentially similar to that used in the air fatigue test programme. The test rig was described in section 3.2.1. Fatigue testing in a controlled seawater environment required additional equipment. The node to be fatigue tested was enclosed by a purpose designed environmental chamber, this allowed for distortion in the chord and brace, whilst minimising the load transmitted through the chamber. The front of the environmental chamber was constructed from Plexiglass[®] to allow the weld toe to be observed during the test. The test apparatus is shown schematically in figure 5.4, a photograph of the rig is given in figure 5.5.

Cathodic protection was applied through a platinum coated, titanium wire anode, mounted to the inspection window. The anode was positioned to provide a uniform potential around the weld toe, and the potential was controlled through a potentiostat attached to a reference electrode. The reference electrode was positioned close to the weld toe. An area from approximately 50 mm from the brace and chord weld toe to 50 mm outside of the corrosion cell was painted with a two part epoxy paint to reduce the current required to maintain cathodic protection. The corrosion cell was then assembled and filled with chilled synthetic seawater prepared to ASTM D1141 (table 5.1). The specimen potential was measured and the specimen cathodically charged gradually from the potentiostat, so that the current never exceeded 3A. The potential was checked regularly throughout the fatigue tests with a second reference electrode. The potential was maintained within 15 mV of the prescribed voltage throughout the test (generally the voltage deviated by less than 5 mV of that prescribed). In the event of electrical failure, the potentiostat was powered through a back up battery which cut in automatically within 30 seconds of mains failure.

Synthetic (biologically inert) sea water, prepared to ASTM D1141 (table 5.1), was continuously circulated around the joint and chiller reservoir. The temperature of the sea water was maintained at 8-10°C and fully aerated. The pH of the sea water was monitored and observed to stay between 7.8 and 8.2.

To avoid the possibility of polluting the seawater, magnetic particle inspection MPI (section 5.3.3) was not used to find the location of a crack. The N1 life was determined from the interpolation of the ACPD crack depth data to where the deepest point was observed to grow continuously. The ACPD technique was used to monitor the crack depth. The technique is described in chapter 4.3.1. The spot welded ACPD terminals were attached at spacings of 10 mm between sites, the spacing was reduced to 5 mm in the vicinity of the chord saddle (the anticipated crack initiation site). The ACPD field wires were attached to small screws which were fixed to the specimen, outside of the corrosion cell, so that they were almost perpendicular to the chord surface. The field injection points were located so that the reference voltage readings were as near uniform as possible, using the procedure described in chapter 4.3.2. Prior to fatigue testing of the tubular joints in the current test programme, the crack voltage, reference voltage and a calculated initial depth reading were determined. Subsequent depth readings were then adjusted to account for the initial depth reading and two dimensional field effects.

The test conditions of the individual corrosion fatigue tests are summarised in detail in table 5.3. The effect of the environment on the crack propagation rate was discussed in detail in section 1.5.4.1. The environmental conditions in the following tests were aimed at reproducing typical North Sea conditions, and represent similar environmental conditions to those of both the X85 compact tension specimen tests and corrosion fatigue tests of BS4360.50D tubular joints. The stress waveform and frequency were chosen to simulate offshore operating conditions. The hot spot stress amplitude was determined from the stress concentration factor, obtained in chapter 3. The actuator was set to dump pressure in the event of the load exceeding 110% of the prescribed maximum load, limiting the size of any possible overload. The maximum load was monitored independently with a peak reading digital volt meter.

The number of cycles was recorded using an electro-mechanical counter, the ACPD crack depth D1, the temperature and pH of the seawater, reference electrode voltage, potentiostat voltage and current were regularly monitored. Corrosion fatigue tests were terminated when the crack penetrated the inside chord wall. This was determined by mounting a level switch to the seawater reservoir. The level switch automatically cut off the servo actuator when the reservoir level fell.

5.3.2 Results

Specimen W1 was reacted against W3; W5 was reacted against W6; S3 was reacted against S1; S2 was reacted against S4. When S4 failed, S4 was removed from the rig and S2 was reacted against W4. Only the corrosion fatigue tests W1, W5, S2, S3, S4

are considered in this chapter. Specimens W5, S2, S3 and S4 were fatigue tested until the crack achieved partial or full chord penetration. The specimens were then sectioned. Section planes and positions along the cracked chord surface, were identified by their distance (in millimetres), from the top crown position.

A crack growing predominantly in a plane perpendicular to the brace surface, such as that seen in the air FCAW specimens, is referred to as a W type crack and a crack growing in a plane predominantly parallel to the chord surface, such as that seen in the air SMAW specimen, is referred to as a S type crack. W1 and W5 were FCAW specimens. S2, S3 and S4 were SMAW specimens.

Several interruptions occurred during each of the tests. However, the interruptions were not thought to have influenced the test results. This was because the level of cathodic protection and the environmental conditions, were maintained during all interruptions to the fatigue programme. The crack growth behaviour was therefore assumed to be representative of crack growth under the prescribed conditions.

W1

Specimen W1 was fatigue tested at a hot spot stress range of 200 MPa. This test was designed to provide corrosion fatigue crack growth and endurance data for the FCAW specimens. Prior to fatigue testing, the node was soaked under standard test conditions for a period of 14 days. After 3,085,000 cycles, no sign of crack initiation was observed and the test was terminated.

W5 (figures 5.6,5.7 & 5.8)

W1 was retested as W5 at a hot spot stress range of 300 MPa. This test was designed to provide corrosion fatigue crack growth data for the FCAW specimens. A crack initiated at 130,000 cycles. The test was terminated at 423,477 cycles when the crack penetrated the chord wall and seawater was observed to have leaked from the corrosion cell.

Figure 5.6 shows an external view of the fatigue crack. The principal crack initiated at 210 mm from the crown, or 30° above the saddle position. This primary fatigue crack was not confined to the weld toe, but grew into the chord in one direction and into the weld metal in the other direction. A second crack initiated at the saddle at 300,000 cycles. This crack grew rapidly until it coalesced with the primary crack. The secondary crack followed the weld toe. The surface appearance of the chord showed evidence for other more minor cracks initiating and growing to coalesce and, in some

cases, intersect. The cracked area extended around the weld toe and broke into the chord at several positions.

Examination of the sectional views showed that the primary crack was a type W crack, whereas the secondary crack was a type S crack. Severe crack branching was observed, particularly at sections 340 to 400. Crack branching was not observed closer to the saddle position and in the vicinity of the principle crack. The crack depth at section 220 was 26 mm. The cracks intersected at some points (e.g. section 250).

Figure 5.7 shows the crack depth as a function of distance from the crown position. The position of the primary crack relative to the ACPD probes meant it was difficult to assess the aspect ratio (e.g. section 160). A secondary crack initiated at the saddle after approximately 305000 cycles and grew rapidly to a depth of 6 mm. The secondary crack then grew at a similar rate to the primary crack. At no point was the secondary crack deeper than the primary crack.

The crack depth was corrected for the two dimensional field. Crack depth readings for the crack at the deepest position are shown in figure 5.8. The measured crack depth was checked as a function of load at 360,000 cycles. No variation in the measured crack depth was noted. The crack growth rate showed a transition from increasing crack growth rates to an approximately constant crack growth rate prior to the crack penetrating the chord wall.

S2 (figures 5.9, 5.10 and 5.11)

S2 was fatigue tested at a hot spot stress range of 235 MPa. The purpose of this test was to obtain fatigue crack growth data and endurance life data for the SMAW specimens for $13\text{MPa}\sqrt{\text{m}} \leq \Delta K \leq 20\text{MPa}\sqrt{\text{m}}$. Prior to fatigue testing, the node was soaked under standard test conditions for a period of 14 days. Fatigue initiation was noted at 30,000 cycles. The test was terminated at 458,465 cycles when seawater was observed to have leaked from the corrosion cell and the crack penetrated the chord wall.

Figure 5.9 shows an external view of the fatigue crack. The fatigue crack in specimen S2 initiated at the saddle position. The crack remained principally confined to the chord weld toe. The sectional views show type S fatigue crack growth (section 295), however at positions closer to the crown, crack growth was on a plane almost perpendicular to the chord surface (sections 85 and 505, figure 5.9). Although some crack branching was observed (e.g. section 85, figure 6.10), no crack branching was observed at the saddle. At some positions (sections 240 and 200) the cracks intersected, resulting in material breaking away from the chord.

Figure 5.10 shows the uncorrected crack depth as a function of distance from the crown position. The crack aspect ratio was estimated from this diagram. The variation of the crack aspect ratio with the crack depth is shown in figure 5.18.

The crack depth was corrected to account for the two dimensional field. Crack depth readings for the crack at the deepest point are shown in figure 5.11. For crack depth readings greater than 8 mm the measured crack depth varied with the applied load, consequently the recorded depth was that taken at a constant maximum load. The variation of the ACPD crack depth with the applied load is discussed below. The crack growth rate fell for cracks longer than 25 mm.

S3 (Figs 5.12, 5.13 and 5.16)

S3 was fatigue tested at a hot spot stress range of 306 MPa. The purpose of this test was to obtain fatigue crack growth data and endurance life data for the SMAW specimens for $20\text{MPa}\sqrt{\text{m}} \leq \Delta K \leq 27\text{MPa}\sqrt{\text{m}}$. Prior to fatigue testing the node was soaked under standard test conditions for a period of 46 days. Fatigue initiation was noted at less than 10,000 cycles. The test was terminated after 327,173 cycles with no sign of seawater leakage through the chord.

Figure 5.12 shows an external view of the fatigue crack. The fatigue crack initiated at the saddle position and remained confined to the weld toe. Surface examination of the chord weld toe surface revealed several positions where adjacent cracks had intersected, resulting in material breaking away from the chord (e.g. position 345). The sectional views showed through thickness cracking, despite the fact that no seawater leakage was detected. Extensive cracking was noted, particularly at sections away from the saddle positions (e.g. section 190 and 345). Supplementary cracks ran parallel to the main crack at sections 410, 345 and 190. The supplementary crack was not linked to the principle crack at section 410. The crack sections showed type S cracking.

Figure 5.13 shows the uncorrected crack depth as a function of the distance from the crown position. Unfortunately, the crack aspect ratio could only be estimated from four profiles. This was because the ACPD crack depth became erratic after 20,549 cycles. According to the ACPD readings the profile obtained for the maximum applied load at 67,000 cycles, was actually deeper than the crack profile obtained for the maximum applied load at 78,232 cycles! The variation of the crack aspect ratio with the crack depth is shown in figure 5.18.

The crack depth was corrected for the two dimensional field. Crack depth readings for the deepest point of the crack are shown in figure 5.14. Crack growth was very rapid to a depth of 7 mm, thereafter crack growth readings became unreliable.

S4 (figures 5.15, 5.16, and 5.17)

S4 was fatigue tested at a hot spot stress range of 261 MPa. The purpose of this test was to obtain fatigue crack growth data and endurance life data for the SMAW specimens for $18\text{MPa}\sqrt{\text{m}} \leq \Delta K \leq 22\text{MPa}\sqrt{\text{m}}$. Prior to fatigue testing, the node was soaked under standard test conditions for a period of 14 days. Fatigue initiation was noted at 10,000 cycles. The test was terminated at 203,943 cycles when the crack penetrated the chord wall and seawater was observed to have leaked through the chord.

Figure 5.15 shows an external view of the fatigue crack and sectional views of the crack. The fatigue crack in specimen S4 initiated close to the saddle position and remained confined to the weld toe. Surface examination of the chord weld toe surface revealed several positions where adjacent cracks had intersected, resulting in chord material breaking away from the chord (e.g. position 405). The sectional views of S4 (figure 5.15), showed no crack branching, however there was evidence of cracks intersecting (section 150). The crack sections show type S cracking.

Figure 5.16 shows the uncorrected crack depth as a function of the distance from the crown position. The aspect ratio was estimated from the crack profiles. The variation in the crack aspect ratio with the crack depth is shown in figure 5.18.

Fatigue crack growth rates are for the deepest point of the fatigue crack. The crack depth was adjusted for the two dimensional field. The crack depth is shown as a function of elapsed cycles in figure 5.17. For crack depth readings greater than 8 mm the measured crack depth varied with the applied load, consequently the recorded depth is that taken at a constant maximum load. The crack growth rate fell for cracks greater than 25 mm long.

Crack Fractography.

The crack surface of specimens W1/W5 and S2 were examined using a scanning electron microscope. This was done to enable a comparison to be made with the fracture surface of the air fatigue tested specimens W6 and S1.

The crack surface of the corrosion fatigue FCAW specimen, W5, is shown in figure 5.19a and 5.19b. Figure 5.19a shows the crack surface for early crack growth ($a < 4$ mm). The crack surface was smooth compared to later crack growth and on a plane

normal to the weld toe. This was similar to the early crack growth surface of specimens W6 and S1. Later crack growth ($a > 4$ mm) at position 305 was characterised by flat platelets approximately parallel to the chord surface. This was similar to the crack growth shown in specimen S1.

The crack surface of the corrosion fatigue, SMAW specimen, S2 is shown in figure 5.20a and 5.20b. Figure 5.20a shows the crack surface for early crack growth ($a < 4$ mm). The crack surface was smooth compared to later crack growth (the scale on the surface was due to salt deposits) and on a plane normal to the weld toe. This was similar to the early crack growth surface of specimens W6 and S1. Later crack growth ($a > 4$ mm) at position 305 was characterised by flat platelets approximately parallel to the chord surface. This was similar to the crack growth shown in specimen S1 and was associated with the presence of the manganese sulphate inclusions.

5.3.3 Discussion of the Results

5.3.3.1 Corrosion Fatigue Crack Propagation

The external views of the crack in the SMAW specimen, differed from the external view of the crack in the FCAW specimen. The crack in the SMAW specimens adhered closely to the weld toe. This contrasted with the cracks in the FCAW specimen, where the cracks broke away from the weld toe and into the chord material. This was similar to that seen in the air fatigued specimens and was attributed to the difference in the notch stress at the weld toe.

The sectional views of the SMAW specimens show the corrosion fatigue cracks to be S type cracks. This meets one of the conditions for applying the SMAW, Y value equation (equation 4.13) to the corrosion fatigue test. The severe cracking seen in specimen S3 was similar to lamellar tearing. Lamellar tearing is associated with the presence of manganese sulphide inclusions [e.g. Easterling, 1992]. However it is difficult to say whether the additional crack planes parallel to the principal crack, initiated before or after, the principal crack penetrated the chord wall. The cracking in specimen S3, was more severe than was observed in either S1 or S2 and S4. Crack branching appeared to increase under a combination of high stress and cathodic protection in seawater. This could be due to either hydrogen embrittlement, or interaction between the manganese sulphide inclusions and hydrogen evolved during cathodic protection. The influence of the inclusions on the corrosion fatigue crack growth rate is discussed in section 5.3.8.2.

The sectional views of the FCAW specimen W5, show the corrosion fatigue crack at section 220 to be type W cracking. This meets one of the conditions for applying the

FCAW, Y value equation (equation 4.12) to the corrosion fatigue test. The secondary crack showed S type cracking, despite the weld process being FCAW. It is thought that the primary crack resulted in the chord bending where the crack penetrated the inner chord wall and resulted in the deflection of the secondary crack path. The primary crack was always deeper than the secondary crack and equation 4.12 was used to model the stress intensity factor. The position of the primary crack relative to the saddle meant that the geometric stress was considerably lower than the hot spot stress. Using the UCL stress distribution the geometric stress was 75% of the hot spot stress at the saddle position. Using the geometric stress at the primary crack, instead of the hot spot stress, had the effect of reducing the SIF range necessary to cause a particular corrosion fatigue crack growth rate. It was decided to characterise the SIF range using the geometric stress range at the primary crack rather than the hot spot stress.

The surface length of the crack for the SMAW specimens was of concern. The much longer crack paths observed with type S cracking, meant that, even with similar aspect ratios to typical tubular steel joints, there was potential for greater loss of stiffness before N3 failure occurs. In addition the crack path would have important implications for the remaining strength of the tubular joint. The existing convention is to assess the remaining life of the tubular joint as the number of cycles before chord wall penetration is achieved. Thereafter, the crack is assumed to grow as a through thickness crack and failure follow rapidly. The residual strength of a cracked component can also be assessed by reference to a failure assessment diagram. This assesses failure by comparing the propensity to failure by a brittle or ductile fracture mechanism to the propensity to failure by net section yielding [PD6493:1991]. Cheataini [1994], has published several proposed solutions for plastic collapse load of tubular joints, based on adaptations to the peak load formulae recommended in the HSE guidance [DEn, 1984]. The proposed formulae basically state that the plastic collapse load is proportional to the remaining ligament area. The residual joint strength would be greatly reduced if the surface area of the crack was significantly greater than that of a typical tubular joint crack, irrespective of the effect of the crack profile on the SIF. This would be particularly noticeable in fully reversed bending or axial loading, where cracks grow on opposite sides of the brace.

Similarity between the crack aspect ratios of the tubular joint tests was regarded as a precondition for the use of the empirical Y value formulae. The crack aspect ratio for the corrosion fatigued specimens was similar to that of the air tests (figure 4.18). The difference was not large enough to significantly affect the SIF.

5.3.3.2 Fracture Mechanics Analysis

The corrosion fatigue, tubular specimens had similar types of cracking and aspect ratios to their respective air specimens. It was therefore assumed that the empirical Y value equations (equations 4.13 and 4.14) could be used to accurately determine the SIF range for the corrosion fatigue tests. These formulae were applied to a depth of 30 mm in the case of the S type cracked specimens and to through thickness wall penetration in the case of W type cracked specimens. The hot spot stress was used to determine the SIF range in the case of specimens S2, S3 and S4. The geometric stress at the deepest point of the principal crack was used to determine the SIF range in the case W5, for the reasons discussed above.

Crack growth rates were determined using the seven point incremental polynomial method [ASTM E647,1993] for specimens W5, S2 and S4. In the case of specimen S3, there were few reliable crack depth measurements and the secant method [ASTM E647,1993] was used to determine the crack growth rate up to a depth of 7 mm. The ACPD measurement of crack depth was observed to vary with the actuator load for specimen S3, and to a lesser degree with specimens S2 and S4 (Appendix VII). This phenomenon was not noted with either the air specimen S1 or with specimens W5 and W6. It is thought that the errors were due to salts bridging the crack and were peculiar to corrosion fatigue conditions and S type cracking. The resultant error in the ACPD measurements could have important consequences, not only to the situation discussed above, but also to the inspection of ring stiffened joints. Where crack depth variation was suspected, the depth was estimated at the peak actuator load.

Each tubular joint test resulted in crack growth data being obtained for a restricted range of ΔK . For this reason, the crack growth data for tests W5, S2, S3 and S4 are shown together (figure 5.21). Figure 5.21 shows corrosion fatigue crack growth data for the SIF range $9\text{MPa}\sqrt{\text{m}} \leq \Delta K \leq 27\text{MPa}\sqrt{\text{m}}$. The corrosion fatigue crack growth rate experienced in the FCAW specimen (W5), varied from 3 to 5 times the air fatigue crack growth rate. Comparison with the corrosion fatigue crack growth rate measured for the X85 compact tension specimens, shows the corrosion fatigue rate was above that of X85 compact tension specimens for the region $8\text{MPa}\sqrt{\text{m}} \leq \Delta K \leq 12\text{MPa}\sqrt{\text{m}}$. Comparison with crack growth data for other higher strength steels (figure 1.37), showed that the corrosion fatigue crack growth rates of the tubular joint crack were in agreement with other steels whereas the X85 compact specimen data was anomalous. It is therefore logical to model the corrosion fatigue behaviour of X85 steel joints, on the tubular data for the FCAW specimen for $9\text{MPa}\sqrt{\text{m}} \leq \Delta K \leq 12\text{MPa}\sqrt{\text{m}}$, rather than the compact tension specimen data. For $\Delta K \geq 12\text{MPa}\sqrt{\text{m}}$ the FCAW specimen corrosion fatigue crack growth rates were significantly lower than those of the

compact tension specimens. The FCAW specimen data supported the existence of a threshold value ΔK_{TH} for the corrosion fatigue at about $8 \text{ MPa}\sqrt{\text{m}}$. This agrees with BS4360.50D variable amplitude, tubular joint test, results for specimens tested with cathodic protection [Austin, 1994]. Further tests, involving variable amplitude loading, are needed to support the existence of a threshold value for the SIF when a joint is protected with cathodic protection.

The corrosion fatigue crack growth rate experienced in the SMAW specimens varied between 3 to 6 times the mean air crack growth rate. The corrosion fatigue crack growth data from the compact tension data agreed closely with the highest rates of crack growth for the tubular joints. However, data from tests S2 and S4 showed considerable scatter. If the data for specimens S2, S4, and W5 are considered together, the crack growth rates in the interval $13 \text{ MPa}\sqrt{\text{m}} \leq \Delta K \leq 22 \text{ MPa}\sqrt{\text{m}}$ are distributed between $2.98 \times 10^{-9} (\Delta K)^{1.36} \leq \frac{da}{dN} \leq 9.98 \times 10^{-11} (\Delta K)^{2.79}$. This high rate of crack growth compared to air crack growth is typical of a hydrogen embrittlement mechanism. Data from S3, was remarkably consistent with the data from tests S2 and S4, considering the extremely high crack growth rates experienced by specimen S3 and the evidence for a crack growth mechanism similar to lamellar tearing. In fact, it is surprising that crack growth rates were not higher for specimen S3. The lower rates of crack growth associated with S3, can be attributed to the relative inaccuracy of the secant method in determining da/dN and by the crack growth rate being limited by the rate of hydrogen diffusion to the advancing crack tip. There was considerable difference between the crack growth rates of S3 and W5 even though both specimens were fatigued at the same hot spot stress range. This was attributed to the position of the primary crack relative to the saddle and the resultant lower SIF range. If the lower SIF range of the FCAW specimen is considered, then the FCAW and SMAW data are remarkably consistent. For $\Delta K \geq 12 \text{ MPa}\sqrt{\text{m}}$ the highest rates of corrosion fatigue crack growth rates were close to those of the compact tension specimens.

It was noted that the crack growth rate decelerated when the SMAW cracks reached a depth of about 30 mm (figures 5.11 and 5.17). This was associated with the crack reaching the projected brace inside wall and the crack changing direction to penetrate the chord wall. Under these conditions the SIF range could no longer be determined from equation 4.13.

Current recommended fatigue design practice for steels with a yield strength less than 400 MPa in sea water with cathodic protection gives upper bound values of C and m as: $C=7.3 \times 10^{-11}$; $m=3$. On the basis of the above tubular joint tests, there is no reason to suggest that corrosion fatigue crack growth rates for the X85 material exceed the

existing guidelines (figure 5.23). It is interesting to note that the corrosion fatigue crack growth rates were below the PD6493:1991 guidelines despite the presence of manganese sulphide inclusions.

Closer examination of the corrosion fatigue crack growth chart showed that the high crack growth rates measured in the tubular joint tests, were confined to shallow growth ($a < 4$ mm). Figure 5.22 compares crack growth rates for shallow growth ($a < 4$ mm) with crack growth rates for deeper crack growth ($a > 7$ mm). The two regimes can be clearly distinguished for $3\text{MPa}\sqrt{\text{m}} \leq \Delta K \leq 20\text{MPa}\sqrt{\text{m}}$. The crack growth rate for the shallow cracks is almost double that of the deeper cracks. These findings compare favourably with research done on variable amplitude corrosion fatigue tests of BS4360.50D steel tubular joints by Austin [1992]. Austin found that corrosion fatigue crack growth rates for cracks of between 2 and 7 mm grew at about 5 times the rate of cracks deeper than 7 mm at the equivalent SIF range.

The reason for different crack growth rates for shallow and deeper cracks can be explained by several factors. The more obvious explanation is that the shallow cracks were not subject to crack closure to the same degree as the deep cracks, and that crack closure in the corrosion fatigue specimens was in addition to any closure effects seen in the air fatigue tested specimens. It was shown (chapter 1.5.2), that the presence of these calcium chloride and other salts can lead to significant crack retardation. Indeed evidence from the compact tension corrosion fatigue tests confirmed this. The influence of crack closure would depend on the crack tip opening displacement, which would be dependent on the orientation of the crack and mode of loading. Obviously these differ significantly between the shallow and deep phases of crack growth. It is therefore probable that calcareous deposits had a significant effect on the crack growth rate, and were at least partly responsible for the slower crack growth rates observed in the deeper cracks. The variation in the ACPD crack growth readings is evidence that crack closure takes place for deeper cracks. In addition the precipitation of calcium chloride on the metal surface is believed to have an important role in limiting the availability of hydrogen.

It can also be argued that the redistribution of the residual stress has a significant effect on the corrosion fatigue crack growth rate. It was suggested that the residual stress redistributes itself as the crack grows and that the effective load ratio and ΔK_{eff} varied with the level of residual stress (chapter 1.4.2.3). Applying these features to corrosion fatigue tubular joint crack growth, the combined high residual stresses and cyclic stress would result in:

(i) a region where the combined residual stress and applied maximum stress were equal to the yield stress and where the corrosion fatigue crack growth would be modelled by corrosion fatigued data obtained at high load ratios;

(ii) a region where the combined peak cyclic stress and residual stress were below the yield stress and corrosion fatigue could be modelled at lower load ratios;

Incorporating the residual stress redistribution model [Monahan ,1994] with corrosion fatigue crack growth data obtained by Thorpe [1983] for BS4360.50D corrosion fatigue data (chapter 1.5.4.1 and figure 1.34) would provide an explanation for the high rates of crack growth experienced by the shallow cracks and the lower rates of crack growth experienced by the deeper cracks. Further experimental work would be needed to verify this hypothesis for X85 steels.

The effect of crack length on the crack tip potential was examined in section 1.5.4.2. Maahn [1986] has shown that the crack tip potential is positive, compared to the external potential. This could provide another explanation for the reduced crack growth rate for the deep cracks in comparison to the shallow cracks. A secondary effect of greater crack length is to limit the availability of hydrogen to the crack tip as hydrogen is no longer available from bulk charging of the tubular surface [Turnbull, 1986].

It is very difficult to separate the influence of crack closure, from that of residual stress effects and potential variation. However, the close correlation between the compact tension results and the tubular joint results suggest that it may be possible to isolate the effect of residual stress from the tubular joint results and account for some of the experimental scatter. This would require further experimental work to obtain the corrosion fatigue crack growth rate at known lower R ratios.

Using the recommended fatigue guidelines, leads to a conservative estimate of the remaining life. Austin [1992] suggested that corrosion fatigue crack growth for BS4360.50D steels can be accurately modelled using separate crack growth rate expressions for cracks less than and greater than 7 mm long. Figure 5.22 confirms that corrosion fatigue crack growth rates for X85 steels differ between cracks less than 4 mm long and greater than 7 mm long. Corrosion fatigue crack growth can be modelled on the basis of these two curves for the crack depths of $a < 4$ mm and $a > 7$ mm. Using the crack growth rate expression for $a < 4$ mm, in the region $4 \text{ mm} < a < 7$ mm gives a conservative prediction of the crack growth rate. Analysis was limited to $\Delta K \leq 27 \text{MPa}\sqrt{\text{m}}$, because of a lack of data for higher SIF ranges. It should also be noted that no data for deep cracks ($a < 7$ mm) were available for $\Delta K \leq 12 \text{MPa}\sqrt{\text{m}}$. Analysis of the X85 tubular joint data, leads to the following equations, assuming $\Delta K_{\text{TH}} = 8 \text{MPa}\sqrt{\text{m}}$:

$$(\Delta K \leq 8 \text{MPa}\sqrt{\text{m}}) \quad \frac{da}{dN} = 0 \quad (5.2)$$

$$(a \leq 7\text{mm}, 8\text{MPa}\sqrt{\text{m}} \leq \Delta K \leq 13\text{MPa}\sqrt{\text{m}}) \quad \frac{da}{dN} = 3.0476 \times 10^{-13} \Delta K^{5.048} \quad (5.3)$$

$$(a \leq 7\text{mm}, 13\text{MPa}\sqrt{\text{m}} \leq \Delta K \leq 27.3\text{MPa}\sqrt{\text{m}}) \quad \frac{da}{dN} = 9.98 \times 10^{-11} \Delta K^{2.79} \quad (5.4)$$

$$(7\text{mm} \leq a, 8\text{MPa}\sqrt{\text{m}} \leq \Delta K \leq 12.07\text{MPa}\sqrt{\text{m}}) \quad \frac{da}{dN} = 3.0476 \times 10^{-13} \Delta K^{5.048} \quad (5.5)$$

$$(7\text{mm} \leq a, 12.07\text{MPa}\sqrt{\text{m}} \leq \Delta K \leq 18.61\text{MPa}\sqrt{\text{m}}) \quad \frac{da}{dN} = 2.98 \times 10^{-9} \Delta K^{1.36} \quad (5.6)$$

$$(7\text{mm} \leq a, 18.61\text{MPa}\sqrt{\text{m}} \leq \Delta K \leq 27.3\text{MPa}\sqrt{\text{m}}) \quad \frac{da}{dN} = 1.15 \times 10^{-13} \Delta K^{4.84} \quad (5.7)$$

The above equations were used to predict fatigue crack growth rates for the tubular joint tests W5, S2, S3, S4. This was done by adopting the following procedure:

1) The extent of crack depth was divided into 40 logarithmic increments:

$$x = \frac{\log(a_f) - \log(a_i)}{40} \quad (5.8)$$

where a_0 is the initial flaw depth (taken as 0.15 mm) and a_f is the final depth (taken as the chord wall thickness). The crack depth at the end of each increment was calculated from:

$$a_j = 10^{\log_{10}(a_0) + jx} \quad (5.9)$$

2) ΔK was calculated at the beginning and end of each increment from equations 4.13 and 4.14. The average value was used in equations 5.2 to 5.7 to determine da/dN_j . The number of cycles consumed in the increment was then calculated from:

$$\Delta N_j = \frac{a_j - a_{j-1}}{(da/dN)_j} \quad (5.10)$$

3) The number of cycles N_j is then calculated from:

$$N_j = \sum_{a_0}^{a_j} \Delta N_i \quad (5.11)$$

As can be seen from figures 5.24a to 5.24d, the split depth equations provide a greatly improved estimate of the remaining lives of all the X85 tubular joint specimens, compared to the PD6493:1991 equations. However, the use of these equations for endurance prediction, is dependent on accurate calculation of the initiation life. If a model incorporating residual stress redistribution were shown to explain the

difference between deep crack growth and shallow crack growth, then it would be possible to justify the use of split depth models for remaining life calculations. The above calculations illustrate the potential benefits which could arise from using such an approach. In the absence of crack growth data at lower R ratios and a more complex residual stress model for corrosion fatigue, it would be wiser to consider variation in the corrosion fatigue data as being due to experimental scatter and to base fatigue calculations on the upper bound of the corrosion fatigue data.

5.3.4 Stress Endurance Results

The N1, N3 and N3* (defined in chapter 4) endurance lives for specimens W5, S2, S3 and S4 are presented in table 5.4. A graphical comparison with BS4360.50D tubular joint, corrosion fatigue data is made in figures 5.25 and 5.26. Results are compared to the endurance life predicted using the corrosion fatigue T' curve (equation 1.3). The T' curve has been adapted to corrosion fatigue conditions by imposing a penalty of 0.5 on the air T' curve (chapter 1.5.5). Endurance lives and the T' curve have been standardised to a thickness of 20 mm using equations 1.4 and 1.6.

5.3.4.1 N1 Endurance Data

The crack initiation of welded tubular joints was discussed in chapter 1.4.2 and the influence of cathodic protection on the crack initiation process was discussed in chapter 1.5.3. It was noted that it was normal to consider tubular joints as having weld defects from which fatigue cracks can propagate. If fatigue cracks are assumed to propagate from preexisting flaws, then the N1 life represents the number of cycles for the crack to propagate to a detectable size. Detection of the N1 endurance life in corrosion fatigue conditions is particularly difficult. The use of MPI in an enclosed seawater environment would lead to seawater pollution and was deemed unacceptable. Therefore N1 detection was by the ACPD technique. As noted previously, the accuracy of this technique depends on the probe spacing and the position of the crack relative to the probes. Therefore, the N1 lives given in this chapter are for the greatest number of cycles for crack initiation to take place and may be closer to N2 in reality. However, the N1 life allows for a comparison to be made between the FCAW and SMAW specimens and with the BS4360.50D steel tubular joints. Unfortunately, little data is available for the N1 life of BS4360.50D tubular joints under conditions of corrosion protection and constant amplitude loading, the data points shown in figure 5.25 are estimated from the crack growth curve derived by Wilson [1986].

Comparison shows that the SMAW tubular specimen N1 lives of specimens S2 and S4 are in broad agreement with data obtained by Wilson for BS4360.50D tubular

joints protected at -850 mV. The endurance life of N3 was substantially lower. There was no improvement in the initiation life as a result of using the higher yield strength material. There was no evidence for the restoration of the air N1 life when compared to BS4360.50D data (figure 5.25) or to the X85 data (c.f. figure 4.21). However, the N1 life of W1 is greater than 97.6% of the N3 endurance for BS4360.50D tubular joints in an air environment. This extended life shows that there is evidence for an improvement in the N1 life as a result of using the FCAW process. The lower SIF range for the FCAW specimens, combined with lower corrosion fatigue crack growth rates and the existence of a threshold SIF range would explain the extended N1 life of the FCAW specimens. This finding was in line with the extended air fatigue N1 results of the FCAW specimens discussed in chapter 4, which was attributed to the weld profile rather than any increase in the yield strength of the steel. Evaluation of the initiation life using a strain life approach would require additional material data (section 1.4.2.1).

5.3.4.2 N3 Endurance Results

The evaluation of the N3 life of the SMAW specimens was complicated by the crack path. It was argued in section 4.3.5.1, that a more realistic measure of the endurance life, was to determine the number of cycles for the crack to reach a depth equivalent to that of the chord wall thickness (the N3* endurance life). The N3* endurance lives are therefore presented with the N3 life for the SMAW specimens.

Comparison of the N3 life of the FCAW tubular joint with the N3 life of the BS4360.50D tubular joints, showed that W1 had a longer life than that typical of the BS4360.50D tubular joints tested in air environment. This represented a significant increase in the N3 endurance life at a hot spot stress range of less than 200 MPa. At the higher hot spot stress range of 300 MPa, the N3 endurance life was equal to that shown typically by a BS4360.50D tubular joint, despite the fact that the joint had been previously fatigued at 200 MPa. Both W1 and W5 exceeded the recommended design guidelines. The evidence from tests W1 and W5 was that the existing guidelines can be used to predict a conservative value for the FCAW specimens constructed from API 5L X85 steel.

Comparison of the N3 life of the SMAW tubular joint with the N3 life of the tubular joints, shows that the N3 lives of S2 and S4 were equivalent to the N3 lives of the BS4360.50D specimens. The N3 life of S3 was difficult to determine, but estimating the N3* life of specimen S3 from figure 5.14, resulted in an endurance life slightly lower than that typical of the BS4360.50D specimens. The N3* life of all the X85 tubular joints were just in excess of the recommended design guidelines.

Given the similarities between the N1 lives of the SMAW tubular joints, the similarity between the corrosion fatigue crack growth rates and the similarity between the empirical Y value and the TPM and AVS equations, there is no reason why there should be any substantial difference between the endurance lives of the BS4360.50D and X85 tubular joints. The evidence suggests that the adapted T' curve can be used for SMAW specimens constructed from API 5L X85 steel to predict a conservative value for the corrosion fatigue endurance life. However, more joints would need to be tested before this can be confirmed.

It should also be noted that the extended fatigue initiation lives and low shallow crack growth rates could be reproduced in the SMAW specimens by weld toe grinding or TIG dressing, in much the same way as was recommended for the air specimens (section 4.3.5.2). This would lead to the advantage of extended life, without the disadvantages of reduced toughness or poor weld profiling. If, as the above results would suggest, the advantage of extended life was present under conditions of cathodic protection, then the use of higher strength steels would have commercial benefits for offshore applications. The influence of weld toe grinding and TIG dressing on the fatigue life of higher strength steels is therefore worthy of further investigation.

5.4 Conclusions

- 1) The corrosion fatigue crack path has been shown to be similar to the fatigue crack path of the air fatigue tested tubular joints tested in the current test programme. The fatigue crack path was believed to be influenced by the weld geometry, weld mismatch, through thickness stress and the presence of manganese sulphide impurities in the steel.
- 2) The corrosion fatigue crack growth rate have been determined in terms of ΔK for the API 5L X85 steel tubular joints.
- 3) Corrosion fatigue crack growth rates for both SMAW and FCAW tubular joints of X85 structural tubing can be conservatively modelled using current PD6493:1991 fatigue guidelines for steels of yield strength below 400 MPa i.e. Paris Law constants of $C=7.3 \times 10^{-11}$ and $m=3$ (MPa, m units).
- 4) Corrosion fatigue crack growth rates have been shown to differ for cracks of less than 4 mm and more than 7 mm. Alternative suggestions were proposed to explain the difference in the crack growth rates.

5) Constant amplitude tests on four tubular welded double T joints of X85 structural tubing in seawater, show that the existing fatigue guidance recommended T' curve gave a conservative prediction of the endurance life, where the joint is protected at a potential of -1000 mV (vs Ag/AgCl).

**TABLE 5.1:CHEMICAL COMPOSITION OF SUBSTITUTE SEAWATER
[ASTM D1141]**

Compound	Concentration (g/L)
NaCl	24.53
MgCl ₂ .6H ₂ O	5.20
Na ₂ SO ₄	4.09
CaCl ₂	1.16
KCl	0.695
NaHCO ₃	0.201
KBr	0.101
H ₃ BO ₃	0.027
SrCl ₂ .6H ₂ O	0.025
NaF	0.003

Chlorinity of this substitute seawater is 19.38

The pH (after adjustment with 0.1 M NaOH solution) is 8.2.

TABLE 5.2 COMPACT TENSION TEST CONDITIONS

Load range	R ratio	Test frequency	Environment	CP level (vs Ag/AgCl)
3.4	0.7	0.167	Seawater	-1000 mV
5	0.7	0.167	Seawater	-1000 mV

TABLE 5.3 TUBULAR JOINT TEST CONDITIONS

Test No.	Weld Process	Hot Spot Stress Range (MPa)	R Ratio	Test Frequency (Hz)	Environment	CP level vs Ag/AgCL
W1	FCAW	200	0.05	0.167	Sea water	-1000mV
W5 ¹	FCAW	300	0.05	0.167	Sea water	-1000mV
S2	SMAW	235	0.05	0.167	Sea water	-1000mV
S3	SMAW	306	0.05	0.167	Sea water	-1000mV
S4	SMAW	261	0.05	0.167	Sea water	-1000mV

1 Previously tested as W1.

**TABLE 5.4 INITIATION AND TOTAL LIFE ENDURANCE DATA:
CORROSION FATIGUE SPECIMENS**

Specimen	Hot Spot Stress Range MPa	Initiation Life N1	Through Wall Thickness Life N3 (N3*)	Comments
W1	200			No sign of initiation after 3,085,000 cycles
W5	300	130,000 cycles	423,477 cycles	Previously tested as W1
S2	235	30,000 cycles	458,465 cycles (141,000 cycles)	
S3	306	0 cycles	<327,173 cycles (46,000 cycles)	No obvious sign of N3, though crack reached depth of 20mm after 56,000 cycles
S4	261	10,000 cycles	203,943 cycles (75,000 cycles)	

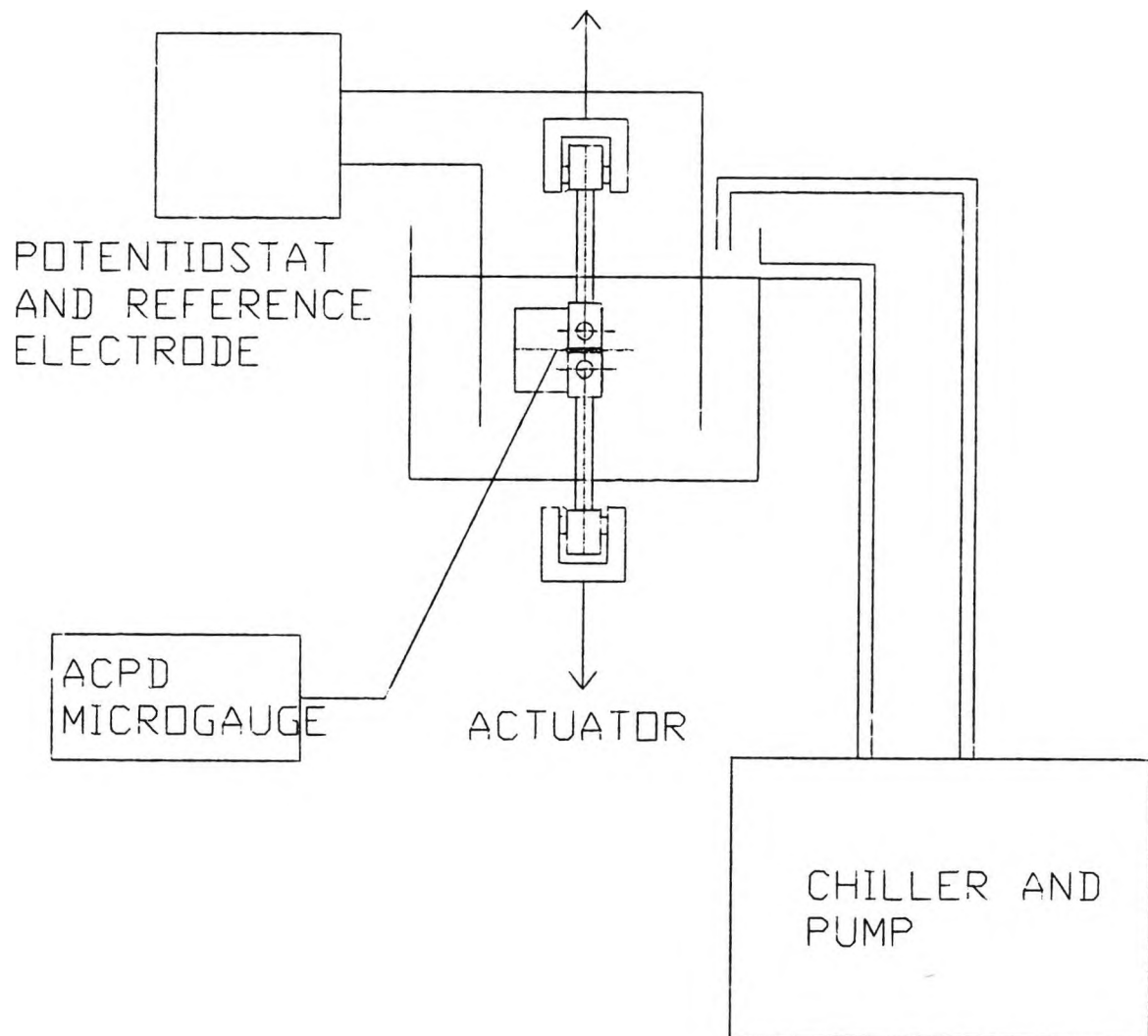


Figure 5.1 Schematic of compact tension corrosion fatigue rig.

Figure 5.2 Corrosion Fatigue Crack Growth Rates for X85 Structural Steel, Compact Tension Specimens, Cathodic Protection (-1000mV vs. Ag/Cl), R=0.7

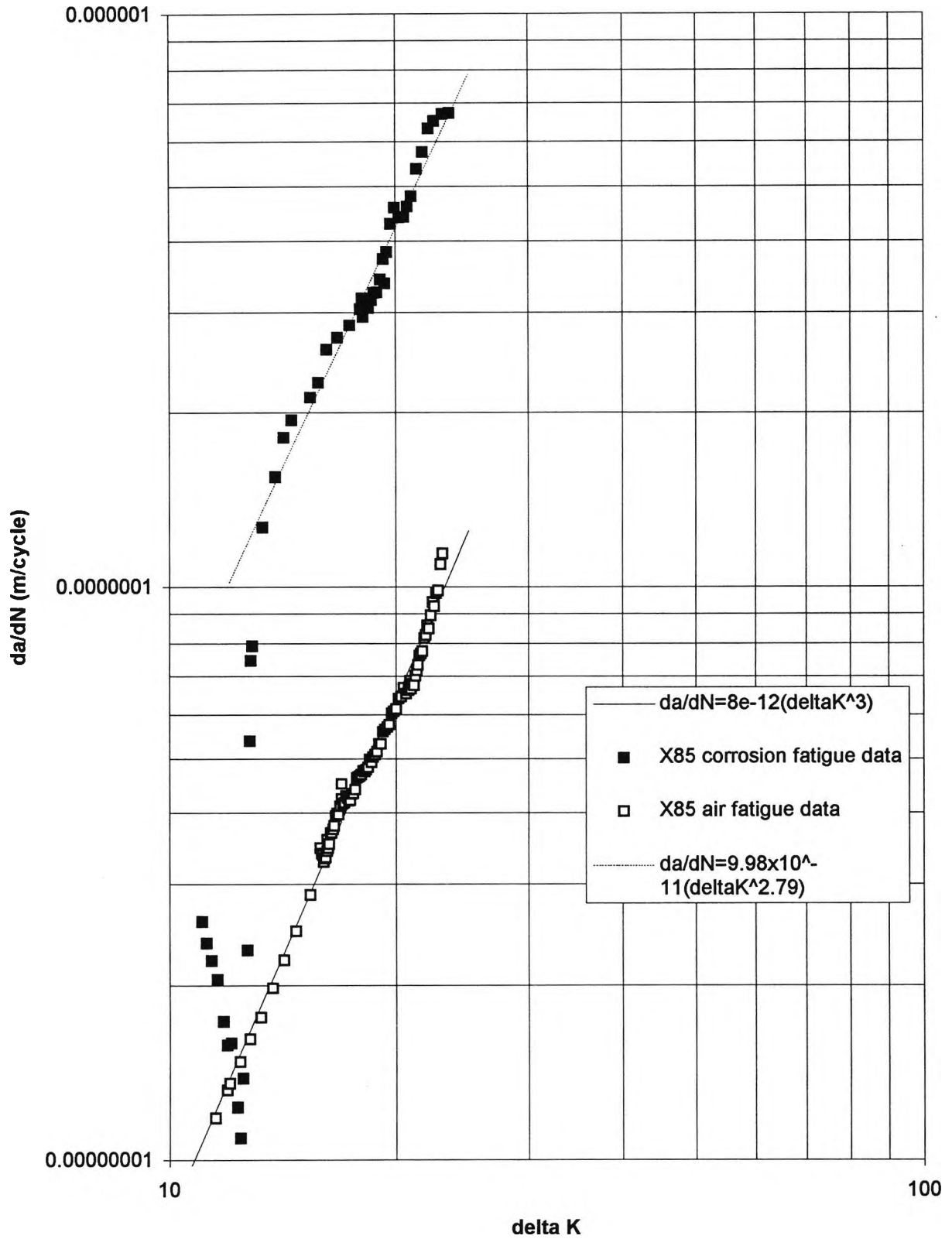
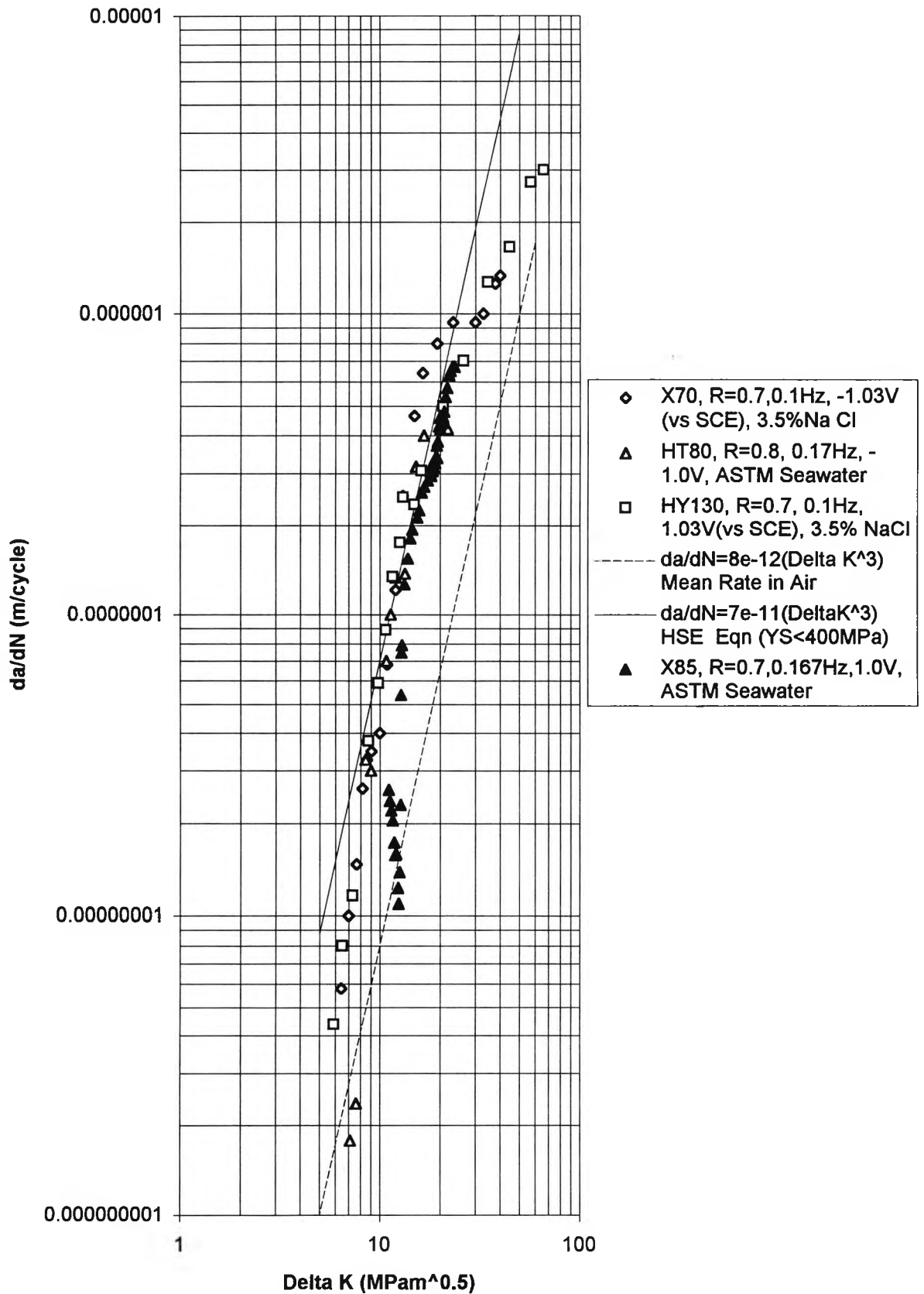


Figure 5.3: Comparison of Corrosion Fatigue Data for High Strength Steels with Cathodic Overprotection



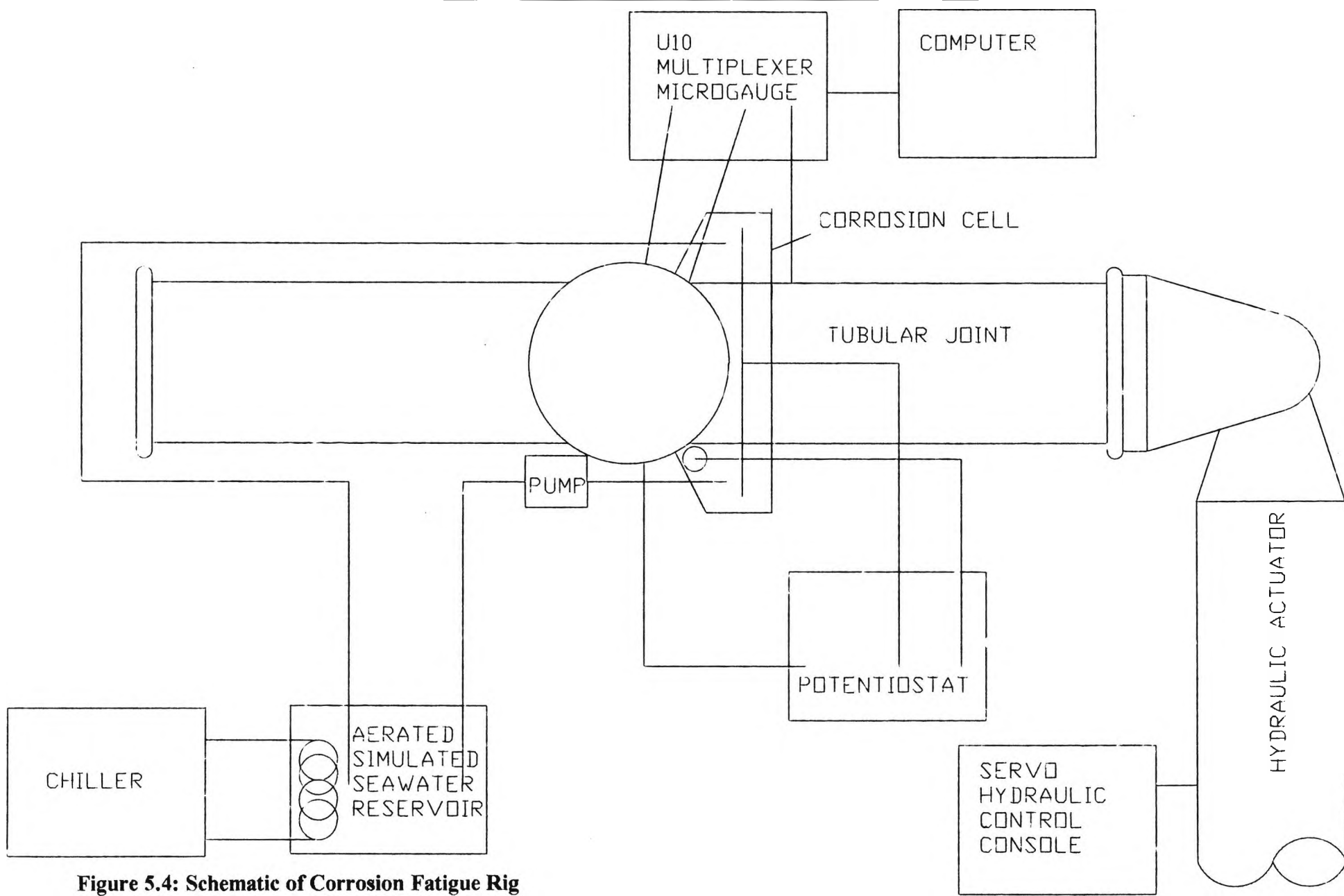


Figure 5.4: Schematic of Corrosion Fatigue Rig

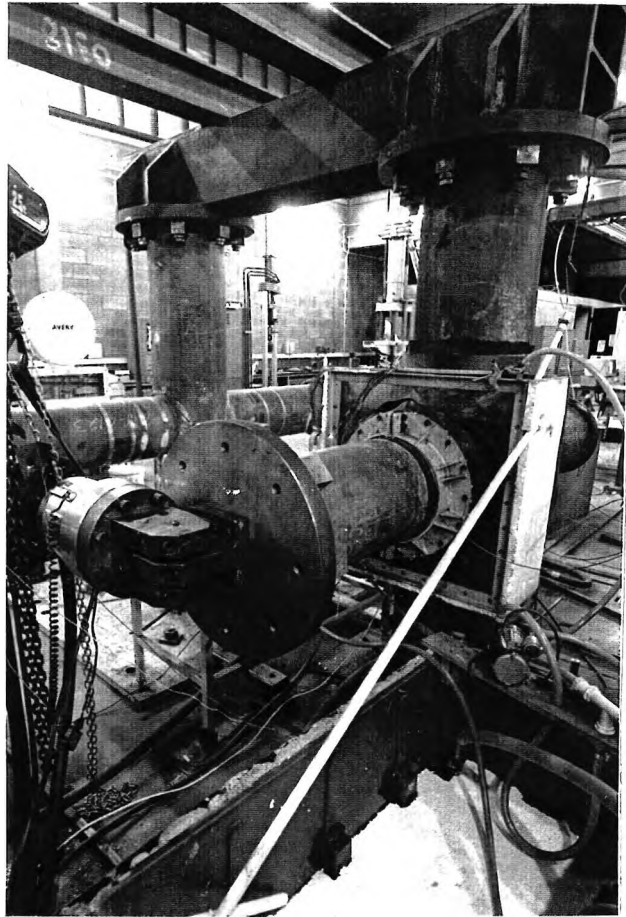
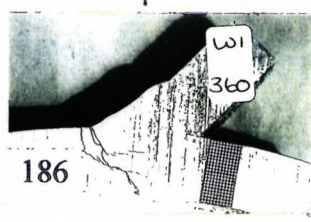
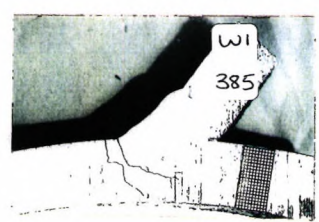
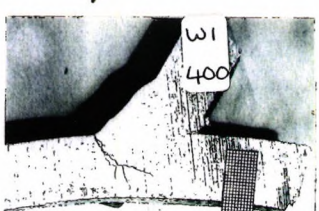
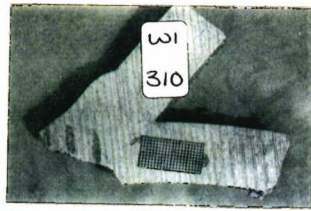
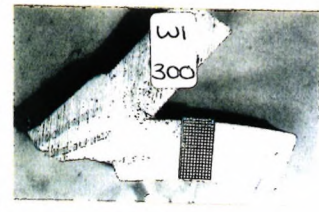
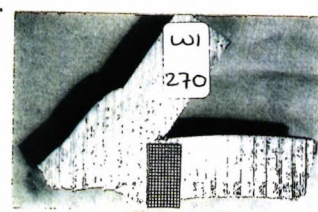
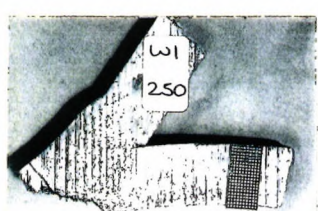
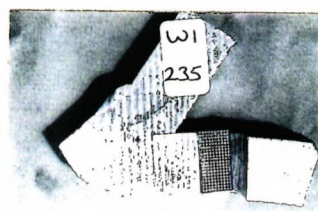
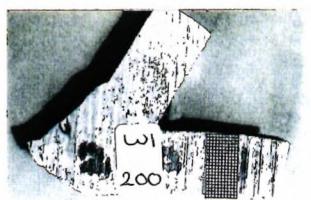
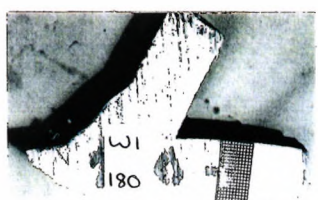
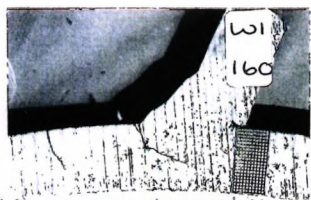


Figure 5.5: Photograph of Tubular Joint, Corrosion Fatigue Rig



186

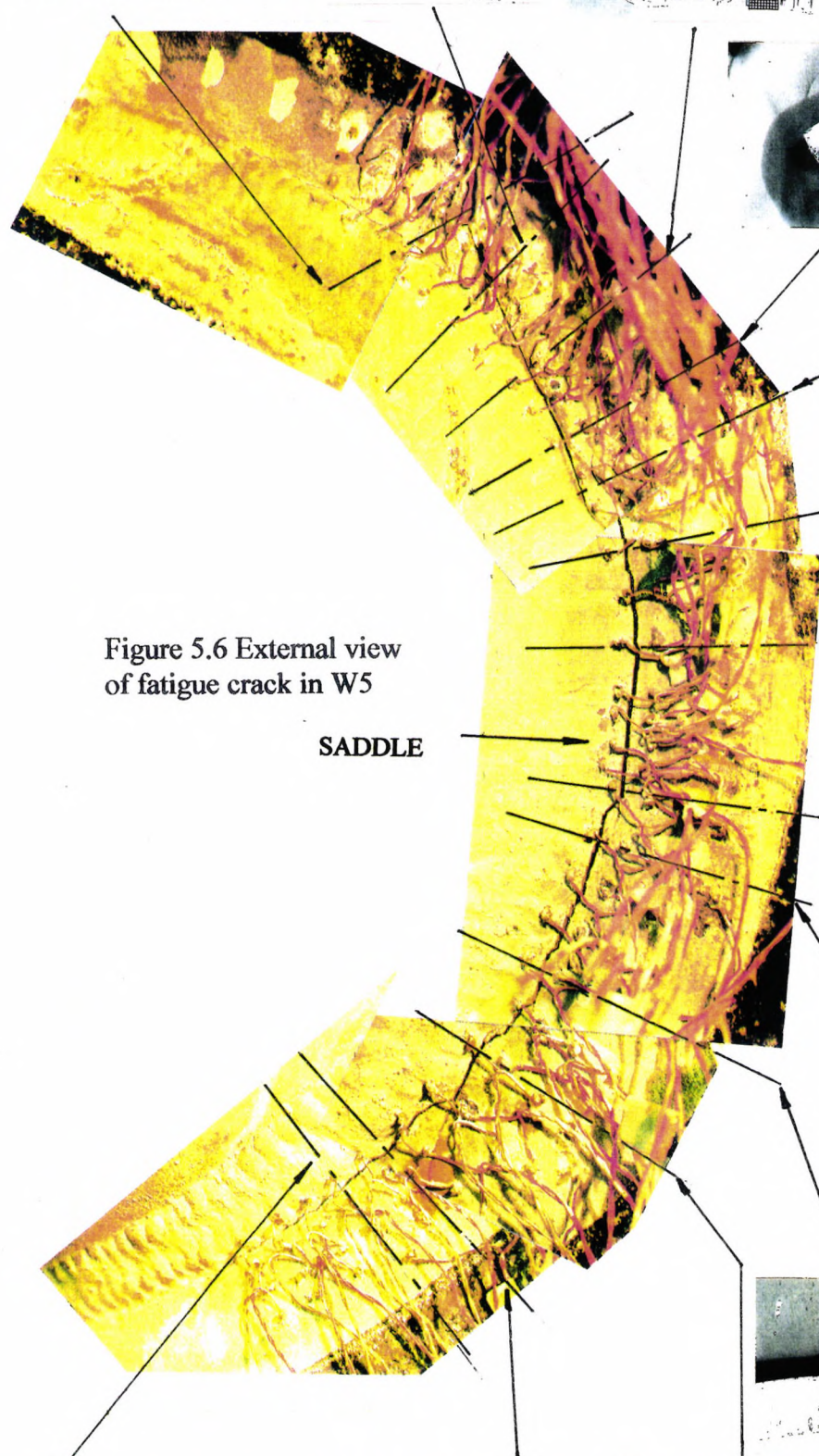
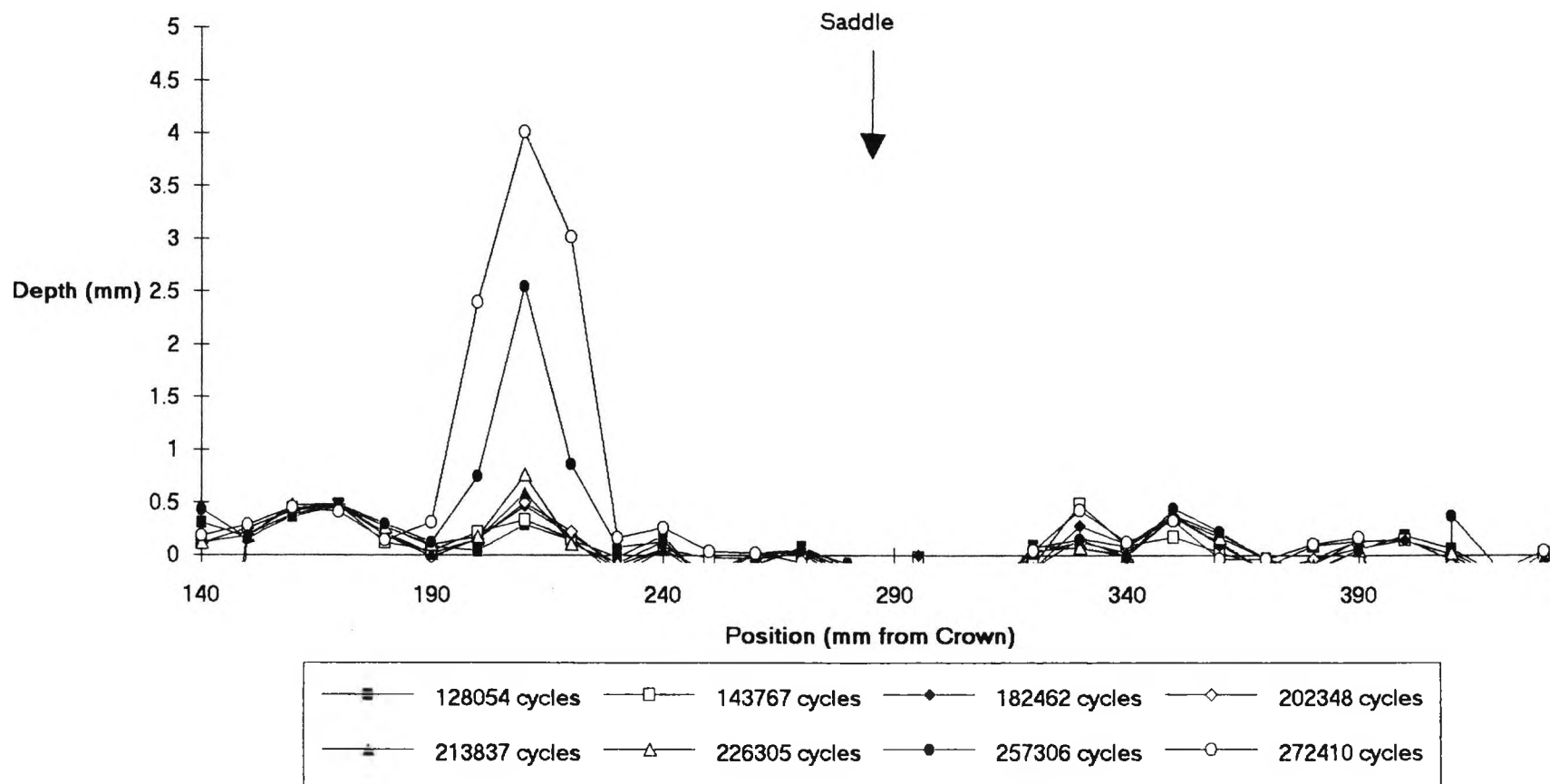


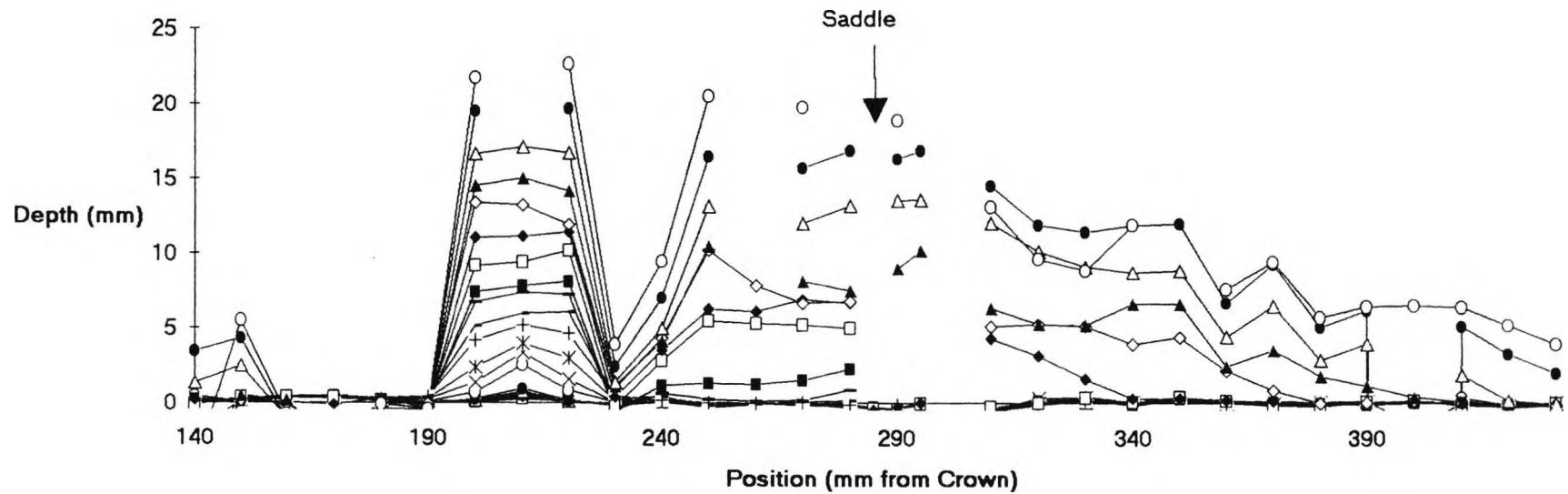
Figure 5.6 External view of fatigue crack in W5

SADDLE

**Figure 5.7a: W5 Corrosion Fatigue Crack Profile
Uncorrected Depth. Depth <5mm**

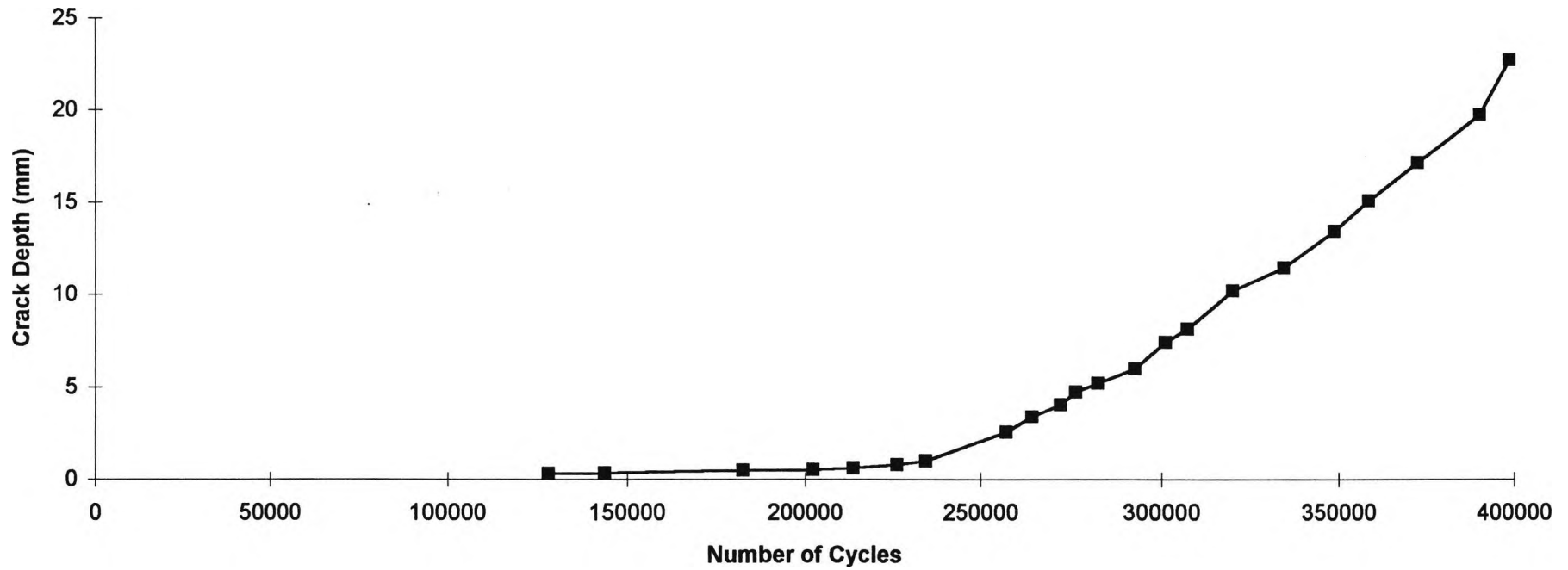


**Figure 5.7b: W5 Corrosion Fatigue Crack Profile
Uncorrected Depth**



■	128054 cycles	□	143767 cycles	◆	182462 cycles	◇	202348 cycles	▲	213837 cycles
△	226305 cycles	●	234421 cycles	○	257306 cycles	×	264520 cycles	*	272410 cycles
+	282715 cycles	←	292751 cycles	→	301148 cycles	■	307160 cycles	□	319863 cycles
◆	334292 cycles	◇	348713 cycles	▲	358516 cycles	△	372657 cycles	●	390407 cycles
○	398890 cycles								

**Figure 5.8: Corrosion Fatigue Crack Growth Data: Specimen W5
Saddle Hot Spot Stress Range: 300MPa**



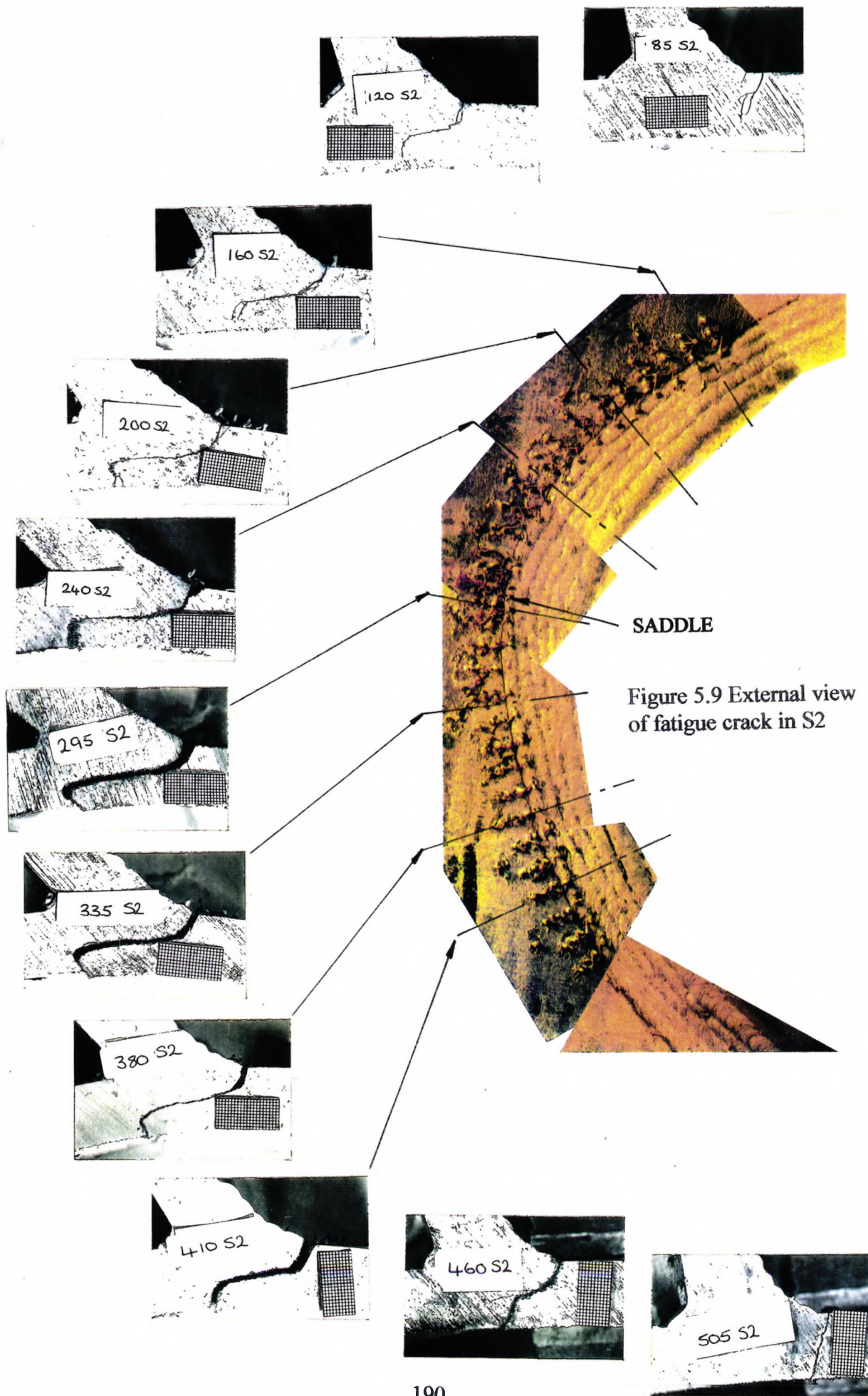
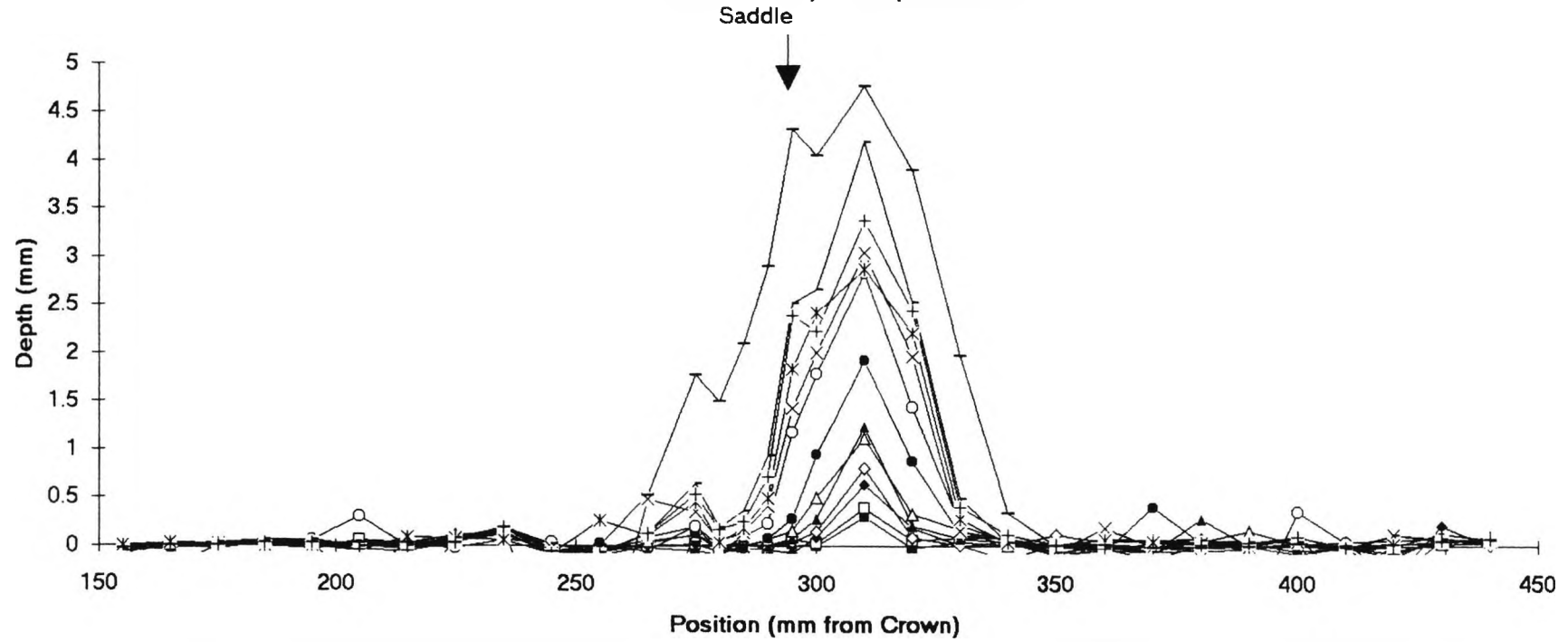


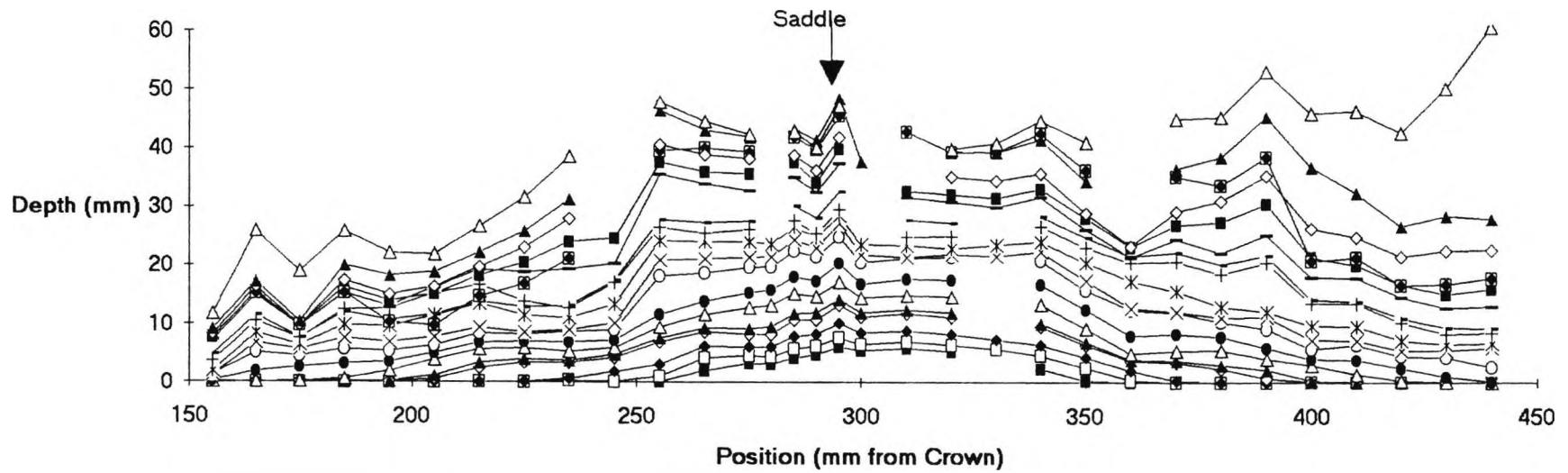
Figure 5.9 External view of fatigue crack in S2

Figure 5.10a: S2 Corrosion Fatigue Crack Profile
Uncorrected Depth. Depth <5mm.



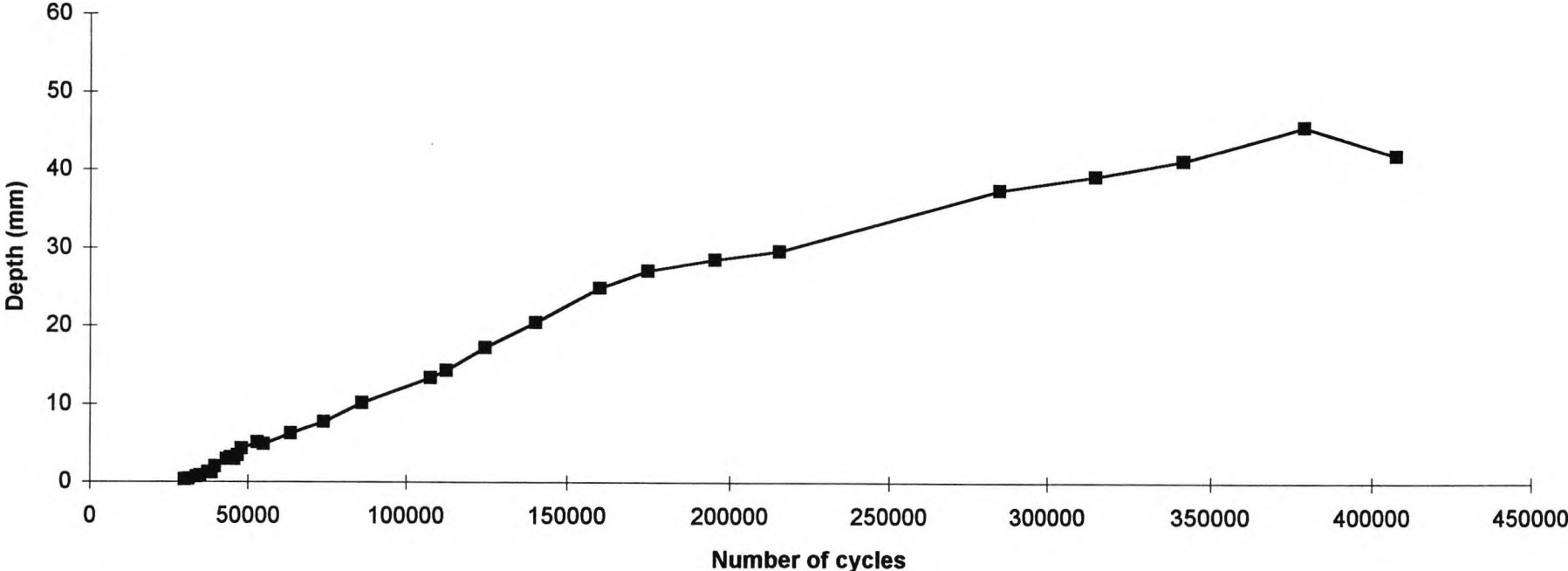
—■—	30000 cycles	—□—	31216 cycles	—◆—	33648 cycles	—◇—	34864 cycles	—▲—	37250 cycles
—△—	38452 cycles	—●—	39540 cycles	—○—	43199 cycles	—×—	44416 cycles	—*—	45632 cycles
—+—	46849 cycles	—	48066 cycles	—	54763 cycles				

**Figure 5.10b: S2 Corrosion Fatigue Crack Profile
Uncorrected Depth. Depth>5mm**



■ 63350 cycles	□ 74102 cycles	◆ 86193 cycles	◇ 107672 cycles	▲ 112634 cycles
△ 124686 cycles	● 140282 cycles	○ 159864 cycles	× 174623 cycles	* 195261 cycles
+ 217432 cycles	— 230674 cycles	— 284900 cycles	■ 315091 cycles	□ 341740 cycles
◆ 378835 cycles	◇ 407752 cycles	▲ 438053 cycles	△ 458465 cycles	

Figure 5.11: Corrosion Fatigue Crack Growth Data: Specimen S2
Hot Spot Stress Range: 235MPa



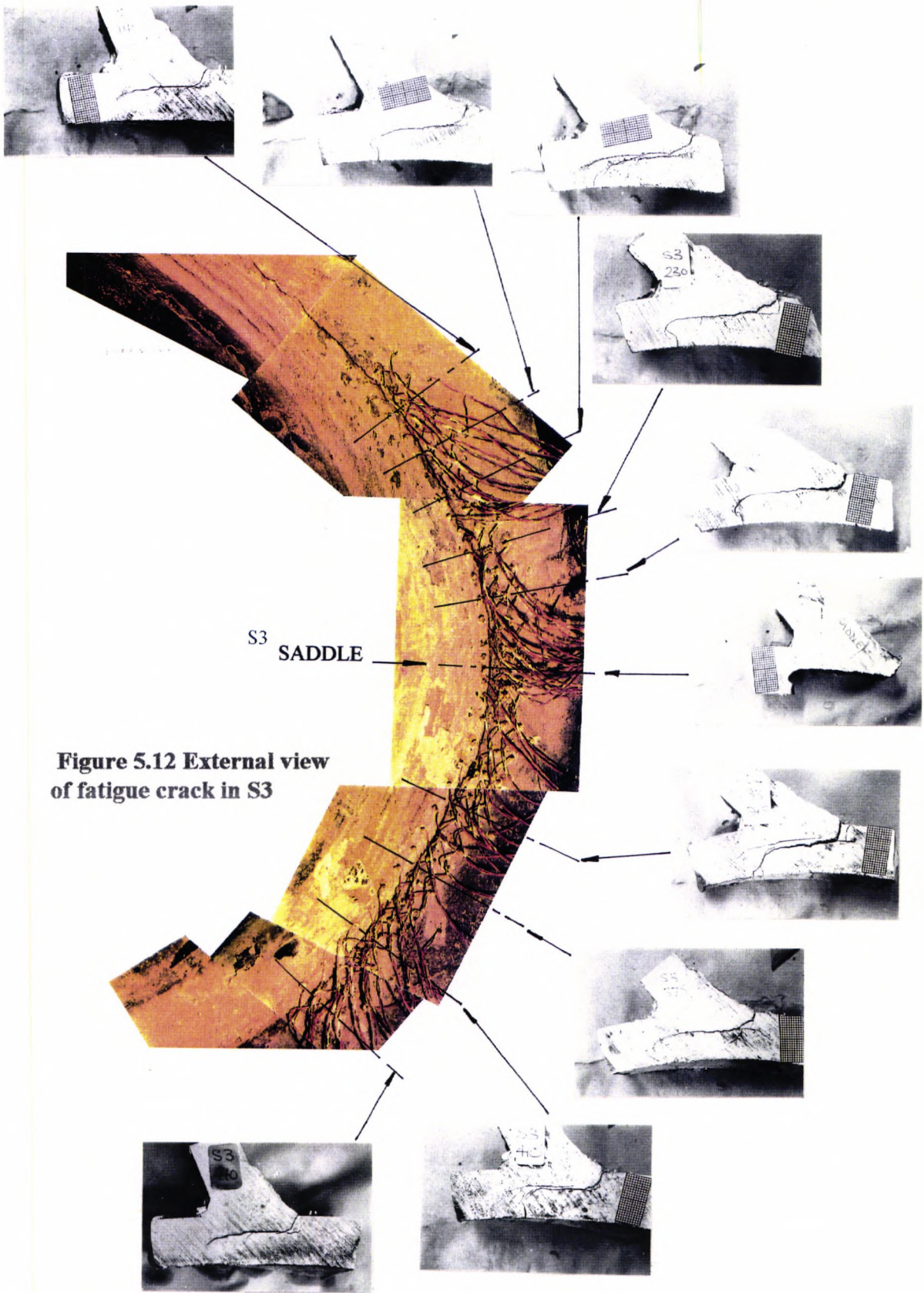
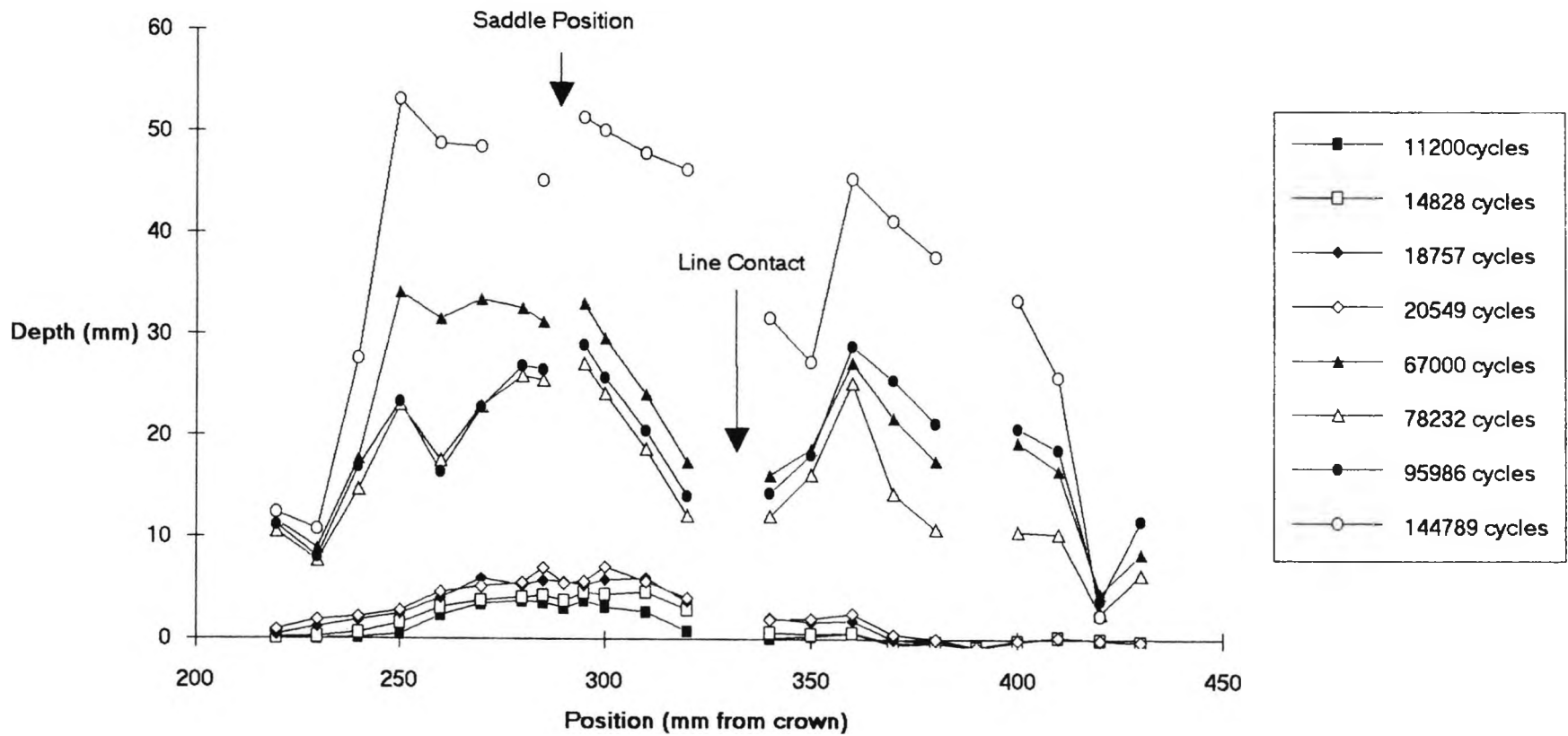
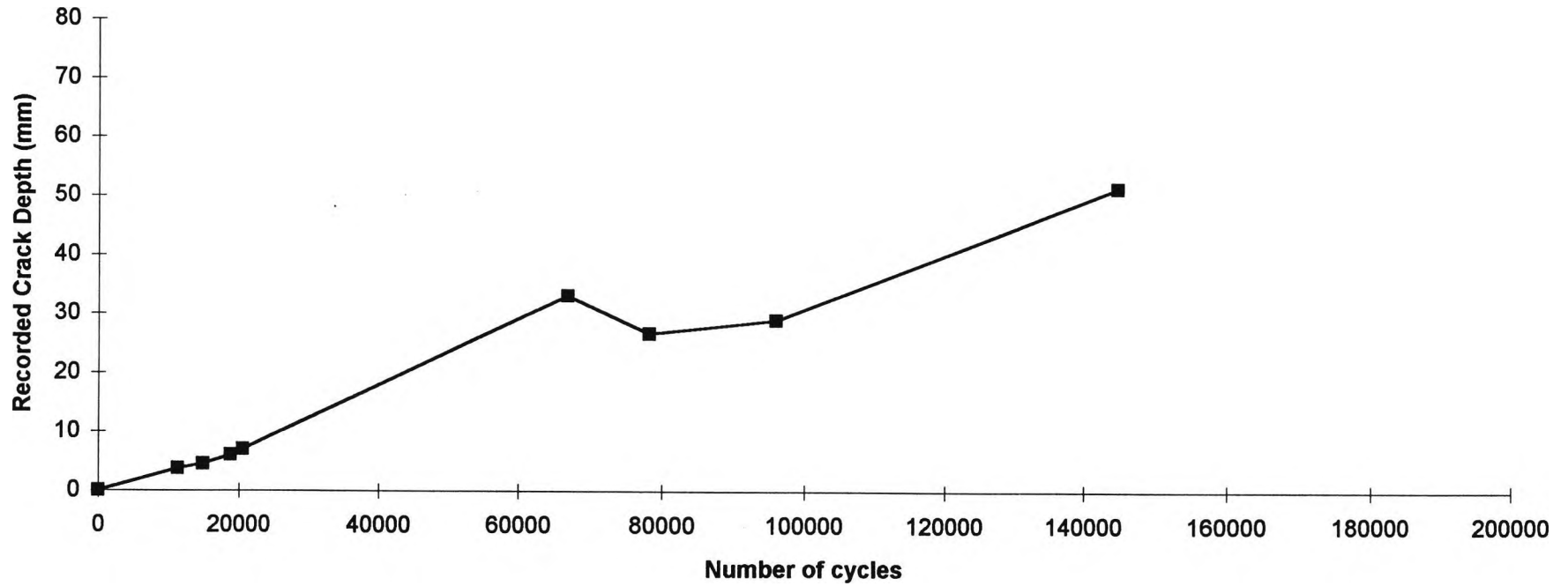


Figure 5.12 External view of fatigue crack in S3

Figure 5.13: S3 Corrosion Fatigue Crack Profile: Uncorrected Depth



**Figure 5.14: Corrosion Fatigue Crack Growth Data: Specimen S3
Hot Spot Stress Range: 306MPa**



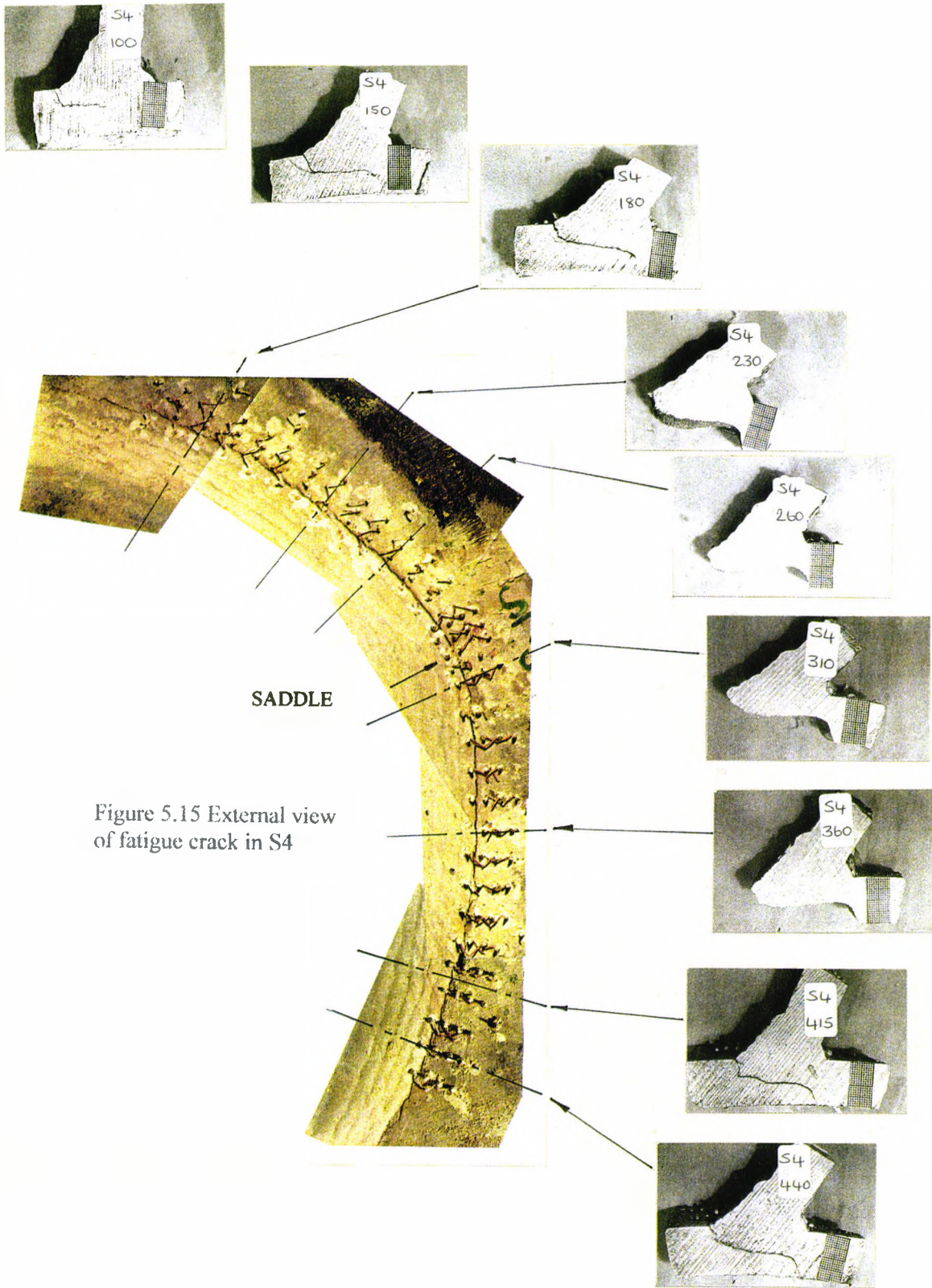


Figure 5.15 External view of fatigue crack in S4

Figure 5.16a: S4 Corrosion Fatigue Crack Profile: Uncorrected Depth. Depth <5mm

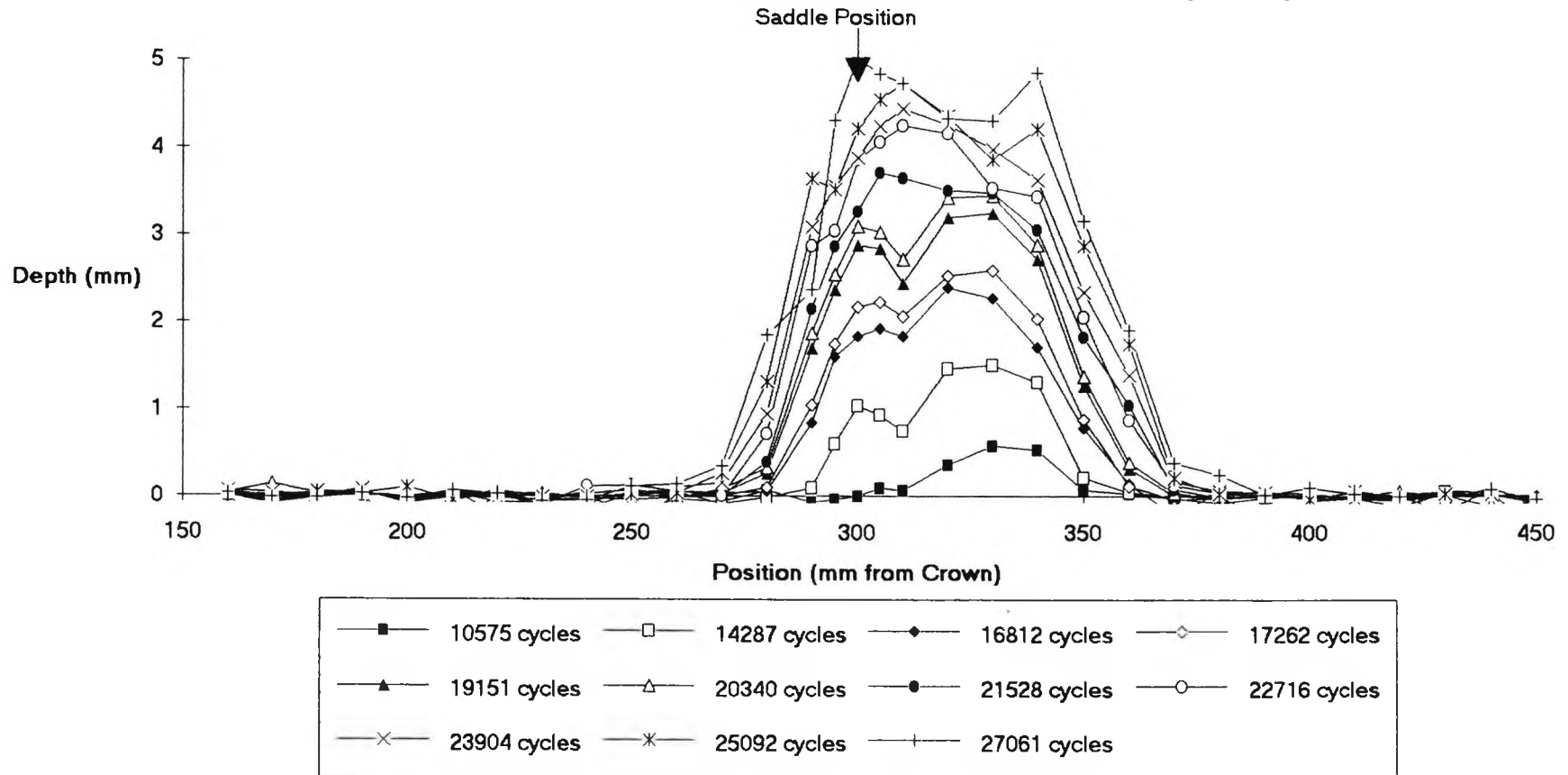
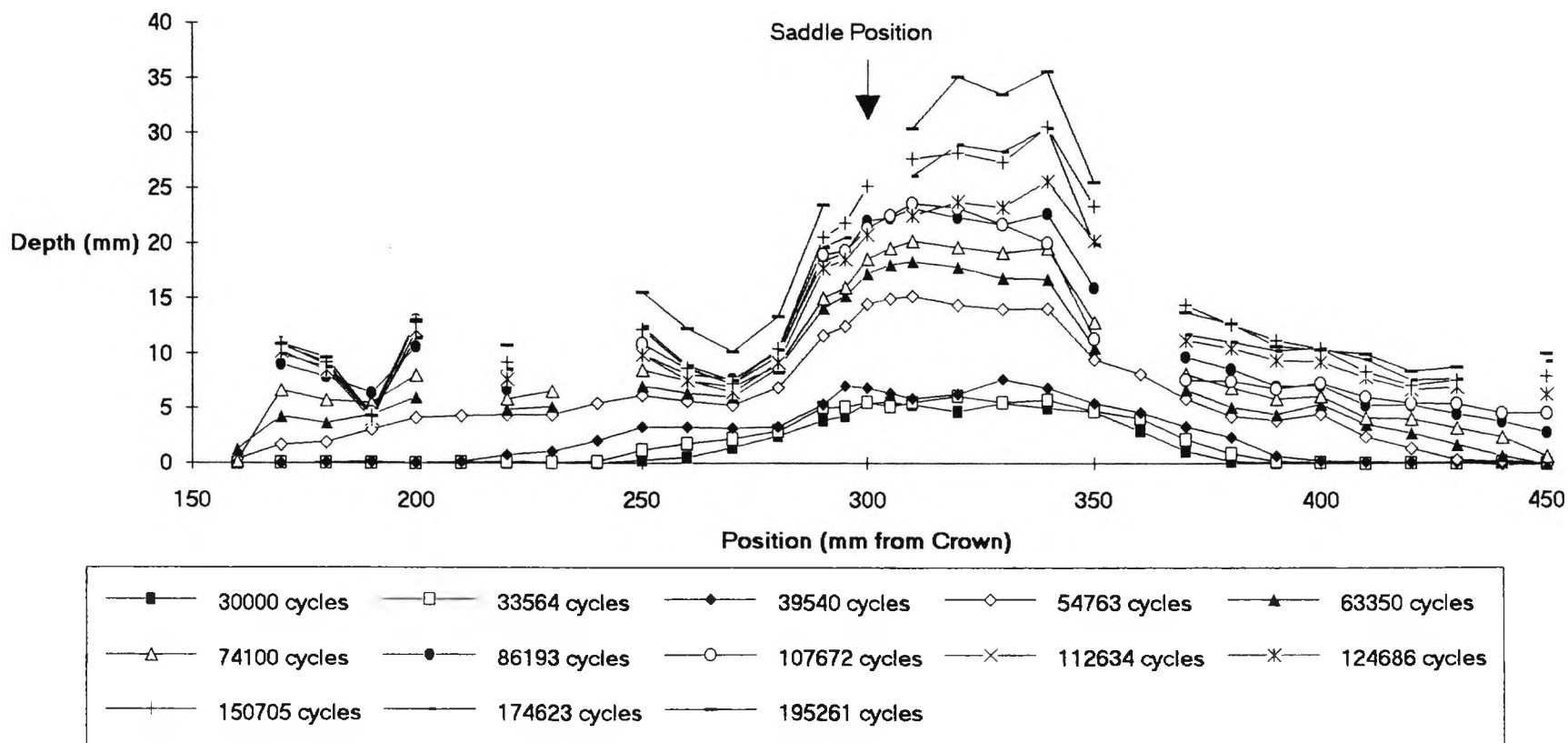


Figure 5.16b: S4 Corrosion Fatigue Crack Profile: Uncorrected Depth. Depth >5mm



**Figure 5.17: Fatigue Crack Growth Data: Specimen S4
Hot Spot Stress Range: 261MPa**

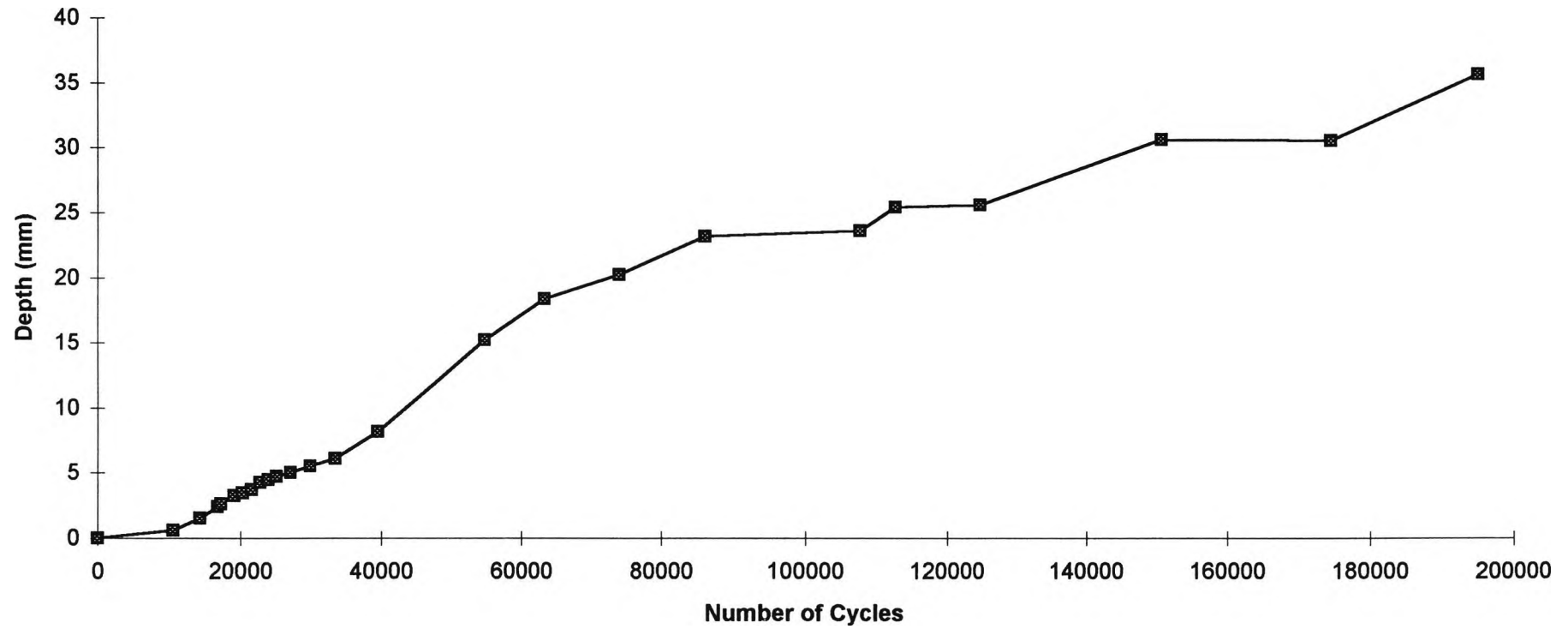
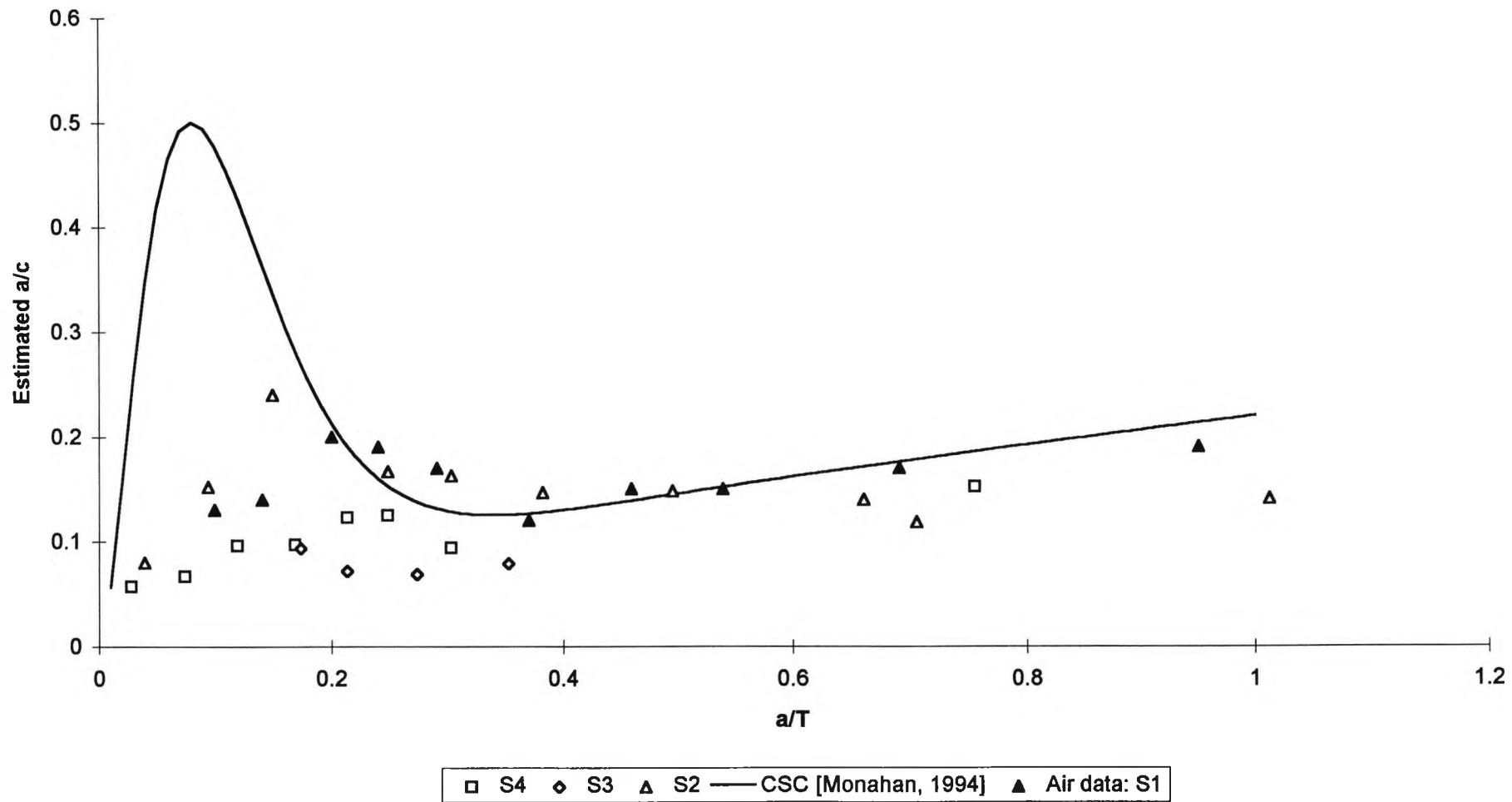


Figure 5.18: Seawater Crack Aspect Ratio



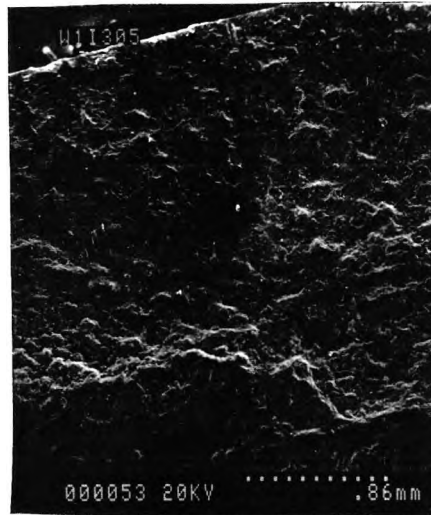


Figure 5.19a: Fracture surface for specimen W1/W5 (cracks < 4 mm)



Figure 5.19b: Fracture surface for specimen W1/W5 (cracks > 4 mm)

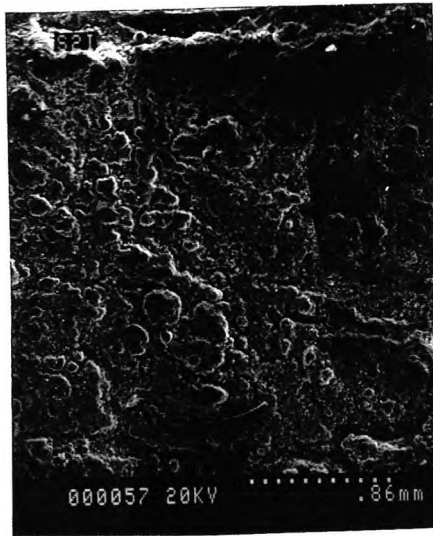


Figure 5.20a: Fracture surface for specimen S2(cracks < 4 mm)

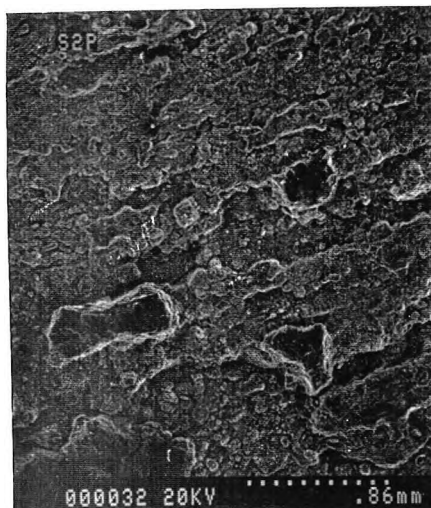


Figure 5.20b: Fracture surface for specimen S2(cracks > 4 mm)

Figure 5.21: X85 Tubular Joint, Corrosion Fatigue Data.

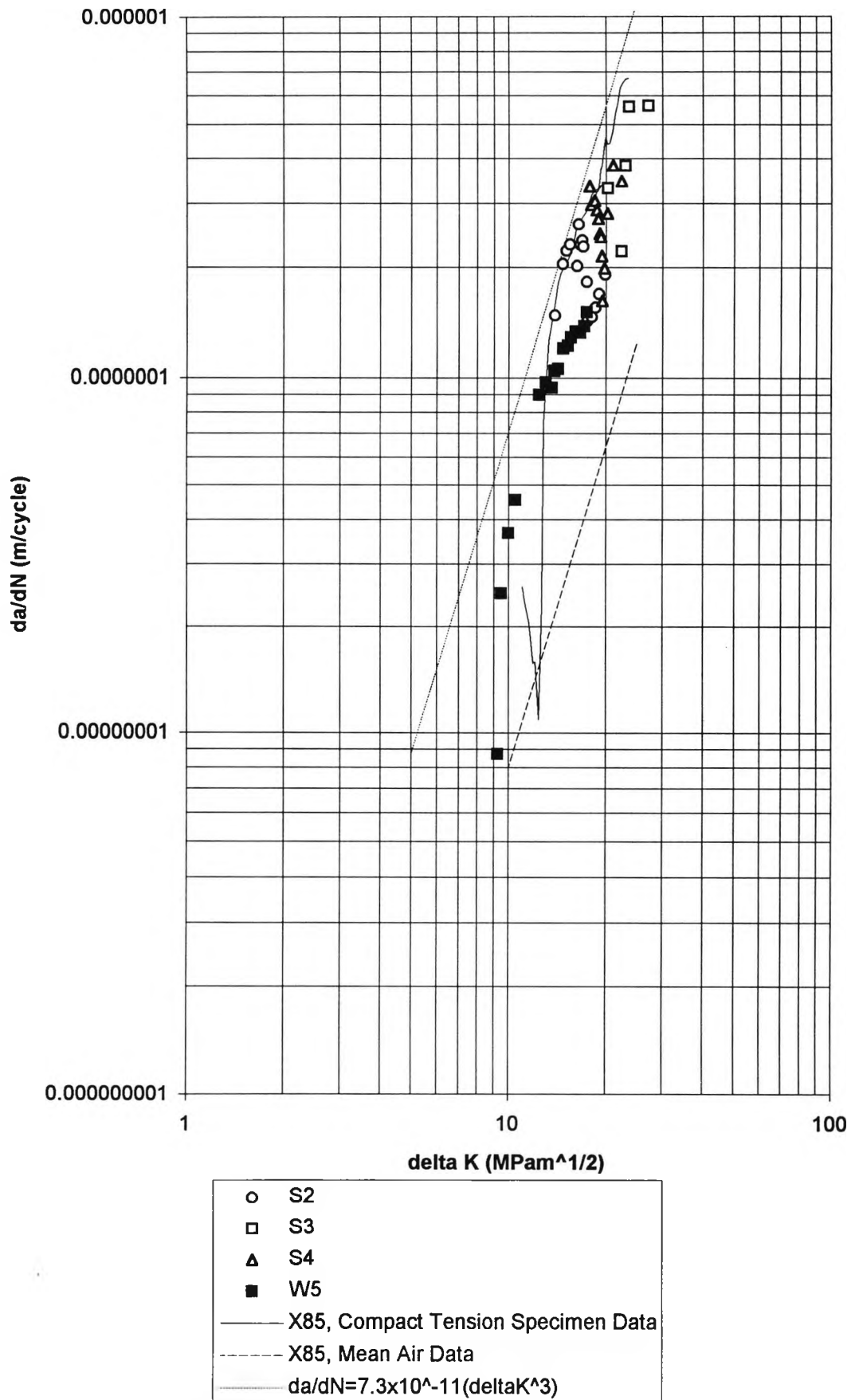
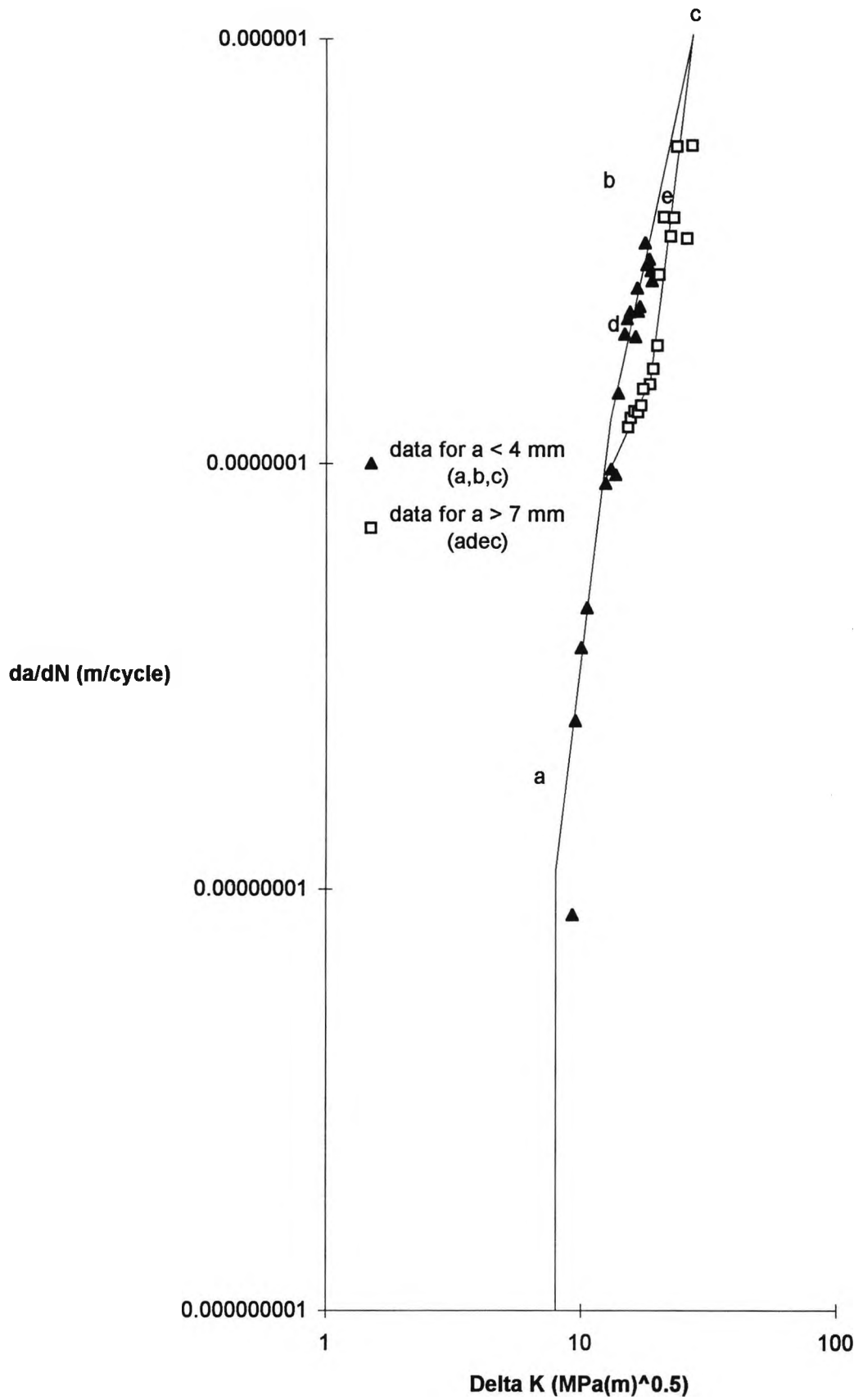
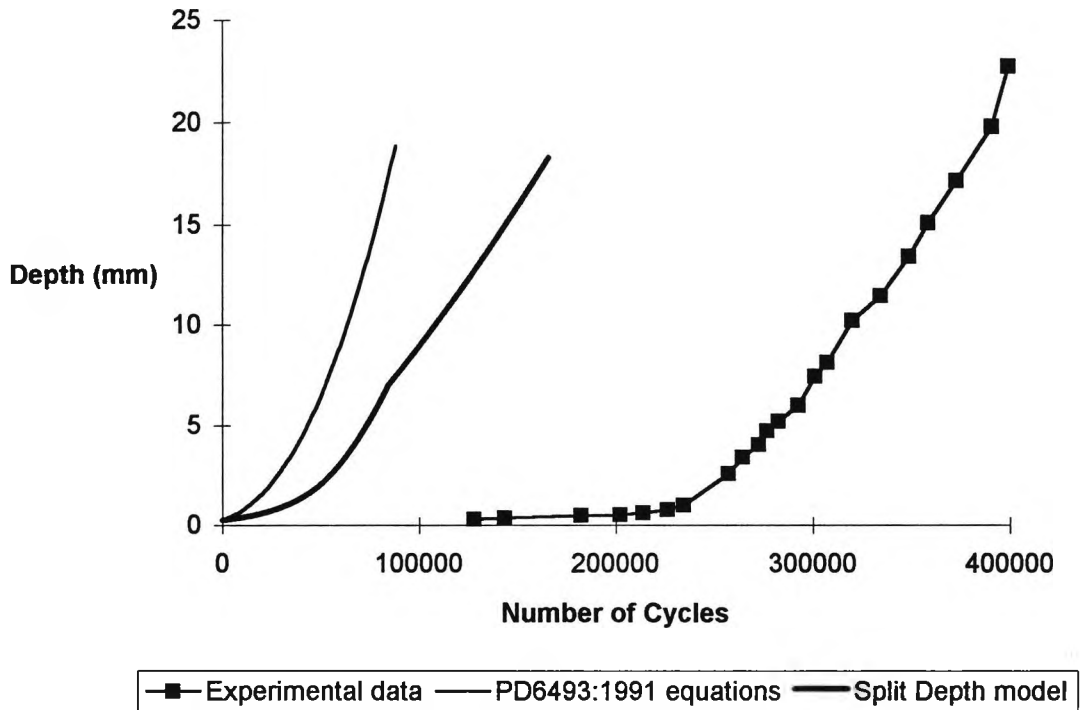


Figure 5.22 Comparison of Data for Shallow Crack Growth and Deep Crack Growth



**Figure 5.23a: Corrosion Fatigue Crack Growth Data:
Specimen W5
Saddle Hot Spot Stress Range: 300MPa**



**Figure 5.23b: Corrosion Fatigue Crack Growth Data:
Specimen S2
Hot Spot Stress Range: 235MPa**

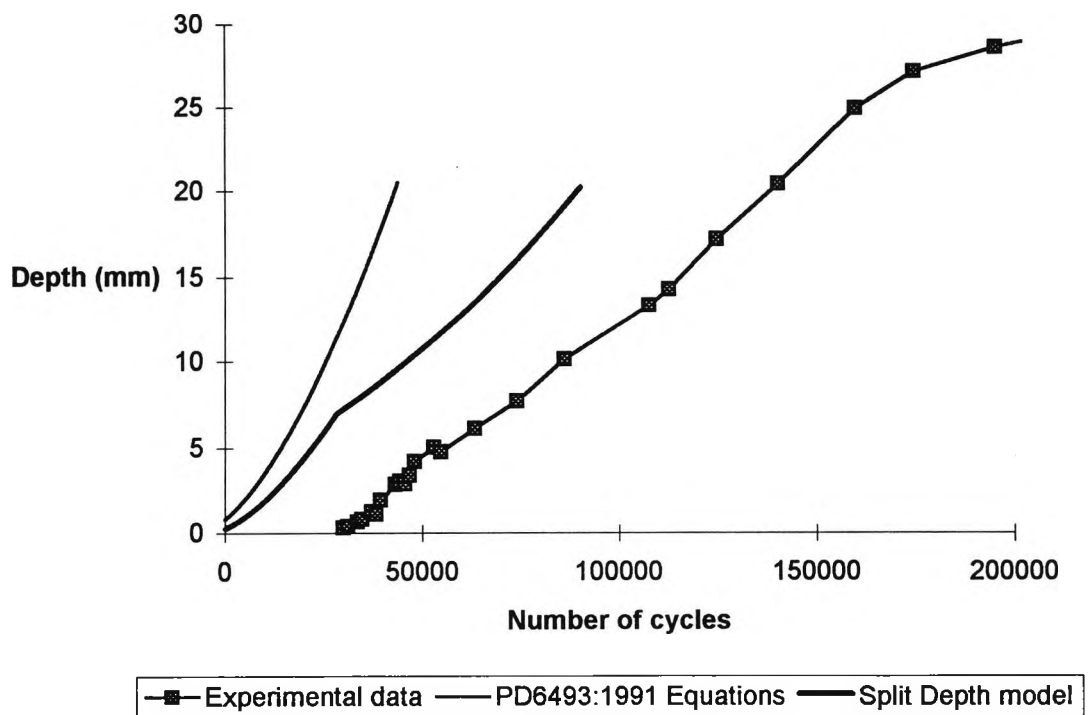


**Figure 5.23c: Corrosion Fatigue Crack Growth Data:
Specimen S3
Hot Spot Stress Range: 306MPa**

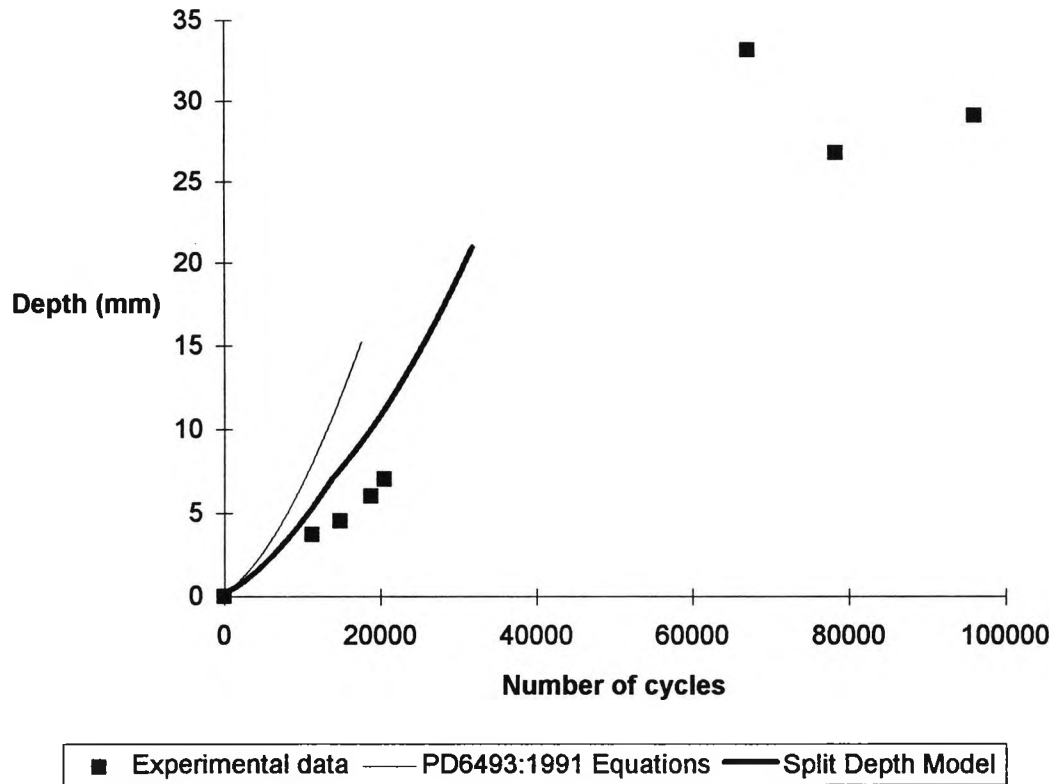


**Figure 5.23d: Fatigue Crack Growth Data: Specimen S4
Hot Spot Stress Range: 261MPa**

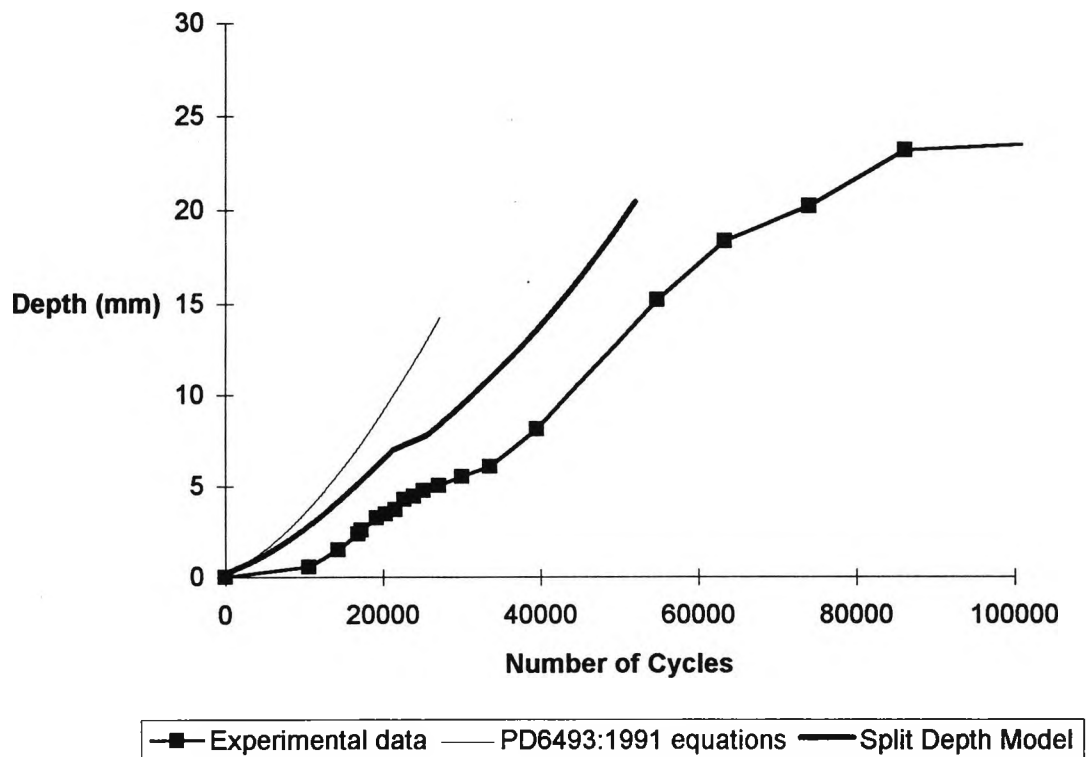


Figure 5.24: Comparison of Corrosion Fatigue N1 Endurance Data With T' Curve

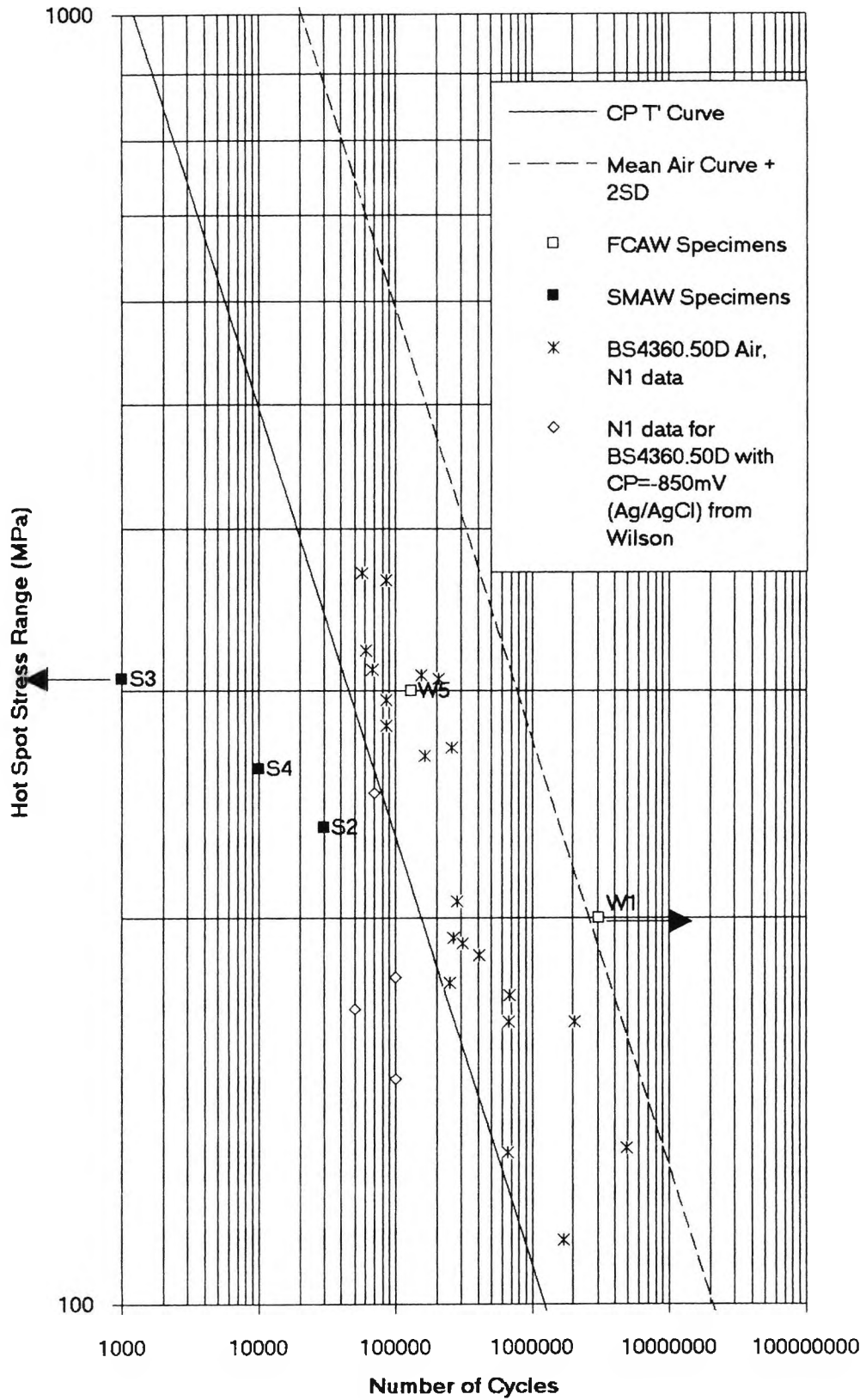
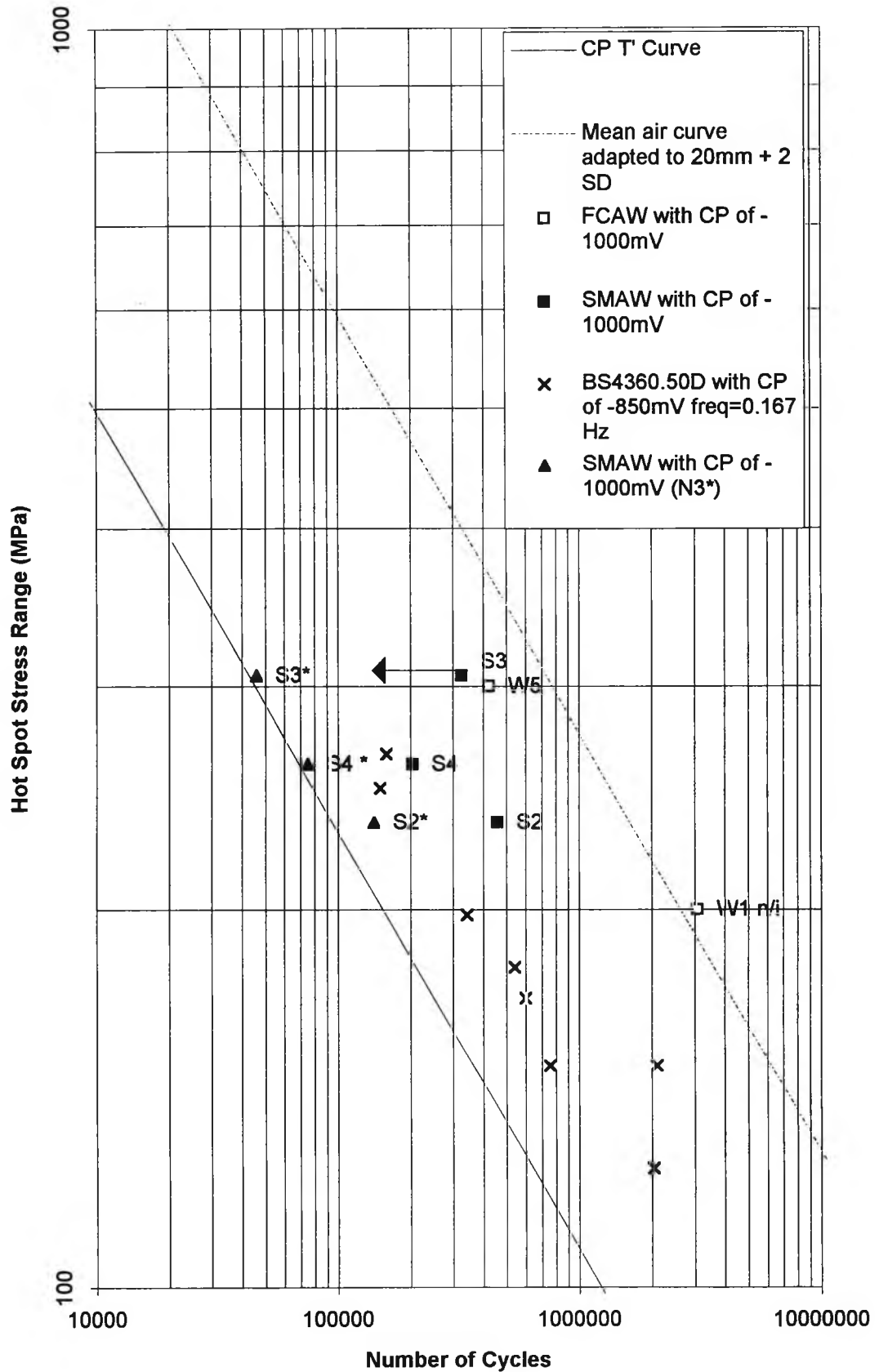


Figure 5.25: Comparison of Corrosion Fatigue N3
Endurance Data with T' Curve (n/i no initiation)



6. THE IMPLICATIONS OF THE RESEARCH

6.1. Scope of chapter

It has been shown that the accuracy with which the remaining life of high strength steel tubular type joints can be assessed, for corrosion fatigue conditions, is dependent on:

- the accurate prediction of the stress field in the vicinity of the weld toe;
- the accuracy of the stress intensity factor solution;
- the scatter of the crack growth data for the specific steel and the accuracy with which the crack path can be predicted.

In the case of realistic offshore conditions, remaining life calculations are also dependent on the accurate modelling of the wave loadings. The remaining life can be estimated by using conservative input assumptions. However, if full advantage is to be taken of life extension, then the input assumptions need to be refined.

During the course of this research, several observations were made which have implications for the accurate prediction of the stress field and the accurate evaluation of the stress intensity factor. These observations were not linked to the use of higher strength steels but are more general. Specific observations have been made regarding the use of a particular high strength steel. It is of interest to know how representative the results obtained for the API 5L X85 steel, are of other high strength steels and how the results obtained in this research could be used for in real applications. The purpose of this chapter is to:

- summarise the observations made in previous chapters and point out where these observations are of general interest to tubular joint design;
- discuss the corrosion fatigue results in the context of other high strength steels to determine how representative the API 5L X85 steel is of other high strength steels;
- discuss how the corrosion fatigue results could be used for variable amplitude loading.

6.2 Implications of Research for General Tubular Joint Design.

The tubular joint air fatigue tests were designed with the primary objective, of providing a reference curve to assess the Y value for the assessment of the corrosion fatigue trials. However, in the course of fulfilling this objective, the air trials provided useful information relevant to tubular joint design more generally.

6.2.1 The Implications for the Air Fatigue of Tubular Joints

6.2.1.1 Stress Field Prediction

The presence of a second brace reduced the hot spot stress concentration factor of the multibrace joint, though only marginally. More accurate estimation of the stress concentration factor provides a useful means for extending the remaining life of a component. In addition, the degree of bending was shown to vary only marginally with the addition of the second brace (this is discussed further in the addenda).

6.2.1.2 Variation in Crack Path

The crack path of the stringer welded specimens was shown to differ significantly from the crack path of the weave welded specimens and both were shown to differ to the crack paths typical of previous tubular joint fatigue trials. The deviation of the crack path from normal to the chord surface was attributed to a combination of local geometry effects, stresses acting in the through thickness direction, weld mismatch effects and the presence of inclusions in the steel. The possibility of the crack deviating from a path perpendicular to the weld toe has implications relevant to all grades of tubular joint. While it is not certain that the deviation of the crack was due to the presence of through thickness stresses alone, it does suggest that in certain geometries where the chord is stiffened, such as ring stiffened joints and some jack up chord brace configurations, there is the possibility that cracks may deviate from a path perpendicular to the chord surface. Solutions for the SIF based on the assumption that the geometry is analogous to a semi elliptical crack in a flat plate, cannot be used where the crack path deviates. It is therefore necessary to determine the geometric conditions where the stress field can no longer be adequately represented by bending and membrane components in the chord wall.

It was argued in chapter 5 that both the remaining strength and stiffness of the tubular joint will be reduced by crack growth on a plane parallel to the chord surface. The loss of strength and stiffness resulting from these extremely long cracks, makes it logical

to redefine the N3 failure criteria for tubular joints, so that N3 is reached when the crack grows to a depth equal to the thickness of the chord or brace in which the crack is growing.

6.2.1.3 Accuracy of SIF Modelling

The empirical AVS and TPM equations were shown to predict the stringer welded SIF with a high degree of accuracy. This was somewhat surprising given the deviation in the crack path, but helps to confirm the accuracy of these equations.

6.2.1.4 Influence of Weld Toe Radius

The SIF is significantly affected by the weld toe radius. Differences in the crack growth rate were observed at depths of up to $0.4T$. This suggested that the SIF was affected by the weld toe stress, even when the crack grew out of the notch stress region. The effect of the blended, wide weave weld toe radius on reducing the SIF together with lower notch stresses had the effect of extending the endurance in both air and seawater environments. However, it was shown by previous authors [Pisarski *et al*, 1987] that the wide weave weld technique adopted here could lead to low fracture toughness in the weld metal. The use of the wide weave technique to achieve weld blending would therefore not be possible for North Sea applications. This does not preclude the use of weave weld techniques for warm sea applications. The wide weave results also suggests that other techniques, such as TIG dressing of the weld toe and weld toe grinding, could result in improved endurance for stringer welded joints, without a loss in toughness. The subject of weld improvement techniques for high strength steels has not been extensively studied and deserves further research.

6.2.2. The Implications for the Corrosion Fatigue of Tubular Joints

It should be pointed out that while the following points are specific to the corrosion fatigue of tubular joints in a seawater environment, the points made for air fatigue are also relevant to the corrosion fatigue of tubular joints.

6.2.2.1 Variation of ACPD signal

In applications where the crack path is expected to deviate from normal to the chord surface (such as tubular joints with stiff chord members, reinforced sections or poor steel quality), and where the crack is filled with wet salt deposits, results from the corrosion fatigue tests of the X85 show the use of ACPD may provide unconservative estimates of the crack depth. This has obvious implications for the in service inspection of such structures.

6.2.2.2 Modelling of Tubular Joint Crack Growth Behaviour with Compact Tension Data.

The use of compact tension or compact bend specimens for determining corrosion fatigue crack growth rates is obviously cheaper than full scale tubular joint trials. However, certain factors have been identified, both by the present and previous authors, which can lead to differences between the corrosion fatigue behaviour of compact specimens and full scale joints:

- Applied load ratio: From previous work, it is apparent that the load ratio has a major influence on the corrosion fatigue crack growth rate. A conservative estimate of the corrosion fatigue crack growth rate would be based on specimens tested at a high R ratio (i.e. $R = 0.7$). This would agree with measurements of the residual stress taken at the weld toe of tubular joints. However, the use of high R ratio in the calculation of remaining lives may lead to a conservative estimation of crack growth rates for deeper cracks.
- Pre-soak period and conditions: Pre-soak has an important influence on the intake of hydrogen by the specimen. In addition to the period of pre-soak, the temperature of the specimen and load conditions are also important. For the compact specimen to represent a real component, the pre-soak period, environmental conditions and load should reflect of the service conditions of the component. Where high residual weld stresses are expected, the pre-soak load should reflect this.
- Geometric considerations: The effect of geometry and specimen thickness were considered in chapter 5. It was argued that the degree of hydrogen embrittlement was related to: the distance of the hydrogen embrittled process zone from the hydrogen charged surface; the process zone size; and the supply of hydrogen to the crack tip. The size of the process zone depends on the constraint of the material at the crack tip. The supply of hydrogen to the process zone, depends on whether hydrogen charging occurs at the side walls of the compact specimen, or at the crack tip. The degree of hydrogen embrittlement also depends on the rate of crack growth relative to the supply of hydrogen to the process zone. The rate of hydrogen embrittled crack growth will therefore be dependent on the thickness of the compact specimens. Thin compact specimens will have a higher rate of crack growth than thick compact specimens, due to side wall charging and constraint effects. For deeper cracks in tubular joints, the use of thick specimens may provide a better estimate of the crack growth rate provided the load ratio and pre-soak conditions are representative of service conditions.

6.2.2.3 Variation of Crack Growth Rate with Depth

It was shown in chapter 5, that the corrosion fatigue crack growth rate was depth dependent and could be accurately modelled by equations 5.2 to 5.7. This agreed with findings from Austin [1994] for other grades of steel. Lower crack growth rates for deeper cracks were rationalised by several mechanisms, including changes in the residual weld stress distribution but may be simply due to scatter in the crack growth data. Further experimental work, preferably with other grades of high strength steel, would be needed before lower crack growth rates can be ascribed to residual stress effects. If lower residual stress levels were shown to account for lower crack growth rates then advantage could be taken of this mechanism to extend the predicted life.

6.3 Implications of the Research for Tubular Joints Constructed from Higher Strength Steels.

6.3.1 Air Fatigue of Higher Strength Steels

Some of the implications of the results from the air fatigue trials were summarised in the previous section as being relevant to tubular joint design generally. This section discusses whether the X85 results are representative of other high strength steels as a class and highlights those findings applicable to other high strength steels.

6.3.1.1 Crack Growth Rate Prediction.

Within the SIF range $10 \text{ MPa}\sqrt{\text{m}} \leq \Delta K \leq 20 \text{ MPa}\sqrt{\text{m}}$, fatigue crack growth for API 5L X85 steel could be characterised using the Paris Law, with values of $C = 8 \times 10^{-12}$; $m = 3$ (units $\text{MPa}\sqrt{\text{m}}$). These values agreed closely with other high strength steels such as HY130, A517Q, HT80 and X70 and also with lower grade steels such as BS4360.50D equivalent steels. The crack growth rate constants comply with current PD6493.1991 guidelines for air fatigue to steels of 600 MPa yield strength and below. On the basis of other test results it can be argued that the current PD6493: 1991 guidelines should be extended to cover higher grades of steel. However, the API 5L X85 steel was of too low a yield strength to support this argument. While the current research complies with existing guidelines, there was no evidence to support claims that any advantage could be taken of lower crack growth rates for the fatigue of higher strength steels in non aggressive environments.

6.3.1.2 Steel Quality

The presence of the manganese sulphide inclusions show steel quality is of primary importance in specifying structural steels for offshore use. This mitigates against the

use of the older class of high strength steels as discussed in chapter 2. It should be pointed out that many existing jack up rigs have been constructed using the older grade of steel. However, the newer class of microalloyed high strength steels have been shown to have much lower levels of impurities and steel quality should be less of a problem.

6.3.1.3 Endurance Prediction

The endurance life results showed that the lives of the higher strength tubular joints exceeded the current guidelines set for lower strength joints by the HSE. In some cases (i.e. two of the weave welded specimens) the endurance exceeded the typical life of the lower strength tubular joints by a significant degree. The extension of the N3 life was attributed to the blended weld radius of the weave welded specimens and the consequent lower weld toe stress and lower SIF of the short crack ($a < 0.5T$). Where low temperature fracture toughness is less critical (such as the warmer sea conditions of the South China Seas) there may be advantages to using a wide weave technique for high strength steels, provided the weld toe has a blended profile at all positions. Additional fracture toughness data would be needed to support this argument.

6.3.2 Corrosion Fatigue of Higher Strength Steels

Existing PD6493.1991 and HSE guidelines are based on research for lower grade steels. It is important to examine how the results from the API 5L X85 steel differ from results for lower grade and other high grade steels. On the basis of these comparisons recommendations can be made regarding the extension of the existing guidelines to higher strength steels.

6.3.2.1 Crack Growth Behaviour

Corrosion fatigue rates for the API 5L X85 steel are compared to typical corrosion fatigue crack growth rates for BS4360.50D structural steels in figure 6.1. For simplicity the BS4360.50D corrosion fatigue crack growth rates are shown by a scatter band representing a range of observed crack growth rates. The corrosion fatigue crack growth rates measured in the X85 steels agreed relatively closely with the corrosion fatigue crack growth rates measured in the BS4360.50D grade steels. However, the plateau region of crack growth experienced by the BS4360.50D steels was less pronounced for the X85 grade steel tubular joints. On the basis of the above comparison, it would appear that initial concerns about high rates of crack growth in higher strength steels were unjustified. This supports the argument that the existing PD6493:1991 guidelines should be extended to higher grades of steel. It was

interesting to note that the corrosion fatigue crack growth rates were comparable to those of BS4360.50D grade steels, despite the presence of the manganese sulphide inclusions in the X85 grade steel.

It is important to know how representative API 5L X85 is of other high strength steels. Figure 6.2 shows a comparison between the X85 tubular joint corrosion fatigue test data with test data for other high strength steels obtained under conditions of cathodic overprotection and in a similar environment. A comparison of data is aided by considering the crack growth data for a SIF range of $10 \text{ MPa}\sqrt{\text{m}} < \Delta K < 30 \text{ MPa}\sqrt{\text{m}}$ separately to that of crack growth data for a SIF range of $6 \text{ MPa}\sqrt{\text{m}} < \Delta K < 10 \text{ MPa}\sqrt{\text{m}}$.

The corrosion fatigue crack growth rates from the X85 compact tension specimens in the SIF range $10 \text{ MPa}\sqrt{\text{m}} < \Delta K < 30 \text{ MPa}\sqrt{\text{m}}$ were lower or comparable to those of the HT80, HY130 steels [King *et al*, 1992] and is comparable to the scatter band for steels of yield strength 460 to 640 MPa obtained by Billingham & Laws [1994]. However the corrosion fatigue data is much lower than that obtained for the X70 steel [King *et al*, 1992]. The corrosion fatigue data from the HY 130, HT80 steels and steels investigated by Billingham & Laws [1994], reinforce the argument that the current PD6493:1991 guidelines for the prediction of crack growth rates can be extended to steels of a yield strength in excess of 400 MPa. However, the data from the X70 tests, (where the corrosion fatigue crack growth rates greatly exceed the current PD6493:1991 guidelines for a steel with a yield strength of less than 400 MPa) shows the dangers of generalising any conclusions from the X85 tubular joint data to all other high strength steels.

The X85, corrosion fatigue data for tubular joint crack growth and compact tension crack growth in the SIF range of $6 \text{ MPa}\sqrt{\text{m}} < \Delta K < 10 \text{ MPa}\sqrt{\text{m}}$ shows relatively poor agreement with corrosion fatigue data for the X70, HT80 and HY130 steels. The difference between the X85 data and the data for the other high strength steels is complicated by several factors such as the lack of confidence in the X85 compact tension data and the scarcity of tubular joint crack growth data for these values of SIF range. The X85 tubular joint corrosion fatigue data for $\Delta K < 9 \text{ MPa}\sqrt{\text{m}}$, may point to a threshold effect at or near $\Delta K = 9 \text{ MPa}\sqrt{\text{m}}$. A similar threshold effect was seen for the HT80 steel, but was not observed in the HY130 and X70 steels. Given the HY130 and X70 corrosion fatigue data, the application of reduced crack growth rates for $\Delta K < 10 \text{ MPa}\sqrt{\text{m}}$ to all higher strength steels cannot be justified. In order to verify the corrosion fatigue crack growth rates for $\Delta K < 10 \text{ MPa}\sqrt{\text{m}}$, it would be useful to test specimens using variable amplitude loading, so as to measure crack growth rates for deeper cracks at a low SIF range. This is an area where more data could lead to

substantially prolonged estimates of the remaining life and deserves further investigation.

In chapter 2, two basic grades of high strength steel were recognised, the first group consisting of older steels manufactured using a high alloy content to achieve high strengths, and the second group consisting of newer grades of micro alloyed high strength steels. The newer microalloyed steels generally have greatly reduced levels of impurities and may be subject to lower corrosion fatigue rates than the results for the X85 steel suggest. However, evidence from corrosion fatigue experiments of SENB specimens suggests that while these newer steels may have lower corrosion fatigue crack growth rates at potentials close to the recommended level of 850 mV, at cathodic potentials of -1000mV, corrosion fatigue rates are comparable to those of BS4360.50D grades [Spurrier, 1995]. This would appear to reinforce the argument that under realistic offshore conditions no advantage can be made of reduced corrosion fatigue rates. Further work would reveal if the newer grades of microalloyed steels perform better than the X85 results suggest.

6.3.2.2 Endurance Behaviour

The endurance data from the X85 steel was compared to typical endurance data for BS4360.50D type grades in chapter 5. To summarise the principal findings, the lives of the X85 tubular joints were comparable to, or better than those typical of BS4360.50D tubular joints. It should be pointed out that:

- i) the restricted number of tests means that no firm conclusions can be drawn from these results alone;
- ii) the difference in the crack path between that typically seen in tubular joints, and that seen in the X85 tests, complicates any direct comparison.

The endurance data for the X85 steel tubular joints also agreed with experimental evidence for 450 MPa yield strength steel tubular joints obtained using variable amplitude loading [Vinas Pich, 1994] which showed good agreement between BS4360.50D and BS7191.455F endurance data (see figure 1.39).

As welded tubular joint data for higher strength steels is restricted, it is of interest to compare the X85 tubular joint endurance results, to data obtained for high strength steel plate to plate joints and T plate joints. As was noted in chapter one, experimental results for welded plate joints from Tubby and Booth, [1991] showed little difference between the corrosion fatigue endurance lives of 430 MPa and 470 MPa grade steels and BS4360.50D steels. However, as was also noted in chapter one, welded plate endurance results for a 490 MPa steel, RQT 501 [Bateson *et al*, 1988] at -1100 mV,

were lower than those predicted using the current HSE guidelines. It is difficult to draw any firm conclusions from a consideration of the collective tubular and plate data. The available evidence would point to some higher strength steels showing comparable performance to BS4360.50D steels under conditions of cathodic overprotection and other steels showing reduced performance. However, the X85 tubular joint endurance results help to reinforce the general argument for the extension of the T' curve to higher grades of steel. There was some evidence to suggest that the weave welded specimens showed superior endurance behaviour compared to the stringer welded specimens. Any improvement in the corrosion fatigue behaviour of the weave welded specimens can be ascribed to low notch stresses and relatively low SIFs. As with the corrosion fatigue crack growth data, any recommendations for endurance prediction would appear to be dependent on the choice of steel and the level of cathodic protection. Additional work to distinguish between the endurance performance of the micro alloyed high strength steels and other high strength steels, may help to extend the application of endurance guidelines to higher strength steels as a class, and deserves further research.

6.4 Application of Constant Amplitude Data to Variable Amplitude Corrosion Fatigue of Tubular Joints.

The application of the corrosion fatigue crack growth rates for higher strength steels, to variable amplitude loading is obviously of practical interest, even though variable amplitude loading was not the primary subject of this research. Approaches to the analysis of variable amplitude loading are described below:

6.4.1. Endurance Life Prediction

Traditionally, endurance life prediction for variable amplitude loading, can be assessed from the following equation, given that the stress history can be divided into k discrete stress ranges:

$$\sum_{i=1}^k \frac{n}{N} = M \quad 6.1$$

where

M is the Miner's Summation.

Under conditions of air fatigue, M is equal to one. It should be noted that for the case of corrosion fatigue, N is often based on the mean air life. In which case M provides a measure of the effect of environment and is referred to as the environmental reduction factor ERF. This approach has been modified by Dover and Hibberd [1977], so that

the variable amplitude stress can be represented for a set of discrete k discrete stress ranges, by an equivalent stress:

$$S_h = \left(\sum_{i=1}^k (\Delta S_i)^m P(\Delta S_i) \right)^{\frac{1}{m}} \quad 6.2$$

where

S_h	is the weighted average stress range
ΔS_i	is the individual range
$P(\Delta S_i)$	is the probability of stress range ΔS_i
m	is the negative inverse slope of the T' curve.

Where the slope of the T' curve changes to incorporate low stress range, m is taken from that part of the T' curve corresponding to the stress range ΔS_i . The above method is equally applicable to air and corrosion fatigue endurance prediction.

6.4.2. Incremental Crack Growth Prediction and Variable Amplitude Loading

Crack growth can be determined from the Paris Law for air fatigue, by estimating the crack growth corresponding to a given SIF range and summing the contributions to crack growth over the SIF range distribution. It follows that the SIF distribution can be represented by an equivalent SIF range:

$$\Delta K_h = \left(\sum_{i=1}^k (\Delta K_i)^m P(\Delta K_i) \right)^{\frac{1}{m}} \quad 6.3$$

where

ΔK_h	is the weighted average stress range,
ΔK_i	is the individual range of ΔK ,
$P(\Delta K_i)$	is the probability of SIF range ΔK_i
m	is the Paris Law exponent.

and $\Delta K_i > \Delta K_{th}$.

For corrosion fatigue, it is normal to represent the da/dN versus ΔK data by a number of segments. Assuming $\Delta K = Y\sqrt{\pi \cdot a}$, and that the probability of the stress range is known as a function of stress range, equation 6.3 can then be modified to calculate an equivalent crack growth rate [Kam and Dover, 1989]:

$$\frac{da}{dN} = \sum_{i=1}^n \left\{ C_i (Y\sqrt{\pi \cdot a})^{m_i} \int_{\Delta K_{i-1}}^{\Delta K_i} (\Delta S)^{m_i} P(\Delta S) d(\Delta S) \right\}^{\frac{1}{m_i}} \quad 6.4.$$

where i = corresponding segment in the da/dN versus ΔK curve.

	m	$=$	slope of segment i
	n	$=$	number of segments
and	ΔS_0	$=$	0
	ΔS_n	$=$	∞

The above approach is shown schematically in figure 6.3. This approach allows the crack growth rate to be calculated as the crack increases in depth. The remaining life can then be calculated from numerical integration of equation 6.4.

6.4.3. Application of Constant Amplitude Data to Variable Amplitude Loading.

Equations 6.1 to 6.4 provide a method of estimating the remaining life or endurance of a tubular joint, subject to variable amplitude loading, from the constant amplitude da/dN versus ΔK curve and S-N curve. In particular, equations 5.2, 5.3, and 5.4 should provide a conservative estimate of the remaining life for a X85 grade steel. However, variable amplitude loading is complicated by several factors, including: the difficulty in predicting a relevant stress history for a particular structure; associated problems of representative methods of cycle counting; and load interaction effects. These features have already been addressed by previous research programmes [e.g. Austin, 1994; Vinas Pich, 1994]. However, no work has been done on the variable amplitude fatigue of tubular structures constructed from grades of steel with yield strengths in excess of 550 MPa. It would be useful to research variable amplitude, corrosion fatigue of such structures. In addition, it would be useful to develop a standard wave action stress history, specifically for jack up structures.

Variable amplitude studies would help to confirm if any depth effect could be noticed. If a depth effect were noted, it may prove interesting to compare crack growth with compact specimen data obtained at different load ratios, to see if residual stress effects could be used to predict lower rates of crack growth. In addition variable amplitude loading could be used to confirm any threshold effect and would help to verify the crack growth models described in section 6.4.1 and 6.4.2.

6.5 Summary of Chapter

This chapter has provided an overview of the findings of the previous chapters, as they relate to crack growth in tubular joints in general and high strength steels in particular. Several important findings were discussed which have implications for the design and inspection of all grades of tubular joint. In addition the results obtained in previous chapters have been discussed in the wider context of corrosion fatigue results

for other high strength steels. The X85 grade of steel studied, showed crack growth rates and endurance performance comparable to that of BS4360.50D and many other grades of high strength steel. In view of these results there was no evidence to support arguments that the higher strength steels show significantly worse corrosion fatigue behaviour than steels with yield strength of less than 400 MPa. However, there was no equally no evidence to support the view that high strength steels showed significantly better corrosion fatigue performance than steels with yield strength of less than 400 MPa. It was also pointed out that there was wide variation between the corrosion fatigue performance of different steels in the high strength category. The research supports the extension of the existing fatigue guidelines to steels of yield strength of 600 MPa, but that the corrosion fatigue performance of individual steels should be based on a case by case consideration. It was further suggested that there was need for further research involving other high strength steels both at constant amplitude and variable amplitude loading.

Figure 6.1: X85 Tubular Joint, Corrosion Fatigue Data.

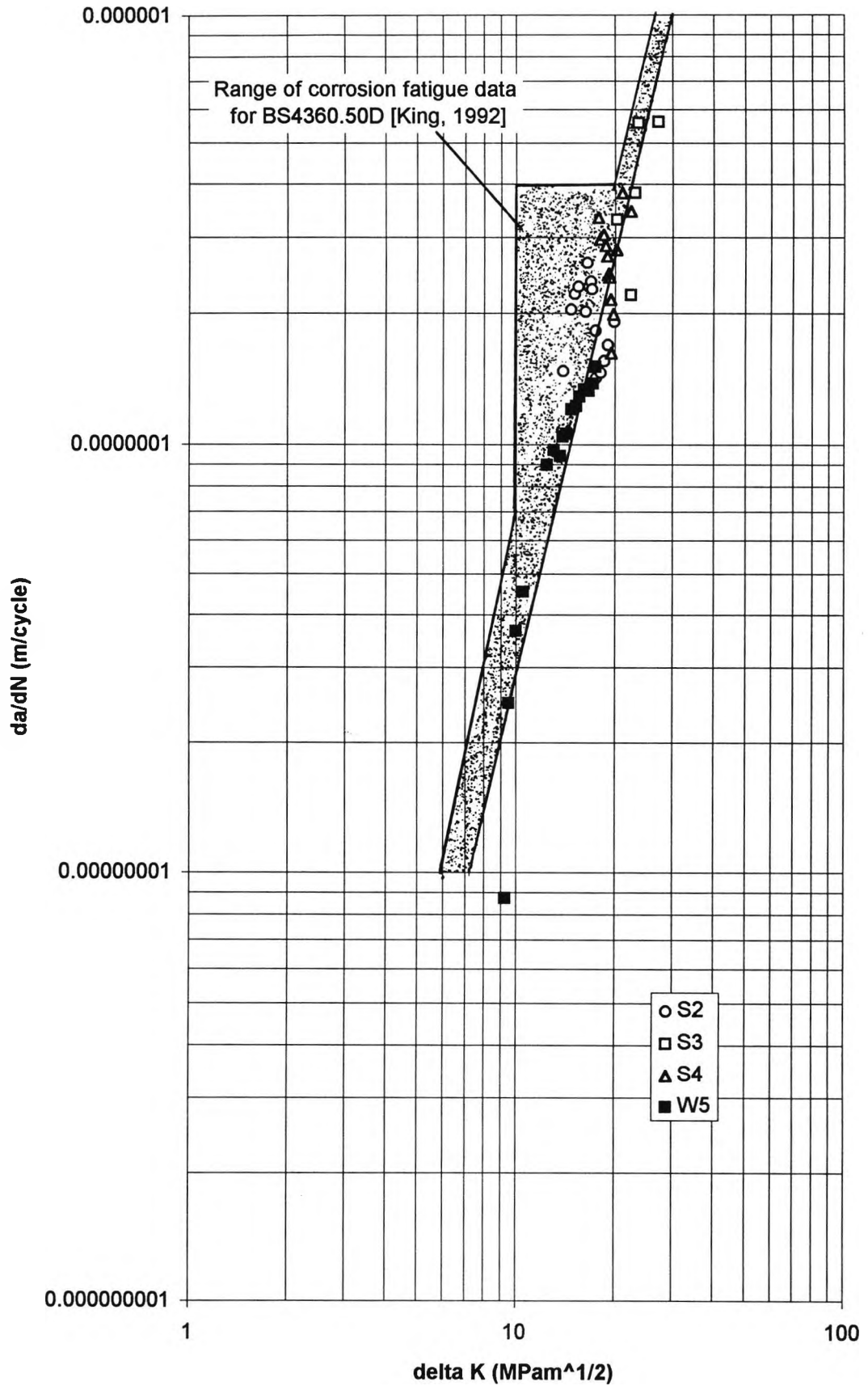


Figure 6.2: Comparison of Corrosion Fatigue Data for High Strength Steels with Cathodic Overprotection

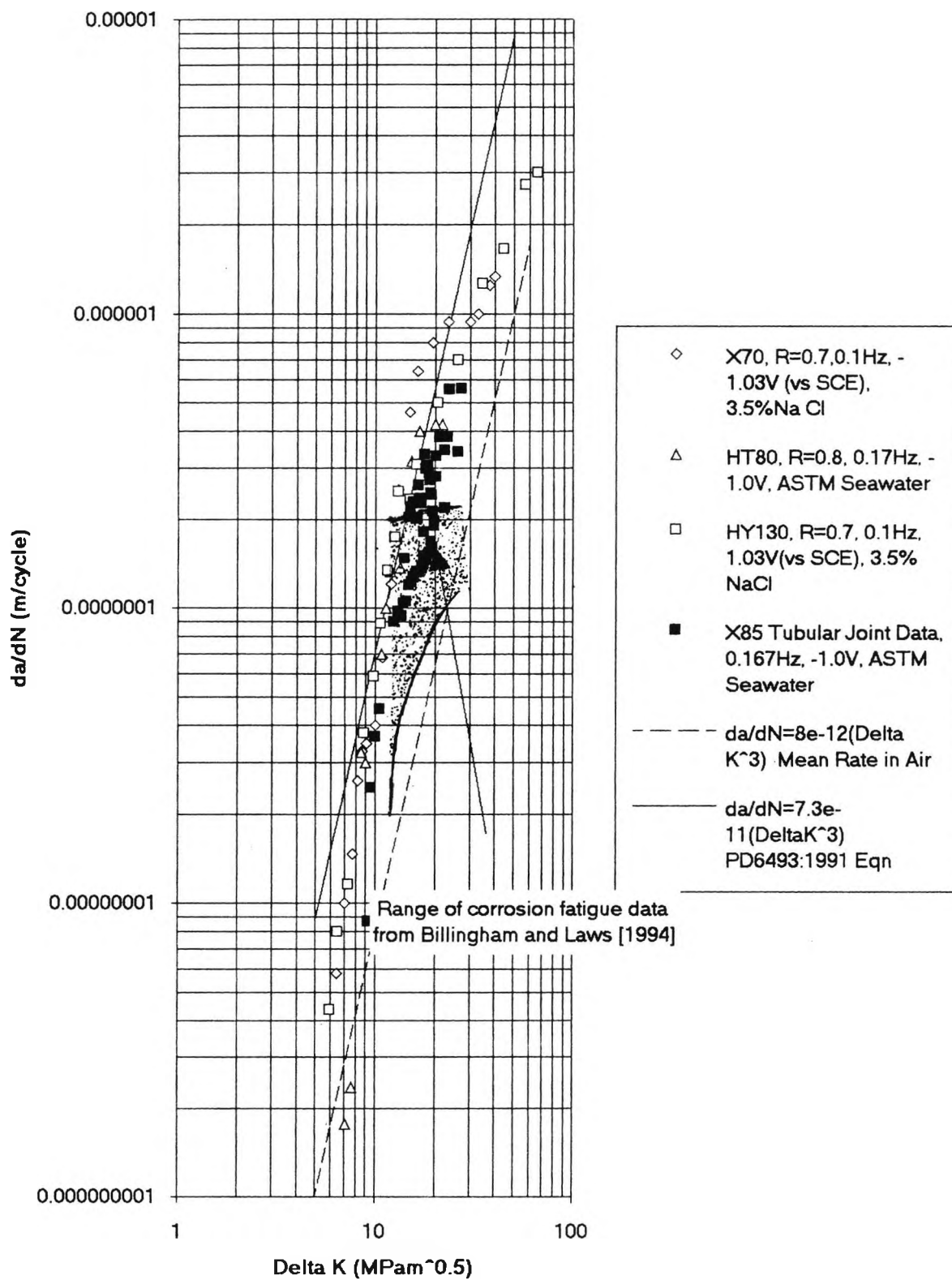
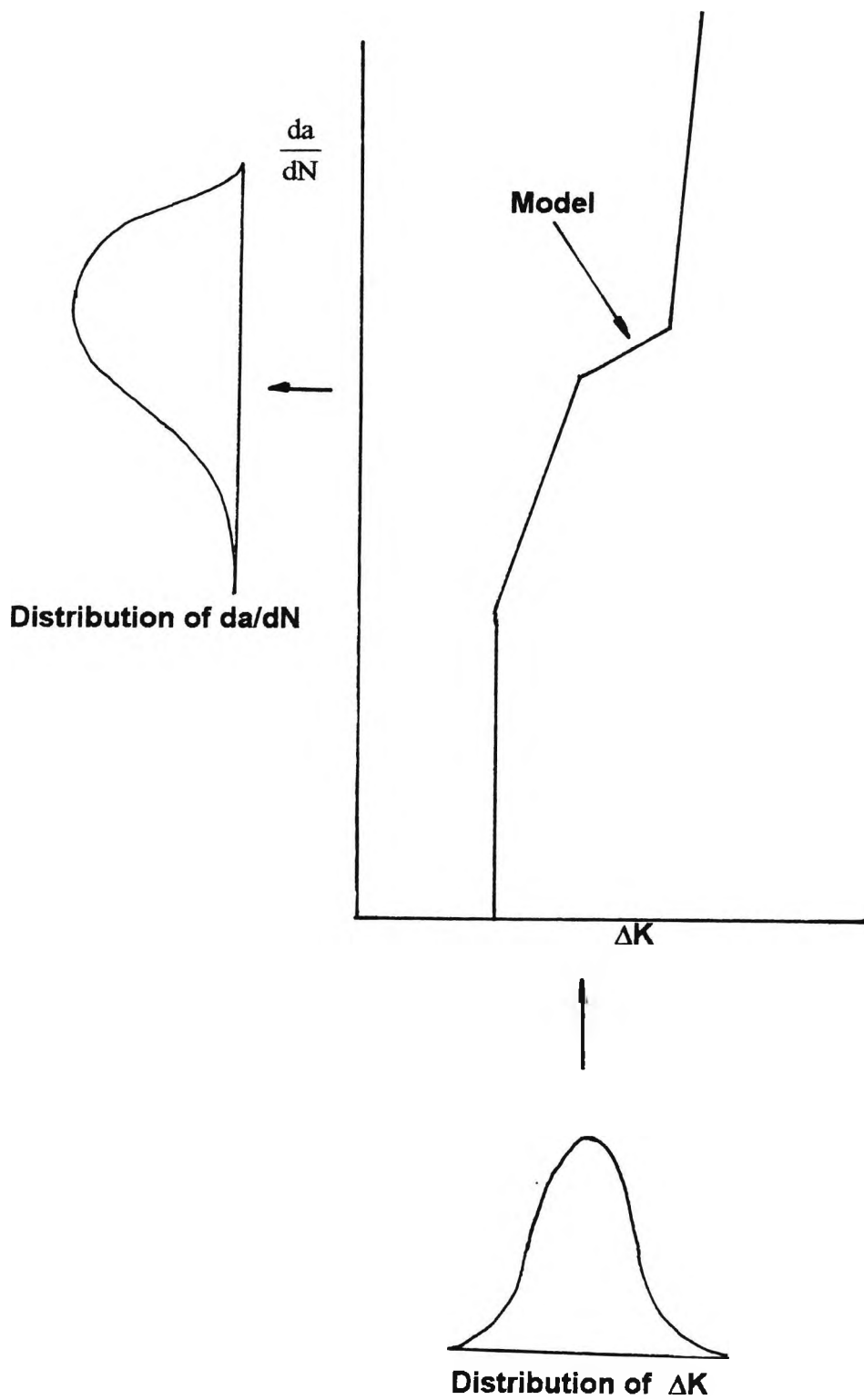


Figure 6.3: Procedure to calculate equivalent crack growth rate



7. SUMMARY, CONCLUSIONS AND FURTHER WORK.

7.1 Scope of Chapter

This chapter presents a summary of the main findings of this thesis. Recommendations are made for future work that would enhance or extend the findings of this thesis.

7.2. Summary of Thesis

This study was prompted by a lack of understanding of the corrosion fatigue behaviour of high strength steel, welded tubular joints, in seawater under conditions of cathodic overprotection. Jack up rigs, use steels with yield strengths of between 500 MPa and 700 MPa. The use of cathodic protection on offshore rigs often results in the steel having a potential of less than -850 mV (versus Ag/ AgCl). Current fatigue guidance is for steels with a yield strength of less than 400 MPa in a seawater environment with cathodic protection. It was considered that the combination of excessive overprotection and higher yield strength could lead to more rapid crack growth than was normal for lower strength steels. It was also discovered that jack up rigs use a flux cored arc welding process. This process results in a weave weld type finish, as opposed to a conventional stringer weld type finish associated with the shielded metal arc welding process.

Chapter one reviewed the principal methods of determining the endurance life and remaining life of a tubular joint under corrosion fatigue conditions. The chapter discussed, different methods of stress analysis and alternative ways of predicting the stress distributions in the welded tubular joint. The endurance life and fracture mechanics approach were both discussed together with various ways of estimating the stress intensity factor. The influence of cathodic protection together with the effect of various environmental and physical variables on the corrosion fatigue process were discussed. The accuracy with which the corrosion fatigue crack growth can be predicted is dependent on: (i) the accuracy with which the stress distributions can be predicted; (ii) the accuracy with which the stress intensity factor range can be predicted and (iii) the consistency of the corrosion fatigue crack growth rate with respect to the stress intensity factor range. It was concluded that the effect of cathodic protection on the corrosion fatigue process could be assessed by fatigue testing representative tubular joints using representative offshore conditions.

To determine the corrosion fatigue behaviour of the high strength steel tubular joints, two double T joint test specimens were fabricated with the flux cored arc welding process and two double T joint specimens were fabricated using the shielded metal arc welding process and fatigue tested using out of plane bending. Chapter two discussed the selection of a suitable material for the tubular specimens, representative of a typical steel used for jack up construction. Chapter two also gave details of the fabrication, geometry and material properties of the test specimens.

Chapter three reported on the experimental stress analysis of the tubular test specimens. The experimental values for the hot spot stress concentration factor were compared to values predicted using commonly used parametric solutions for the stress concentration factor. The transverse weld, stress distributions associated with the tubular joint were also investigated and compared to commonly used parametric solutions. The predicted hot spot stress was found to be conservative. Further experiments showed: (i) the second brace had a marginal effect on stiffened the chord, but this could not account for the discrepancy between the parametric solutions and the measured SCF and (ii) the stiffening effect of the second brace on the chord, led to only marginal variation in the ratio of bending stress to tension stress.

Chapter four reported on fatigue crack growth in an X85 steel tubular joint, in an air environment. In addition to providing endurance life data, the crack growth rate was determined. Paris Law data was obtained from compact tension fatigue tests of the X85 steel. The Paris Law data was shown to be similar to data for BS4360.50D steel. The stress intensity factor range for the tubular joint, was obtained from transformation of the Paris Law and the empirical Y value (used to evaluate the SIF range), was determined as a function of the hot spot stress. The Y value was shown to vary between the FCAW and SMAW specimens, this was probably due to variation in the local weld toe profile. The FCAW and SMAW specimens were shown to have different crack paths. The crack path was believed to be partly due to the weld toe and global geometry of the specimens, and partly due to the presence of manganese sulphide inclusions. Both the AVS and TPM stress intensity factor equations were shown to predict the crack growth rate in the cracked tubular specimens to a high degree of accuracy. The endurance life of the specimens was higher than that predicted using current HSE guidelines for welded tubular joints with a yield strength of less than 400 MPa.

Chapter five reported on corrosion fatigue crack growth in a X85 tubular joint protected at a potential of -1000mV (vs Ag/AgCl). The corrosion fatigue tests provided endurance data in addition to crack growth data. The crack paths were shown to be similar to the crack paths of the specimens fatigue tested in air. The

ACPD crack depth was shown to be dependent on the applied load for S type cracks in a seawater environment. The corrosion fatigue crack growth rate data were lower than HSE predicted corrosion fatigue crack growth rate guidelines for steels with a yield strength less than 400 MPa. The corrosion fatigue crack growth rate for cracks deeper than 7 mm, was shown to be lower than that of cracks less than 4 mm deep at the corresponding SIF range. Explanations have been proposed to account for this. The endurance life of the corrosion fatigue specimens, was higher than that predicted using current HSE guidelines for welded tubular joints with a yield strength of less than 400 MPa.

Chapter 6 highlighted those findings which were relevant to tubular joint design in general and to the air and corrosion fatigue of high strength steels in particular. A comparison was made between the corrosion fatigue performance of the API 5L X85 grade steel and other grades of high strength steel and steels similar to BS4360.50D. It was found that the performance of API 5L X85 was broadly similar behaviour to that of other high strength steels with some important qualifications. There was no evidence in support of the use of additional penalties for the crack growth rate or endurance behaviour on the basis of the current research.

7.3 Summary of Conclusions.

- 7.3.1** The Lloyd Registry parametric equations and Efthymiou parametric equations gave a conservative estimate of the brace and chord SCF for this geometry. The UCL equations gave a good estimate of the chord circumferential stress distribution.
- 7.3.2** The double T joint studied was shown to have a marginally lower chord SCF and different bending stress to membrane stress ratios compared to single T joints. This effect was shown to be dependent on the node geometry. The node geometry was believed to have a significant effect on the orientation of the crack growth plane.
- 7.3.3** Constant amplitude, fatigue tests on four welded, tubular double T joints in air show that the existing fatigue guidance recommended T' curve gave a conservative prediction for the N3 endurance life of tubular joints constructed from an API 5L X85 grade.
- 7.3.4** Constant amplitude fatigue tests on four welded, tubular, double T joints in a sea water environment with applied cathodic protection of -1000mV (vs Ag/AgCl) show that the existing fatigue guidance recommended T' curve

adapted for corrosion fatigue conservative prediction for the N3 endurance life of tubular joints constructed from an API 5L X85 grade.

- 7.3.5 Existing PD6493:1991 values for ferritic steels with a yield strength below 600 MPa of $C=9.5 \times 10^{-12}$ and $m=3$ (MPa, m units) are conservative for use with X85 structural tubing, to describe air fatigue crack growth.
- 7.3.6 The AVS and TPM models provide a conservative estimate of the SIF range for the stringer welded joints, the TPM method being more conservative. Both methods are more conservative when applied to the weave welded specimens. The difference between the empirical Y values was rationalised as being partly due to differences in the weld profile.
- 7.3.7 The corrosion fatigue crack growth rates for both SMAW and FCAW tubular joints of API 5L X85 structural tubing protected at a potential of -1000 mV (versus Ag/AgCl), were less than those predicted using PD6493:1991 guidelines for steels with a yield strength of less than 400MPa.
- 7.3.8 The crack paths in the API 5L X85 tubular joints were different to those observed in BS4360.50D tubular joints. The different crack path led to substantially longer cracks developing before chord wall penetration (N3) took place. The longer crack path, combined with a low aspect ratio could result in a reduction in the remaining strength and stiffness of the joint prior to chord wall penetration, compared to BS4360.50D tubular joints
- 7.3.9 API 5L X85 structural steels showed evidence of Manganese Sulphide inclusions. These inclusions result in planes of weakness which influence subsequent crack growth paths and lead to crack branching. Care should be taken when purchasing such steels to avoid such inclusions.

7.4 Further Work

The following work would contribute to a better understanding of corrosion fatigue crack growth in offshore steel tubular joints:

- 7.4.1. Establish influence functions for the bending stress to membrane stress ratio of multibrace nodes and verify the Efthymiou influence function for the hot spot stress.
- 7.4.2. Establish the tubular joint geometrical parameters under which through thickness chord stresses become significant.

- 7.4.3. Establish material data for the strain life prediction of crack initiation of suitable high strength steels in air and seawater environments.
- 7.4.4. Establish corrosion fatigue, compact tension data for X85 steel, under conditions of cathodic protection at load ratios of less than 0.7, to isolate the residual stress effects from crack closure effects in the tubular joint tests.
- 7.4.5. Establish a standardised stress history for jack up tubular joints.
- 7.4.6. Fatigue test, cathodically protected, high strength steel tubular joints in a seawater environment, using the standardised stress history, to evaluate the corrosion fatigue crack growth rate under realistic service conditions.
- 7.4.7. Conduct a comparative study on corrosion fatigue of other high strength steels suitable for jack up construction.
- 7.4.8. Conduct further air fatigue tests and corrosion fatigue tests to investigate the use of weld improvement techniques (particularly weld toe dressing and weld toe grinding) with high strength steels.

ADDENDA

The Influence of the Degree of Bending on the Endurance of Tubular Specimens.

The T' curve derives a lower bound estimate of the endurance based on the hot spot stress of tubular nodal joints and takes no account of the degree of bending. For certain cases (particularly for in plane bending where two braces are mounted to a common chord and reacted against each other) the degree of bending is much lower than that experienced in other loading configurations. Using an estimate of the endurance life which assumes load shedding due to linear moment release, Eide [1994] has predicted that the effect of the change in the degree of bending, is to reduce the endurance of such joints by a factor of 1.5. When the relevant results are modified to account for the degree of bending, the endurance of the specimens are comparable to the endurance of other tubular joint configurations.

Analysis of the acrylic model trials (section 3.3), showed a small but discernible change in the degree of bending between the single T joint and double T joint specimens when tested in out of plane bending. It follows that, for the case of the acrylic model at a given hot spot stress, the membrane and bending stresses will vary for the single and double brace models as follows:

$$\sigma_{hss} = \sigma_M(1 + (\sigma_B/\sigma_M)) \quad (\sigma_M = 0.121\sigma_{hss} \text{ for single brace node})$$

$$(\sigma_M = 0.112\sigma_{hss} \text{ for double brace node})$$

$$\sigma_{hss} = \sigma_B(1 + (1/(\sigma_B/\sigma_M))) \quad (\sigma_B = 0.879 \sigma_{hss} \text{ for single brace node})$$

$$(\sigma_B = 0.888 \sigma_{hss} \text{ for double brace node})$$

i.e. the membrane stress of the single brace node is 9% higher than the membrane stress

of the double T joint at the equivalent hot spot stress, while the bending stress of the single brace node is 1.0 % lower than the bending stress of the double brace node at the equivalent hot spot stress.

As the membrane stress will make a greater contribution to the crack growth (especially for deeper cracks), the change in membrane stress would be expected to affect the endurance life. If the endurance results are adapted to account of the change in the degree of bending by using Eide's results [Eide *et al*, 1994], the measured change in the degree of bending would lead to a change in the endurance life of about 3%. Such a change is insignificant when compared to the scatter inherent in endurance life testing. Haswell [1992] has derived a generalised SIF in terms of the DOB and SCF. Haswell's formula shows a marginal increase in life at deeper crack depths, as expected. However, the difference in the endurance is too low to make a significant difference to the results obtained in the current study.

The degree of bending is marginally higher than the 0.85 described as "average" by Eide [1994] for a typical joint. The endurance life of the double T joint could then be normalised to that of a typical tubular joint, by reducing the endurance life obtained in this study by 13%. It should be noted that the specimens fatigue tested to form the T' database had differing degrees of bending and to make such a study meaningful would require the reanalysis of the T' database. This is made more difficult by a lack of measured bending stress data for the T' specimens.

In addition two qualifications should be noted:

- The β ratio of the specimen was quite high and the effect of additional braces on the stiffness of T joints of lower β ratio may be lower. Also, the effect of the chord rack on the degree of bending of jack up joints may be greater than that shown here.
- Assuming load shedding takes place, the effect of the variation in the B-M ratio on the initiation and early crack growth is more limited. As was noted in chapter 4, the use of simple models based on plate bending (even where load shedding is incorporated) is

somewhat dubious when the crack path deviates to the extent shown in the current test program.

In conclusion, there is no evidence on the basis of current test results to support a significant increase in the endurance of double T joints in comparison to the endurance of single T joints.

The Influence of Residual Stress on the Crack Propagation Rate

The Y value of the FCAW specimens was considerably lower than the corresponding Y value of the SMAW specimens. The difference could be partly attributed to the difference between the weld toe radius of the two weld processes. Independent studies of the effect of weld radius on the SIF using two dimensional, finite element analysis of T plates [Thurlbeck & Burdekin,1992; Niu and Glinka, 1987], confirm that little or no variation of the SIF with weld toe radius can be seen for cracks, where the depth exceeds 0.2 of the plate thickness. This contrasts with the results obtained by the current study, where a noticeable effect was seen at depths of up to 0.4 of the chord thickness. The reason for the differences between the experimental Y values may be either due to the variation in the crack path observed or perhaps to the difference in the residual weld stresses of the two processes.

The residual stress distributions of the two processes are likely to be very different. The SMAW process is likely to lead to yield level residual stresses at the weld toe decaying with depth. The depth to which these stresses decay to zero is determined largely by the heat input [PD6493:1991]. If these stresses are simplified to bending and membrane components, then it is further suggested that the residual stresses will be subject to load shedding in much the same way as the applied stress.

The FCAW welds have a much higher initial heat input, witnessed by an visibly larger heat affected zone. However, the motion of the FCAW process is to weave slowly around the weld. This will result in the heat affected zone cooling and being heated in a number

of cycles. It is therefore possible that this process leads to a degree of post-weld heat treatment and consequently a lower level of residual stress at the weld joint.

Normally the crack growth rate at a weld toe can be assumed to be modelled by compact tension data from tests conducted at a high load ratio, and that the load ratio has little influence on the crack growth rate for tests conducted in air. In contradiction to this view, Vosikovsky [1980] has shown that the load ratio has a measurable effect on the crack growth rate of X70 and HY130 steels in air (see figure 1.32) and that the air crack growth rates at different stress ratios can be normalised to a single curve by plotting the crack growth rate against $\Delta K - B.R$ in place of ΔK . Where B is a constant varying between 3 and 4 depending on the steel. Although the relationship is no longer valid where crack growth extends into region III behaviour (K_C dominated crack growth). This would suggest that for tubular joints constructed from certain steels, the crack growth rate is dependent on the residual stress distribution within the steel. If the FCAW tubular joints were subject to lower residual stresses as a result of the welding processes, this would account for the lower Y value found at crack depths of 0.2 to 0.4 of the plate thickness, compared to the SMAW specimens.

Vosikovsky [1980] has also shown that the same $\Delta K - B.R$ versus crack growth rate relationship, is valid for crack growth in sea water under a variety of conditions, including cathodic protection at the zinc potential. It was suggested (chapter 5) that this may account for some of the scatter in the X85 results. This would need further tests to confirm: that such a load ratio effect occurred in X85 grade steels; the appropriate crack growth constants, and to measure the residual stress distribution in the FCAW specimen.

Additional References Not Contained in the Main Text

EIDE, O.I., SKALLERUD, B., BERGE, S., [1994]. Fatigue of large scale tubular joints - Effects of sea water and spectrum loading, Conference Proceedings: : Fatigue Under Spectrum Loading in Corrosive Environments, Lyngby, Denmark.

HASWELL, J., [1992], A general fracture mechanics model for a cracked tubular joint derived from the results of a finite element parametric study, Conference Proceedings: Offshore Mechanics and Arctic Engineering, Calgary.

REFERENCES

- AAGHAAKOUCHAK, A., GLINKA, G. & DHARMAVASAN, S., [1989]. A load shedding model for fracture mechanics analysis of fatigue cracks in tubular joints, OMAE 1989, ASME, vol III, pp 159-165.
- ASTM E647, [1993]. Standard test method for measurement of fatigue crack growth rates, American Society for Testing and Materials, Philadelphia.
- ASTM D1141, [1992]. Standard specification for substitute ocean water, American Society for Testing and Materials, Philadelphia.
- ATKINSON, J.D. & LINDLEY, T.C., [1977]. The influence of environment on fatigue, Inst. Mech. Eng. Publications, Vol.4, 65-74 (1977).
- AUSTIN, J.A., DHARMAVASAN, S. & DOVER, W.D., [1992]. Variable amplitude corrosion fatigue of tubular welded T-joints (axial): progress report, Internal report, University College London, January 1992.
- AUSTIN, J., [1994]. The role of corrosion fatigue crack growth mechanisms in predicting the fatigue life of offshore tubular joints, PhD Thesis, UCL,
- BATESON, H., LIAN, B. & LINDLEY, C., [1988]. Fatigue properties of a higher strength quenched and tempered steel, Offshore Tubular Joints (Conference Proceedings), Anugraha Centre, Egham, 1988, cited in King *et al* 1992.
- BENHAM, P.P. & WARNOCK, F.V., [1976], Mechanics of Solids and Structures, Pitman Publishing, London,
- BENNETT, W. T. JR., CADIOU, L. & CONDREUSE, L., [1991] Steels for jack up legs, Proceedings of the 3rd International Conference on The Jack Up Drilling Platform, City University London.
- BHUYAN G. & VOSIKOVSKY O., [1989]. Prediction of fatigue crack initiation lives for welded plate T joints based on the local stress- strain approach, International Journal of Fatigue, Vol 11, No 3 pp 153-159.
- BIGNONNET, A., BRAZY, J.L., VALLET, C. & BARRERE, F., [1987], The influence of electrochemical parameters on the corrosion fatigue of a structural steel, Steel in Marine Structures, eds: Noordhoek and de Back, Elsevier, Delft.

BILLINGHAM, J. & LAWS, P. A., Fatigue crack propagation in high strength steels for use offshore, Offshore Mechanics and Arctic Engineering, Volume III, 1994.

BOWES, J., [1993]. Marathon Le Tourneau, Personal Communication.

BROEK, D., [1991]. Elementary Engineering Fracture Mechanics, 4th Edition, Kluwer Academic Publishers.

BROEK, D., [1986]. The Practical Use of Fracture Mechanics, Kluwer Academic Publishers.

BROOK, R. & ZHANG, W., [1994]. The effect of loading on the fatigue crack growth of an offshore structural steel, University of Sheffield. (obtained from author).

BS PD 6493: [1991]. Guidance on Methods for Assessing the Acceptability of Flaws in Fusion Welded Structures, British Standards Institute, London.

BS 6835: [1988]. Determination of the rate of fatigue crack growth in metallic materials, British Standards Institute, London.

BS 7608: [1993]. Fatigue design and assessment of steel structures, British Standards Institute, London.

CHEATAINI, M.J., [1994]. Ultimate strength of cracked and uncracked tubular K joints, Welding in the World, Volume 33, Number 5.

CONGLETON & CRAIG, [1982]. Corrosion Fatigue, Corrosion Processes, Edited R.N. Parkins, Applied Science Publications, 1982.

COLLINS, R & MICHAEL, D. H., (1982). Crack monitoring using AC field measurement - multipliers for semi elliptical cracks. Contract Report No. NCS 362/3007, London Centre for Marine Technology, University College London.

COWLING, M.J. & APPLETON, R.J. [1986]. Corrosion fatigue of a C-Mn steel in seawater solutions, Fatigue and Crack Growth in offshore Structures, IMechE.

CREUSOT LOIRE, [1990] Division Creusot-Marrel, Special A517FCR for Jack- Up Legs, Doc 90/A5, Creusot-Loire Industries.

DAVEY, V. S., [1991], Hydrogen assisted cracking of high strength steels in the legs of jack-up rigs, Proceedings 3rd International Conference on The Jack Up Drilling Platform, City University, London.

DEPARTMENT OF ENERGY, [1984]. Offshore Installations: Guidance on Design and Construction 3rd Edition, HMSO, London

DEPARTMENT OF ENERGY, [1987]. United Kingdom Offshore Steels Research Project- Phase II Final Report, OTH 87 265, HMSO.

DEPARTMENT OF ENERGY, [1988]. United Kingdom Offshore Steels Research Project- Phase 1 Final Report, OTH 88 282, HMSO.

DICKSON, J.I., BLANCHETTE, Y. & BAILLON, J.P., [1986]. The effect of cathodic protection on the propagation of long and short fatigue cracks, eds Vosikovsky O and Lewis K, Conference: Cathodic Protection a +or - in Corrosion Fatigue. CANMET.

DIJKSTRA, O.D. & DE BACH, J., [1981]. Fatigue strength of tubular X and T-joints, Proceedings of EEC Conference on Steel in Marine Structures, Paris.

DOLPHIN, A.S. & TICE, D.R., Effects of cathodic protection potential and stress ratio on fatigue thresholds of structural steels in seawater, UREA Draft Report ND-M-3888(S) cited in [HSE, 1992].

DOVER, W.D., CHARLESWORTH, F.D.W., TAYLOR, K.A., COLLINS, R. & MICHAEL, D.H., [1982]. The Use of A.C. Field Measurements to Determine the Shape and Size of a Crack in a Metal, Eddy Current Characterisation of Materials and Structures. Ed. Birbaun, G. and Free, G., ASTM STP722, pp401-427.

DOVER, W. D. & CONNOLLY, M.P.M, [1986]. Fatigue fracture mechanics assessment of tubular welded Y and K joints. Proc. Int Conf on Fatigue Crack Growth in Offshore Structures. I Mech E, London.

DOVER, W.D., DHARMAVASAN, S., [1982], Fatigue fracture mechanics analysis of T and Y joints, Paper OTC4404 of Offshore Technology Conference. Texas.

DOVER, W.D. & DHARMAVASAN, S., [1984]. Fatigue of offshore Structures- a review, Fatigue 84. Vol III, EMAS.

Eds: DOVER, W. D., & DHARMAVASAN, S., [1989]. Cohesive program of research and development into the fatigue of offshore structures July 1985 to June 1987, SERC.

Eds: DOVER, W. D. & DHARMAVASAN S., [1992]. Cohesive program of research and development into the fatigue of offshore structures July 1985 to June 1987, SERC.

DOVER, W.D. & HOLDBROOK, S.J., [1979]. Fatigue crack growth in tubular welded connections, Proceedings of 2nd. International Conference on Behaviour of Offshore Structures. (BOSS 1979), London.

DOVER, W.D. & MONAHAN, C.C., [1994]. The measurement of surface breaking cracks by the electrical systems ACPD/ ACFM, Fatigue and Fracture of Engineering Materials and Structures, Vol 17, No 12, pp 1485-1492.

DOVER W.D., NIU X, AAGHAAKOUCHAK A, KARE R.F. & TOPP D.A., [1988] Fatigue crack growth in X and multi-brace nodes", Fatigue of Offshore Structures, Ed: Dover, W.D. & Glinka, G., London.

EASTERLING, K., [1992]. Introduction to the Physical Metallurgy of Welding, 2nd. Edition, Butterworth and Heinemann.

EFTHYMIU, M., [1988]. Development of SCF formulae and generalised influence functions for use in fatigue analysis, Proceedings: Offshore Tubular Joints Conference, Surrey.

EFTHYMIU, M., & DURKIN, S., [1985]. Stress Concentrations in T/Y and Gap/Overlap K Joints, BOSS 1985, pp 429-440, Delft.

ELLIOT, K.S. & FESSLER, H., [1987]. Stresses at the weld toes in tubular joints in offshore structures, Cohesive Programme of Research and Development July 1985- June 1987, SERC.

GLINKA, G., DHARMAVASAN, S. & DOVER, W.D., [1987]. An analysis of the effect of residual stress on the initiation and fatigue crack growth in tubular welded joints, Steel in Marine Structures, Elsevier, Amsterdam.

GURNEY, T.R., [1989]. The influence of section thickness on the fatigue strength of welded joints - 10 years on, Proceedings 8th International Conference on Offshore Mechanics and Arctic Engineering, The Hague.

HAMBLY, E.C., [1985]. Fatigue vulnerability of jack up platforms, Proceedings: Institute of Civil Engineers, Part 1, Volume 77, pps161-178, Elsevier.

HEALY, J., BILLINGHAM, J., CHUBB, J.P., JONES, R.L. & GALSWORTHY, J., [1993]. Weldable high strength steels for naval construction, Offshore Mechanics and Arctic Engineering, Volume III-A.

HELLIER, A.K., CONNOLLY, M.P., DOVER W.D. & SUTOMO, J., [1990a]. A parametric study of the ratio of bending to membrane stress in tubular Y and T joints, International Journal of Fatigue, Volume 12, 1, pp 3-11, London.

HELLIER, A.K., CONNOLLY, M.P. & DOVER W.D., [1990b]. Stress concentration factors for tubular Y and T-joints, International Journal of Fatigue, Volume 12, 1, pp 13-23, London.

HELLIER, A.K., CONNOLLY, M.P., & DOVER W.D., [1990c] Prediction of the stress distribution in tubular Y and T-joints, International Journal of Fatigue, Volume 12, 1 pp 25-36, London.

HERTZBERG, R.W., [1989], Deformation and fracture mechanics of engineering materials, John Wiley.

HIBBERD R.D. & DOVER, W.D., [1977] The analysis of random load fatigue crack propagation, Fracture '77, Vol 2, Waterloo, Canada, cited in [Dover *et al*, 1984].

HODGKIESS, T.H & CANNON, M.J., [1985], Corrosion fatigue of steels in seawater; Studies of crack tip electrochemistry, Final Report GL/ MM6, Cohesive program of research and development into the fatigue of offshore structures July 1985 to June 1987, Editors: Dover, W. D., & Dharmavasan, S., SERC

HSE, [1992]. Fatigue Background Guidance Document, OTH 92 390, HMSO.

INTERNATIONAL INSTITUTE OF WELDING, [1971]. Guide to the Welding and Weldability of C-Mn and C-Mn Microalloyed Steels, Publications Document II S/IIW-382-71.

KAM, J.C.P., [1988], Structural integrity of offshore tubular joints, PhD Thesis, Department of Mechanical Engineering, University College London.

KAM, J. & BIRKINSHAW, M., [1993]. The simulation of wave induced fatigue loading of jack up tubular components, Offshore Mechanics and Arctic Engineering, Volume 3B, Materials Engineering, ASME.

KAM, J. & DOVER, W. D., [1988]. Fatigue crack growth in offshore welded tubular joints under real life variable amplitude loading, Fatigue crack growth under variable amplitude loading, Eds: Petit, Davidson, Suresh and Rabbe, Elsevier Science.

KARE, R. F. [1989]. Influence of weld profile on the fatigue crack growth in tubular joints, PhD Thesis, The City University.

KING, R., SHARP, J.V. & NICHOLS, N. W., [1992]. The influence of seawater and cathodic protection on the fatigue performance of high strength steels for jack ups, Conference Proceedings: Offshore Mechanics and Arctic Engineering, Calgary.

KIM, K. & HARRT, W.H., [1993]. Corrosion fatigue of short cracks for higher strength steels in sea water with cathodic protection, Offshore Mechanics and Arctic Engineering, Volume 3B, ASME.

KOMAI, K., NOGUICHI, M., [1987], Low Cycle Corrosion Fatigue of High Tensile Strength Steel and Image Processing of Fracture Surfaces, Conference Proceedings: Low Cycle Fatigue and Elasto Plastic Behaviour of Materials, Munich, pps. 342-347, Elsevier.

LOPEZ-MARTINEZ, L., PETERSEN, R.I. & AGERSKOV H., [1994]. Fatigue life of high strength steel tubular joints, Conference Proceedings: Fatigue Under Spectrum Loading in Corrosive Environments, Lyngby, Denmark.

LUCAS, KA. & ROBINSON, M.J., [1986]. The influence of lattice hydrogen content on the hydrogen- assisted cracking of high strength steel, Corrosion Science, Volume 26, No 9.

LUGG, M.C., [1992]. An introduction to ACPD, Technical Software Consultants.

MAAHN, E., [1986]. Crack tip chemistry under cathodic protection and its influence on fatigue crack growth, editors: Vosikovsky O and Lewis K, Conference: Cathodic Protection a + or - in Corrosion Fatigue. CANMET.

MARATHON LE TOURNEAU, [1983]. Specification for Marathon Le Tourneau MM Structural Tubing, Marathon Le Tourneau, 1983

MARATHON LE TOURNEAU, Private communication.

MARINE TECHNOLOGY DIRECTORATE, [1990]. Design and Operational Guidance for Cathodic Protection of Offshore Structures, Subsea Installations and Pipelines, MTD Pub 90/102.

MASUDA, H., MATSUOKA, S., NISHIJIMA, S. & SHIMODAIRA, M., [1988]. Effect of frequency on corrosion fatigue life prediction of high tensile steel (HT80) in synthetic seawater, Translation: MITS BISI26721, Boshoku Gijutsu (Corrosion, Engineering),37(1), 1988,pp27-32. (Cited in King *et al* 1992)

MONAHAN, C.C., [1994]. Early fatigue crack growth in offshore tubular joints, PhD Thesis, University College London.

MONAHAN, C.C. & HOPKINS, R.M., [1990]. The relative severity of natural and synthetic sea-waters on the fatigue behaviour of cathodically protected steel, Environment Assisted Fatigue, EGF7 (Edited P.Scott) , Mechanical Engineering Publications, London.

MORGAN, H.G., [1987]. Interaction of multiple fatigue cracks, Paper 35, Fatigue of Welded Constructions, April 1987.

MORROW [1979], cited in Glinka G, Dhamavasan S and Dover WD, An analysis of the effect of residual stress on the initiation and fatigue crack growth in tubular welded joints, Steel in Marine Structures, Elsevier 1987

NEILSEN, H.P. & MAAHN, E., [1987]. Environmental Effects in Fatigue Crack Initiation, Steel in Marine Structures, editors Noordhoek and de Back, Elsevier Science.

NEUBER, H., [1961]. Transactions ASME, Journal of Applied Mechanics, Volume 8, p 544. (cited in Hertzberg 1989).

NEWMAN, J.C. & RAJU, I.S., [1981]. An empirical stress intensity factor equation for the surface crack, Engineering Fracture Mechanics, Volume 15, pps 185-192.

NICHOLS, N., Marine Technology Support Unit, Culham, Oxfordshire, Private communication.

NIPPON STEEL CORPORATION, [1984]. Welten, Cat. No. EXE 304 July 1977, Nippon Steel Corporation, Tokyo, Japan.

NIU, X. & GLINKA, G., [1987]. The weld profile effect on stress intensity factors in weldments, International Journal of Fracture, Volume 35: 3-20.

NIU, X. & GLINKA, G., [1989]. Stress intensity factors for semi elliptical surface cracks in welded joints, International Journal of Fatigue, Autumn.

PARIS, P.C., [1962]. The growth of fatigue cracks due to variations in load, PhD Thesis, Lehigh University.

PISARSKI, H.G., JONES, R.L. & HARRISON, P.L., [1987]. Influence of welding procedure on the fracture toughness of welds made with self shielding flux cored wires, 6th International OMAE Symposium, Houston.

PORTER GOFF, R.F.D., PAYNE, J.G & FREE, J.A., [1987] Residual stress in nodes, Cohesive Programme of research and Development July 1985- June 1987, SERC.

PROCTOR, R.P.M., [1986] Detrimental effects of cathodic protection: embrittlement and cracking phenomena, Cathodic Protection: Theory and Practice, editors: Ashworth V and Booker CJL, Ellis Horwood.

RAJPATHAK & HARTT, [1988]. Fatigue crack initiation of selected high strength steels in seawater, Offshore Mechanics and Arctic Engineering.

SAENZ DE SANTA MARIA, M., & PROCTOR, R.P.M., [1986]. Environmental cracking (corrosion fatigue and hydrogen embrittlement) X-70 linepipe steel, Fatigue and Crack growth in Offshore Structures IMech E.

SCULLY, J.A. & MORAN, P.J., [1990]. Influence of strain on hydrogen assisted cracking of cathodically polarized high strength steel, Environmentally Assisted Cracking, ASTM STP 1049

SINES, E.G., [1967] Factors Affecting the fatigue strength of high strength steels, Welding Journal, Volume 14, Number 3, pps 108-116 (cited in HSE, 1992).

SLATER, G., [1991]. Fatigue behaviour of internally stiffened tubular joints, TWI, Confidential to sponsors.

SMEDLEY, P. & FISHER, P., [1991]. Stress concentration factors for simple tubular joints, International Society of Petroleum Engineers, 1991. (obtained from author)

SPURRIER, J. & HEALY, J., [1995]. Effects of overmatching of weld metals used in offshore high strength steel weldments, Marine Technology Directorate, Publication 95/100.

SRAWLEY, J. E., [1976]. Wide range stress intensity factor expressions for ASTM E399 standard toughness fracture toughness specimens, International Journal of Fracture, Volume 12, 475, Martinus Nijhoff Pub (cited in BS 6835).

STACEY A, [1993]. The Significance of Residual Stress in the Defect Assessment of Offshore Structures, Offshore Mechanics and Arctic Engineering, Volume 3b, pps 729-739.

STANGERS CONSULTANTS Ltd, Fortune Lane, Elstree, Herts, Private communication, Ref 207/0879/92/MP/wdb.

SURESH, [1991], Fatigue of Materials, Cambridge University Press.

TECHNICAL SOFTWARE CONSULTANTS, FLAIR software, TSC, Milton Keynes.

TECHNICAL SOFTWARE CONSULTANTS, U10 Crack Microgauge Handbook, TSC, Milton Keynes.

THORPE T.W., SCOTT P.M., RANCE, A. & SILVESTER, D., [1983]. Corrosion fatigue of BS4360.50D structural steel in seawater, International Journal of Fatigue, Volume 5, Number 3, July 1983.

THURLBECK, S.D. & BURDEKIN, F.M., [1992]. Effects of geometry and loading variables on the fatigue design curve for tubular joints, Welding in the World, Volume 30, Number 7/8, pp 189-200.

TOPP, D. & DOVER, W. D., [1987]. Study of calibration procedures for accurately quantifying crack sizes in welded tubular joints, OTH 87 263, HMSO, (cited in Dover & Monahan, [1994]).

TOPPER, T.H., WETZEL, R.H. & MORROW, J., [1969]. J Mater., JMSLA, Vol 4, p200, (cited in Hertzberg 1989).

TUBBY, P.J., & BOOTH, G.S., [1991]. Corrosion fatigue of two weldable high strength steels for offshore structures, Offshore Mechanics and Arctic Engineering, Stavenger.

TURNBULL, A. & FERRISS, D.H., [1986]. Mathematical modelling of the electrochemistry in corrosion fatigue cracks in structural steel cathodically protected in seawater, Corrosion Science, Vol 26, p601.

TURNBULL, A. & GARDNER, M.K., [1982]. Electrochemical polarization studies of BS 4360.50D steel in 3.5% Na Cl, Corrosion Science, Volume 22, Number 7, pp 661-673.

TWADDLE, B.R. & HANCOCK, J.W., [1988]. The development of cracks by surface coalescence, Conference: Fatigue of Offshore Structures, editors Dover WD and Glinka G, EMAS.

UNIVERSITY ENGINEERING GROUP, [1985]. Offshore Research, Volume 2, Design of Tubular Joints for Offshore Structures, UR33, UEG/CIRIA.

VINAS-PICH, J., [1994], The influence of environment, loading and steel composition on fatigue of tubular connections, PhD Thesis, Mechanical Engineering Department, University College London.

VOSIKOVSKY, O., [1975], Fatigue crack growth in a X65 line pipe steel at low cyclic frequencies in aqueous environments, Journal of Engineering Materials and Technology, Transaction of ASME, Series H, Volume 97, No. 4, pp 298 - 304.

VOSIKOVSKY, O., [1978]. Frequency, stress ratio, and potential effects on fatigue crack growth of HY130 steel in salt water, Journal of Testing and Evaluation, Volume. 6, Number 3, pp 175-182, May 1978.

VOSIKOVSKY, O., [1980]. Effect of mechanical and environmental variables on fatigue crack growth rates in steel, Canadian Metallurgical Quarterly, Volume 19, pp 87-97.

VOSIKOVSKY, O., NEILL, W.R., CARLYLE D.A. & RIVARD A., [1986]. PMRL CANMET Report ERP/PMRL 83-27 (OP-J), 1983, cited in Dickson 1986.

VOSIKOVSKY, O. & TYSON, W.R., [1986]. Effects of cathodic protection on fatigue life of steel welded joints in sea-water, Cathodic Protection, a + or - in Fatigue, editors: Vosikovsky O and Lewis K, Conf Cathodic Protection a +or - in Corrosion Fatigue, CANMET.

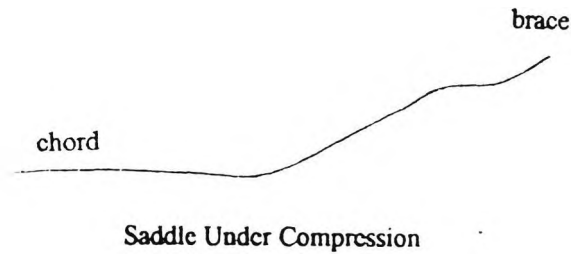
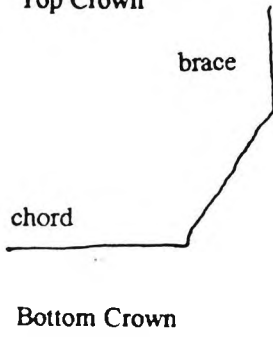
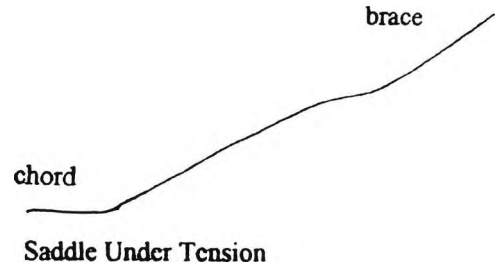
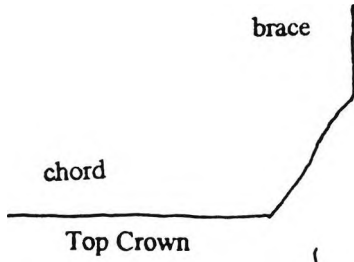
WATKINS, F., [1970]. The fatigue strength of welded joints in high strength steels and methods for its improvement, Fatigue of Welded Structures, Conference, Brighton.

WILSON, T.J., DOVER, W.D., [1986]. Corrosion Fatigue of Tubular Welded T Joints, Paper C136/86, International Conference on Fatigue and Crack Growth in Offshore Structures, Proceedings Institute of Mechanical Engineers, 1986-2, London.

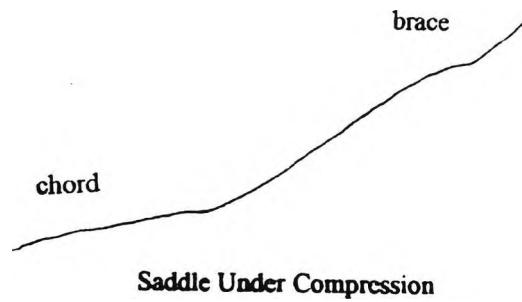
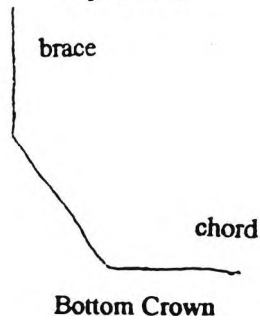
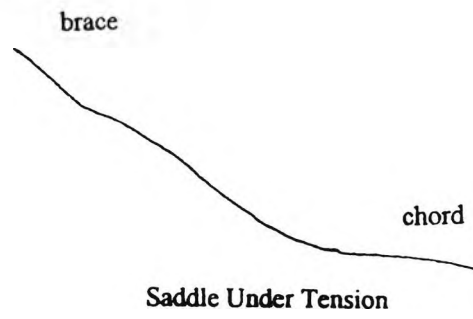
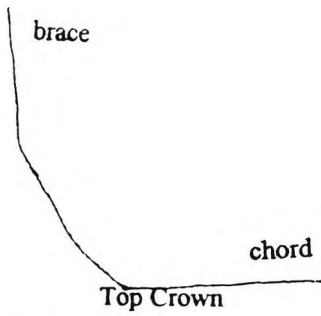
**APPENDIX I : WELD PROFILES AT SADDLE AND CHORD
POSITIONS**

Appendix I Weld Profiles at Crown and Saddle Positions

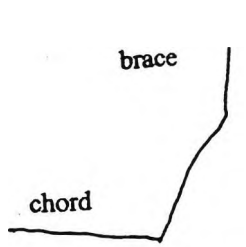
Specimen W1 and W5



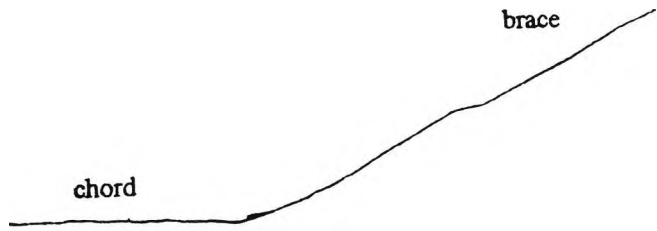
Specimen W2



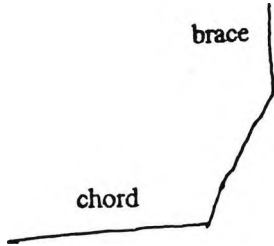
Specimen W3 and W6



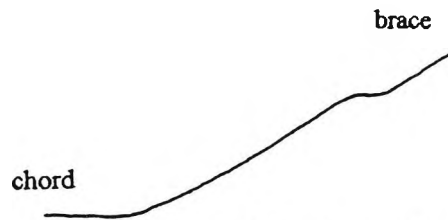
Top Crown



Saddle Under Tension

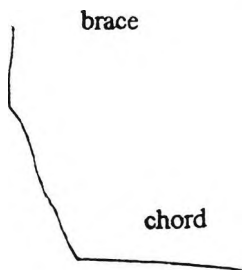


Bottom Crown

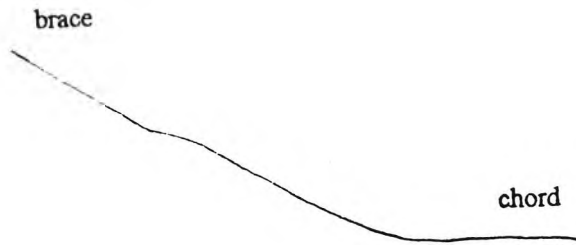


Saddle Under Compression

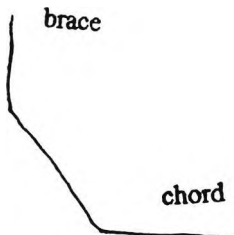
Specimen W4



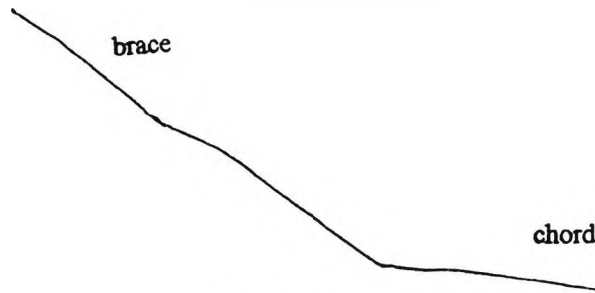
Top Crown



Saddle Under Tension

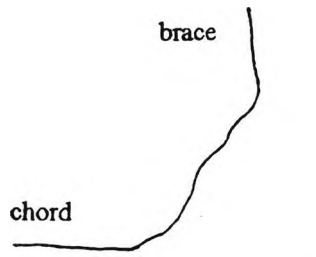


Bottom Crown

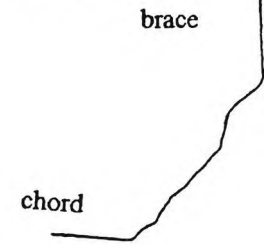


Saddle Under Compression

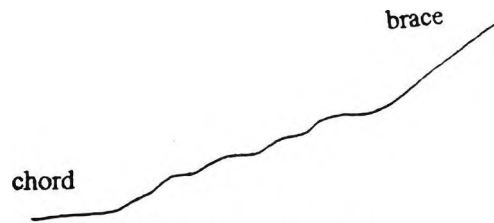
Specimen S1



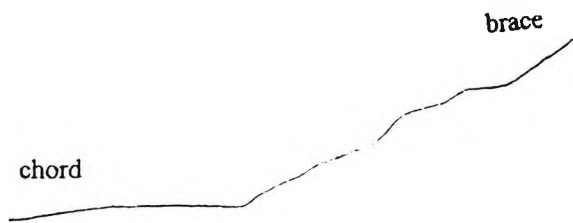
Top Crown



Bottom Crown

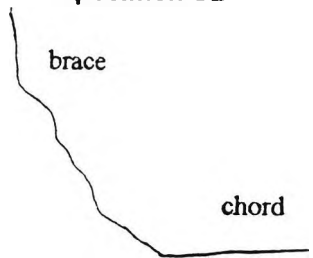


Saddle Under Tension

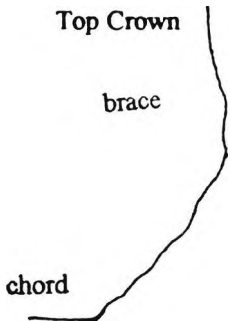


Saddle Under Compression

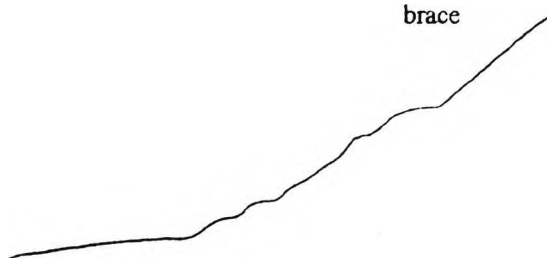
Specimen S2



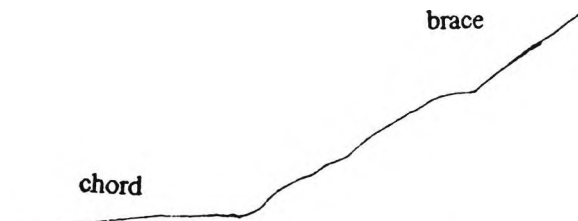
Top Crown



Bottom Crown

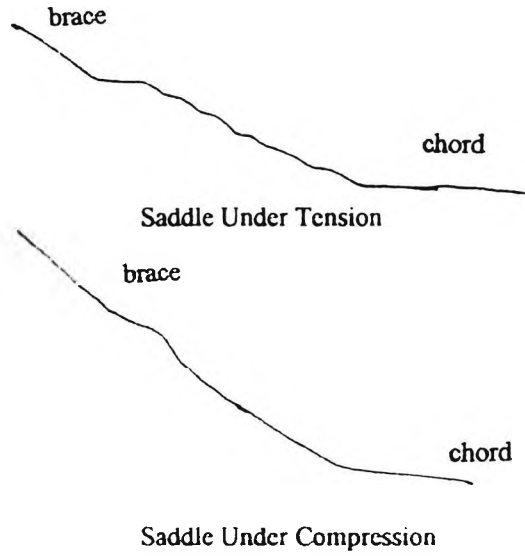
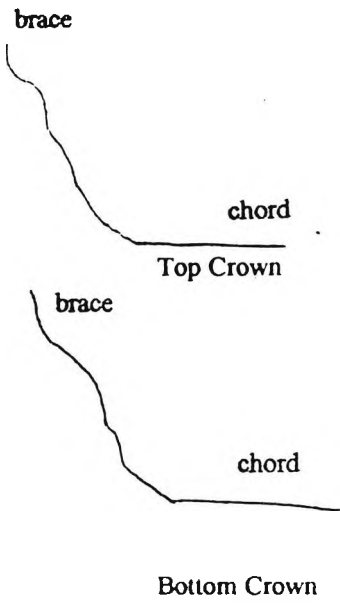


Saddle Under Tension

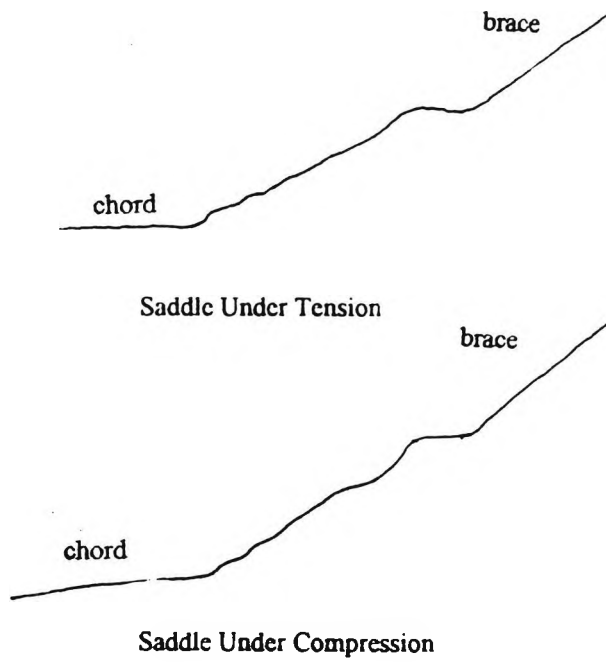
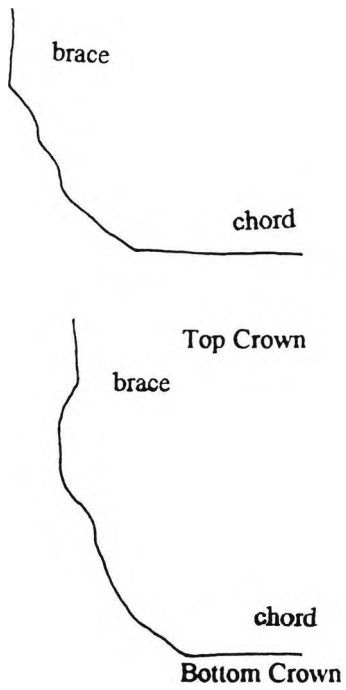


Saddle Under Compression

Specimen S3



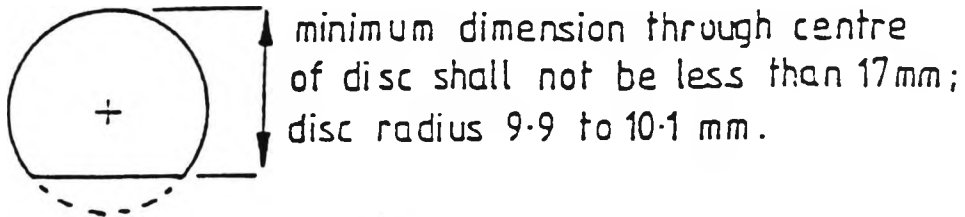
Specimen S4



APPENDIX II : THE IRISH PENNY TEST

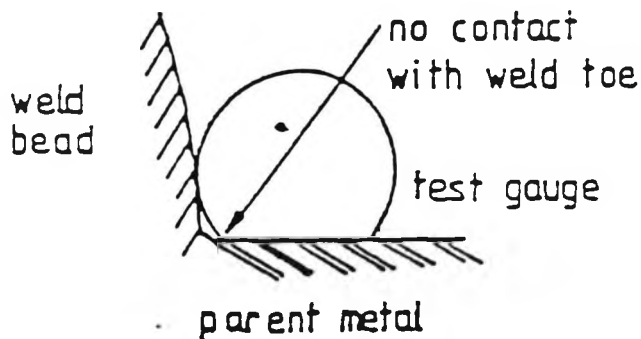
PROCEDURE FOR ASSESSMENT OF WELD PROFILES

This procedure is usually referred to as either the Dime or Irish Penny test. In order to pass the test, the point/corner of the test gauge must be able to touch the weld toe for at least 90% of the length of the weld. Locations where the profile fails the test should be noted for consideration of their significance regarding subsequent performance of the joint.

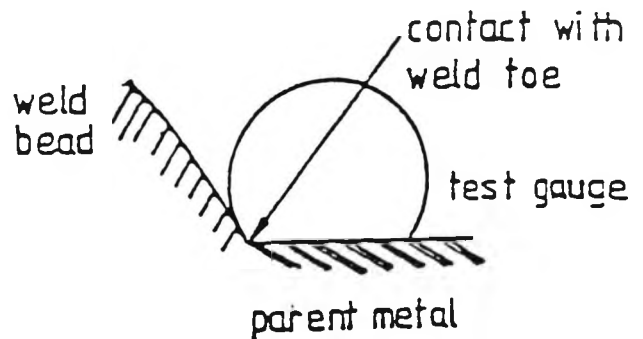


DETAIL OF TEST GAUGE

EXAMPLES OF TEST

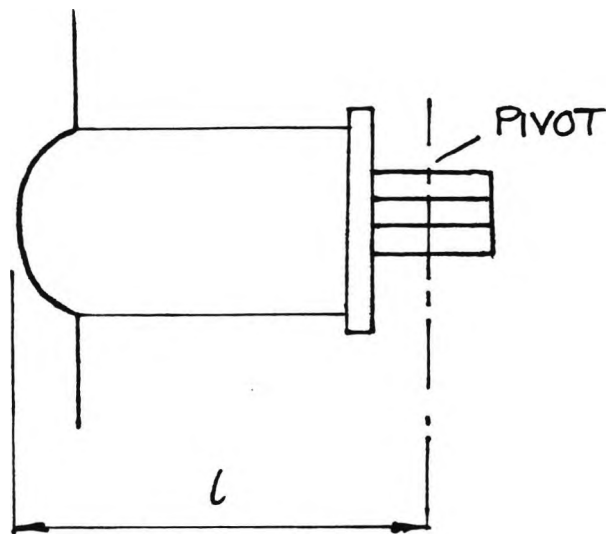


FAIL TEST



PASS TEST

APPENDIX III : CALCULATION OF NOMINAL STRESSES



From Simple Bending Theory

Nominal Stress

$$\sigma = My/I$$

$$I = \pi(r_1^4 - r_2^4)/4$$

$$M = Pl$$

$$\therefore \sigma = 4Plr_1 / (\pi(r_1^4 - r_2^4))$$

APPENDIX IV: VARIATION IN CRACK DEPTH READINGS ASSOCIATED WITH S TYPE CRACKING

A large variation of the ACPD depth reading was noted with specimen S3 at about 63000 cycles. Similar variations were noted in specimens S2 and S4, but only for much deeper cracks. It was decided to investigate how the crack and reference voltages varied with actuator load.

Experimental Procedure

Specimens S3 and S1 were loaded using the test rig described in section 5.3.1, (S3 was immersed in seawater during the test). The brace was loaded using incremental loading varying from 0 kN to the peak service load and then unloaded incrementally. The potential difference at the crack and reference probes were measured using a U10 ACPD crack microgauge.

Results

Figure IV:1 shows the variation in crack and reference voltage with applied load. The reference voltage remained constant, however the crack voltage varied considerably,. If the maximum crack potential difference is the true measure of the crack depth, the minimum measure of the crack depth would lead to a 20mm underestimate of the crack depth (62% error).

Similar results were recorded with specimens S2 and S4, however no significant variations were noted with specimens W5 or any of the air specimens.

Discussion of results

The variation of crack voltage was unexpected. Previous crack closure trials conducted in air [OTH 87 263, 1987] showed the crack voltage to be almost constant with respect to actuator loading for tensile loads. However, significant variation in crack voltage was noted for compressive loading of plate specimens. This would imply that crack closure was taking place in the X85 tubular joint trials, but only under conditions where the crack growth was on a plane approximately parallel to the chord surface and only in conditions of seawater corrosion. It is suggested that the

variation in the ACPD readings was due to calcaereous deposit crack closure, and that the corrosion products formed a conductive "salt bridge" shorting out the crack and giving false crack voltage readings. This has two important implications for tubular joint work: firstly, ACPD and crack depth monitoring by electrical resistance methods is potentially unreliable for certain crack geometries in a seawater environment; secondly, these results indirectly confirm corrosion product crack closure and help to explain the lower than anticipated crack growth rates, noted for the deeper cracks in seawater.

It is suggested that the influence of crack closure on crack depth monitoring techniques is best investigated under seawater corrosion fatigue conditions, as the presence of calcaereous deposits may have a significant influence on the effectiveness of the NDT technique under investigation.

Figure IV.1: Variation in crack potential with load S3 at 67000 cycles

